Polymeric Complexes and Composites for Aerospace and Biomedical Applications

Rui Zhang

Dissertation submitted to the faculty of the Virginia Polytechnic Institute and State University in partial fulfillment of the requirements for the degree of

Doctor of Philosophy

in

Chemistry

Judy S. Riffle

Richey M. Davis

S. Richard Turner

Guoliang Liu

Apr 19, 2018

Blacksburg, VA

Keywords: high-performance polymer, carbon fiber, suspending agent, ionic copolymer, magnetite, particles, imaging, drug delivery

Abstract (academic)

Polymers, among metals and ceramics, are major solid materials which are widely used in all kinds of applications. Polymers are of particular interest because they can be tailored with desirable properties. Polymer-based complexes and composites, which contain both the polymers and other components such as metal oxide/salts, are playing a more and more important role in the material fields. Such complexes and composites may display the benefits of both the polymer and other materials, endowing them with excellent functionalities for targeted applications.

In this dissertation, a great deal of research was conducted to synthesize novel polymers and build polymeric complexes and composites for biomedical and aerospace applications. In chapter 3, two methods were developed and optimized to fabricate sub-micron high-performance polymer particles which were subsequently used to coat onto functional carbon fibers via electrostatic interactions, for the purpose of fabricating carbon fiber reinforced polymer composites. In chapter 4, a novel Pluronic® P85-bearing penta-block copolymer was synthesized and formed complexes with magnetite. The complexes displayed non-toxicity to cells normally but were able to selectively kill cancer cells without killing normal cells when subjected to a low-frequency alternating current magnetic field. Such results demonstrated the potential of such polymeric complexes in cancer treatment. Chapter 5 described the synthesis of several ionic graft copolymers primarily bisphosphonate-containing polymers, and the fabrication of polymer-magnetite complexes. The in-depth investigation results indicated the capability of the complexes for potential drug delivery, imaging, and other biomedical applications. Chapter 6 described additional polymer synthesis and particle or complex fabrication for potential drug delivery and imaging, as well as radiation shielding.

Abstract (public)

Polymers, metals, and ceramics are three major classes of solid materials that are used every day and everywhere. Polymers are of particular significance because they can be tailored to possess certain desirable properties, and, hence, they are playing a more and more important role as substitutes for metals and ceramics in a wide array of applications. Engineering and high-performance polymers were synthesized with excellent properties for biomedical and aerospace applications.

Polymers can be fabricated into composites and complexes which contain not only polymers but also other materials, such as metal oxides/salts, carbon fibers, glass fibers, etc. When composites and complexes are made with sufficient stability, the materials may display the advantages of each component, making them more promising for specific applications.

In this dissertation, effort was focused on developing versatile polymer-based complexes and composites for aerospace and biomedical applications. Chapter 3 describes the fabrication of sub-micron high-performance polymer particles by two methods and they were subsequently coated onto functional carbon fibers for making composites. Chapter 4 describes the synthesis of a novel copolymer that formed complexes with magnetite nanoparticles. The complexes were able to selectively kill cancerous cells without killing normal cells when exposed to an external magnetic field, and thus these materials have potential for cancer treatment. Chapter 5 describes the fabrication of phosphonate-bearing ionic copolymer-magnetite complexes and their potential applications in drug delivery, imaging, and other biomedical applications. Chapter 6 describes the synthesis of polymers and their corresponding complexes for potential drug delivery and imaging, as well as potential radiation shielding applications.

Acknowledgements

First and foremost, I would like to express my greatest gratitude to Professor Judy S. Riffle for her extensive guidance and support. She has taught me tremendously, from polymer science knowledge to synthetic methods and procedures, from lyophilization processes to polymer precipitation requirements, from presentation skills to technical writing. She even assisted me in word-to-word reduction of a literature writing in order to meet word limit requirements. Her positive impacts on me is far beyond education and research. Words cannot describe how grateful I am feeling towards her generous assistance. Meanwhile, I am also very thankful for my committee members, Prof. S. Richard Turner, Prof. Richey M. Davis, and Prof. Guoliang Liu. They have devoted their valuable time to provide me with excellent suggestions and guidance, which are significant.

In addition, I would like to say many thanks to my labmates and collaborators. Dr. Nikorn Pothayee, Dr. Nipon Pothayee, Dr. Nan Hu, Dr. Oguzhan Celebi, Dr. Gregory Miller, Dr. Ran Liu, Dr. Wenrui Zhang, Dr. Andrew Shaver, Dr. Alyssa Master, Dr. Marina Sokolsky-Papkov, Dr. Xiaoling Wang, Dr. Ana C. Bohorquez, Dr. Xu Feng, Mr. Ronald Matthew Joseph, Mr. Jake Fallon, Miss Ami Jo, and other labmates. They either provided excellent collaboration, or great assistance of other work-related issues. My success is indispensable for their excellent collaboration, assistance, and support.

Finally, I would like to express my sincerest gratefulness to my parents, my grandparents, my wife and little one, as well as other family members. Their support, both spiritually and materially, has laid the foundation and endowed me with confidence in doing research in the United States. They are great family members and I am very proud of them.

Authorship Attributions

It has been my greatest pleasure and honor to work under the brilliant guidance of Prof. Judy S. Riffle and other committee members, as well as to work with excellent collaborators who had devoted to the presented work. The contribution of the author of this dissertation to each chapter is listed below.

Chapter 3: Preparation of Sub-Micron High-Performance Polyetherimide Particles for Fabricating Carbon Fiber Reinforced Polymer Composites.

The author was the primary researcher on this topic. The author was responsible for the fabrication of sub-micron PEI particles by nucleation and growth (3.3.4), fabrication of PEI particles using homogenization - solvent evaporation (3.3.5), carbon fiber coating with PEI particles (3.3.6) and all or part of the characterization using NMR, SEM, DLS, and XPS (3.3.7.1-3.3.7.3, and 3.3.7.6). The author is indebted to Jake Fallon and Prof. Michael Bortner for contributing the engineering sections of this paper.

Chapter 4: Design and Synthesis of Pluronic® P85 Block Copolymers for Remote Actuation in Cancer Cell Selective Treatment through Cytoskeletal Disruption.

The author was a co-author in the paper and was in charge of the synthesis of a Br-P85-Br macro-initiator, a p*t*BA-*b*-P85-*b*-p*t*BA copolymer, deprotection of p*t*BA-*b*-P85-*b*-p*t*BA to afford PAA-*b*-P85-*b*-PAA copolymer, and the fabrication of polymer-SMNP (PAA-*b*-P85-*b*-PAA-magnetite nanoparticle) complexes (4.3.3.1-4.3.3.4). The author is indebted to Dr. Alyssa Master, directed by Prof. A. V. Kabanov, for contributing the biological parts of this work.

Chapter 5: Ammonium Bisphosphonate Polymeric Magnetic Nanocomplexes for Platinum Anticancer Drug Delivery and Imaging, with Potential Hyperthermia and Temperature-Dependent Drug Release.

The author was the primary researcher on this topic. The author was responsible for the synthesis of magnetite-graft ionomer complexes (*MGICs*), cisplatin-loaded and carboplatin-loaded *MGICs* (5.3.2.6-5.3.2.8), as well as characterization using ^{1}H and ^{31}P nuclear magnetic resonance (NMR), dynamic light scattering (DLS), inductively coupled plasma atomic emission spectroscopy (ICP-AES) (5.3.3.1-5.3.3.3). The author also conducted relaxivity measurements (5.3.3.6) and *in vitro* release of cisplatin and carboplatin from *MGICs* (5.3.3.7). In addition, the author was partially in charge of the synthesis of an acrylate-functional poly(ethylene oxide) macromonomer, methacrylate-functional bisphosphonate monomers, acrylic acid-containing graft copolymer, poly(ammonium bisphosphonic acid-*g*-ethylene oxide) copolymers (5.3.2.1-5.3.2.4). The author acknowledges the work of Dr. Nan Hu for much of the synthetic development.

Chapter 6: Additional synthesis and fabrication.

The author was responsible for all the detailed synthesis and fabrication in this chapter, while coauthors and collaborators were in charge of other sections.

Table of Contents

List of Abbreviations

PEI: polyetherimide

DCM: dichloromethane

DMSO: dimethyl sulfoxide

PEO: poly(ethylene oxide)

PES: polyethersulfone

PEEK: polyetheretherketone

PPS: poly(phenylene sulfide)

PTFE: polytetrafluoroethylene

DMAc: dimethylacetamide

NMP: N-methyl-2-pyrrolidone

PAASalt: poly(amic acid) salt

PVA: polyvinyl alcohol

PP: polypropylene

PVC: polyvinyl chloride

PE: polyethylene

ILSS: interlaminar shear strength

CFRP: carbon fiber reinforced plastics

ORNL: Oak Ridge National Laboratory

GP: General Purpose

HP: High Performance

SEC: size exclusion chromatography

NMR: nuclear magnetic resonance

XRD: X-ray diffraction

SEM: scanning electron microscope

PMA: poly(methacrylic acid)

NHS: *N*-Hydroxysuccinimide

EDC: 1-ethyl-3-(3-dimethylaminopropyl)carbodiimide

SMNP: superparamagnetic nanoparticles

AC: alternating current

EGF: epidermal growth factor

LMP: lysosomal membrane permeabilization

ICP-MS: inductively coupled plasma-mass spectrometry

CD: Cytochalasin D

TEM: transmission electron microscopy

ICP-AES: inductively coupled plasma atomic emission spectroscopy

DMF: dimethylformamide

AIBN: azobisisobutyronitrile

TMSBr: bromotrimethylsilane

PVP: poly(*N*-vinyl-2-prrolidone)

PDMAEMA: poly(*N*,*N*-dimethyl-aminoethylmethacrylate)

PVBP: poly(4-vinylbenzylphosphonate)

PAA: poly(acrylic acid)

PNIPAM: Poly-*N*-isopropylacrylamide

THF: tetrahydrofuran

TFA: trifluoroacetic acid

PMDETA: *N*,*N*,*N*′,*N*′,*N*″-pentamethyldiethylenetriamine

PBS: phosphate buffered saline

ABS: acetate buffered saline

PB: phosphate buffer

ATRP: atom transfer radical polymerization

RAFT: reversible-addition fragmentation chain-transfer polymerization

ABCs: amphiphilic block copolymers

BICs: block ionic copolymers

PICs: polyion complexes

CMC: critical micelle concentration

LCST: lowest critical solution temperature

MGICs: magnetite-graft ionomer complexes

MBICs: magnetite-block ionomer complexes

MNPs: magnetic nanoparticles

rpm: revolutions per minute

Eq.: equivalent

PDI: polydispersity index

DLS: dynamic light scattering

MRI: magnetic resonance imaging

AC: alternating current

FGs: functional groups

FDA: American Food and Drug Administration

SAR: specific absorption rate

SPION: superparamagnetic iron oxide nanoparticles

Cisplatin (CPT): *cis*-diamminedichloro-platinum (II)

Carboplatin (CAPT): *cis*-diammine (cyclobutane-1,1-dicarboxylate-O,O')-platinum (II)

List of Figures

List of Tables

Chapter 1: Introduction

1.1 Introduction

Polymers have been synthesized and utilized for a long time. They are playing a more and more important role in the modern world and being used in all walks of life, from spacecrafts to automobiles, from medical devices to everyday commodities.[1-4] Based on the specific applications, suitable polymeric materials can be synthesized with desirable properties. Polymeric complexes or composites are of particular interest because they may display the properties of both the polymers and other components, making them more versatile and suitable for many applications.[5-8] For example, carbon fiber reinforced plastics using carbon fibers as reinforcement and polymers as matrices are widely used in the aerospace, automotive, and biomedical fields.[9]

In this dissertation, the emphasis is on the design, synthesis, and fabrication of functional monomers and polymers, as well as polymeric composites and complexes. The purpose is to utilize the as-prepared polymeric materials for aerospace and biomedical applications. A multitude of polymers have been synthesized using different polymerization techniques including conventional free radical polymerization, atom transfer radical polymerization, and ring opening polymerization. Fabrication of several sub-micron nanoparticles with narrow size distributions have also been investigated. The polymers were then used to form either composites with carbon fibers, or colloidal micellar complexes with transition metal oxides/salts. Their potential for aerospace and biomedical applications are also discussed.

Chapter 2 is the literature review which first describes the origin of carbon fibers, different carbon fiber precursors and the manufacturing processes, followed by a review on high-performance polymers, with emphasis on polyetherimides and polyetheretherketones. Thermally stable suspending

agents are then discussed, as well as the fabrication of carbon fiber reinforced plastics and their applications. In part II, drug delivery systems are discussed, with a focus on polymeric micellar drug delivery systems. Common biocompatible polymers which are used in drug delivery are reviewed. The synthetic approaches to make these polymers are also discussed.

In chapter 3, two methods to synthesize high-performance polyetherimide particles have been investigated. They are termed a "nucleation and growth" method, and a "homogenization - solvent evaporation" method. The optimization of reaction conditions and reagent ratios were investigated. The particles were mostly sub-micron in size and could be used as a coating on carbon fibers to fabricate carbon fiber reinforced plastic composites. An ozone plasma treatment was applied and silane coupling agents were reacted with hydroxyl groups on the carbon fibers, leading to significantly increased incorporation of the polymer particles into the fiber-polymer composites. Such materials may be potentially useful for aerospace applications.

Chapter 4 is a combination of our published article - remote actuation of magnetic nanoparticles for cancer cell selective treatment through cytoskeletal disruption. In chapter 4, Pluronic® P85-based pentablock copolymers that were designed and synthesized are described. The polymers were complexed with magnetite nanoparticles to form a core-shell micellar structure that may have potential to be used as drug delivery vehicles. It was found that such complexes had significantly increased intracellular uptake compared to complexes without P85 block, were non-toxic, and were able to selectively kill cancerous cells without significantly affecting non-tumorous cells under a low frequency alternating current magnetic field. The mechanism behind this was found to be cytoskeleton damage induced by magneto-mechanical motion rather than hyperthermia effects or lysosomal membrane permeabilization. Such complexes may have the potential to be used for selectively killing tumorous cells upon exposure to an AC magnetic field at low frequencies.

Chapter 5 is an original paper that was submitted to Journal of Nanomaterials. It describes the design and synthesis of novel bisphosphonate-bearing ionic graft copolymers and their corresponding polymer-magnetite nanocomplexes. The complexes were colloidally stable, and had reasonable sizes and good size distributions. Anti-cancer platinum drugs, cisplatin and carboplatin, were successfully loaded into the complexes and were released in a slow, sustained manner in simulated endosomal and physiological conditions *in vitro*. Therefore, the novel graft ionomer-magnetite nanocomplexes may be useful for drug delivery. In addition, the complexes displayed excellent negative contrast enhancement for MRI imaging, as was determined by both relaxivity studies and phantom magnetic resonance imaging. Moreover, aqueous dispersions of such complexes were found to generate heat under an AC magnetic field of high frequency, thus demonstrating the potential for applications in hyperthermia, as well as temperature-dependent or triggered drug release.

Chapter 6 includes some additional polymer synthesis as well as nanoparticles and complexes fabrication, including functional polydimethylsiloxane polymers and silver nanoparticles. They were used in other research projects as well as published or not yet published papers.

Chapter 7 proposes future directions for some pertinent projects, as well as some non-relevant, but highly interesting and promising research ideas. It describes three different potential projects. The first focuses on the selection of versatile silane coupling agents to coat carbon fibers in order to increase their potential adhesion to polymer matrices to make carbon fiber reinforced composites. The second is aimed at developing a biodegradable copolymer analog to replace non-degradable Pluronic® P85 for biomedical applications, especially for potential drug delivery through the blood-brain barrier. The third describes the development of peptoid libraries for fast screening and fabrication of potential drug delivery systems.

1.2 References

1. Tyutnev, A.; Saenko, V.; Pozhidaev, E.; Ikhsanov, R., Experimental and theoretical studies of radiation-induced conductivity in spacecraft polymers. *IEEE Transactions on Plasma Science* **2015,** *43* (9), 2915-2924.
2. Chandra, A. K.; Kumar, N. R., Polymer Nanocomposites for Automobile Engineering Applications. In *Properties and Applications of Polymer Nanocomposites: Clay and Carbon Based Polymer Nanocomposites*, Tripathy, D. K.; Sahoo, B. P., Eds. Springer Berlin Heidelberg: Berlin, Heidelberg, 2017; pp 139-172.
3. Youssef, A.; Hollister, S. J.; Dalton, P. D., Additive manufacturing of polymer melts for implantable medical devices and scaffolds. *Biofabrication* **2017,** *9* (1), 012002.
4. Guillame, S. M.; Khalil, H.; Misra, M., Green and sustainable polyurethanes for advanced applications. *Journal of Applied Polymer Science* **2017,** *134* (45), 45646.
5. Pothayee, N.; Pothayee, N.; Jain, N.; Hu, N.; Balasubramaniam, S.; Johnson, L. M.; Davis, R. M.; Sriranganathan, N.; Riffle, J. S., Magnetic Block Ionomer Complexes for Potential Dual Imaging and Therapeutic Agents. *Chemistry of Materials* **2012,** *24* (11), 2056-2063.
6. Master, A. M.; Williams, P. N.; Pothayee, N.; Pothayee, N.; Zhang, R.; Vishwasrao, H. M.; Golovin, Y. I.; Riffle, J. S.; Sokolsky, M.; Kabanov, A. V., Remote Actuation of Magnetic Nanoparticles For Cancer Cell Selective Treatment Through Cytoskeletal Disruption. *Scientific Reports* **2016,** *6*.
7. McGrail, B. T.; Sehirlioglu, A.; Pentzer, E., Polymer composites for thermoelectric applications. *Angewandte Chemie International Edition* **2015,** *54* (6), 1710-1723.
8. Phil, E.; Soutis, C., *Polymer composites in the aerospace industry*. Elsevier: 2014.
9. Mallick, P. K., *Fiber-reinforced composites: materials, manufacturing, and design*. CRC press: 2007.

Chapter 2: Literature Review

This literature review is divided into two parts. Part I describes polymeric composites for aerospace applications. Part II focuses on polymeric complexes for biomedical applications. In Part I, the origin of carbon fibers are first introduced, followed by the review of different carbon fiber precursors and the manufacturing processes, high-performance polymers with emphasis on polyetherimides and polyetheretherketones, thermally stable suspending agents, as well as the fabrication of carbon fiber reinforced plastics and their applications. In part II, drug delivery systems are discussed, with a focus on polymeric micellar drug delivery systems. Common biocompatible polymers which are used in drug delivery are reviewed. The synthetic approaches to make these polymers are also discussed.

Part I. Polymeric composites for aerospace applications.

2.1 Carbon fibers

2.1.1 Introduction to carbon fibers

Carbon fibers are engineering materials that are mostly comprised of carbon atoms. Similar to other carbon allotropes such as graphite, diamond, fullerenes, and carbon nanotubes, they have a multitude of merits that have garnered tremendous research interest.[1-2] Carbon fibers can be incorporated into polymer composites, with the advantages of extreme lightweight, ultra-high strength and modulus, and high thermal conductivity, to name a few.[3] The carbon fiber was first documented, fabricated, and patented for use as a filament in the incandescent light bulb by the world famous American inventor and businessman, Thomas Edison, back in 1879.[4] He made a thin strip of bamboo or cotton threads of a certain size and shape to form a filament, and then utilized electricity to "bake"

it at high temperature, thus forming "carbonized" materials.[5] The primary composition of the bamboo and cotton precursor materials is cellulose, which is a natural polymer comprised of repeating units of glucose with C-1 and C-4 glycosidic linkages. The thermal treatment led to char formation, and the product became known as carbon fibers. Though tungsten wires were soon fabricated and widely used as light bulb filaments to replace the carbon fiber filaments, Edison's invention was an important milestone and shed light on the precursor compositions and processes required to fabricate carbon fibers. Edison's carbon fiber filaments were still used on U.S. Navy ships until the 1960s, due to their better stability against ship vibrations in comparison with tungsten counterparts.[4] Edison's contributions are greatly remembered and honored, and his first light bulb is on display in the Thomas Edison Center at Menlo Park in Edison, New Jersey, as is shown in Figure 2.1.[6]

Figure 2.1 Edison's first incandescent light bulb on display in the Thomas Edison Center at Menlo Park, NJ.[6]

The modern investigation and fabrication of carbon fiber materials began in the late 1950s. In 1956, the then Union Carbide and Carbon Corporation (changed name to Union Carbide Corporation in 1957 and is now a wholly owned subsidiary of Dow-DuPont Inc.) opened the Parma Technical Center (now GrafTech International) in Parma, Ohio and recruited many young scientists.[7] Among

them, Dr. Roger Bacon, who was a fresh Ph.D. in physics, was particularly interested in the phenomenon of graphite melting under high temperature and pressure. He used equipment that was similar to carbon arc lamps but that could be used under high pressure, and found that carbon vapors formed and eventually deposited on the lower electrode. When he investigated these deposited carbon materials, he found them to have extraordinary properties such as ultrahigh strengths and moduli. He claimed that "they were long filaments of perfect graphite."[7] In 1959, Curry E. Ford and Charles V. Mitchell in the Parma Technical Center developed a process to use commercial rayon fibers to fabricate high-strength carbon fiber, and they called these "fibrous graphite".[8] Rayon is a semi-synthetic fiber made from regenerated cellulose, so the composition of the starting material was similar to that which Edison had used. The process involved heating the rayon at different temperatures ending as high as 2900-3000 °C, known as carbonization and graphitization, to obtain the carbon fibers.[7] They later filed a patent in 1960 and claimed that the method to make carbon fibers was applicable to all woven and non-woven cellulosic materials, including rayon cord, cloth, and fibers.[8] However, the mechanical properties of these fibers, in particular their moduli, were relatively low. In 1964, Dr. Roger Bacon and his colleagues developed a novel "hot-stretching" process that enabled fabrication of high modulus rayon-based carbon fibers. It involved stretching and orienting the fibers during the low-temperature heat treatment stage and led to a ten-fold increase in Young's modulus of the fabricated carbon fibers.[7] The rayon-based fibers and the new fabrication process seemed so promising that the U.S. Air Force Materials Laboratory provided funding and in-kind support to the Union Carbide Corporation, with the objective of developing high strength, rayon-based carbon fiber composites for aerospace and military applications, including rocket nozzles, spacecraft heat shields, and missile nose tips.[7]

In the US, unsuccessful attempts to synthesize high modulus carbon fibers from polyacrylonitrile (PAN) led to the research focus on rayon-based carbon fibers, while researchers in Japan established the protocol to utilize PAN precursor to fabricate carbon fibers.[7] Dr. Akio Shindo at Japan's former Government Industrial Research Institute in Osaka (GIRIO) successfully developed the process to fabricate PAN-based carbon fibers with high strengths and moduli.[7] The modulus of PAN-based carbon fibers was three-fold higher compared to rayon-based carbon fibers. Moreover, Dr. Shindo's process generated carbon fibers with a high carbon yield of ~50-60%, while the rayon-based materials had much lower carbon yields of approximately 20%. PAN-based carbon fibers are the dominant carbon fiber materials made and used in all kinds of applications in today's world.[9]

The rayon or PAN-based carbon fibers were fabricated with either natural macromolecules or synthetic polymer precursors. The question was: could carbon fibers be made from non-macromolecular precurors? The answer is yes. Leonard Singer who worked in the Parma Technical Center back in the 1960s studied the mechanism of the carbonization process by thermal treatment of coal and petroleum-based organic materials.[7] He found that these treatments led to the formation of pitch, which was a tar-like mixture comprised of mainly aromatic organic compounds with an average molecular weight less than 1000 grams per mole. Natural pitch is typically isotropic, but it could be fabricated to be oriented into layered liquid crystalline forms, leading to anisotropic mesophase pitch.[7] Leonard Singer and his team later designed an instrument to enable the fiber alignment and thermal treatment, and they were able to obtain highly-oriented graphitizable fibers using the pitch precursors. The pitch fibers had ultrahigh elastic moduli and thermal conductivities, but lower tensile strengths.[10]

Other synthetic polymers and naturally-occurring macromolecules were also investigated, including non-heterocyclic aromatic polymers such as polyacenaphthalene, phenolic polymers, polyamides.[3, 11-12] Although some of these featured high carbon yields and could be converted to

graphitic structures, no unique or superior properties were identified.[3] Heterocyclic organic polymers including polybenzimidazole, polytriadiazoles, and polyimides were also exploited.[13-16] Although high modulus carbon fibers were obtained with unique properties and high carbon yields, their cost was prohibitive for large-scale production.[3] Linear thermoplastic polymers such as poly(vinyl alcohol), polypropylene, poly(vinyl chloride), and polyethylene could also be fabricated into carbon fibers, but they had either poor mechanical properties or low carbon yields.[3, 17-18] It is worth noting that, lignin-based carbon fibers have attracted tremendous interest in recent years by the US Department of Energy, and researchers at Oak Ridge National Laboratory have investigated lignin precursors to fabricate carbon fibers, with the objective of significantly reducing overall carbon fiber production costs for potential automobile applications.[19]

Carbon fibers are widely used today as reinforcements with polymer matrices to form composite materials.[20-22] They have broad applications in many fields ranging from aerospace and military tactic gears, to more civilian usage such as automobiles, building materials, sports goods, etc.[23] PAN-based carbon fibers are manufactured and used predominantly, while pitch fibers are also produced and utilized in more limited amounts. Industrial production of rayon-based carbon fibers in the US has been halted to comply with the Environmental Protection Agency, though lab-scale research is still underway to address the waste side-products and other issues.[24] Lignin-based carbon fibers remain under investigation and may significantly reduce carbon fiber production cost if such carbon fibers can be fabricated with good mechanical properties, and if suitable, cheap lignin starting materials are readily available.[25]

2.1.2 Polyacrylonitrile-based carbon fibers

Polyacrylonitrile-based carbon fibers use polyacrylonitrile copolymers as the precursors to fabricate carbon fibers. They are currently the gold standard for aerospace-grade carbon fiber

materials where excellent mechanical properties such as high tensile strength and elastic modulus are required.[26] PAN is generally synthesized from acrylonitrile via conventional free radical solution and suspension polymerization, or more recently by living atom transfer radical polymerization (ATRP) polymerization.[27-28] The acrylonitrile monomer is typically synthesized from propylene with ammonia and air (oxidizer) via a catalytic ammoxidation, which is widely known as the Standard Oil of Ohio (SOHIO) process.[29] However, pure PAN is not suitable for making carbon fibers because it has poor processability, due to its insolubility in many organic solvents and high melting point. This is, in part, because of its highly polar nitrile pendant groups leading to strong dipole-dipole interactions. In order to enable spinning of PAN precursors to fabricate carbon fibers, co-monomers ($\leq$ 5 mol%) such as methyl acrylate and/or itaconic acid, are used as internal plasticizers to lower the melting point and improve solubility and processability.[28] These comonomers are also facilitate cyclization of PAN in the stabilization process during later thermal treatment by enhancing the segmental mobility of the polymer chains and aiding orientation.[30] The crystallinity, crosslinking, branching, molecular weight, and molecular weight distribution of the copolymers all play an important role in determining the properties of the potentially fabricated carbon fibers. The PAN-based copolymer precursors for carbon fibers normally have a molecular weight range of 70,000-260,000 g mol^{-1} and a polydispersity index between 1.5 and 3.0.[31]

Solution (wet) spinning is the preferred method to fabricate PAN fiber precursors, as melt spinning has been found to be difficult without addition of significant amounts of solvents and other plasticizers.[28] In the wet spinning process, as shown in Figure 2.2, the PAN copolymers (~15-30 wt%) are dissolved in a suitable solvent such as DMAc and DMSO, and loaded into a storage tank.[32] The solution is then pumped through a die head to be filtered, and extruded through a spinnerette containing a multitude of capillary holes into a coagulation bath so that solvents are extracted and

fibrous copolymer precursors are formed.[32] The coagulation bath may contain various solutions such as water, ethylene glycol, DMF or their mixtures. The coagulation bath temperature and concentration, the copolymer concentration, and the extrusion and draw-down rates all play an important role in determining the morphology and properties of the fibrous PAN precursors, and will also have an influence on the fabricated carbon fibers.[33-34] After coagulation, The precipitated precursors are washed and further stretched in steam or water to remove remaining solvent and to increase the orientation of the polymer chains.[30] Dry-jet-wet (air gap) spinning has also been developed, in which the extruded solution is jet stretched in an air gap before entering the liquid coagulation bath.[28]

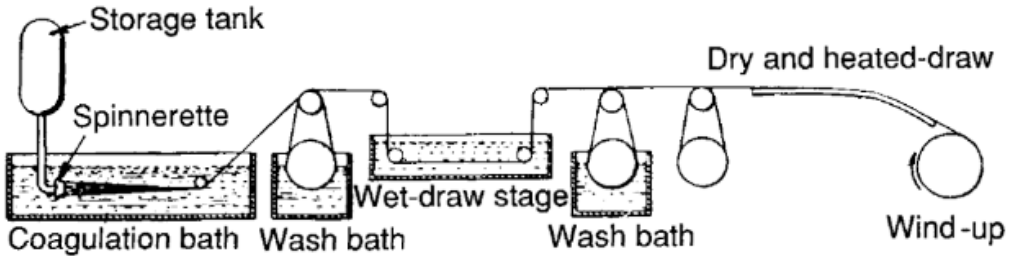

Figure 2.2 Equipment for wet-spinning PAN copolymers to form PAN-based fibers.[32, 35]

The fabrication of PAN-based carbon fibers from solution spun PAN precursors is an energy-intensive, multi-step process that primarily consists of stabilization, carbonization, and optional graphitization.[28] All of these steps involve thermal treatment with varying temperatures and heating rates and are either conducted in air, nitrogen, or argon. They are optimized as needed to fabricate carbon fibers with the desired mechanical properties. Surface treatments are subsequently performed to increase their adhesion to potential substrates or polymer matrices.[36-37]

During the oxidative stabilization step, the spun PAN fibers are first stretched and then heated to a temperature range of 200-300 °C in an oxygen-containing environment. This induces cyclization of the nitrile groups and crosslinking between the carbon atom and the nitrogen atom in adjacent

pendant nitrile groups.[26, 38] During the process, dehydrogenation, aromatization, and oxidation also occurs, thus forming a N-containing, conjugated ladder structure, which can withstand high temperature without melting or degradation during later pyrolysis processes.[39] The oxidative stabilization usually requires a couple of hours with a heating rate of 1-2 °C min^{-1}. Optimized conditions including heating rate, temperature, and duration are important to obtain carbon fibers with excellent mechanical properties.[9]

In the carbonization step, the stabilized PAN fibers are heated under nitrogen from as low as 300 °C to as high as 1800 °C.[28] Non-carbon atoms are evolved in the form of gases such as ammonia, carbon monoxide/dioxide, and hydrogen cyanide, and turbostatic structured carbon fibers are formed.[30] The gases are mostly removed below 1000 °C and the approximate temperatures where gases are released are listed in Figure 2.3. The heating rate, retention time, and final treatment temperature in this stage are also important in determining the mechanical properties of the final carbon fibers, and need to be optimized based on the precursor and stabilization conditions.[40] It has been found that defects are introduced in the final carbon fibers if the carbonization rate is too high, while too low a carbonization rate can lead to fast loss of nitrogen that can damage the fibers.[10] The carbonization can be divided into two steps: a low heating rate, low temperature (below 700 °C) pre-carbonization, followed by a high temperature (~1700 °C) step.[26] The pre-carbonization step has three stages and is typically conducted with a low heating rate, such as 5 °C min^{-1} to lower the mass transfer.[9, 40] The three stages involve primarily crosslinking and aromatization, active pyrolysis, and carbon basal plane elementary formation.[41-43] During the second carbonization step, high heating rate and low retention time (such as 10 minutes) may be used.[26] After this step, the turbostatic carbon fibers are well oriented in the fiber direction, but carbon atoms with tetrahedron-type crosslinking still exist, which endows the carbon fibers with high tensile strengths.[30]

Temperature (°C)	Observation	Interpretation
220	HCN evolved and O_2 chemically bonded	Ladder polymer formation and oxidation of polymer
260	Little changed. No modulus increased	No chain scission
300	Large CO_2 and H_2O evolution; also CO, HCN, and some nitriles. No modulus increased	CO_2 from –COOH groups in oxidized polymer No cross-linking
400	CO_2, H_2O, CO, HCN, and NH_3 evolved. Small evolution of C3 hydrocarbons and nitriles Modulus increased	Cross-linking by intramolecular H_2O elimination
500	Increased H_2 evolution. Some NH_3 and HCN evolved. Modulus increased	Cross-linking by dehydrogenation
600	Reduced H_2 evolution. HCN and trace N_2	Cross-linking by dehydrogenation
700	N_2, HCN, and H_2 evolution. Modulus increased	Cross-linking by dehydrogenation and evolution of N_2
800	Large increase in N_2, H_2, and HCN still evolved. Modulus increased	Cross-linking by evolution of N_2
900	Maximum evolution of N_2, some H_2, and traces of HCN. Modulus increased	Cross-linking by N_2 elimination
1,000	N_2 evolution decreases to approximately the same level as that at 800 °C. Trace H_2 evolved. Modulus increased	Cross-linking by N_2 elimination

Figure 2.3 Gases released during carbonization of PAN-based precursors.[23]

Graphitization is not necessary to make high tensile strength carbon fibers, but to obtain carbon fibers with high moduli, it is required.[28] During this step, the carbonized fibers are stretched to 50-100% elongation and heated under the protection of argon gas up to 3000 °C. Defects in the fibers as well as other non-carbon atoms are mostly removed, forming a graphitic structure containing over 99 % of carbon atoms.[26] Such carbon fibers are generally referred to as graphite fibers. It has been found that the peak tensile strengths for PAN-based carbon fibers are achieved after a thermal treatment temperature of ~1700 °C, while the modulus of such fibers keeps increasing with the thermal treatment temperature.[3] Therefore, there is a tradeoff between tensile strength and modulus. Argon is used instead of nitrogen in this step because nitrogen reacts with carbon and forms cyanogen when the temperature is above 2,000 °C.[44] The use of argon has additional advantages for improving

the mechanical strength of the fabricated carbon fibers, because of the higher density and viscosity of argon over nitrogen.[45] Carbon fiber structures with different thermal treatment temperatures during graphitization is shown in Figure 2.4. After graphitization, the turbostatic crystalline structures are fully oriented in the direction of the fiber axis, which is the cause of the increased modulus and decreased tensile strength of the graphite fibers.[28]

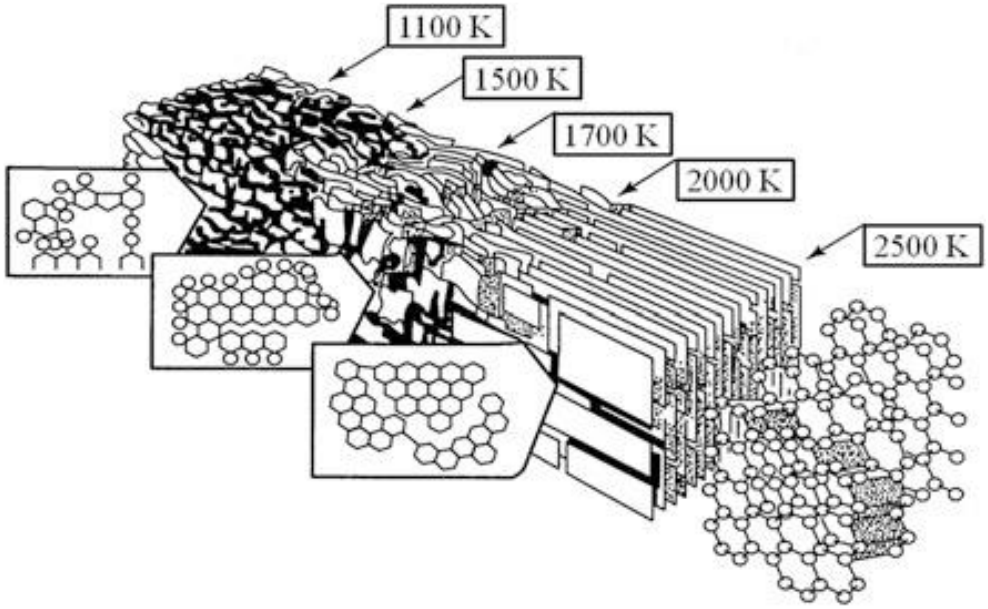

Figure 2.4 Carbon fiber structures with different thermal treatment temperatures during graphitization.[23]

The surface treatment is almost exclusively applied after the formation of carbon or graphite fibers to increase their affinity to the potential matrix. Without such treatments, the fabricated composites have lower interlaminar sheer strengths and suffer from weak bonding and poor adhesion.[3] One goal is to increase the wettability of the carbon fiber. The treatments can be categorized as oxidative and non-oxidative, liquid phase or gas phase, as well as chemical or electrochemical.[3, 46] The non-oxidative approach typically involves depositing "carbon whiskers" or grafting polymers onto the carbon fiber surfaces, but this is relatively uncommon and not typically used industrially.[3]

Ozone treatment at room temperature has been found to generate oxygen-containing species such as hydroxyl groups and carbonyl groups on the surfaces of the carbon fibers.[47] Nitric acid-based oxidative treatment has also been found to introduce acidic functional groups onto the fibers.[48-49] Zhang et al. have prepared carbon fiber-polyarylacetylene composites by first treating the carbon fibers with oxygen plasma, $LiAlH_4$, and then vinyl silsesquioxane coupling agents.[50] XPS results indicated that vinyl groups were successfully introduced onto the fiber surfaces, so that they could be coupled with the polyarylacetylene, leading to increased interfacial shear strength. Metals including nickel coatings on carbon fibers were found to create composites with good interfacial and mechanical properties, due to high metal surface free energy-induced increased wettability.[23] Generally speaking, liquid oxidation treatment, in particular, the anodic oxidation treatment, is widely used commercially, because it is inexpensive, fast, and convenient, and may significantly increase the shear strengths of the composites.[46, 51] It involves an electrolysis reaction using the carbon fibers as the anode and an acid (such as nitric acid) or a salt (such as ammonium sulfate) as the electrolyte. Ammonium sulfate is often widely used because it is less expensive and non-corrosive compared to acids. During the process, carbonyl groups such as carboxylic acids are introduced onto the surfaces of the carbon fibers to improve the cohesion of the potential fiber-matrix composites.[46] Excess electrolytes are then washed off and the surface-functionalized carbon fibers are then sized.

The process to fabricate PAN-based carbon fibers and graphite fibers are well-established and widely used, and over 90% of carbon fibers are made from PAN-based precursors because of their excellent mechanical properties and reproducibility. However, the drawback is conspicuous as well. First of all, the solution spun PAN precursors have much higher cost compared to natural polymers such as cellulose and lignin. The cost to synthesize the PAN-precursors is over 50% of the overall cost to make PAN-based carbon fibers, as is indicated in Figure 2.5. The polymers may contain toxic

and carcinogenic acrylonitrile monomers and careful purification is required.[52] More importantly, all the thermal treatment steps need either stretching or have a slow heating rate and consume a lot of energy. Therefore, the carbon fiber are mostly used in high-end applications such as aerospace, military gears, and high-end automobiles.

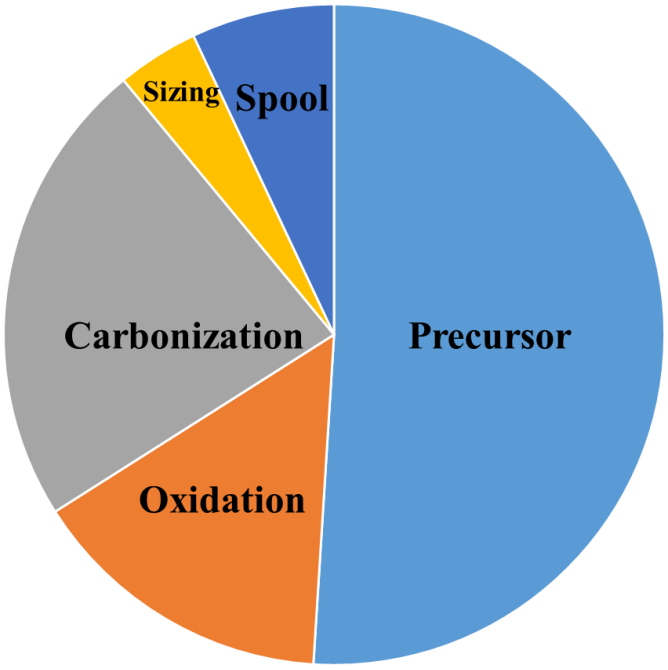

Figure 2.5 Cost distribution to fabricate PAN carbon fibers.[25, 53]

2.1.3 Pitch-based carbon fibers

Pitch is a complex, black or dark mixture of primarily polyaromatic and heterocyclic compounds containing over 80% of carbon, with an average molecular weight of several hundred, and it is formed by a combination of thermal decomposition, hydrogen transfer, and oligomerization reactions.[54] It has been utilized to fabricate commercial carbon fibers by Union Carbide Corporation since the 1970s.[55] There are a multitude of potential sources of pitch. Among them, petroleum asphalt and coal tar are the primary sources to fabricate carbon fibers industrially, and they can be obtained by either

destructive distillation of coal, or by the refining of petroleum.[46] The sources and the processing conditions play a vital role in determining the chemical composition of the pitch.[56] For example, typical components found in coal tar pitch are shown in Figure 2.6, and include aromatic compounds such as fluorene and benzo-(α)-pyrene.[46] Pyrolysis of poly(vinyl chloride) may also afford pitch fibers, but at a higher cost. The naturally-occurring pitch is usually isotropic, and it can be stretched and oriented into layered liquid crystalline states so that anisotropic, mesophase pitch forms with enhanced mechanical properties.[7] It is preferred to melt-spin pitch into fibrous precursors, and to subsequently treat it thermally in a manner similar to PAN-fiber treatment. Oxidative stabilization, carbonization, and optionally graphitization, can be applied to convert the precursors into carbon fibers or graphite fibers.[28, 46] Isotropic pitch can be fabricated into a general purpose, low strength and low modulus carbon fiber at a low cost. To form a pitch-based carbon fiber with good mechanical properties, either mesophase pitch precursors as starting materials are used, or an expensive hot stretching treatment is applied to the isotropic pitch precursors during the thermal treatment procedures.[46] Mesophase pitch precursors can be made either by thermal polymerization of petroleum and coal-tar pitches, or by the catalytic polymerization of pure compounds such as naphthalene.[46] The steps to fabricate pitch-based carbon fibers and graphite fibers (general purpose graphite and high performance graphite) from their starting materials are shown in Figure 2.7.

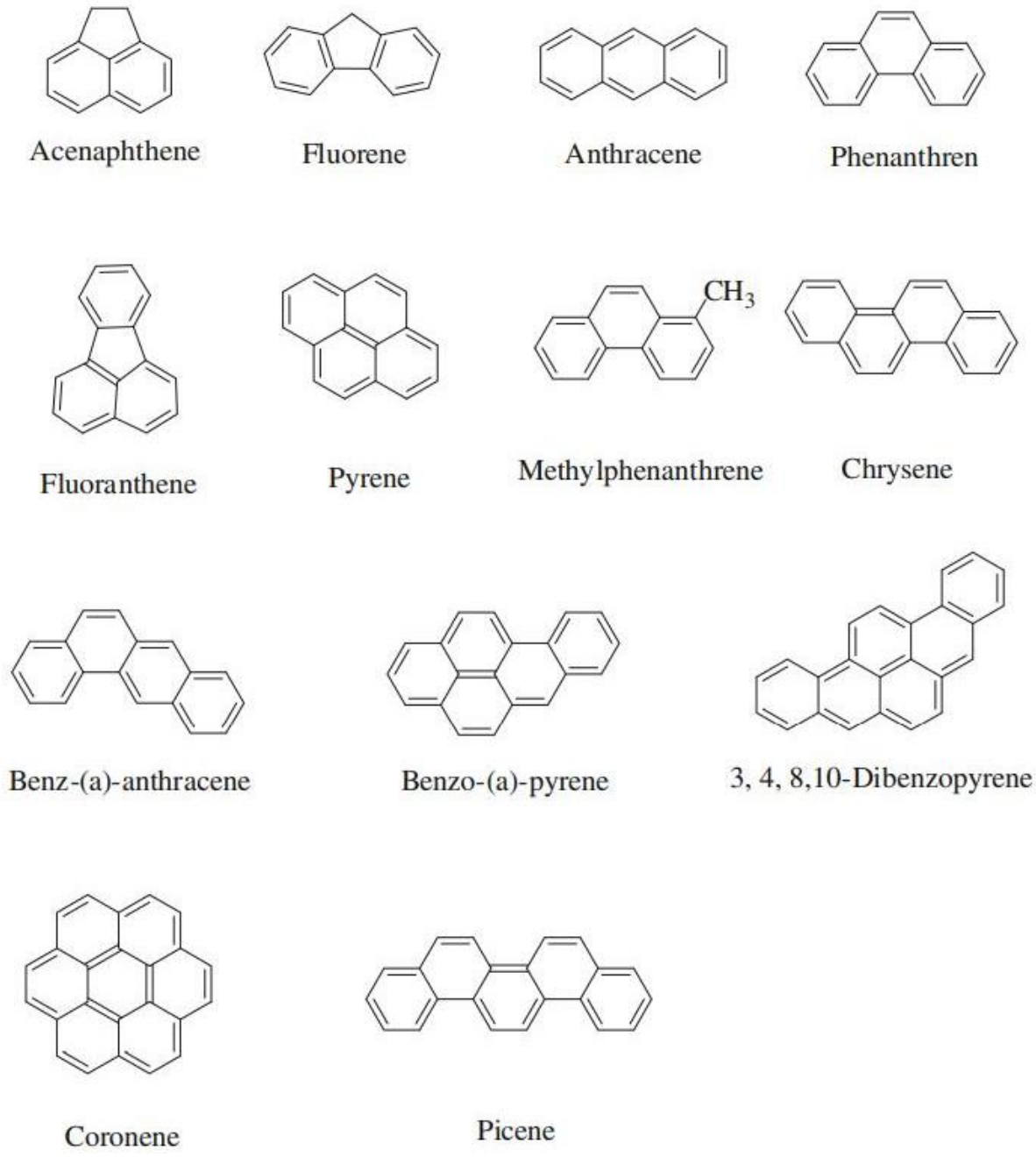

Figure 2.6 Common aromatic compounds found in coal tar pitch.[46]

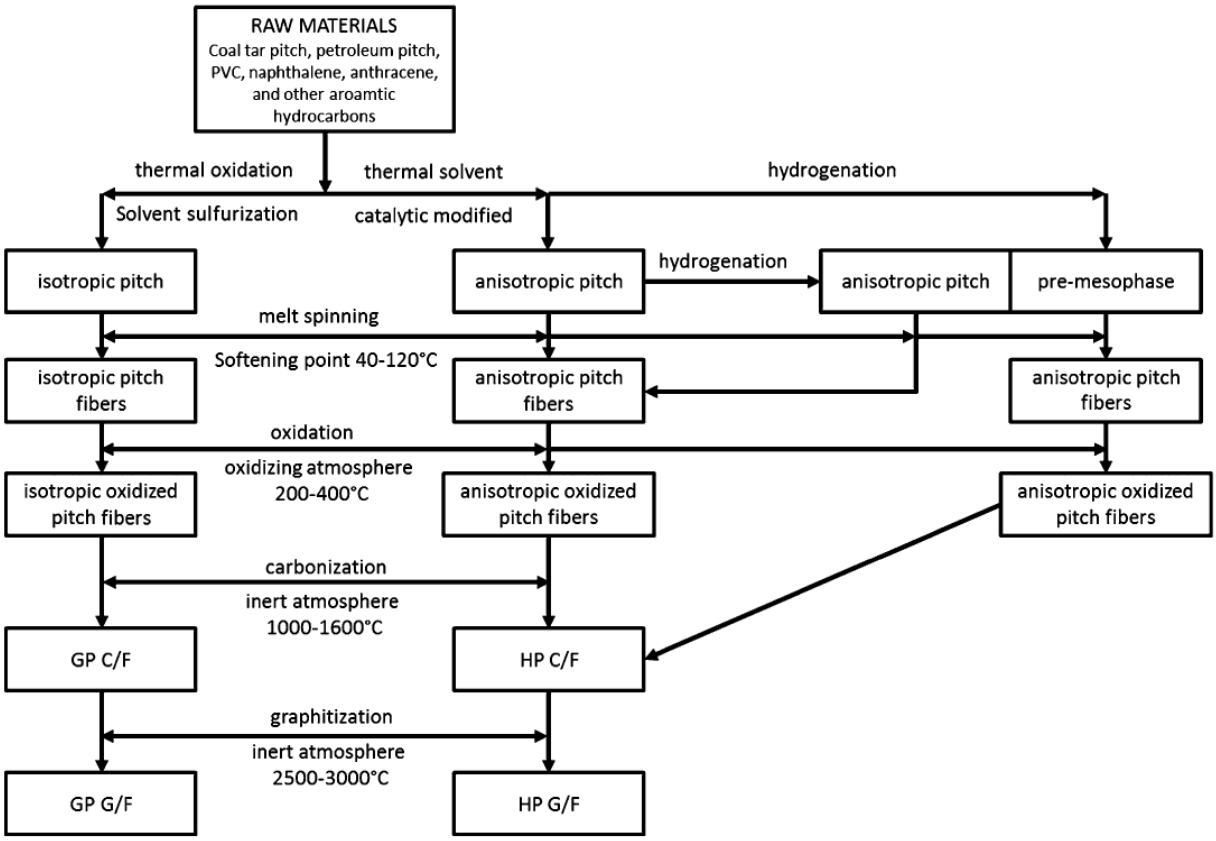

Figure 2.7 Processes for the fabrication of carbon fibers using pitch precursors.[28] GP is general purpose pitch and HP is high performance pitch.

Compared to PAN precursors, pitch precursors are much lower cost, and have higher char yields and better crystal orientation.[57] The corresponding mesophase graphitic pitch-based carbon fibers also have higher elastic moduli and superior thermal and electric conductivities along the fiber direction, but its tensile strength is lower than PAN-based carbon fibers and they are brittle.[46] Pitch carbon fibers are primarily used in applications ranging from aircraft brakes to space satellite structures, where heat management is critical.[7] In 2015 and 2016, Advanced Carbon Products LLC (Hitchins, KY) has reported and patented a continuous short residence-time manufacturing process for the production of isotropic and anisotropic mesophase pitch precursors from petroleum pitch, reportedly with a

potential low cost of less than \$1.50 lb^{-1}.[58-60] However, the processing of pitch-based precursors to afford mesophase pitch carbon fibers at a significantly lower cost still remains a great challenge.

2.1.4 Lignin-based carbon fibers

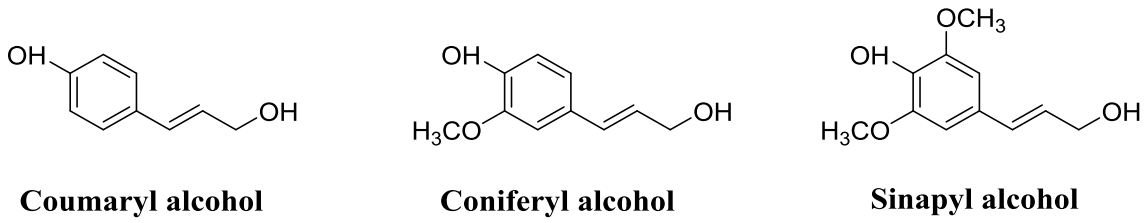

Figure 2.8 Monomers which make up lignin.[53]

Lignin is comprised of high molecular weight (racemic) aromatic heteropolymers deriving from three monomeric units (as shown in Figure 2.8), and is commonly present in all plants, constituting ~20-30% of the dry weight of wood and woody biomass.[61] It has the second highest natural abundance (~30% of the organic carbon in the biosphere) just after cellulose, and more than 50 million tons per year are produced worldwide as waste in biofuel and paper manufacturing processes.[25, 62-63] A typical lignin chemical structure is shown in Figure 2.9. Lignin is renewable with high carbon content (≥ 60 %) and is also independent of the oil price. With increasing petroleum prices, the prices of PAN and pitch-based carbon fibers will also increase, while lignin-based carbon fibers may not be affected. It has been estimated that using lignin as a precursor to fabricate carbon fibers could reduce the overall carbon fiber cost by more than 80%.[53] Therefore, it has aroused tremendous research interest in the US, Sweden, Germany, Canada, Japan, etc. Nippon Kayaku Company in Japan was the first to investigate and manufacture lignin-based carbon fibers dating back to the 1960s and 1970s, using high molecular weight additives such as poly(vinyl alcohol) or PAN during the manufacturing process.[28] Fukuoka and Mikawa from the Nippon Kayaku Company reviewed the process to fabricate lignin-based carbon fibers, and the fibers were commercialized on a pilot scale under the name of

Kayacarbon in the 1970s.[64-65] The process utilized alkaline lignosulfonate solutions and added poly(vinyl alcohol) as an additive, and the materials were dry-spun and carbonized with high heating rates.[28] The merits of this method were low cost, high carbon yield, wide lignin sources to choose from, and no thermo-stabilization was needed. However, it was found that such graphitized Kayacarbon fibers contained pores and heterogeneous structures, as measured by X-ray diffraction and scanning electron microscopy.[66] Since 1972, Mansmann has filed several patents in the US, Germany and Great Britain for the manufacture of lignin carbon fibers using lignin sulfonates as precursors and poly(ethylene oxide) (MW of ~5k, and ≤ 5 wt%) as a polymeric additive to improve spinnability.[28, 67] The research and commercial production of lignin-based carbon fibers mainly ceased in the 1970s, possibly due to breakthroughs in the development of PAN and pitch-based carbon fibers.

In the early 1990s, research interest in fabrication of lignin-based fibers attracted great interest again. Investigations focused on melt-spinning of the lignin precursors, compared to the previously dominant "wet-and-dry" approach. Thermal stabilization was required for such methods, which involved applying very slow heating rates in air to the lignin precursors while keeping the temperature below the glass transition temperature of the lignin materials to avoid fusion.[28] There are generally five major steps to fabricate lignin-based carbon fibers from lignin precursors by the melt-spinning method (Figure 2.10).[53] First, when lignin is separated from plants either by physical or chemical methods, it is precipitated to afford lignin powder. The powders are washed with water and dried. Next, the lignin powders are extruded and pelletized. The pellets of lignin are then melt-spun, heat-treated in an oxidation step, then carbonized to convert the lignin into carbon fibers. The oxidation step is conducted in an oven with air at 200-300 °C, and it typically requires 1.5-2 hours. The oxygen diffuses into the lignin materials, leading to increased crosslinking, and the brown starting material

becomes black with an increased melting point.[53] The carbonization step takes place in a furnace under a nitrogen stream. The oxidized lignin fibers are treated at temperatures up to 1500 °C for approximately 10 minutes, thus affording lignin-based carbon fibers. A graphitization step may be performed to obtain structural carbon fibers (graphite fibers) with better mechanical properties. The simplified manufacturing process of lignin-based carbon fibers is shown in Figure 2.11.

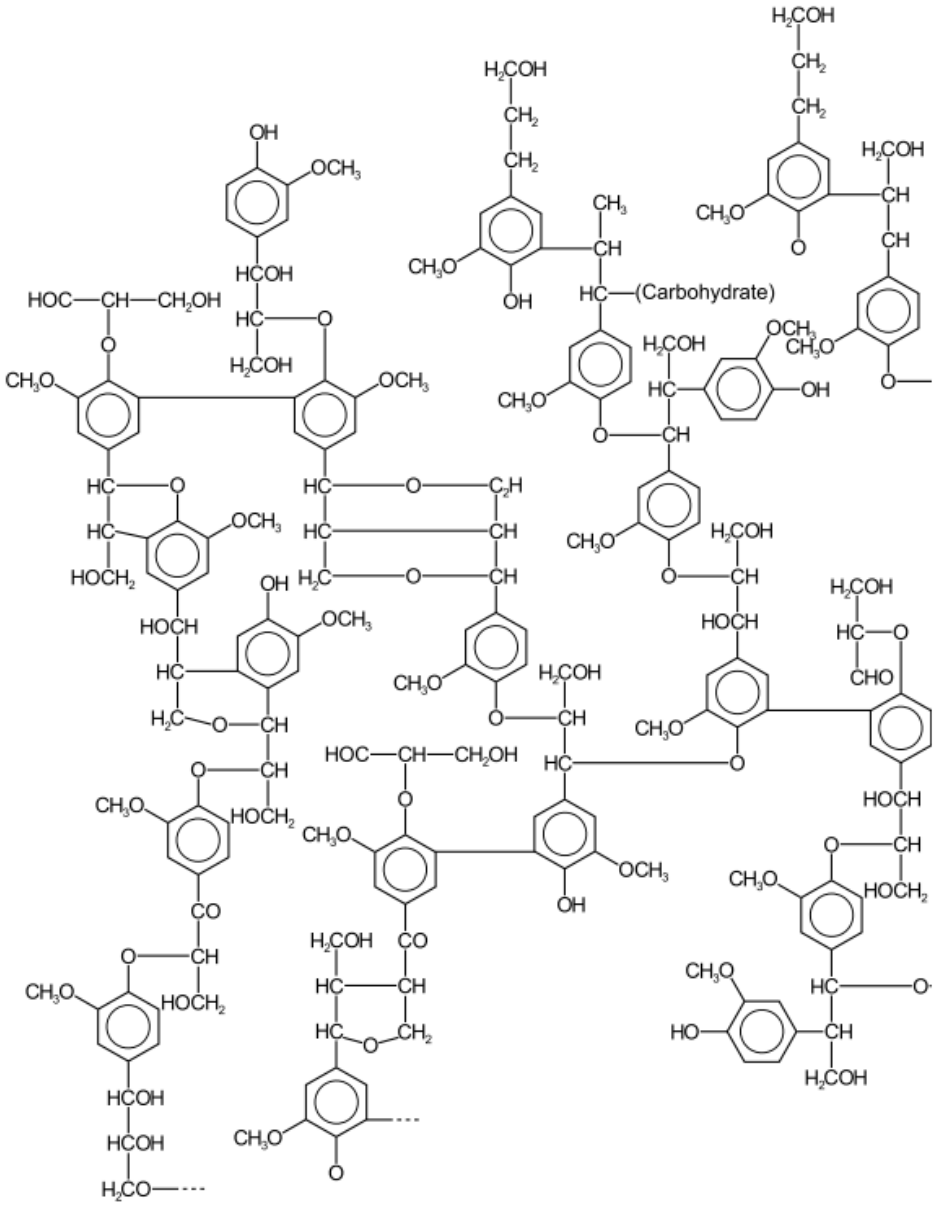

Figure 2.9 An example of lignin chemical structure.[68]

Figure 2.10 Different stages of lignin appearance from lignin precursors to form lignin-based carbon fibers.[53]

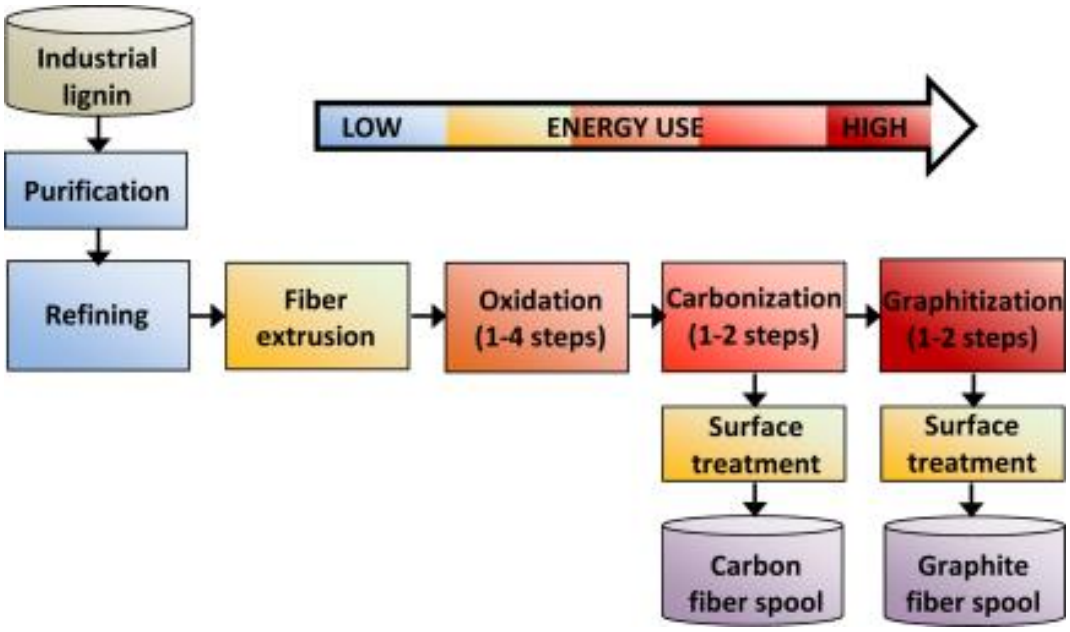

Figure 2.11 Simplified carbon fiber production from a technical grade lignin.[66]

One major disadvantage of melt-spinning to make lignin carbon fibers is that during oxidative stabilization of the lignin fiber precursors, extremely low heating rates (as low as 0.2 to 1 °C min^{-1}) are required.[69] However, the relative simplicity without use of a solvent, and fast speed to manufacture the fiber tows make it a preferred method over the wet and dry approach. The wet and dry method uses an organic solution of precursor fiber that is extruded under heat and pressure through an air gap before entering a coagulation bath Sudo and Shimizu used steam-exploded lignin from birch wood chips and then hydrogenated the lignin with Raney-Ni under basic conditions (250 °C for 60 minutes) to create melt-spinnable lignin precursors.[70] However, the hydrogenated lignin could not be used directly for melt-spinning process due to a low viscosity and low glass transition temperature. The problem was solved with an extra thermal treatment step by exposing the modified lignin at 300-350 °C for 30 minutes under vacuum or nitrogen.[28] Still, the carbon yield was very low at ~ 16%. They later reported a modified method which generated phenolated lignin precursors.[71] A steam-process was also used, followed by reacting the lignin with phenol or creosote at 180 to 300 °C for 2-5 hours using 2% *para*-toluenesulfonic acid as a catalyst. This created phenolated lignin precursors which could make lignin carbon fibers with similar mechanical properties, but with a significantly increased carbon yield of ~ 44%. However, an additional thermal treatment under vacuum at a relatively lower treatment temperature (220-280 °C) was needed. Uraki reported using organosolv lignin to melt spin lignin carbon fibers.[72] The organosolv lignin was obtained from pulping birch wood with aqueous acetic acid and 0.32% sulfuric acid. Partial acetylation occurred during the process, and no additional chemical treatment was required before melt-spinning, thermo-stabilization, and carbonization to fabricate the lignin-based carbon fibers. The preparation of the lignin precursor was simplified in this approach, but the heating rate during thermo-stabilization was low at 0.5 C min^{-1} in pure oxygen. The carbon yield was only ~33%. Kadla investigated the fabrication of lignin carbon

fibers using three commercial lignin sources: Organosolv lignin (Alcell^{TM}, Repap), softwood kraft lignin (Indulin AT^{TM}, Westvaco, now Ingevity Corporation) and hardwood kraft lignin (Westvaco).[73] The kraft lignins were washed extensively with de-ionized water and dilute hydrochloric acid to remove salt and ash before thermal treatment. The Alcell lignin carbon fiber was made at a rate of 0.2 °C min^{-1} to 250 °C during thermo-stabilization and 3 °C min^{-1} to 1000 °C during carbonization with a carbon yield of ~42%.[66] The hardwood kraft lignin was melt-spun at a temperature (~200 °C) and a much faster rate of 2 °C min^{-1} for thermo-stabilization, with a 48% carbon yield. The softwood kraft lignin could not be melt spun. Fabrication of lignin-based carbon fibers from other lignin sources, *i.e.*, Alamo switchgrass (panicum virgatum), was also reported.[74] The lignin was isolated using a proprietary organosolv process, and it was melt-spun, thermo-stabilized at a rate of 0.02 °C min^{-1} up to 250 °C, and carbonized to afford lignin carbon fiber. A novel "lignoboost process" which is a method for lignin removal from alkaline pulping liquors, and membrane ultrafiltration were also used to isolate and purify lignin precursors, and lignin carbon fibers were fabricated.[75-76] Doping or mixing other polymers with lignin to fabricate lignin carbon fibers has also been investigated. In one recent study, researchers in Zoltek Corp. (now Toray Carbon Fibers) studied blends of PAN with lignin precursors to fabricate carbon fibers.[77] Although the fiber properties improved when more PAN was incorporated, there seemed to be immiscibility issues between the PAN and lignin, leading to the formation of porous materials.

Fabrication of lignin-based carbon fibers has attracted a great deal of interest in the US since 2001, and the U.S. Department of Energy was particularly interested as they launched their automotive lightweight materials research program, with the aim of fabricating low-cost carbon fiber composites as substitutes for steel/metal alloys in cars.[78] Their objective was to significantly reduce the vehicle weight without sacrificing durability, thus leading to significantly reduced fuel

consumption and greenhouse gas emissions. PAN and pitch-based carbon fibers were deemed to be too costly for wide applications in non-high-end cars. Thus, the program was justified by the need to fabricate mid-range-performance carbon fiber composites at a low cost and high volume.[79] Using lignin precursors was proposed as one promising solution. Oak Ridge National Laboratory is leading the research and development of lignin-based carbon fibers. First of all, they developed novel advanced procedures for atmospheric pressure plasma oxidation and microwave assisted plasma carbonization for the manufacturing of carbon fibers. Using these techniques significantly reduced the residence time by one-third, and the energy consumption in the oxidation and carbonization process was also reduced by half, leading to much lower overall cost to fabricate carbon fibers.[80] Secondly, they demonstrated the capability to fabricate lignin-based carbon fibers from both kraft and Organosolv-pulped hardwood lignin precursors with high melt spinning speeds, which is almost 3-fold faster than the same process for commercial mesophase pitch fibers and 4-fold faster than the commercial wet spinning speed of PAN-based fibers.[81] Most importantly, they developed a novel method for continuous melt spinning of multifilament tow from a kraft pulped softwood lignin without purification, using a purified hardwood lignin as a plasticizing agent.[82] Previous studies on softwood lignin rendered it unsuitable for melt spinning due to lack of fusibility due to a high glass transition temperature. Softwood lignin contains over 90% of coniferyl alcohol and some *para*-coumaryl alcohol monomeric units, while hardwood lignin contains coniferyl alcohol and synapyl alcohol monomeric units with varying ratios.[83-84] The structural difference endows hardwood lignin with excellent spinnability and thermal mobility, while softwood lignins have faster thermo-stabilization times.[85-88] The novel process enabled the fabrication of softwood lignin using continuous melt spinning, which overcomes the disadvantages of spinnability and thermal stability of softwood lignin, while maintaining its advantages. It significantly lowered the overall cost to fabricate carbon

fibers, which may be a significant advance. With the trilateral efforts of ORNL and the Department of Energy offices, GrafTech International has fabricated GRAFSHIELD™ and FiberForm® based on lignin-based carbon fibers for high-temperature insulation. This may be the first commercial use of lignin carbon fiber.[19, 89] The commercialization of lignin-based carbon fibers could be a milestone and may attract more research interest in this renewable and abundant lignin material.

Although some breakthroughs in fabrication and optimization of lignin-based carbon fibers have been made, its large-scale manufacture and utilization are not yet available compared to the predominant usage of PAN-based and pitch-based carbon fibers. Issues and challenges lie in the following fields. 1) Lignin sources for fabrication of fibers: Despite the extremely high abundance, the compositions from different sources, such as hardwood *vs* softwood, are significant. To obtain starting lignin precursors with similar, if not identical, compositions between different batches are crucial in making lignin carbon fibers with consistent, reproducible properties. Therefore, a stable supply chain would be required. 2) The purity and processability of lignin precursors: Results have indicated that unpurified lignin-based carbon fibers can be made. However, such fibers have poor mechanical properties. Therefore, it is important to effectively extract, purify, and convert lignin at a low cost, either by physical or chemical means, so that the overall cost to fabricate these carbon fibers could remain low. 3) Oxidation and carbonization time, and production volume: For example, the thermo-stabilization process needs to be optimized. In some studies, the heating rate was as low as 0.02 °C min^{-1} up to 250 °C. To enable fabrication of low-cost carbon fibers, high volume production with rapid oxidation and carbonization in a continuous process would be necessary.

2.2 High-performance polymers

2.2.1 Introduction to high-performance polymers

High-performance polymers, which are also known as high-performance plastics, refer to synthetic macromolecules with high-temperature stability and superior mechanical properties and chemical resistance.[90] They are usually more expensive than commodity plastics, and they normally have a lower production volume, but they are used in a wide array of applications where their superior properties are required.[91] It is estimated that high-performance polymers are approximately 3 to 20 times as expensive as engineering plastics, while their market share is only about 1%.[92] Among them, fluoropolymers such as polytetrafluoroethylene have the highest market share at ~45%, while sulfur-bearing aromatic polymers and polyaromatic ethers and ketones have 20% and 10%, respectively.[93] Most high-performance polymers are step-growth polymers that are synthesized by polycondensation reactions. They can be semi-crystalline or amorphous. For example, polyetherimide and polyethersulfone are amorphous, while polyetheretherketone and poly(phenylene sulfide) are semi-crystalline. The structures of several high-performance polymers are shown in Figure 2.12.

Although there is no widely accepted definition or boundary between commodity plastics and high-performance polymers, high-performance polymers are considered to at least possess a short-term heat resistance temperature of up to 250 °C, and should have continuous service temperatures of ~160 °C.[90] They may also have high strength, stiffness, chemical resistance, and excellent electrical properties, and these superior properties are mostly attributed to the increased aromaticity and conjugation in the monomeric repeating unit. Polytetrafluoroethylene is an exception that has excellent properties but is not aromatic. It has excellent heat and chemical resistance and is used as coating materials for magnetic stir bars and cookware where high-temperature resistance and chemical inertness is required. Liquid crystalline polymers are another important class of high-

performance polymers with low thermal expansion coefficients, high-temperature stabilities, and low inflammability, and these are widely used to make composites for electrical and optical components.[94]

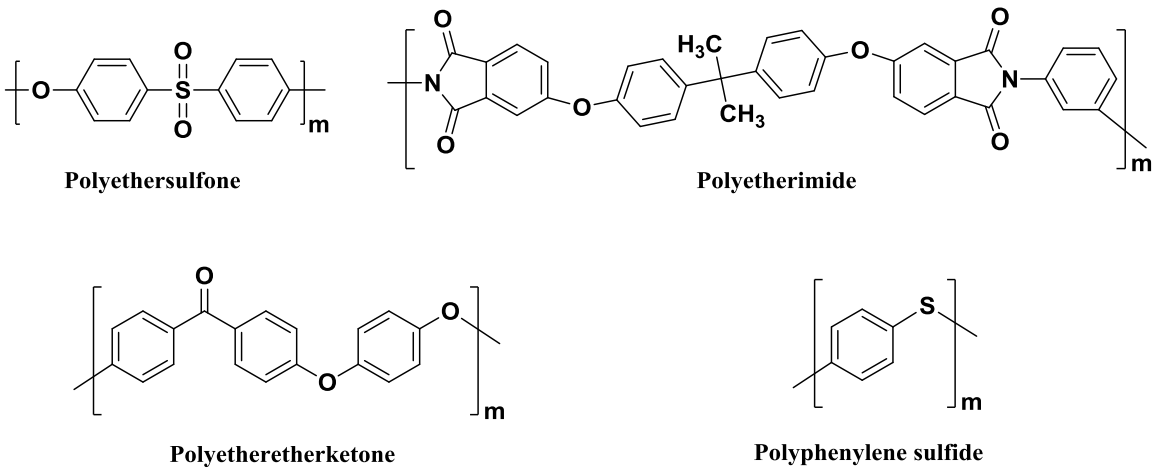

Figure 2.12 The structures of some common high-performance polymers.

2.2.2 Polyether ether ketone (PEEK)

PEEK, with the systematic name of poly(oxy-1,4-phenyleneoxy-1,4-phenylenecarbonyl-1,4-phenylene), is a semi-crystalline high-performance polymer with exceptional mechanical properties and chemical resistance, and it has a continuous service temperature of up to 260 °C (500 °F).[95] It has a glass transition temperature of ~143 °C and a melting temperature of 343 °C. In PEEK, the rigid phenyl rings are linked by stiff ketone linkages and flexible ether linkages. Since there are two ether linkages and one ketone linkage, it is commonly called "polyether ether ketone". PEEK was first produced in the laboratories of the Imperial Chemical Industries (ICI) in the UK in 1978 and commercialized in 1981.[96] It is synthesized by step-growth polymerization of hydroquinone and 4,4'-difluorobenzophenone as monomers in polar aprotic solvents such as diphenylsulphone, with potassium carbonate as a base and at a high temperature of 150-300 °C.[97]

Commercial neat PEEK in produced in various forms including powders, granules, fibers and films.[97] For example, Victrex produces PEEK fibers (Zyex) and films (Stabar), while Solvay produces KetaSpire® as pellets. Glass fiber and carbon fiber reinforced PEEK are also commercially available. Injection molding, compression molding, and extrusion processing are generally used to process PEEK. PEEK-based composites have been used in various applications in the fields of aerospace, automobile, and as medical implants. For instance, PEEK is widely used as lightweight interior and exterior materials, as well as assembly components in aircrafts, as substitutes for metal and metal alloys including aluminum, titanium, and other metallic components.[98] PEEK-based materials are up to 70% lighter than the metals while maintaining their excellent thermal and mechanical properties under harsh conditions including high temperature and pressure.[98] This enables a significant reduction of fuel consumption, operation cost, and greenhouse gas emissions. PEEK-based biomaterials are also widely used as orthopedic, spinal implants and in other biomedical fields because of their strong, inert, and biocompatible nature.[99] For example, implantable PEEK-OPTIMA™ polymers developed by Invibio Inc. are used in spinal reconstruction, arthroscopy, joint reconstruction, trauma, dental and cranio-maxillofacial procedures.[100] They have also developed the first human implantation of a cervical interbody fusion device using their PEEK-OPTIMA™ - hydroxyapatite composite materials.[101]

2.2.3 Polyetherimide (PEI)

Neat polyetherimide (PEI) is an amorphous high-performance polymer with a glass transition temperature of 217 °C. It possesses excellent mechanical, thermal, and electrical properties, as well as a high strength-to-weight ratio.[102] Compared to another high-performance polymers such as PEEK, the mechanical properties of PEI are slightly inferior, but it has high heat resistance, inherent flame retardancy, low smoke generation, and is also less expensive. Therefore, PEI has been widely used in

aerospace and automotive applications.[73-74, 103-107] Most polyimides are difficult to manufacture because they require high processing temperatures and are often imidized as films from solutions.[108] However, PEI has flexible ether linkages on the polyimide backbone, so it is melt-processable at a relatively low temperature without compromising the excellent properties of the imide characteristics.[109-110]

PEI was first commercially manufactured under the trade name of ULTEM® by General Electric (GE) Plastics in 1982 (now SABIC after the acquisition in 2007).[111-112] It is produced as powders or pellets as neat PEI or with reinforcement materials such as glass fibers. PEI is typically synthesized by a two-step process. The first step is a polycondensation which is conducted at room temperature or low temperature using dianhydride and aromatic diamine monomers in a polar aprotic solvent such as dimethylacetamide or *N*-methyl-2-pyrrolidone.[113] The formed poly(amic acid) intermediate is then heated in solution to form the corresponding polyetherimide by a cyclodehydration reaction.

PEI has good processability and is generally processed by injection/compression molding or extrusion. PEI films are fabricated by melt extrusion or solvent casting, while PEI fibers are prepared via melt spinning.[102] It is used in fields such as aerospace, automotive, electrical and electronics, membranes, and in the medical sector. For example, Khayet et al. reported fabrication of a fluorinated surface modifying polymer PEI blend.[114] The blend was solvent cast to form a membrane and found them to be promising for water desalination applications. Oh et al. reported fullerenol-based electroactive artificial muscles by casting ionic polyhydroxylated fullerene nanoparticles in a sulfonated PEI matrix.[115] The composite was biocompatible, and displayed desirable high water uptake and proton conductivity, as well as large motion ranges and high blocking forces, which made them a promising candidate for biomedical devices such as active stents and catheters.[115]

2.3 Thermally-stable suspending agents

A suspending agent is a chemical compound that helps to disperse and stabilize insoluble solids or liquids in water or other media. These suspending agents self-assemble on the surfaces of particles and decrease inter-particle attraction via steric or electrostatic repulsion forces.[116] In some cases, they may also act as thickening agents by increasing the viscosities of the dispersions. Common suspending agents include natural macromolecules such as methylcellulose polysaccharides, and synthetic polymers such as poly(vinyl alcohol).[117-119] Polysaccharide-based suspending agents are widely used in food and pharmaceutical applications because of their excellent biocompatibility. Poly(vinyl alcohol) is the most frequently used suspending agent in suspension polymerization of a multitude of vinyl-bearing monomers, such as vinyl chloride. However, neither polysaccharide nor poly(vinyl alcohol)-based suspending agents have good mechanical properties or thermal stabilities, and they also usually lack chemical resistance. Therefore, they cannot be used in applications where increased temperature or other harsh environmental conditions are present. A thermally-stable suspending agent would be required for these situations.

Poly(amic acid) is the intermediate compound to synthesize polyetherimide, and it is also an important thermally-stable suspending agent in its salt form.[120-122] The poly(amic acid) can be synthesized from a dianhydride such as 4,4'-(4,4'-isopropylidenediphenoxy)bis(phthalic anhydride) (also known as Ultem dianhydride) and a diamine such as *meta*-phenylenediamine by step-growth polymerization. Phthalic anhydride can be used as an end-capping agent to avoid active functional groups at the polymer chain ends. Designed end groups may also enable the use of NMR techniques to measure the molecular weight of the polymer to a certain limit. Size exclusion chromatography cannot be used directly to measure such polymers in DMAc because the polymers aggregate in the columns, but dipolar aprotic solvents with added phosphorus pentoxide have been shown to be

effective SEC solvents for these poly(amic acid) salts. Poly(amic acid) aqueous solutions are susceptible to hydrolytic degradation and are not stable for a long time in water. Therefore, amines such as dimethylethanolamine may be added to form more stable poly(amic acid) salts in either organic or aqueous solutions. To obtain poly(amic acid) salts with fixed anions and ammonium cations, a tertiary amine may be used to react with the poly(amic acid) in a stoichiometric amount. The poly(amic acid) salts have been shown to have increased solubility in methanol, ethanol, and water, which are less toxic and cheaper solvents than the ones needed for the analogous poly(amic acid)s.[123-124] Another advantage of making the corresponding salts rather than the acids is that the salt may also assist the formation and coating of nanoparticles in solution due to electrostatic repulsion, and this could increase the stability of the coated particles. The poly(amic acid) salts can be thermally cyclized to form the corresponding polyimides in solution or during a composite fabrication process. For example, The poly(amic acid) ammonium salt can be imidized through cyclodehydration by thermal treatment at ~300 °C.[125]

The synthesis of poly(amic acid)s has been investigated widely. Poly(amic acid)s are usually synthesized in polar organic solvents such as DMAc at room temperature in an inert atmosphere for a couple of hours.[126-128] Exposure to moisture in air may lead to hydrolysis of the poly(amic acid), thus in turn reducing the mechanical properties of the corresponding PEI or potential PEI-based composites after imidization.[129] Therefore, poly(amic acid) salts with medium to high molecular weight are needed to be imidized to PEI with desirable mechanical properties.[130]

2.4 Coupling agent treatments on carbon fibers

As has been discussed previously, surface treatment is usually a requirement for carbon fibers that are to be incorporated into polymer matrix composites. Plasma treatments and acid treatments are widely used to introduce functional groups onto the carbon fiber surfaces to increase their

wettability and potential adhesion with the polymer matrix.[131-134] Additionally, coupling agents may be used alone or in combination with the plasma or oxidative acid treatments to functionalize the carbon fibers. Silane coupling agents have been of great importance because of their excellent commercial availability and easy application. Some chemical reactions of silane coupling agents are shown in Figure 2.13. They are normally used with glass fibers because of their strong chemical binding with the glass, but they have also been utilized with carbon fibers.[135-136] The objective is to have the silane coupling agent act as a molecular bridge at the interface between the inorganic fiber and the organic polymer matrix, thus increasing the shear strength and adhesion of the fabricated composites.[137]

For example, Nie reported PAN-based carbon fibers with an epoxy sizing that were simultaneously plasma treated and reacted with a 3-methacryloxypropyltrimethoxysilane coupling agent. Their objective was to prepare carbon fiber reinforced-polyimide matrix composites with good mechanical properties.[138] The plasma was a quasi-neutral gas comprised of charged and neutral particles containing cations and electrons, and the charged particles should activate and react with the fiber surface, thus introducing functional groups. In particular, hydroxyl groups were introduced onto the surfaces of the carbon fibers.[131] The hydroxyl groups react with the silicon on the silane coupling agent to form C-O-Si bonds.[139-140] Unfortunately, the chemistry of the methacryloxy-functional fiber surface was not designed correctly to couple with the polyimide matrix. The tensile properties of the composites were degraded relative to the analogous untreated fibers. In another study, organofunctional (3-chloropropyl)trimethoxysilane was used to couple pitch-based carbon fibers which had no other surface or sizing treatments to furanyl resins.[137] It is reasonable that the hydroxyl groups on the resin would react with the silane coupling agent, but it is not understood what the mechanism for coupling to the pitch fibers would be. Following composite formation, they were heat

treated at 2600 °C to carbonize the materials. Significantly increased tensile strengths of the carbonized materials were observed with the coupling agent treatments. The use of a cyclic azasilane coupling agent may enable vapor deposition onto the fibers, which may lead to a streamlined manufacturing process, without using solvents and generating by-products at a very fast speed by a ring opening reaction. The use of trialkoxysilanes may enable potential crosslinking, thus leading to increased binding strength. Introducing appropriate functional groups onto the fibers may enable potential chemical binding between the fibers and the functional polymer matrix, which could be a huge advantage compared to physical interactions alone.

2.5 Carbon fiber reinforced composites

Carbon fiber reinforced plastics can be fabricated into important engineering composites with continuous carbon fibers as reinforcement materials and the polymers as matrices.[20] The fiber to matrix ratio is usually at least 60:40 by volume for advanced composite materials.[141] If high-performance polymers are used, the composites may demonstrate the advantages of both the polymers and the carbon fibers, with excellent mechanical and thermal properties, as well as very high strength-to-weight ratios.[142-143] The matrices can be either thermosets or thermoplastics. Such polymer matrices reinforced with carbon fibers have high shear strengths wherein the interface materials between the fibers and matrix can help to transfer load from the fiber to the matrix around a fiber break. This in turn allows for the load to be carried throughout the material so that the load carried by the bundle becomes important.[144] These merits have made carbon fiber reinforced polymers important in a variety of applications including aerospace, automotive, and for sporting goods.[145]

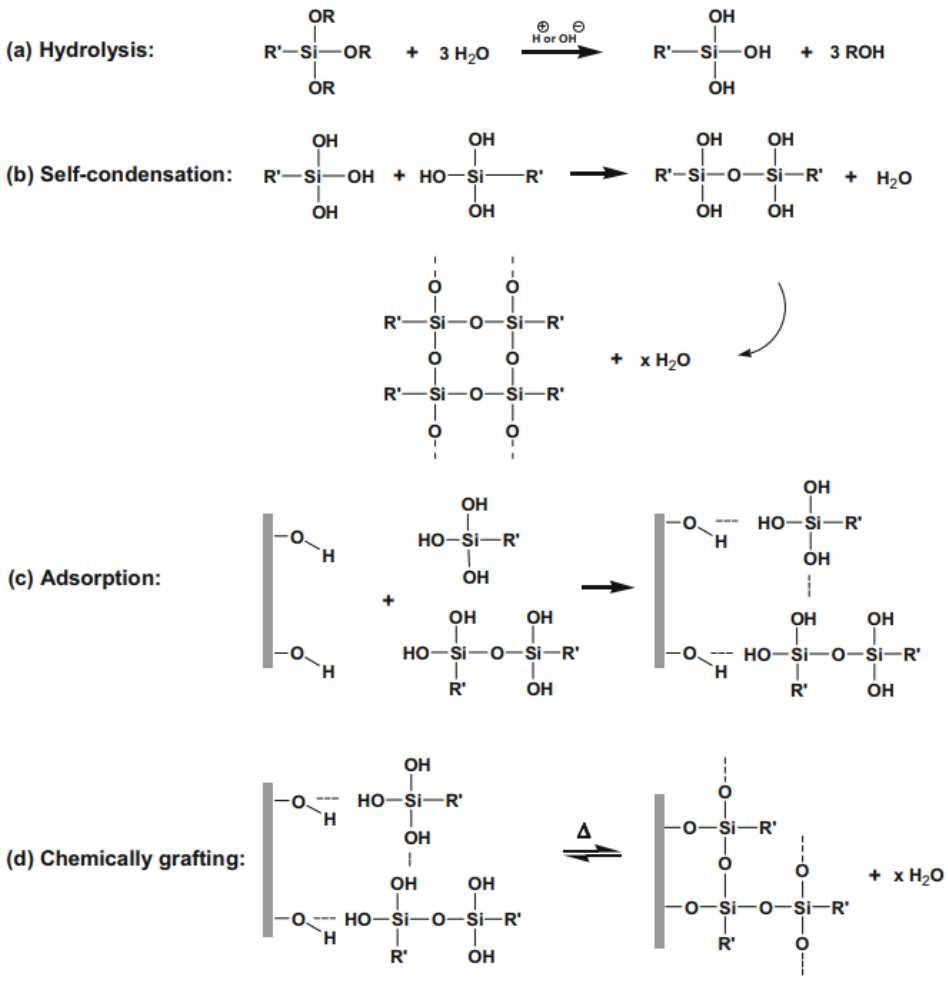

Figure 2.13 Silane hydrolysis, coupling and crosslinking.[135]

Commercial carbon fibers can be made from PAN, pitch, rayon, or lignin precursors, with PAN-based carbon fibers comprising ~90% of the market. The advantages of PAN-based carbon fibers are the well-established manufacturing procedures and equipment, high reproducibility, and the corresponding carbon fibers may have ultra-high tensile strengths and excellent moduli.[146] Carbon fibers made from mesophase pitch are also in production due to their ultra-high elastic moduli.[145] In recent years, a lot of effort has been undertaken by the US Department of Energy at Oak Ridge National Laboratory with the objective of fabricating low-cost carbon fibers for automotive

applications.[78] Their approach is to use either recycled textile PAN copolymers, or naturally-abundant, bio-regenerable lignin to fabricate carbon fibers at a much lower overall cost.

As for the polymer matrix, thermosetting resins including epoxies, unsaturated polyesters, vinyl esters, phenolic resins, bismaleimides, and cyanate esters are used. Thermoset epoxy matrices are most widely used in composite materials for aerospace applications.[145] Alternatively, high-performance thermoplastic polymers such as PEI, PEEK and poly(phenylene sulfide) may be used, which would enable composites with excellent mechanical properties under harsh environments such as high or low temperatures. Amorphous polymers such as PEI can be more easily melt processed relative to semi-crystalline PEEK or poly(phenylene sulfide).

There are several methods to manufacture carbon fiber reinforced polymers, such as vacuum bagging, resin infusion under vacuum, compression molding, and pultrusion, and these can be applicable to both thermoplastic and thermoset polymers.[145] For example, epoxy prepreg can be prepared by wetting and impregnating the carbon fibers with neat liquid polymer resins, or in polymer solution by dipping, spraying, or film pressing.[97, 147] Subsequently, layers of pre-impregnated sheets can be stacked on top of one another to be consolidated in a vacuum bag, and cured by applying simultaneous heat and pressure in an autoclave.[144] Thermoplastic polymer matrices such as PEI can be used to make the composites using similar methods but without the curing requirement. However, a major challenge for manufacturing carbon fiber reinforced composites using thermoplastics such as PEI as a matrix is the high viscosity of the polymer which limits inter-diffusion and may lead to incomplete or uneven impregnation of the PEI matrix into the fiber sheets. If processing time and temperature are not optimized and sufficiently long, the composite will be susceptible to damage under load due to decreased mechanical properties.[108, 148-149]

Perhaps one of the most important applications of carbon fiber reinforced composites is their usage in aerospace applications for both military and civil aircraft. The F22 fighter aircraft contain ~25 wt% of carbon fiber reinforced composites, while the outer skin of the Northrop Grumman B-2 Spirit aircraft are almost exclusively made of polymer composites.[145] The newest Boeing 787 Dreamliner has composites comprising half of the aircraft's overall weight (80% by volume), and most of the composites are carbon fiber reinforced polymer composites.[150] It mainly utilizes an intermediate modulus T800S carbon fiber with a highly toughened epoxy matrix.[151] The majority of the airframe is made of composites. This enables a 20-25% reduction of fuel consumption as well as greenhouse gas emissions. More importantly, fatigue and any corrosion will be minimized with these composites compared to metals or alloys, and this should lead to reduced maintenance requirements and increased service time.[150] Later, the Airbus A350 extra wide body aircrafts were produced by Airbus Corp. to compete with the Boeing 787 Dreamliner. Composites make up ~53 wt% of the aircraft weight, and it is the first time that the outer and center wing boxes have been made of carbon fiber reinforced composites.[152] PEI and PEEK-based carbon fiber reinforced composites are also used. Composites with carbon fibers and a PEI matrix are strong, durable, lightweight, and retain desirable mechanical properties and excellent flame resistance along with low smoke and toxicity at high temperatures, and may be used for aircraft interiors such as arm and foot rests, as well as tray table arms.[153] For example, THERMOCOMP™ EC008PXQ developed by SABIC which is made of 40% carbon fiber with an ULTEM matrix can be fabricated with thin-walled molded parts for aircraft interior components, technical parts, and structural elements, leading to weight reductions of ~50% while maintaining excellent stiffness and flow characteristics, as well as significantly increased strength.[153] It is predicted that carbon fiber reinforced composites may be increasingly used in

aerospace applications, leading to fewer greenhouse emissions and longer trips possible without refueling.

Another important application of carbon fiber reinforced composites is in the automotive field. The US Department of Energy reported that reducing the weight of all US vehicles by 10% would reduce carbon dioxide emissions by 72 million metric tons each year.[154] At this stage, carbon fiber reinforced composites are used mostly in high-end automobiles or racing cars. For example, the McLaren 570S has carbon fiber reinforced polymer composites for almost all of its structural panels and body frame, and its dry weight is only 3,150 lbs.[155] More commonly, carbon fiber reinforced composites are used to fabricate hoods, decklids, spoilers, and scuttle panels of vehicles to achieve higher performance or better aesthetics.[156-157] More recently, SABIC, in collaboration with Kringlan Composites (Otelfingen, Switzerland) and other partners, has fabricated the world's first strong, lightweight, and stylish wheels using PEI-based carbon fiber reinforced composites, as shown in Figure 2.14.[158] However, the high cost and difficulties associated with scalability of manufacturing processes for carbon fiber reinforced composites still limits their wider application in the automotive industry.[159-160] To establish lower cost, streamlined, large-scale fabrication and processing methods for these composites is key to broaden their applications. The automotive industry may use mid-range-performance carbon fibers to make the composites, which may significantly reduce the overall cost. Lignin-based carbon fibers are of particular interest due to the availability of lignin and potential cost reduction. However, investigations with lignin-based carbon fibers remain on the lab scale and there is a long way to go before the low-cost lignin-based fibers could be in large-scale production.

Figure 2.14 First all carbon fiber reinforced composite-based wheels made by SABIC and their collaborators.[158]

Part II. Polymeric complexes for biomedical applications.

2.6 Overview of drug delivery

Drug delivery is the methodology for delivering pharmaceuticals to achieve desirable therapeutic effects in humans or animals.[161] Drug delivery has aroused tremendous interest due to a lack of sufficient treatment for many diseases. Although all kinds of drugs have been produced, their efficacies have been limited due to various reasons. First, drugs have to be delivered to pathologic sites so that they can perform their therapeutic functions.[162] Conventional drug delivery relies on intravenous injection (IV), oral intake, inhalation, and transdermal delivery, mostly without drug carriers. In these situations, drugs are directly or indirectly delivered to the bloodstream, then possibly delivered to pathological sites. Optimal drug efficacy can be achieved only when the drug concentration is in the therapeutic window, which is the range between the maximum toxic concentration (MTC) and minimum effective concentration (MEC). Figure 2.15 demonstrates concentrations and relative efficacies after administration of an oral drug. If the drug concentration

falls below the MEC, no therapeutic effects may be achieved. If the concentration is higher than the MTC, toxicity effects become more prominent, leading to side effects or more disastrous consequences. Therefore, it is of utmost importance to achieve and maintain the drug concentration in the optimal therapeutic window. However, most modern drugs have low water solubility and the optimal concentration cannot be achieved easily. Intravenous injection allows drugs to go into blood circulation directly, but the other methods do not enable this. For example, oral drugs have to go through the stomach before they can be absorbed in the small intestine and eventually go into the bloodstream. The concentration of drugs cannot be precisely controlled. Moreover, active ingredients in drugs may be changed in the stomach due to the significantly lower pH environment. Even if the drugs go into circulation, they may be eliminated quickly without identifying and reaching pathologic sites, due to their small sizes and non-targeting properties.

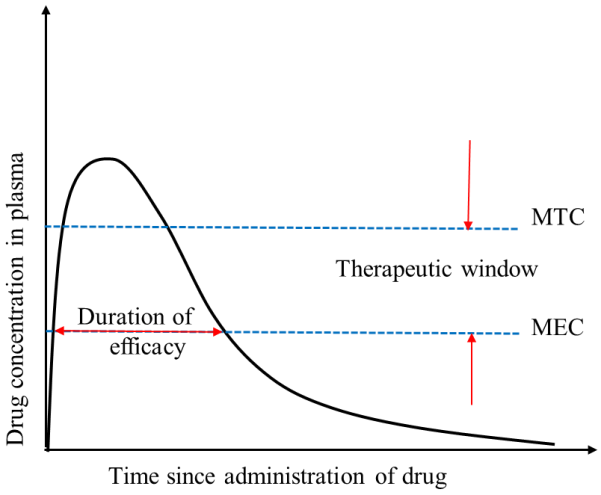

Figure 2.15 Typical drug concentrations and efficacies in plasma after an oral drug administration.

Since conventional drug delivery has lots of limitations, research has been conducted to develop versatile drug delivery systems. The prototype of the drug delivery carrier dates back to 1834, when Mothes and DuBlanc prepared and patented the first capsules which were made of gelatin.[163] Drugs

in solid or liquid form were loaded inside the capsules. Low solubility for some drugs was solved. Such "carriers" also minimized drug loss in the stomach. Drugs in capsules are still widely used today. However, this approach is limited to oral drug delivery and is not applicable for other types of drug administration. The serum levels of drugs are still difficult to control. More versatile drug delivery systems were needed. Novel drug delivery systems were developed to improve drug bioavailability, increase drug circulation time, minimize drug loss prior to delivery, avoid immune response, and ultimately, target circulation to pathological sites.[164-165] A large numbers of delivery systems have been developed and tested for drug delivery applications.[162, 166-169] Typical drug delivery carriers include nanoparticles, liposomes, micelles, and hydrogels.[170] Polymeric materials are versatile and can be utilized in all of these carrier types.[171-174]

2.7 Polymer-based drug delivery systems

Polymer-based drug delivery systems have attracted significant interest and a multitude of such platforms have been developed and characterized.[162, 166-169, 175-177] The use of polymers as carriers has played a key role in the advancement of drug delivery technologies. Most polymers can be synthesized easily on a large scale with good reproducibility and relatively low cost. Their sizes, molecular weights and size distributions can be well-controlled by using living polymerization techniques. Their shapes and physiological properties can also be tailor-made. There are generally two types of polymer drug delivery systems based on the drug loading mechanism. The less common one is the "polymer-drug conjugate" that uses the functional groups of the polymer to directly link to the drug, or connect via a linker.[178] The majority utilize polymeric materials to form micelles. The drugs are then loaded into the micellar "container" via physical or chemical means.[179] Well-designed polymeric micellar systems also enjoy advantages such as high stability under physiological conditions and high drug loading capacity.[162] Those micellar polymeric architectures are usually within the size of 10-200 nm.

They are big enough to avoid renal excretion, leading to increased circulation time in the bloodstream. More importantly, they allow potential passive-targeting due to the enhanced permeation and retention (EPR) effect, as pathological sites differ from normal sites in properties such as temperature, pH, vasculature permeability, and surface charge.[180-181] Block copolymer-based micelles are among the most widely investigated polymer drug delivery systems.[162, 167, 182] They are characterized by the presence of long sequences of different monomers. Block copolymers for drug delivery usually have at least one of the blocks being hydrophilic.[183] There are two common types of block copolymer systems: Non-ionic amphiphilic and ionic block copolymers. Amphiphilic block copolymers have a hydrophilic block and a hydrophobic segment, and they form core-shell micellar structures via self-assembly in aqueous media, due to hydrophobic interactions of the hydrophobic block(s).[184] The ionic block copolymers are typically comprised of an ionic segment and a nonionic hydrophilic block. They also form complexes with a core-shell structure when mixed with other oppositely charged species.[185-186] Examples of polymer-based spherical micelles and their proposed structures are shown in Figure 2.16. In either type of the block copolymers, a hydrophilic block forms the shell of the micellar structures. Either the ionic block or the hydrophobic segment forms the core of the micelles.[162] Drugs which are hydrophobic or ionic can be loaded into the core section of the micellar structures due to hydrophobic, electrostatic or other physical or chemical interactions.[179] This significantly increases drug solubility and bioavailability. The hydrophilic shell assists in maintaining the hydrodynamic stability of the complexes. By using highly biocompatible macromolecules as the shell, drug circulation time can be significantly increased, without triggering an immune response from the host.[178] It is also possible to endow the shell surface of the micelles with certain functional groups. These functional groups may interact specifically and bind to certain ligands, thus leading to active

targeting.[187] It is also feasible to introduce pH or temperature-responsive polymer segments to these systems, thus allowing potential triggered drug release.[188-189]

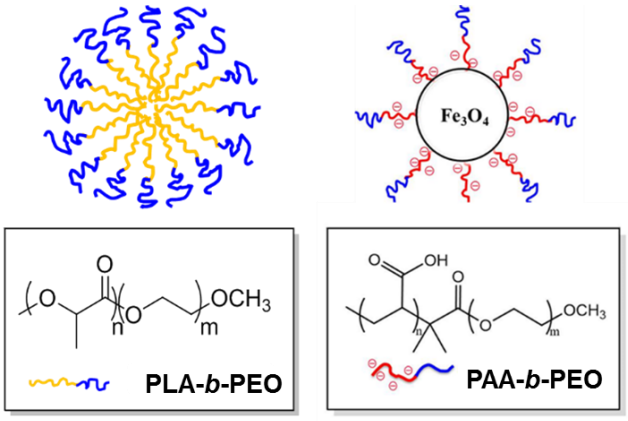

Figure 2.16 Examples of non-ionic amphiphilic and ionic block copolymer based micellar structures

2.8 Living polymerization for the synthesis of well-defined block copolymers

2.8.1. Overview of the synthesis of block copolymers

The block copolymers for drug delivery applications are typically addition polymers which are prepared by chain growth reactions. In some cases, it is feasible to grow both blocks at the same time. For example, Seo et al.[190] successfully performed a one-step synthesis of cross-linked block copolymers of poly(lactide)-*b*-poly(styrene). However, in most cases, one homopolymer is synthesized before growing the other block. In order to obtain well-defined polymers with specific molecular weights, living polymerization methods, such as reversible-addition fragmentation chain-transfer polymerization (RAFT), atom transfer radical polymerization (ATRP), or living anionic/cationic ring-opening polymerization (ROP), have to be used.[165, 191] It is noteworthy that the synthesis of the block copolymers sometimes may need more than one technique to be used if the two or more homopolymers must be synthesized by different methods. ROP is mostly utilized to synthesize polyesters such as polylactide, polyglycolide, and polycaprolactone, while the other two

are applicable to monomers with vinyl groups. One of the biggest advantages of living polymerization is that the molecular weight of potential polymers can be tailor-made based on the initial monomer to initiator ratio. The polymer product also has narrow molecular weight distributions and well-defined architectures. This is because there is no irreversible chain termination or chain transfer until the monomers are depleted, or inhibitors such as oxygen are introduced.[192] As long as the rate of the initiation is much faster compared to the rate of propagation, the molecular weight distribution of the growing chain, as well as the final polymer product, should be narrow.[193] This can be quite important for polymers for drug delivery vehicles, which requires the polymer "containers" to be relatively uniform in sizes and stabilities. Another quite significant benefit is that such polymers can be easily functionalized. This enables easy addition of another polymer chain or targeting ligands which may be utilized for targeted delivery. Moreover, it is possible to functionalize the starting materials on two or more sites, making simultaneous growth of polymer chains on different sites easy to achieve with targeted molecular weight.

2.8.2 Atom transfer radical polymerization (ATRP)

ATRP is among the most efficient, robust and successful controlled polymerization techniques for living polymerization.[194] It was developed by Professor Krzysztof Matyjaszewski at Carnegie Mellon in 1994. In ATRP, free radical initiators, such as azobisisobutyronitrile (AIBN) or benzoyl peroxide (BPO), are not used. It uses dormant species of alkyl halides. It also uses activators, which are typically low-oxidation-state metal complexes, as well as a ligand. The most commonly used metal complex is copper(I) bromide (cuprous bromide).[194] The ligands are often amines, and an example is *N,N,N',N''*-pentamethyldiethylenetriamine (PMDETA). Once the reaction begins, the halogen groups are chelated to the copper catalyst and radicals are generated. Differently from conventional free radical polymerization which has no control over propagation, the radicals in ATRP

reversibly bind to the halogens quickly and set up an equilibrium. That avoids uncontrolled growth of the propagating chain, and leads to formation of polymers with relatively uniform molecular weights and narrow molecular weight distributions. The simplified ATRP mechanism is shown in Figure 2.17. ATRP has been employed by our group[195] to synthesize diblock poly(*tert*-butyl acrylate)-*b*-poly(ethylene oxide) (P*t*BA-*b*-PEO). The copolymer was subsequently selectively deprotected to afford an ionic block copolymer and was used to form complexes with magnetite and manganese (II). The synthetic route for the copolymer is shown in Figure 2.18. Their potentials as drug delivery carriers and magnetic resonance imaging agents were investigated. Due to the use of ATRP, the copolymers had targeted molecular weights and narrow size distributions, and they also had well-defined core-shell micellar structures, as well as excellent hydrodynamic stabilities. Zhang et al.[196] utilized ATRP to synthesize $MnFe_2O_4$-polystyrene nanoparticles. A carboxylate-functional alkyl halide initiator was chemically attached to the surface of the nanoparticles. The surface functionalized nanoparticles were then used as macroinitiators for the subsequent ATRP to grow polystyrene from their surfaces. This resulted in the formation of polystyrene-coated $MnFe_2O_4$ nanoparticles with core-shell structures smaller than 15 nm.

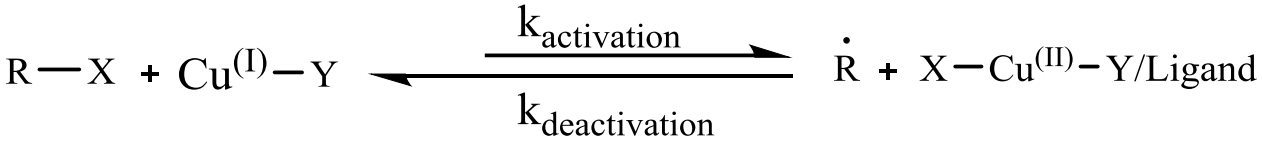

Figure 2.17 ATRP reaction simplified mechanism.

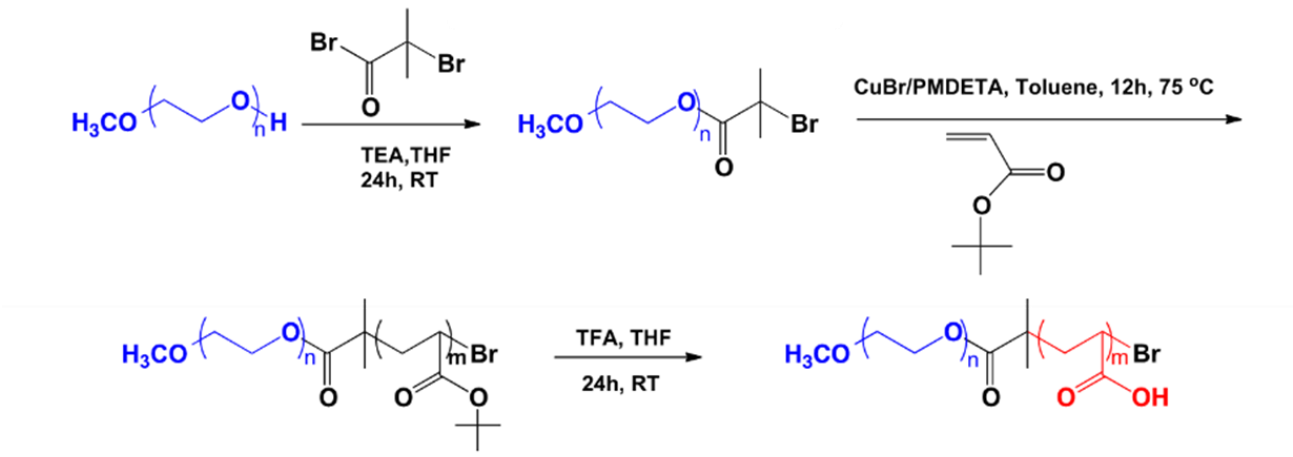

Figure 2.18 Synthesis of PEO-*b*-PAA for potential drug delivery.[195]

2.8.3 Reversible addition-fragmentation chain transfer polymerization (RAFT)

RAFT polymerization is also a versatile and widely used technique for synthesizing well-defined polymer architectures.[193] The first report of RAFT as a controlled polymerization to synthesize poly(butyl methacrylate) homopolymers and block copolymers was reported in 1995.[197] The term "RAFT" was designated later when Thang[198] et al. polymerized various monomers using thiocarbonylthio compounds as chain transfer agents (RAFT agents). Differently from ATRP, RAFT polymerization still utilizes conventional free radical initiators such as AIBN or BPO. The difference between conventional free radical polymerization and RAFT is the use of the RAFT agents. The RAFT agent, predominantly comprised of thiocarbonylthio compounds, plays the key role in making RAFT a controlled polymerization. The generated radicals react with the agent, and the growing chains become dormant. Since this step is completely reversible, the radicals can be regenerated and react with monomers. The mechanism for the RAFT is illustrated in Figure 2.19. RAFT polymerization has been found to be widely applicable where conventional free radical polymerization may be usable. It can be conducted in emulsion, solution, suspension, or bulk, and

with a wide range of temperatures and solvents, including water.[198] Compared to ATRP, RAFT exhibits excellent tolerance to a diverse range of functional groups, thus a great deal of polymers with neutral, anionic, cationic and even zwitterionic monomers have been successfully synthesized via RAFT.[199-201] It has significantly broadened the scope of functionalized polymer materials for potential drug delivery applications. RAFT also enables easy end-group fabrication and conjugation by reducing the thiol end-group moiety following polymerization. RAFT to synthesize block copolymers for drug delivery applications has been reported. For example, Luo et al.[173] synthesized poly(*N*-vinylpyrrolidone)-*b*-poly(styrene-*alt*-maleic anhydride) and poly(*N*-vinylpyrrolidone)-*b*-poly(*N*,*N*-dimethylaminoethyl methacrylate) via RAFT. They used a pair of oppositely charged block ionomers to form micelles and loaded Co A as a sample water-soluble drug and studied the drug release. McCormick et al.[199] utilized RAFT to synthesize anionic poly(*N*-(3-aminopropyl)methacrylamide hydrochloride)-*b*-poly(*N*-isopropylacrylamide) (PAMPA-b-PNIPAM) and poly(sodium 2-acrylamido-2-methylpropane sulfonate) (PAMPS). The two copolymers were rapidly mixed in aqueous solution and were found to form ionically cross-linked vesicles due to interpolyelectrolyte complexation. The vesicle structures were found to be stable in a pH range of 0-10.5, as well as with sodium chloride concentrations up to 0.8 M, which shows potential for drug delivery.

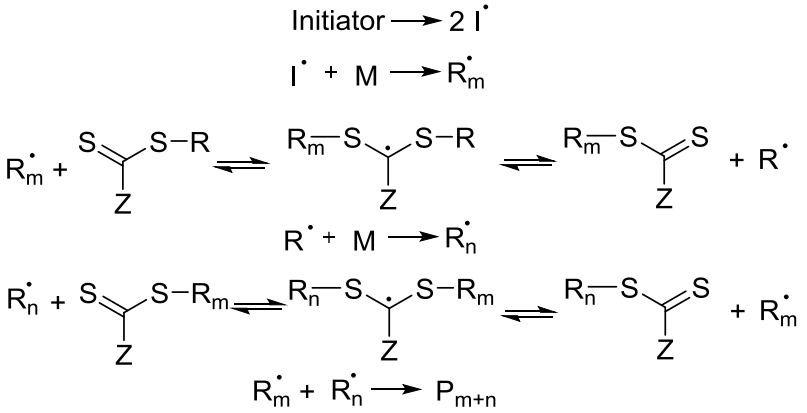

Figure 2.19 Mechanism of the RAFT process.

2.8.4 Anionic ring opening polymerization (ROP)

Ring opening polymerization has a long history in polymer science, as the famous Nylon 6, or polycaprolactam was synthesized by ROP, invented by Paul Schlack in the 1930s.[202] Based on the reaction mechanisms, ROP can be categorized into radical ROP, ionic (cationic or anionic) ROP, and ring opening metathesis polymerization (ROMP). Typical cyclic monomers for ROP are listed in Table 2.1. The driving forces for ROP are the ring strain and steric constraints, and 3-8 membered rings may be polymerized as the polymerization reaction is favored due to enthalpy loss.[203] In this review, only anionic ROP is discussed. In anionic ROP, an anionic species serves as a nucleophile and attacks the partially positive carboxylate carbons on the ring systems, generating another anion, thus allowing the propagation of the polymerization reaction. For anionic polymerization, the initiators can be 1) radical anions formed by mixing naphthalene and potassium or sodium metal in dry THF; 2) carbanions such as n-butyl lithium; or 3) alcoholate.[203] Our group[204] has used 3-hydroxypropyldimethylvinylsilane and potassium naphthalide in THF as initiators to synthesize functional poly(ethylene oxide) in a Parr pressure reactor, as is shown in Figure 2.20. Anionic ROP can be a living polymerization reaction that enables the synthesis of polymers with targeted molecular weights and block lengths, by adjusting the ratios of the monomers to the initiators. It is still widely used for the synthesis of poly(ethylene oxide), Nylon 6, 11, 12, as well as poly(caprolactone), poly(glycolic acid) and poly(lactic acid). Kayandan[204] synthesized poly(ethylene oxide)-*b*-poly(DL-lactide) by using vinyldimethylsilyl propoxy functional poly(ethylene oxide), potassium naphthalide, and recrystallized DL-lactide. For the synthesis of these polylactones and polylactides, since their monomers are relatively stable ring systems, a transition metal catalyst is usually used to facilitate the ROP reaction. The most effective and widely used catalyst is tin(II) 2-ethyl-hexanoate (stannous octoate).[205-206]

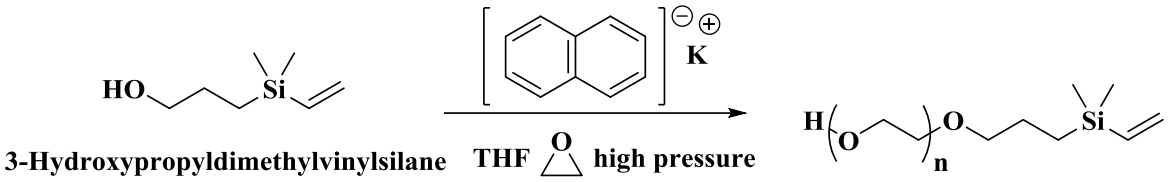

Figure 2.20 An example of the synthesis of functional poly(ethylene oxide) in a Parr reactor.

Table 2.1 Typical cyclic monomers for ROP.[203]

Name	Structures	Ring size	Mechanism
Olefin		4, 5, 8	Metathesis
Ether		3, 5-7	Cationic, anionic, coordination
Lactone		4, 5-8	Cationic, anionic, coordination

2.9 Important polymer building blocks for drug delivery

2.9.1 Poly(ethylene oxide) (PEO)

The hydrophilic poly(ethylene oxide) has been and will continue to be the "golden rule" for drug delivery, due to its easy synthesis, excellent biocompatibility, commercial availability, and resistance to protein adsorption.[207] PEO and poly(ethylene glycol) (PEG) are the same materials. PEO with various molecular weights and different functional moieties have been commercialized and are widely available for the synthesis of block copolymers with different compositions, topologies, and functionalities. Many polymeric micellar drug delivery systems have core-shell micellar structures, and the hydrophilic shell is mostly comprised of PEO-based polymers. Poly(ethylene oxide-*b*-acrylate) (PEO-*b*-PAA) ionomer complex drug delivery systems have been widely investigated. Poly(ethylene oxide-b-lactide) (PEO-*b*-PLA) amphiphilic block copolymers are another important class of block copolymers for potential drug delivery. Generally, the molecular weight of the PEO

block in these copolymers for drug delivery is less than 5k Daltons, and they are usually commercially available. For the synthesis of PEO-bearing block copolymers, a PEO macromonomer is often synthesized and end-functionalized to enable polymerization of another block(s). The hydroxyl groups on PEO allow direct ROP to copolymerize with cyclic monomers such as lactide or caprolactone. End-functionalization is necessary in order to copolymerize with other monomers such as *tert*-butyl acrylate by ATRP. It is also possible to introduce functional moieties on the initiator terminal. This may allow the introduction of another polymer segment, or even targeting ligands, onto the surface of the polymeric micelles, thus making actively-targeted drug delivery possible.[208]

2.9.2 Amphiphilic P85 Pluronics®

Pluronics® are amphiphilic PEO-*b*-poly(propylene oxide)-*b*-PEO triblock copolymers. Pluronic® triblock copolymers with different compositions are available from BASF chemical company. They are synthesized by initial polymerization of propylene oxide, followed by growing ethylene oxide from both ends.[162] They have been widely used in various applications and have aroused great interest recently for potential drug delivery.[209-213] Quite a few advantages lead to the preferred use of Pluronics® for drug delivery applications. First of all, based on the study of Kabanov's group, low molecular weight Pluronics® at low concentrations did not show cytotoxicity.[214] Second, Pluronics® are commercially available in a multitude of block lengths and molecular weights.[184] Pluronics® with different compositions have different properties, and their drug delivery profiles may be different. This may be exploited and tailored for specific drug delivery applications. More importantly, Pluronics®, especially P85-bearing complexes, has been shown to be capable of sensitizing multi-drug resistant (MDR) tumor cells, inhibiting drug efflux transporters, and increasing the cytotoxicity of drugs. P85 has also found to be capable of temporarily disrupting and opening the blood-brain barrier (BBB), which is crucial for treating malignant brain tumors.[162, 215-217] Up to now,

due to the presence of this barrier, treatment of brain tumors have been seriously limited compared to other types of tumors. The BBB is comprised of endothelial cells with continuous tight junctions between the blood vessels and the interstitial fluid where the brain cells are located.[218] In order to treat brain tumors, anti-cancer drugs have to cross the BBB and enter the interstitial fluid environment. However, the BBB filters and prohibits most unknown substances from crossing it. Only certain species such as oxygen, glucose, hormones, insulin, and certain amino acids can cross it via passive diffusion, carrier-mediated transport or receptor-mediated endocytosis.[219] P85-containing nanocarriers are promising candidates for delivering drugs to the brain and have aroused tremendous research interest recently. P85 has 26 repeating units of ethylene oxide on both ends and an average molecular weight of 4600 grams per mole. In P85, the central poly(propylene oxide) plays an important role in interacting with biological entities. Poly(propylene oxide) has a pendant methyl group, which makes it relatively hydrophobic, compared to hydrophilic PEO. It enables better interactions with hydrophobic cell membranes, leading to increased intracellular uptake. Our recent study in collaboration with the Kabanov group at the University of North Carolina at Chapel Hill compared the intracellular uptake of PEO-*b*-poly(acrylate) and PEO-*b*-poly(methacrylate)-magnetite nanoparticles. The latter displayed slightly better intracellular uptake in several cell lines, which may also be attributed to the presence of the α-methyl group. Interestingly, P85-bearing complexes were taken up significantly more in all cell lines. We have collaborated with Professor Kabanov on a project utilizing P85-containing ionic copolymer-magnetite nanoparticles for remote and selective control of cancer treatment by magneto-mechanical actuation. P85 was utilized to form a pentablock copolymer by growing *tert*-butyl acrylate blocks on both ends and subsequently removing the *tert*-butyl groups. The copolymer was endowed with terminal ionic poly(acrylate) blocks, two hydrophilic PEO blocks, and a central, hydrophobic PPO block (P85PAA). The polymer structure is shown in Figure 2.21. The

P85PAA was then complexed with magnetite nanoparticles with an average diameter of 8 nm. The complexes were used for selective treatment of human breast tumor cells in vitro by employing an ultra-low frequency AC magnetic field. This led to the death of cancer cells without perceptible heat generation as well as lysosomal disruption. It was found that when the AC field was applied, the cell death was caused by mechanical motion rather than hyperthermia. The AC field triggered the magnetic nanoparticles to generate rotational forces, which led to cytoskeletal disruption in cancer cells, while healthy cells were unaffected. It is a novel concept to utilize magneto-mechanical actuation of magnetic nanoparticles for remote and selective control of cancer treatment. Shen et al.[220] successfully utilized P85-*b*-polyethyleneimine together with D-α-tocopheryl poly(ethylene glycol) 1000 succinate micellar nanoparticles to deliver twist small hairpin RNA and paclitaxel (a potent anti-cancer drug). An in vivo study showed increased circulation and cellular uptake of both RNA and paclitaxel in the cancer cells. The toxicity of the drug-loaded complexes was much lower than paclitaxel alone. The in vivo study based on a mouse model also demonstrated that this system could inhibit both the growth and metastasis of tumor cells.

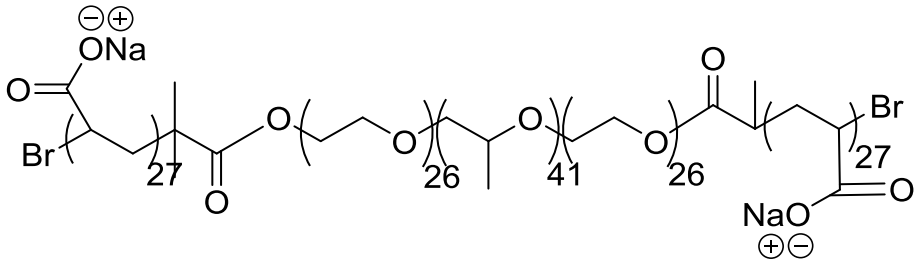

Figure 2.21 P85PAA synthesized in our lab for investigation in drug delivery.

2.9.3 Poly(lactic acid) and poly(glycolic acid)

Poly(lactic acid) and poly(glycolic acid) have been widely used in tissue engineering due to their biodegradable and biocompatible features, and their simple production.[221-225] They are usually

synthesized by ROP using their cyclic dimers as monomers. The monomers are named 3,6-dimethyl-1,4-dioxane-2,5-dione and 1,4-dioxane-2,5-dione respectively and are shown in Figure 2.22. Lactide has one additional methyl group compared to glycolide, and this leads to differences in their properties and reactivities. Poly(glycolic acid) is a highly crystalline thermoplastic polymer while poly(lactic acid) is a bit more complicated. The lactide dimers have two chiral centers with a plane of symmetry. There are three possible poly(lactic acid) polymers, with either D, L, or DL configurations. The structures of all three cyclic dimers are shown in Figure 2.22. The poly(L-lactide), also known as PLLA, is a semi-crystalline polymer. The same can be said of PDLA, which is an enantiomer of PLLA. The D,L mixture, however, or blends of the isomers are amorphous. Amorphous polymers are more vulnerable to hydrolysis, thus degrading faster than semi-crystalline polymers.[226] Poly(lactic acid-co-glycolic acid) random copolymers, termed PLGA, have been widely used for biological applications in drug delivery. The degradation of poly(lactic acid) and poly(glycolic acid) is due to hydrolysis of the ester bonds. In poly(lactic acid), the additional methyl group leads to increased hydrophobicity as well as steric hindrance, compared to poly(glycolic acid). Water is less able to access the ester bond, making poly(lactic acid) more hydrolytically stable with longer degradation times. The ratios of the PLA-PGA units in the copolymers can be carefully designed, so that an optimized degradation rate can be reached.

ROP is utilized for the synthesis of these polyesters using alcohols as initiators. The reaction can be conducted in the melt at elevated temperatures or in dry toluene under reflux conditions. $Sn(Oct)_2$ is commonly used as the catalyst. After the reaction, the polymers can be isolated by precipitation in chilled diethyl ether and drying under vacuum at elevated temperatures.[204] PLA and PGA polymers and copolymers have been reported for drug delivery. For example, Xue et al.[227] synthesized amphiphilic poly(acrylic acid)-*b*-poly(DL-lactide) to form micelles and evaluated its potential for pH-

responsive drug delivery. Prednisone acetate was used as a sample drug for an in vitro study. The drugs were released quickly at pH 7.4 but released a minimal amount at pH 1.4. The cytotoxicity of the polymeric carrier was found to be low based on MTT assay experiments. The results indicated that PAA-*b*-PDLLA could be a potentially safe and effective drug carrier with pH-responsive functions. Cheng et al.[228] synthesized and studied carboxylate-terminated poly(D,L-lactide-*co*-glycolide)-*b*-poly(ethylene glycol) copolymers for in vivo targeted drug delivery. They prepared polymeric nanoparticles conjugated to A10 Aptamers (single-stranded DNA or RNA, short for ssDNA and ssRNA). Increased delivery to prostate tumors was achieved. This also demonstrated the possibility of using PLGA-based nanoparticles for drug delivery.

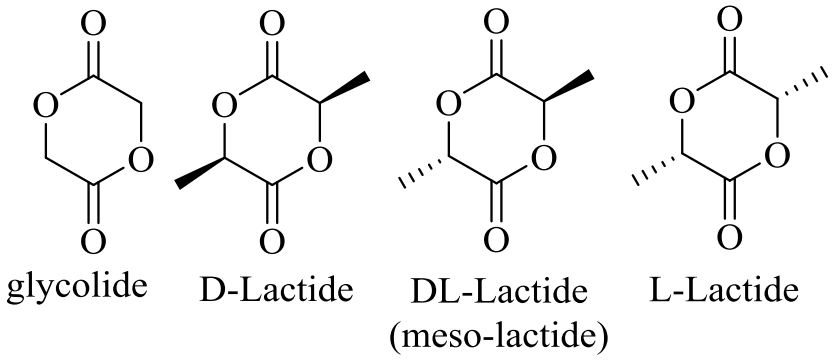

Figure 2.22 The structures of cyclic dimers of glycolide, D-lactide, L-lactide, and DL-lactide.

2.9.4 Poly(caprolactone)

Poly(caprolactone) is another important hydrophobic, semi-crystalline polymer used in biological fields such as tissue engineering and drug delivery.[229-232] It has excellent biocompatibility, bioresorbability, biodegradability, and good miscibility with other polymers. These advantages make it ideal for drug delivery applications.[233] The monomer, caprolactone, is a seven-membered ring cyclic ester. The increased hydrocarbon methylene groups per repeating unit of polycaprolactone, compared to poly(lactic acid) and poly(glycolic acid), lead to significantly increased hydrophobicity and

hydrolytic stability. Polycaprolactone degrades much slower than poly(lactic acid) or poly(glycolic acid), and such advantages were utilized to synthesize PLGA copolymers for tailoring the degradation duration for drug delivery systems.[234] Similar to poly(lactide), poly(caprolactone) is usually synthesized by anionic ROP using $Sn(Oct)_2$ as the catalyst. There are various papers describing the use of polycaprolactone-based polymers for drug delivery. Chen et al.[229] synthesized PCL-*b*-PEO based amphiphilic hyperbranched polymers for targeted drug delivery. The core contained Boltorn H40 (a hyperbranched aliphatic polyester) and hydrophobic PCL, while the shell contained hydrophilic PEO conjugated with targeting moieties of folic acid. Paclitaxel and 5-fluorouracil were used as sample drugs and were loaded into the polymeric nanoparticles. Drug release and targeting effects were investigated in vitro. Enhanced cell inhibition was achieved, demonstrating the potential as drug delivery carriers. Allen et al.[235] synthesized and used polycaprolactone-*b*-poly(ethylene oxide) micelles for delivery of neurotrophic agents FK506 (tacrolimus, an immunosuppressive drug) and L-685,818 (a non-immunosuppressive analog of FK506). The polymeric carrier had good in vitro stability, biocompatibility, and drug loading capability. Sustained release of the reagents further revealed the potential of such polymeric micelles for delivery applications.

2.10 Summary

In summary, the utilization of functional polymers to form composites and complexes were described. Their potential applications in aerospace and biomedical applications were discussed. High-performance polymers such as PEI and PEEK could be synthesized and fabricated into composites as carbon fiber reinforced polymers. The fabrication of the polymer matrices, different carbon fibers from various precursors, and composite with surface treatment were investigated. In part II, drug delivery systems and the important, biocompatible polymer structures to build such systems were described and their synthetic and fabrication methods were discussed.

2.11 References

1. Hirsch, A., The era of carbon allotropes. *Nature materials* **2010,** *9*, 868.
2. Donnet, J.-B.; Bansal, R. C., *Carbon fibers*. CRC Press: 1998.
3. Chand, S., Review carbon fibers for composites. *Journal of materials science* **2000,** *35* (6), 1303-1313.
4. Bacon, R.; Moses, C. T., Carbon Fibers, from Light Bulbs to Outer Space. In *High Performance Polymers: Their Origin and Development*, Springer: 1986; pp 341-353.
5. Stainsby, A., Time for a change. *Electronics and Power* **1985,** *31* (10), 728.
6. Edison's Incandescent Lamp. http://ethw.org/Edison%27s_Incandescent_Lamp (accessed Mar 8, 2018).
7. American Chemical Society National Historic Chemical Landmarks. High Performance Carbon Fibers. . http://www.acs.org/content/acs/en/education/whatischemistry/landmarks/carbonfibers.html (accessed Mar 8, 2018).
8. Ford, C. E.; Mitchell, C. V., Fibrous graphite. Google Patents: 1963.
9. Yusof, N.; Ismail, A., Post spinning and pyrolysis processes of polyacrylonitrile (PAN)-based carbon fiber and activated carbon fiber: A review. *Journal of Analytical and Applied Pyrolysis* **2012,** *93*, 1-13.
10. Huang, X., Fabrication and properties of carbon fibers. *Materials* **2009,** *2* (4), 2369-2403.
11. Ezekiel, H. M. In *Graphite fibers from an aromatic polyamide yarn*, Appl. Polym. Symp, 1969; p 315.
12. Bansal, J.-B. D. a. R., Fibers, Carbon. Marcel Dekker, New York: 1984.
13. Ezekiel, H., Preprints ACS Div. ofOrg. Coatings: 1971.
14. Ezekiel, H. M.; Spain, R. In *Preparation of graphite fibers from polymeric fibers*, Journal of Polymer Science: Polymer Symposia, Wiley Online Library: 1967; pp 249-265.
15. Bhat, G.; Schwanke, R., Thermal properties of a polyimide fiber. *Journal of Thermal Analysis and Calorimetry* **1997,** *49* (1), 399-405.
16. Acatay, K., Carbon fibers. In *Fiber Technology for Fiber-Reinforced Composites*, Elsevier: 2017; pp 123-151.
17. Boucher, E.; Cooper, R.; Everett, D., Preparation and structure of saran-carbon fibres. *Carbon* **1970,** *8* (5), 597-605.
18. Jenkins, G. M.; Kawamura, K., *Polymeric carbons: carbon fibre, glass and char*. Cambridge University Press: 1976.
19. Recent Progress in Producing Lignin-Based Carbon Fibers for Functional Applications. https://www.osti.gov/servlets/purl/1224679 (accessed Mar 6, 2018).
20. Soutis, C., Carbon fiber reinforced plastics in aircraft construction. *Materials Science and Engineering: A* **2005,** *412* (1), 171-176.
21. Meier, U., Carbon fiber-reinforced polymers: modern materials in bridge engineering. *Structural Engineering International* **1992,** *2* (1), 7-12.
22. Bakis, C. E.; Bank, L. C.; Brown, V.; Cosenza, E.; Davalos, J.; Lesko, J.; Machida, A.; Rizkalla, S.; Triantafillou, T., Fiber-reinforced polymer composites for construction—State-of-the-art review. *Journal of composites for construction* **2002,** *6* (2), 73-87.
23. Park, S. J., Carbon Fibers. In *Springer Series in Materials Science* [Online] Hull, R., Jagadish, C., Osgood, R. M., Parisi, J., Seong, T., Uchida, S., Wang, Z. M., Ed. Springer: 2015.

24. Tauriello, J.; Doyle, S.; Ellis, R. In *A Sustainable and Secure Source of Carbonized Rayon for Solid Rocket Motor Nozzles*, 41st AIAA/ASME/SAE/ASEE Joint Propulsion Conference & Exhibit, 2005; p 3796.
25. Mainka, H.; Täger, O.; Körner, E.; Hilfert, L.; Busse, S.; Edelmann, F. T.; Herrmann, A. S., Lignin–an alternative precursor for sustainable and cost-effective automotive carbon fiber. *Journal of Materials Research and Technology* **2015,** *4* (3), 283-296.
26. Rahaman, M. S. A.; Ismail, A. F.; Mustafa, A., A review of heat treatment on polyacrylonitrile fiber. *Polymer Degradation and Stability* **2007,** *92* (8), 1421-1432.
27. Morgan, P., Carbon fibers and their composites CRC press: Boca Raton. *FL, USA* **2005**.
28. Frank, E.; Steudle, L. M.; Ingildeev, D.; Spörl, J. M.; Buchmeiser, M. R., Carbon fibers: precursor systems, processing, structure, and properties. *Angewandte Chemie International Edition* **2014,** *53* (21), 5262-5298.
29. American Chemical Society National Historic Chemical Landmarks. The Sohio Acrylonitrile Process. . https://www.acs.org/content/acs/en/education/whatischemistry/landmarks/acrylonitrile.html (accessed Mar 6, 2018).
30. Frank, E.; Hermanutz, F.; Buchmeiser, M. R., Carbon fibers: precursors, manufacturing, and properties. *Macromolecular materials and engineering* **2012,** *297* (6), 493-501.
31. Chung, D., Carbon Fiber Composites Butterworth. Heinemann, Newton, MA: 1994.
32. Buckley, J. D.; Edie, D. D., *Carbon-carbon materials and composites*. William Andrew: 1993; Vol. 1254.
33. Bajaj, P.; Sreekumar, T. V.; Sen, K., Structure development during dry–jet–wet spinning of acrylonitrile/vinyl acids and acrylonitrile/methyl acrylate copolymers. *Journal of Applied Polymer Science* **2002,** *86* (3), 773-787.
34. Knudsen, J., The influence of coagulation variables on the structure and physical properties of an acrylic fiber. *Textile Research Journal* **1963,** *33* (1), 13-20.
35. Ram, M. J.; Riggs, J. P., Process for the production of acrylic filaments. Google Patents: 1972.
36. Vautard, F.; Ozcan, S.; Meyer, H., Properties of thermo-chemically surface treated carbon fibers and of their epoxy and vinyl ester composites. *Composites Part A: Applied Science and Manufacturing* **2012,** *43* (7), 1120-1133.
37. Montes-Morán, M. A.; Martínez-Alonso, A.; Tascón, J. M. D.; Paiva, M. C.; Bernardo, C. A., Effects of plasma oxidation on the surface and interfacial properties of carbon fibres/polycarbonate composites. *Carbon* **2001,** *39* (7), 1057-1068.
38. Nataraj, S.; Yang, K.; Aminabhavi, T., Polyacrylonitrile-based nanofibers—A state-of-the-art review. *Progress in Polymer Science* **2012,** *37* (3), 487-513.
39. Dalton, S.; Heatley, F.; Budd, P. M., Thermal stabilization of polyacrylonitrile fibres. *Polymer* **1999,** *40* (20), 5531-5543.
40. Fitzer, E.; Frohs, W.; Heine, M., Optimization of stabilization and carbonization treatment of PAN fibres and structural characterization of the resulting carbon fibres. *Carbon* **1986,** *24* (4), 387-395.
41. Liu, J.; Wang, P.; Li, R., Continuous carbonization of polyacrylonitrile‐based oxidized fibers: Aspects on mechanical properties and morphological structure. *Journal of Applied Polymer Science* **1994,** *52* (7), 945-950.
42. Ko, T. H.; Li, C. H., The influence of pre‐carbonization on the properties of PAN‐based carbon fibers developed by two‐stage continuous carbonization and air oxidation. *Polymer composites* **1995,** *16* (3), 224-232.

43. Goodhew, P.; Clarke, A.; Bailey, J., A review of the fabrication and properties of carbon fibres. *Materials Science and Engineering* **1975,** *17* (1), 3-30.
44. Damodaran, S.; Desai, P.; Abhiraman, A., Chemical and physical aspects of the formation of carbon fibres from PAN-based precursors. *Journal of the Textile Institute* **1990,** *81* (4), 384-420.
45. Rahaman, M. S. A., A.F. Ismail, A. Mustafa, *Polym. Degrad. Stab.* **2007,** *92*, 1421.
46. Park, S.-J.; Heo, G.-Y., Precursors and Manufacturing of Carbon Fibers. In *Carbon Fibers*, Springer Netherlands: Dordrecht, 2015; pp 31-66.
47. Park, S.-J.; Kim, B.-J., Roles of acidic functional groups of carbon fiber surfaces in enhancing interfacial adhesion behavior. *Materials Science and Engineering: A* **2005,** *408* (1-2), 269-273.
48. Zhang, G.; Sun, S.; Yang, D.; Dodelet, J.-P.; Sacher, E., The surface analytical characterization of carbon fibers functionalized by H2SO4/HNO3 treatment. *Carbon* **2008,** *46* (2), 196-205.
49. Wu, Z.; Pittman Jr, C. U.; Gardner, S. D., Nitric acid oxidation of carbon fibers and the effects of subsequent treatment in refluxing aqueous NaOH. *Carbon* **1995,** *33* (5), 597-605.
50. Zhang, X.; Huang, Y.; Wang, T.; Liu, L., Influence of fibre surface oxidation–reduction followed by silsesquioxane coating treatment on interfacial mechanical properties of carbon fibre/polyarylacetylene composites. *Composites Part A: Applied Science and Manufacturing* **2007,** *38* (3), 936-944.
51. Drzal, L. T.; Rich, M. J.; Lloyd, P. F., Adhesion of graphite fibers to epoxy matrices: I. The role of fiber surface treatment. *The Journal of Adhesion* **1983,** *16* (1), 1-30.
52. S. R. Sandler, Polymer Synthesis, Academic Press, New York/London, 1974.
53. Mainka, H.; Täger, O.; Stoll, O.; Körner, E.; Herrmann, A. S. In *Alternative precursors for sustainable and cost-effective carbon fibers usable within the automotive industry*, Society of plastics engineers (automobile division)–automotive composites conference & exhibition, 2013.
54. Singer, L. S., The mesophase in carbonaceous pitches. *Faraday discussions of the Chemical Society* **1985,** *79*, 265-272.
55. Delhaes, P., *Fibers and composites*. CRC Press: 2003; Vol. 2.
56. Berrueco, C.; Álvarez, P.; Díez, N.; Granda, M.; Menéndez, R.; Blanco, C.; Santamaria, R.; Millan, M., Characterisation and feasibility as carbon fibre precursors of isotropic pitches derived from anthracene oil. *Fuel* **2012,** *101*, 9-15.
57. Mora, E.; Blanco, C.; Prada, V.; Santamarıa, R.; Granda, M.; Menendez, R., A study of pitch-based precursors for general purpose carbon fibres. *Carbon* **2002,** *40* (14), 2719-2725.
58. Coming to carbon fiber: Low-cost mesophase pitch precursor. https://www.compositesworld.com/news/coming-to-carbon-fiber-low-cost-mesophase-pitch-precursor (accessed Mar 6, 2018).
59. Malone, D. P.; Lee, D. M., Turbulent mesophase pitch process and products. Google Patents: 2016.
60. Malone, D. P.; Lee, D. M., Single stage pitch process and product. Google Patents: 2015.
61. Martone, P. T.; Estevez, J. M.; Lu, F.; Ruel, K.; Denny, M. W.; Somerville, C.; Ralph, J., Discovery of lignin in seaweed reveals convergent evolution of cell-wall architecture. *Current biology* **2009,** *19* (2), 169-175.
62. Hu, J.; Zhang, Q.; Lee, D.-J., Kraft lignin biorefinery: A perspective. *Bioresource technology* **2018,** *247*, 1181-1183.
63. Boerjan, W.; Ralph, J.; Baucher, M., Lignin Biosynthesis. *Annual Review of Plant Biology* **2003,** *54* (1), 519-546.
64. Mikawa, S., Lignin-based carbon fiber. *Chem. Econ. Eng. Rev* **1970,** *2*, 43-46.
65. Fukuoka, Y., Carbon fiber made from lignin (Kayacarbon). *Jap Chem Quart* **1969**.

66. Baker, D. A.; Rials, T. G., Recent advances in low-cost carbon fiber manufacture from lignin. *Journal of Applied Polymer Science* **2013,** *130* (2), 713-728.
67. Mansmann M. GB Pat 1, 764 (1974).
68. Potumarthi, R.; Baadhe, R. R.; Bhattacharya, S., Fermentable Sugars from Lignocellulosic Biomass: Technical Challenges. In *Biofuel Technologies: Recent Developments*, Gupta, V. K.; Tuohy, M. G., Eds. Springer Berlin Heidelberg: Berlin, Heidelberg, 2013; pp 3-27.
69. Baker, D. A.; Gallego, N. C.; Baker, F. S., On the characterization and spinning of an organic-purified lignin toward the manufacture of low-cost carbon fiber. *Journal of Applied Polymer Science* **2012,** *124* (1), 227-234.
70. Sudo, K.; Shimizu, K., A new carbon fiber from lignin. *Journal of Applied Polymer Science* **1992,** *44* (1), 127-134.
71. Sudo, K.; Shimizu, K.; Nakashima, N.; Yokoyama, A., A new modification method of exploded lignin for the preparation of a carbon fiber precursor. *Journal of Applied Polymer Science* **1993,** *48* (8), 1485-1491.
72. Uraki, Y.; Kubo, S.; Nigo, N.; Sano, Y.; Sasaya, T., Preparation of carbon fibers from organosolv lignin obtained by aqueous acetic acid pulping. *Holzforschung-International Journal of the Biology, Chemistry, Physics and Technology of Wood* **1995,** *49* (4), 343-350.
73. Kadla, J. F.; Kubo, S.; Venditti, R. A.; Gilbert, R. D.; Compere, A. L.; Griffith, W., Lignin-based carbon fibers for composite fiber applications. *Carbon* **2002,** *40* (15), 2913-2920.
74. Meek, N.; Penumadu, D.; Hosseinaei, O.; Harper, D.; Young, S.; Rials, T., Synthesis and characterization of lignin carbon fiber and composites. *Composites Science and Technology* **2016,** *137*, 60-68.
75. Tomani, P., The lignoboost process. *Cellulose Chemistry & Technology* **2010,** *44* (1), 53.
76. Nordström, Y.; Norberg, I.; Sjöholm, E.; Drougge, R., A new softening agent for melt spinning of softwood kraft lignin. *Journal of Applied Polymer Science* **2013,** *129* (3), 1274-1279.
77. Alternative precursor R&D: Lignin in the lightweighting limelight. . https://www.compositesworld.com/articles/alternative-precursor-rd-lignin-in-the-lightweighting-limelight (accessed Feb 20, 2018).
78. Griffith, W.; Compere, A.; Leitten, C.; Shaffer, J. In *Low Cost Carbon Fiber for Transportation Appliations*, INTERNATIONAL SAMPE TECHNICAL CONFERENCE, Citeseer: 2002; pp 959-967.
79. Compere, A. *Low cost carbon fiber from renewable resources*; Citeseer: 2001.
80. Transportation Solutions Using Carbon Fiber.
https://web.ornl.gov/sci/manufacturing/docs/CarbonFiber_Brochure.pdf (accessed Mar 6, 2018).
81. Warren, C. D. D., Lower Cost Carbon Fiber Precursors.
82. Baker, F. F. S. Low Cost Carbon Fiber from Renewable Resources. https://energy.gov/sites/prod/files/2014/03/f13/lm_03_baker.pdf (accessed Feb 24, 2018).
83. Adler, E., Lignin chemistry—past, present and future. *Wood science and technology* **1977,** *11* (3), 169-218.
84. Nimz, H., Beech lignin—proposal of a constitutional scheme. *Angewandte Chemie International Edition* **1974,** *13* (5), 313-321.
85. Hosseinaei, O.; Harper, D. P.; Bozell, J. J.; Rials, T. G., Improving Processing and Performance of Pure Lignin Carbon Fibers through Hardwood and Herbaceous Lignin Blends. *International journal of molecular sciences* **2017,** *18* (7), 1410.

86. Hosseinaei, O.; Harper, D. P.; Bozell, J. J.; Rials, T. G., Role of physicochemical structure of organosolv hardwood and herbaceous lignins on carbon fiber performance. *ACS Sustainable Chemistry & Engineering* **2016,** *4* (10), 5785-5798.
87. Norberg, I.; Nordström, Y.; Drougge, R.; Gellerstedt, G.; Sjöholm, E., A new method for stabilizing softwood kraft lignin fibers for carbon fiber production. *Journal of Applied Polymer Science* **2013,** *128* (6), 3824-3830.
88. Kubo, S.; Kadla, J. F., Poly (ethylene oxide)/organosolv lignin blends: Relationship between thermal properties, chemical structure, and blend behavior. *Macromolecules* **2004,** *37* (18), 6904-6911.
89. Alternative precursor R&D: First commercial use of lignin carbon fiber? https://www.compositesworld.com/articles/alternative-precursor-rd-first-commercial-use-of-lignin-carbon-fiber (accessed Mar 6, 2018).
90. Platt, D. K., *Engineering and high performance plastics market report: a Rapra market report*. iSmithers Rapra Publishing: 2003.
91. Mittal, V., *High performance polymers and engineering plastics*. John Wiley & Sons: 2011.
92. Parker, D.; Bussink, J.; van de Grampel, H. T.; Wheatley, G. W.; Dorf, E. U.; Ostlinning, E.; Reinking, K.; Schubert, F.; Jünger, O.; Wagener, R., Polymers, High‐Temperature. *Ullmann's Encyclopedia of Industrial Chemistry* **2002**.
93. High-performance plastics. https://en.wikipedia.org/wiki/High-performance_plastics (accessed Mar 6, 2018).
94. Finkelmann, H., Liquid Crystalline Polymers. *Angewandte Chemie International Edition in English* **1987,** *26* (9), 816-824.
95. High-performance Plastics for Aviation and Aerospace. http://www.sdplastics.com/ensinger/aerodef.pdf (accessed Mar 7, 2018).
96. May, R., Polyetheretherketones. In *Encyclopedia of Polymer Science and Technology*, John Wiley & Sons, Inc.: 2002.
97. Cogswell, F. N., *Thermoplastic aromatic polymer composites: a study of the structure, processing and properties of carbon fibre reinforced polyetheretherketone and related materials*. Elsevier: 2013.
98. High performance thermoplastic solutions for aerospace challenges. http://www.vestamid.com/sites/lists/re/documentshp/flyer%20aerospace%2003-2017.pdf (accessed Mar 6, 2018).
99. Kurtz, S. M.; Devine, J. N., PEEK biomaterials in trauma, orthopedic, and spinal implants. *Biomaterials* **2007,** *28* (32), 4845-4869.
100. Reach the PEEK: How polymer implants can be used for trauma. https://www.medicalplasticsnews.com/news/opinion/reach-the-peek/ (accessed Mar 6, 2018).
101. INVIBIO BIOMATERIAL SOLUTIONS – A WORLDWIDE INNOVATIVE LEADER. https://invibio.com/about (accessed Mar 8, 2018).
102. Ibeh, C. C., *Thermoplastic materials: properties, manufacturing methods, and applications*. CRC Press: 2011.
103. Rosas, J. M.; Berenguer, R.; Valero-Romero, M. J.; Rodríguez-Mirasol, J.; Cordero, T., Preparation of Different Carbon Materials by Thermochemical Conversion of Lignin. *Frontiers in Materials* **2014,** *1* (29).
104. Keane, P.; Chua, C. K.; Joshi, S. C., Embedding Electronics In Printing ULTEM 9085 Quadcopter. **2016**.
105. Misra, A. K.; Grady, J. E.; Carter, R., Additive Manufacturing of Aerospace Propulsion Components. **2015**.

106. Chuang, K. C.; Grady, J. E.; Draper, R. D.; Shin, E.-S. E.; Patterson, C.; Santelle, T. D., Additive Manufacturing and Characterization of Ultem Polymers and Composites. **2015**.
107. Galoone, A.; Ariante, M.; Fusco, G.; Flores, F. F.; Bizzarro, G.; Zinno, A.; Prota, A. In *Thermoplastic composite structure for mass transit vehicle: design, computational engineering and experimental validation,* 15th European Conference on Composite Materials, 2012; pp 24-28.
108. Hou, M.; Ye, L.; Lee, H. J.; Mai, Y. W., Manufacture of a carbon-fabric-reinforced polyetherimide (CF/PEI) composite material. *Composites Science and Technology* **1998,** *58* (2), 181-190.
109. Johnson, R. O.; Burlhis, H. S., Polyetherimide - a New High-Performance Thermoplastic Resin. *Journal of Polymer Science-Polymer Symposia* **1983,** (70), 129-143.
110. Davies, M.; Hay, J. N.; Woodfine, B., Polyetherimides—synthesis and structure-property relationships. *High Performance Polymers* **1993,** *5* (1), 37-45.
111. Heath, D.; Wirth, J., Polyetherimides. Google Patents: 1974.
112. Serfaty, I. W., Polyetherimide: A Versatile, Processable Thermoplastic. In *Polyimides: Synthesis, Characterization, and Applications. Volume 1*, Mittal, K. L., Ed. Springer US: Boston, MA, 1984; pp 149-161.
113. POLYETHERIMIDE (PEI).
http://polymerdatabase.com/polymer%20classes/Polyetherimide%20type.html (accessed Mar 6, 2018).
114. Essalhi, M.; Khayet, M., Surface segregation of fluorinated modifying macromolecule for hydrophobic/hydrophilic membrane preparation and application in air gap and direct contact membrane distillation. *Journal of membrane science* **2012,** *417*, 163-173.
115. Rajagopalan, M.; Oh, I.-K., Fullerenol-Based Electroactive Artificial Muscles Utilizing Biocompatible Polyetherimide. *ACS Nano* **2011,** *5* (3), 2248-2256.
116. Suspending Agent. https://www.scribd.com/doc/96522642/Suspending-Agent (accessed Mar 8, 2018).
117. Johnston, D.; Gray, M. R.; Reed, C. S.; Bonner, F. W.; Anderson, N. H., A Comparative Evaluation of Five Common Suspending Agents Used in Drug Safety Studies. *Drug Development and Industrial Pharmacy* **1990,** *16* (12), 1893-1909.
118. Ormondroyd, S., The influence of poly(vinyl alcohol) suspending agents on suspension poly(vinyl chloride) morphology. *British Polymer Journal* **1988,** *20* (4), 353-359.
119. Bao, Y. Z.; Liao, J. G.; Huang, Z. M.; Weng, Z. X., Influences of individual and composed poly (vinyl alcohol) suspending agents on particle morphology of suspension poly (vinyl chloride) resin. *Journal of Applied Polymer Science* **2003,** *90* (14), 3848-3855.
120. Brink, A. E.; Lin, M. C.; Riffle, J. S., A high-performance electrostatic stabilizer for poly(ether ether ketone) particles. *Chemistry of Materials* **1993,** *5* (7), 925-929.
121. Texier, A.; Davis, R. M.; Lyon, K. R.; Gungor, A.; McGrath, J. E.; Marand, H.; Riffle, J. S., Fabrication of PEEK/carbon fibre composites by aqueous suspension prepregging. *Polymer* **1993,** *34* (4), 896-906.
122. Nohara, L. B.; Costa, M. L.; Alves, M. A.; Takahashi, M. F. K.; Nohara, E. L.; Rezende, M. C., Processing of high performance composites based on peek by aqueous suspension prepregging. *Materials Research* **2010,** *13* (2), 245-252.
123. Cai, D. D.; Su, J. F.; Huang, M.; Liu, Y. H.; Wang, J. J.; Dai, L. X., Synthesis, characterization and hydrolytic stability of poly (amic acid) ammonium salt. *Polymer Degradation and Stability* **2011,** *96* (12), 2174-2180.

124. Yang, J.; Lee, M.-H., A water-soluble polyimide precursor: Synthesis and characterization of poly(amic acid) salt. *Macromolecular Research* **2004,** *12* (3), 263-268.
125. Tyan, H.-L.; Liu, Y.-C.; Wei, K.-H., Enhancement of imidization of poly(amic acid) through forming poly(amic acid)/organoclay nanocomposites. *Polymer* **1999,** *40* (17), 4877-4886.
126. Lan, T.; Kaviratna, P. D.; Pinnavaia, T. J., On the nature of polyimide-clay hybrid composites. *Chemistry of Materials* **1994,** *6* (5), 573-575.
127. Morikawa, A.; Iyoku, Y.; Kakimoto, M.-a.; Imai, Y., Preparation of a new class of polyimide-silica hybrid films by sol-gel process. *Polymer Journal* **1992,** *24* (1), 107.
128. Yang, C. P.; Hsiao, S. H., Effects of various factors on the formation of high molecular weight polyamic acid. *Journal of Applied Polymer Science* **1985,** *30* (7), 2883-2905.
129. Krishnan, P. S. G.; Vora, R. H.; Chunga, T. S., Synthesis, characterization and kinetic study of hydrolysis of polyamic acid derived from ODPA and m-tolidine and related compounds (vol 42, pg 5165, 2001). *Polymer* **2001,** *42* (21), 8921-8921.
130. Ghosh, M., *Polyimides: Fundamentals and Applications*. Taylor & Francis: 1996.
131. Wu, G. M., Oxygen plasma treatment of high performance fibers for composites. *Materials Chemistry and Physics* **2004,** *85* (1), 81-87.
132. Xie, J.; Xin, D.; Cao, H.; Wang, C.; Zhao, Y.; Yao, L.; Ji, F.; Qiu, Y., Improving carbon fiber adhesion to polyimide with atmospheric pressure plasma treatment. *Surface and Coatings Technology* **2011,** *206* (2), 191-201.
133. Jang, J.; Yang, H., The effect of surface treatment on the performance improvement of carbon fiber/polybenzoxazine composites. *Journal of materials science* **2000,** *35* (9), 2297-2303.
134. Pittman Jr, C.; He, G.-R.; Wu, B.; Gardner, S., Chemical modification of carbon fiber surfaces by nitric acid oxidation followed by reaction with tetraethylenepentamine. *Carbon* **1997,** *35* (3), 317-331.
135. Xie, Y.; Hill, C. A.; Xiao, Z.; Militz, H.; Mai, C., Silane coupling agents used for natural fiber/polymer composites: A review. *Composites Part A: Applied Science and Manufacturing* **2010,** *41* (7), 806-819.
136. Gelest Silane Coupling Agents Connecting Across Boundaries. https://www.gelest.com/wp-content/uploads/Goods-PDF-brochures-couplingagents.pdf (accessed Mar 9, 2018).
137. Iwashita, N.; Psomiadou, E.; Sawada, Y., Effect of coupling treatment of carbon fiber surface on mechanical properties of carbon fiber reinforced carbon composites. *Composites Part A: Applied Science and Manufacturing* **1998,** *29* (8), 965-972.
138. Wenzhong, N., The effect of coupling agents on the mechanical properties of carbon fiber-reinforced polyimide composites. *Journal of Thermoplastic Composite Materials* **2015,** *28* (11), 1572-1582.
139. Lee, H.; Ohsawa, I.; Takahashi, J., Effect of plasma surface treatment of recycled carbon fiber on carbon fiber-reinforced plastics (CFRP) interfacial properties. *Applied Surface Science* **2015,** *328*, 241-246.
140. Cech, V.; Prikryl, R.; Balkova, R.; Grycova, A.; Vanek, J., Plasma surface treatment and modification of glass fibers. *Composites Part A: Applied Science and Manufacturing* **2002,** *33* (10), 1367-1372.
141. Naaman, A. E. In *High performance fiber reinforced cement composites: classification and applications*, CBM-CI international workshop, Karachi, Pakistan, Citeseer: 2007; pp 389-401.
142. Unterweger, C.; Duchoslav, J.; Stifter, D.; Fürst, C., Characterization of carbon fiber surfaces and their impact on the mechanical properties of short carbon fiber reinforced polypropylene composites. *Composites Science and Technology* **2015,** *108*, 41-47.

143. de Leon, A. C.; Chen, Q.; Palaganas, N. B.; Palaganas, J. O.; Manapat, J.; Advincula, R. C., High performance polymer nanocomposites for additive manufacturing applications. *Reactive and Functional Polymers* **2016,** *103*, 141-155.
144. Campbell, F. C., *Manufacturing Processes for Advanced Composites*. Elsevier Science: 2003.
145. Mallick, P. K., *Fiber-reinforced composites: materials, manufacturing, and design*. CRC press: 2007.
146. Chae, H. G.; Newcomb, B. A.; Gulgunje, P. V.; Liu, Y.; Gupta, K. K.; Kamath, M. G.; Lyons, K. M.; Ghoshal, S.; Pramanik, C.; Giannuzzi, L.; Şahin, K.; Chasiotis, I.; Kumar, S., High strength and high modulus carbon fibers. *Carbon* **2015,** *93*, 81-87.
147. Newell, G. C.; Buckingham, R. O.; Khodabandehloo, K., The automated manufacture of prepreg broadgoods components - A review of literature. *Composites Part a-Applied Science and Manufacturing* **1996,** *27* (3), 211-217.
148. Offringa, A. R., Thermoplastic composites - Rapid processing applications. *Composites Part a-Applied Science and Manufacturing* **1996,** *27* (4), 329-336.
149. Peng, Y. X.; Chi, Y. L.; Dong, W. M.; Sun, D. M., Wear properties of polyetherimide and carbon fiber-reinforced polyetherimide composite. *Journal of Thermoplastic Composite Materials* **2014,** *27* (7), 949-957.
150. 787 DREAMLINER BY DESIGN. http://www.boeing.com/commercial/787/by-design/#/advanced-composite-use (accessed Mar 6, 2018).
151. Cheng, Y., Preliminary fuselage structural configuration of a flying-wing type airline. **2012**.
152. Hellard, G. In *Composites in airbus. A long story of innovations and experiences*, Global Investor Forum Workshop, 2008.
153. INNOVATIVE PLASTICS LIGHTWEIGHT+COMPLIANT Next Generation Solutions for Aircraft Designers https://sfs.sabic.eu/wp-content/uploads/resource_pdf/1366634996-58446190-SABIC-PLA-4036+Aircraft.pdf (accessed Mar 6, 2018).
154. Energy, U. S. D. o., *Quadrennial Technology Review 2015*. U.S. Department of Energy: 2015.
155. The Carbon-Fiber Future: It's About More Than Speed. https://www.livescience.com/53995-carbon-fiber-may-finally-be-coming-to-cars-everywhere.html (accessed Mar 6, 2018).
156. Cabrera‐Ríos, M.; Castro, J. M., An economical way of using carbon fibers in sheet molding compound compression molding for automotive applications. *Polymer composites* **2006,** *27* (6), 718-722.
157. Stachel, P. In *Carbon fibre reinforced SMC for automotive applications*, 5th Automotive Seminar–SMC/BMC-New challenges in Automotive, Landshut, 2006.
158. SABIC AND KRINGLAN DEVELOPING WORLD'S FIRST THERMOPLASTIC CARBON COMPOSITE WHEEL. https://www.sabic.com/en/news/3926-sabic-and-kringlan-developing-world-s-first-thermoplastic-carbon-composite-wheel (accessed Mar 6, 2018).
159. Beardmore, P.; Johnson, C. F., The potential for composites in structural automotive applications. *Composites Science and Technology* **1986,** *26* (4), 251-281.
160. Koronis, G.; Silva, A.; Fontul, M., Green composites: A review of adequate materials for automotive applications. *Composites Part B: Engineering* **2013,** *44* (1), 120-127.
161. P. Prasad, P. P., D. Rao, T. Shrivastav and R. Ge, Bird's Eye View on the Recent Advances in Drug Delivery Systems. *Journal of Biomaterials and Nanobiotechnology* **2011,** *Vol. 2 No. 5A*, 544-556.
162. Kabanov, A. V.; Batrakova, E. V.; Alakhov, V. Y., Pluronic® block copolymers as novel polymer therapeutics for drug and gene delivery. *Journal of Controlled Release* **2002,** *82* (2–3), 189-212.

163. Podczeck, F.; Jones, B. E., *Pharmaceutical capsules*. Pharmaceutical Press: 2004.
164. Torchilin, V., Micellar Nanocarriers: Pharmaceutical Perspectives. *Pharmaceutical Research* **2007,** *24* (1), 1-16.
165. Torchilin, V. P., Structure and design of polymeric surfactant-based drug delivery systems. *Journal of Controlled Release* **2001,** *73* (2–3), 137-172.
166. Yang, J., Stimuli-responsive drug delivery systems. *Advanced Drug Delivery Reviews* **2012,** *64* (11), 965-966.
167. Kataoka, K.; Harada, A.; Nagasaki, Y., Block copolymer micelles for drug delivery: design, characterization and biological significance. *Advanced Drug Delivery Reviews* **2001,** *47* (1), 113-131.
168. Hoare, T. R.; Kohane, D. S., Hydrogels in drug delivery: Progress and challenges. *Polymer* **2008,** *49* (8), 1993-2007.
169. Allen, T. M.; Cullis, P. R., Liposomal drug delivery systems: From concept to clinical applications. *Advanced Drug Delivery Reviews* **2013,** *65* (1), 36-48.
170. Louguet, S.; Rousseau, B.; Epherre, R.; Guidolin, N.; Goglio, G.; Mornet, S.; Duguet, E.; Lecommandoux, S.; Schatz, C., Thermoresponsive polymer brush-functionalized magnetic manganite nanoparticles for remotely triggered drug release. *Polymer Chemistry* **2012,** *3* (6), 1408-1417.
171. Pothayee, N.; Pothayee, N.; Hu, N.; Zhang, R.; Kelly, D. F.; Koretsky, A. P.; Riffle, J. S., Manganese graft ionomer complexes (MaGICs) for dual imaging and chemotherapy. *Journal of Materials Chemistry B* **2014,** *2* (8), 1087-1099.
172. Wang, H.; Zhao, P.; Su, W.; Wang, S.; Liao, Z.; Niu, R.; Chang, J., PLGA/polymeric liposome for targeted drug and gene co-delivery. *Biomaterials* **2010,** *31* (33), 8741-8748.
173. Luo, Y.; Yao, X.; Yuan, J.; Ding, T.; Gao, Q., Preparation and drug controlled-release of polyion complex micelles as drug delivery systems. *Colloids and Surfaces B: Biointerfaces* **2009,** *68* (2), 218-224.
174. Gong, C.; Qi, T.; Wei, X.; Qu, Y.; Wu, Q.; Luo, F.; Qian, Z., Thermosensitive Polymeric Hydrogels As Drug Delivery Systems. *Current Medicinal Chemistry* **2013,** *20* (1), 79-94.
175. Peer, D.; Karp, J. M.; Hong, S.; Farokhzad, O. C.; Margalit, R.; Langer, R., Nanocarriers as an emerging platform for cancer therapy. *Nat Nano* **2007,** *2* (12), 751-760.
176. Langer, R., Drug delivery and targeting. *Nature* **1998,** *392* (6679 Suppl), 5-10.
177. Lavasanifar, A.; Samuel, J.; Kwon, G. S., Poly(ethylene oxide)-block-poly(l-amino acid) micelles for drug delivery. *Advanced Drug Delivery Reviews* **2002,** *54* (2), 169-190.
178. Pasut, G.; Veronese, F. M., Polymer–drug conjugation, recent achievements and general strategies. *Progress in Polymer Science* **2007,** *32* (8–9), 933-961.
179. Gaucher, G.; Dufresne, M.-H.; Sant, V. P.; Kang, N.; Maysinger, D.; Leroux, J.-C., Block copolymer micelles: preparation, characterization and application in drug delivery. *Journal of Controlled Release* **2005,** *109* (1–3), 169-188.
180. Prabhu, R. H.; Patravale, V. B.; Joshi, M. D., Polymeric nanoparticles for targeted treatment in oncology: current insights. *International journal of nanomedicine* **2015,** *10*, 1001.
181. Muggia, F. M., Doxorubicin-polymer conjugates: further demonstration of the concept of enhanced permeability and retention. *Clinical cancer research* **1999,** *5* (1), 7-8.
182. Park, J.-S.; Akiyama, Y.; Yamasaki, Y.; Kataoka, K., Preparation and Characterization of Polyion Complex Micelles with a Novel Thermosensitive Poly(2-isopropyl-2-oxazoline) Shell via the Complexation of Oppositely Charged Block Ionomers†. *Langmuir* **2006,** *23* (1), 138-146.
183. Allen, C.; Maysinger, D.; Eisenberg, A., Nano-engineering block copolymer aggregates for drug delivery. *Colloids and Surfaces B: Biointerfaces* **1999,** *16* (1–4), 3-27.

184. Adams, M. L.; Lavasanifar, A.; Kwon, G. S., Amphiphilic block copolymers for drug delivery. *Journal of pharmaceutical sciences* **2003,** *92* (7), 1343-1355.
185. Oh, K. T.; Bronich, T. K.; Bromberg, L.; Hatton, T. A.; Kabanov, A. V., Block ionomer complexes as prospective nanocontainers for drug delivery. *Journal of Controlled Release* **2006,** *115* (1), 9-17.
186. Bontha, S.; Kabanov, A. V.; Bronich, T. K., Polymer micelles with cross-linked ionic cores for delivery of anticancer drugs. *Journal of Controlled Release* **2006,** *114* (2), 163-174.
187. Su, J.; Chen, F.; Cryns, V. L.; Messersmith, P. B., Catechol Polymers for pH-Responsive, Targeted Drug Delivery to Cancer Cells. *Journal of the American Chemical Society* **2011,** *133* (31), 11850-11853.
188. Guo, X.; Li, D.; Yang, G.; Shi, C.; Tang, Z.; Wang, J.; Zhou, S., Thermo-triggered Drug Release from Actively Targeting Polymer Micelles. *ACS Applied Materials & Interfaces* **2014,** *6* (11), 8549-8559.
189. Liu, Y.; Wang, W.; Yang, J.; Zhou, C.; Sun, J., pH-sensitive polymeric micelles triggered drug release for extracellular and intracellular drug targeting delivery. *Asian Journal of Pharmaceutical Sciences* **2013,** *8* (3), 159-167.
190. Seo, M.; Murphy, C. J.; Hillmyer, M. A., One-Step Synthesis of Cross-Linked Block Polymer Precursor to a Nanoporous Thermoset. *ACS Macro Letters* **2013,** *2* (7), 617-620.
191. Bayo-Puxan, N.; Dufresne, M.-H.; Felber, A. E.; Castagner, B.; Leroux, J.-C., Preparation of polyion complex micelles from poly(ethylene glycol)-block-polyions. *Journal of Controlled Release* **2011,** *156* (2), 118-127.
192. Szwarc, M., Living polymers. Their discovery, characterization, and properties. *Journal of Polymer Science Part A: Polymer Chemistry* **1998,** *36* (1), IX-XV.
193. Graeme, M., RAFT Polymerization ? Then and Now. In *Controlled Radical Polymerization: Mechanisms*, American Chemical Society: 2015; Vol. 1187, pp 211-246.
194. Matyjaszewski, K.; Tsarevsky, N. V., Nanostructured functional materials prepared by atom transfer radical polymerization. *Nat Chem* **2009,** *1* (4), 276-288.
195. Pothayee, N.; Pothayee, N.; Jain, N.; Hu, N.; Balasubramaniam, S.; Johnson, L. M.; Davis, R. M.; Sriranganathan, N.; Riffle, J. S., Magnetic Block Ionomer Complexes for Potential Dual Imaging and Therapeutic Agents. *Chemistry of Materials* **2012,** *24* (11), 2056-2063.
196. Vestal, C. R.; Zhang, Z. J., Atom Transfer Radical Polymerization Synthesis and Magnetic Characterization of MnFe2O4/Polystyrene Core/Shell Nanoparticles. *Journal of the American Chemical Society* **2002,** *124* (48), 14312-14313.
197. Krstina, J.; Moad, G.; Rizzardo, E.; Winzor, C. L.; Berge, C. T.; Fryd, M., Narrow Polydispersity Block Copolymers by Free-Radical Polymerization in the Presence of Macromonomers. *Macromolecules* **1995,** *28* (15), 5381-5385.
198. Chiefari, J.; Chong, Y. K.; Ercole, F.; Krstina, J.; Jeffery, J.; Le, T. P. T.; Mayadunne, R. T. A.; Meijs, G. F.; Moad, C. L.; Moad, G.; Rizzardo, E.; Thang, S. H., Living Free-Radical Polymerization by Reversible Addition−Fragmentation Chain Transfer: The RAFT Process. *Macromolecules* **1998,** *31* (16), 5559-5562.
199. Li, Y.; Lokitz, B. S.; McCormick, C. L., Thermally Responsive Vesicles and Their Structural "Locking" through Polyelectrolyte Complex Formation. *Angewandte Chemie International Edition* **2006,** *45* (35), 5792-5795.
200. Donovan, M. S.; Lowe, A. B.; Sanford, T. A.; McCormick, C. L., Sulfobetaine-containing diblock and triblock copolymers via reversible addition-fragmentation chain transfer polymerization in aqueous media. *Journal of Polymer Science Part A: Polymer Chemistry* **2003,** *41* (9), 1262-1281.

201. Pai, T. S. C.; Barner-Kowollik, C.; Davis, T. P.; Stenzel, M. H., Synthesis of amphiphilic block copolymers based on poly(dimethylsiloxane) via fragmentation chain transfer (RAFT) polymerization. *Polymer* **2004,** *45* (13), 4383-4389.
202. Paul, S., Manufacture of amines of high molecular weight, which are rich in nitrogen. Google Patents: 1938.
203. Nuyken, O.; Pask, S., Ring-Opening Polymerization—An Introductory Review. *Polymers* **2013,** *5* (2), 361.
204. Kayandan, S. Synthesis and Characterization of Poly (lactide) Functional Oligomers and Block Copolymers. Virginia Tech, 2013.
205. Libiszowski, J.; Kowalski, A.; Duda, A.; Penczek, S., Kinetics and mechanism of cyclic esters polymerization initiated with covalent metal carboxylates, 5. End-group studies in the model ε-caprolactone and L,L-dilactide/Tin(II) and zinc octoate/butyl alcohol systems. *Macromolecular Chemistry and Physics* **2002,** *203* (10-11), 1694-1701.
206. Kowalski, A.; Libiszowski, J.; Biela, T.; Cypryk, M.; Duda, A.; Penczek, S., Kinetics and Mechanism of Cyclic Esters Polymerization Initiated with Tin(II) Octoate. Polymerization of ε-Caprolactone and l,l-Lactide Co-initiated with Primary Amines. *Macromolecules* **2005,** *38* (20), 8170-8176.
207. Jeon, S. I.; Lee, J. H.; Andrade, J. D.; De Gennes, P. G., Protein—surface interactions in the presence of polyethylene oxide. *Journal of Colloid and Interface Science* **1991,** *142* (1), 149-158.
208. Yang, Z.; Tang, W.; Luo, X.; Zhang, X.; Zhang, C.; Li, H.; Gao, D.; Luo, H.; Jiang, Q.; Liu, J., Dual-Ligand Modified Polymer-Lipid Hybrid Nanoparticles for Docetaxel Targeting Delivery to Her2/neu Overexpressed Human Breast Cancer Cells. *Journal of Biomedical Nanotechnology* **2015,** *11* (8), 1401-1417.
209. Bennadja, Y.; Beaunier, P.; Margolese, D.; Davidson, A., Fine tuning of the interaction between Pluronic surfactants and silica walls in SBA-15 nanostructured materials. *Microporous and Mesoporous Materials* **2001,** *44–45*, 147-152.
210. Černigoj, U.; Štangar, U. L.; Trebše, P.; Krašovec, U. O.; Gross, S., Photocatalytically active TiO 2 thin films produced by surfactant-assisted sol–gel processing. *Thin Solid Films* **2006,** *495* (1), 327-332.
211. Lu, Y., Surfactant‐Templated Mesoporous Materials: From Inorganic to Hybrid to Organic. *Angewandte Chemie International Edition* **2006,** *45* (46), 7664-7667.
212. Park, T. G.; Cohen, S.; Langer, R., Poly (L-lactic acid)/pluronic blends: characterization of phase separation behavior, degradation, and morphology and use as protein-releasing matrixes. *Macromolecules* **1992,** *25* (1), 116-122.
213. Zhao, X.; Ma, X.; Sun, J.; Li, D.; Yang, X., Enhanced Catalytic Activities of Surfactant-Assisted Exfoliated WS2 Nanodots for Hydrogen Evolution. *ACS Nano* **2016**.
214. Batrakova, E. V.; Dorodnych, T. Y.; Klinskii, E. Y.; Kliushnenkova, E. N.; Shemchukova, O. B.; Goncharova, O. N.; Arjakov, S. A.; Alakhov, V. Y.; Kabanov, A. V., Anthracycline antibiotics non-covalently incorporated into the block copolymer micelles: in vivo evaluation of anti-cancer activity. *British Journal of Cancer* **1996,** *74* (10), 1545-1552.
215. Shaik, N.; Giri, N.; Elmquist, W. F., Investigation of the micellar effect of pluronic P85 on P‐glycoprotein inhibition: Cell accumulation and equilibrium dialysis studies. *Journal of pharmaceutical sciences* **2009,** *98* (11), 4170-4190.
216. Kabanov, A. V.; Batrakova, E. V.; Miller, D. W., Pluronic® block copolymers as modulators of drug efflux transporter activity in the blood–brain barrier. *Advanced Drug Delivery Reviews* **2003,** *55* (1), 151-164.

217. Sun, J.-j.; Xie, L.; Liu, X.-d., Transport of carbamazepine and drug interactions at blood-brain barrier. *Acta Pharmacologica Sinica* **2006,** *27* (2), 249.
218. Azad, T. D.; Pan, J.; Connolly, I. D.; Remington, A.; Wilson, C. M.; Grant, G. A., Therapeutic strategies to improve drug delivery across the blood-brain barrier. *Neurosurgical focus* **2015,** *38* (3), E9.
219. Bhaskar, S.; Tian, F.; Stoeger, T.; Kreyling, W.; de la Fuente, J. M.; Grazú, V.; Borm, P.; Estrada, G.; Ntziachristos, V.; Razansky, D., Multifunctional Nanocarriers for diagnostics, drug delivery and targeted treatment across blood-brain barrier: perspectives on tracking and neuroimaging. *Particle and Fibre Toxicology* **2010,** *7* (1), 1-25.
220. Shen, J.; Sun, H.; Xu, P.; Yin, Q.; Zhang, Z.; Wang, S.; Yu, H.; Li, Y., Simultaneous inhibition of metastasis and growth of breast cancer by co-delivery of twist shRNA and paclitaxel using pluronic P85-PEI/TPGS complex nanoparticles. *Biomaterials* **2013,** *34* (5), 1581-1590.
221. Schneider, C. A.; Rasband, W. S.; Eliceiri, K. W., NIH Image to ImageJ: 25 years of image analysis. *Nat. Methods* **2012,** *9*, 671.
222. Dorati, R.; Colonna, C.; Tomasi, C.; Genta, I.; Bruni, G.; Conti, B., Design of 3D scaffolds for tissue engineering testing a tough polylactide-based graft copolymer. *Materials Science and Engineering: C* **2014,** *34*, 130-139.
223. Lopes, M. S.; Jardini, A.; Maciel Filho, R., Poly (lactic acid) production for tissue engineering applications. *Procedia Engineering* **2012,** *42*, 1402-1413.
224. Sakai, R.; John, B.; Okamoto, M.; Seppälä, J. V.; Vaithilingam, J.; Hussein, H.; Goodridge, R., Fabrication of polylactide ‐ based biodegradable thermoset scaffolds for tissue engineering applications. *Macromolecular materials and engineering* **2013,** *298* (1), 45-52.
225. Hutmacher, D. W., Scaffold design and fabrication technologies for engineering tissues—state of the art and future perspectives. *Journal of Biomaterials Science, Polymer Edition* **2001,** *12* (1), 107-124.
226. Kissel, T.; Li, Y.; Unger, F., ABA-triblock copolymers from biodegradable polyester A-blocks and hydrophilic poly(ethylene oxide) B-blocks as a candidate for in situ forming hydrogel delivery systems for proteins. *Advanced Drug Delivery Reviews* **2002,** *54* (1), 99-134.
227. Xue, Y.-N.; Huang, Z.-Z.; Zhang, J.-T.; Liu, M.; Zhang, M.; Huang, S.-W.; Zhuo, R.-X., Synthesis and self-assembly of amphiphilic poly(acrylic acid-b-dl-lactide) to form micelles for pH-responsive drug delivery. *Polymer* **2009,** *50* (15), 3706-3713.
228. Cheng, J.; Teply, B. A.; Sherifi, I.; Sung, J.; Luther, G.; Gu, F. X.; Levy-Nissenbaum, E.; Radovic-Moreno, A. F.; Langer, R.; Farokhzad, O. C., Formulation of functionalized PLGA–PEG nanoparticles for in vivo targeted drug delivery. *Biomaterials* **2007,** *28* (5), 869-876.
229. Chen, S.; Zhang, X.-Z.; Cheng, S.-X.; Zhuo, R.-X.; Gu, Z.-W., Functionalized amphiphilic hyperbranched polymers for targeted drug delivery. *Biomacromolecules* **2008,** *9* (10), 2578-2585.
230. Allen, C.; Yu, Y.; Maysinger, D.; Eisenberg, A., Polycaprolactone-b-poly (ethylene oxide) block copolymer micelles as a novel drug delivery vehicle for neurotrophic agents FK506 and L-685,818. *Bioconjugate Chemistry* **1998,** *9* (5), 564-572.
231. Kweon, H.; Yoo, M. K.; Park, I. K.; Kim, T. H.; Lee, H. C.; Lee, H.-S.; Oh, J.-S.; Akaike, T.; Cho, C.-S., A novel degradable polycaprolactone networks for tissue engineering. *Biomaterials* **2003,** *24* (5), 801-808.
232. Williams, J. M.; Adewunmi, A.; Schek, R. M.; Flanagan, C. L.; Krebsbach, P. H.; Feinberg, S. E.; Hollister, S. J.; Das, S., Bone tissue engineering using polycaprolactone scaffolds fabricated via selective laser sintering. *Biomaterials* **2005,** *26* (23), 4817-4827.

233. Dash, T. K.; Konkimalla, V. B., Poly-ϵ-caprolactone based formulations for drug delivery and tissue engineering: A review. *Journal of Controlled Release* **2012,** *158* (1), 15-33.
234. Woodruff, M. A.; Hutmacher, D. W., The return of a forgotten polymer—Polycaprolactone in the 21st century. *Progress in Polymer Science* **2010,** *35* (10), 1217-1256.
235. Allen, C.; Yu, Y.; Maysinger, D.; Eisenberg, A., Polycaprolactone-b-poly(ethylene Oxide) Block Copolymer Micelles as a Novel Drug Delivery Vehicle for Neurotrophic Agents FK506 and L-685,818. *Bioconjugate Chemistry* **1998,** *9* (5), 564-572.

Chapter 3: Preparation of Sub-Micron High-Performance Polyetherimide Particles for Fabricating Carbon Fiber Reinforced Polymer Composites

3.1 Abstract

The fabrication of high-performance polymer - carbon fiber composites have attracted a great deal of research, industrial and government interest. In this study, high-performance polyetherimide particles in sub-micron sizes were prepared by two different methods - a nucleation and growth process, and a homogenization - solvent evaporation approach. Two thermally stable suspending agents were synthesized and utilized for particle fabrication. Carbon fibers from both poly(acrylonitrile) and pitch precursors were treated with ozone to form hydroxyl groups on their surfaces, then reacted with a cyclic azasilane to afford surface-tethered amino groups. The polyetherimide particles were subsequently coated onto the carbon fibers. The untreated and functionalized carbon fibers were studied using scanning electron microscopy and X-ray photoelectron spectroscopy. The results indicated that high-performance polyetherimide particles may be fabricated and dispersed in aqueous dispersions, and that such particles can be incorporated in carbon fiber - polymer composites.

3.2 Introduction

Carbon fiber reinforced polymer composites are extensively used in a multitude of applications due to their high strength-to-weight ratio, excellent mechanical properties, and thermal stability.[1-2] Their properties make them excellent material candidates for a wide array of applications in the automotive, aerospace and marine industries.[3-6] The manufacturing processes and materials that are

used to produce the composites vary significantly, thus allowing for properties to be tailored for specific applications and environments.[7]

Carbon fiber reinforced polymer matrix composites are usually comprised of either chopped (short) or continuous fibers held together by the polymer. The matrix consists of a thermosetting or thermoplastic polymer, with each material type providing its own unique advantages.[5] Epoxy resins, which are examples of thermosetting polymers, are one of the most widely used classes of matrices.[2] There is continued interest in using high-performance thermoplastic polymers as alternatives to thermosets as the matrix phase for various composite applications.[8] This is largely due to the potential for rapid processing of thermoplastic materials, improved fracture toughness, and reduction in labor requirements.[9] Common high-performance polymers used in these applications include polyetherimide (PEI) and polyetheretherketone (PEEK).[8] These thermoplastic materials allow for relatively high continuous operating temperatures while maintaining mechanical properties, thus making them potential alternatives for thermosetting matrices.[10-11]

Several production methods are utilized for manufacturing carbon fiber reinforced thermoplastic materials, which include processing the polymers in hot melt, solution, suspension, and dry powder forms.[12-16] Powder coating with thermoplastic materials is of great interest, especially if one could utilize sub-micron particles that may allow for high carbon fiber volume fractions (>60%) while maintaining a uniform dispersion of the two phases in the composites.[12] Hot melt and solution prepregs are also widely used to make such fiber-polymer composites.[16-19] Both thermoplastic and thermosetting polymers may be used in such methods with tetrahydrofuran (THF) and (NMP) as examples of solvents for solution prepregs.[18] Suspension prepregs also have potential as these may be produced from polymer particles in aqueous suspensions that contain suspension stabilizers such

as poly(amic acid) ammonium salts.[15] By using environmentally-friendly water instead of expensive, high-boiling solvents such as NMP, suspension prepregs would have significant cost advantages.

Numerous processes could potentially produce thermoplastic particles, but the current commercial process is to physically grind particles to reduce their sizes. Thermoplastic particles for fiber composite applications could potentially be applied to the fibers in a dry powder form or from an aqueous dispersion.[18, 20] Particles dispersed in a liquid require a steric or electrostatic suspension stabilizer or emulsifier to coat the particle surfaces and improve the suspension stability. It is reasoned that the stability of the suspension could greatly influence the fiber coating process. Suspension stabilizers for dispersing thermoplastic particles in water have been previously investigated by a number of researchers. Giraud et al. studied the influence of various suspending agents and compositions in an "emulsion-solvent evaporation" process for producing thermoplastic nanoparticles.[21] Sodium dodecyl sulfate and benzalkonium chloride agents were investigated in various concentrations, and the resulting particle sizes and suspension stabilities were determined. The authors investigated optimal conditions and parameters for producing PEI nanoparticles that would provide maximum interfacial coverage of the PEI on the carbon fibers. The suspension stabilizers introduced variations as they were inherently located at the interface of the matrix and reinforcing fibers.[15] A recent study by Cheng et al. reported the benefits of using surfactants as compatibilizers for polymer composite systems. They analyzed the influence of sodium dodecyl sulfate (SDS) and sodium dodecylbenzene sulfonate as compatibilizers on multi-walled carbon nanotube/polypropylene composites.[22] The results indicated that the surfactants improved dispersion of the multi-walled carbon nanotubes in the polypropylene matrix and increased the mechanical properties of the composites. However, thermogravimetric analysis of the surfactants indicated the low-temperature degradation of these components which may result in decreased mechanical

properties if their composites are used continuously at high temperatures.[22] Chai et al. reported the preparation of several amorphous polymer microspheres from solutions using poly(vinyl alcohol) (PVA) as the suspension stabilizer.[23] The polymers included polyimide, PEI, poly(ether ketone), poly(phenylene oxide), polysulfone, and poly(vinylidene fluoride). The polymer concentrations, PVA concentrations, stirring speed, and precipitation temperature were varied to optimize conditions for fabricating microspheres with narrow size distributions.[23]

We have previously reported uniform sub-micron polyimide particles prepared by a solution nucleation and growth process.[24] Each of two polyimides were dissolved in a mixed homogeneous solvent comprised of water and NMP at 80-90 °C, and sub-micron polymer particles with narrow size distributions were obtained by controlling the cooling rate down through the cloud point where the system evolved from a homogeneous state to a final phase-separated (precipitated) state.[24]

Herein, we present two methods - a nucleation and growth process, and a homogenization - solvent evaporation process, for fabricating sub-micron high-performance polyetherimide particles. Poly(vinyl alcohol) was used in the nucleation and growth process and was removed after formation of the particles to preserve the thermal stability of the polyetherimide. By contrast, thermally-stable poly(amic acid) salts and sulfonated polyimide suspension stabilizers were synthesized and incorporated into the homogenization – solvent evaporation particle fabrication process. Controlled experiments were conducted to optimize the reagent ratios and reaction conditions to obtain particles with desirable sizes and narrow size distributions. Both the homogenization - solvent evaporation and nucleation and growth processes demonstrated the capability of producing stable aqueous suspensions of PEI particles with small particle sizes and relatively tight particle size distributions. The homogenization method has potential advantages including excellent scalability, and thus it may be the preferred method for large-scale fabrication of such particles. Moreover, the particles were

coated onto poly(acrylonitrile)-based and pitch-based carbon fibers. This demonstrated their potential for composite fabrication and other coating applications.

3.3 Experimental

3.3.1 Materials

Triethylamine (TEA, 99.5%), poly(vinyl alcohol) (PVA, average MW 85,000-124,000, 87-89% hydrolyzed), sodium dodecyl sulfate (SDS, ACS reagent, ≥99.0%), and *N*,*N*-dimethylethanolamine (Purum, ≥98%) were purchased from Sigma Aldrich and used as received. Pluronic® F68 was purchased from BASF. *N*-(2-aminoethyl)-2,2,4-trimethyl-1-aza-2-silacyclopentane was purchased from Gelest and used as received. Dimethylacetamide (DMAc, 99.5%, HPLC grade), 1,2-dichlorobenzene (*o*-DCB, HPLC grade, 98% min), and potassium carbonate were purchased from Alfa Aesar. DMAc and *o*-DCB were dried with calcium hydride (95%, Sigma Aldrich) and phosphorus pentoxide (Acros), respectively, and distilled under vacuum prior to use. *N*-methylpyrrolidone (NMP, ≥99.9%), isopropanol (HPLC grade, ≥99.9%), dichloromethane (DCM, 99.9%), and chloroform (99.99%) were purchased from Fisher Chemical. NMP and dichloromethane were dried with calcium hydride and phosphorus pentoxide and distilled prior to use. Ethanol (200 proof) was purchased from Decon Labs. 3-Aminophenol (*m*-AP, 99%) was purchased from Acros and recrystallized in toluene prior to use. 4,4'-Dichlorodiphenylsulfone-3,3'-disulfonic acid disodium salt (SDCDPS, 99%) was purchased from Akron Polymer Systems. Ultem dianhydride (4,4'-(4,4'-isopropylidene-diphenoxy)bis(phthalic anhydride)) was graciously provided by SABIC. Ultem dianhydride and phthalic anhydride (ACS reagent, ≥ 99%, Sigma-Aldrich) were dried under vacuum at 150 °C, and *m*-phenylenediamine (99%, Sigma-Aldrich) was dried at room temperature under vacuum prior to use. Polyetherimide powders and pellets (PEI, Ultem 1000 Natural) were purchased

from SABIC. Anhydrous toluene (EMD Chemicals, 99.8%) was dried over Na_2SO_4 for 2 h and over CaH_2 overnight, then distilled and stored over activated 3 Å molecular sieves. PAN-based IM7 and pitch-based carbon fibers were provided by the collaborators.

3.3.2 Synthesis of suspending agents - sulfonated polyimide

3.3.2.1 Synthesis of Bis(4,4'-m-aminophenoxy)-3,3'-disulfonate diphenylsulfone monomer (1)

A typical procedure for the synthesis of the disulfonated monomer (1) is provided. *m*-Aminophenol (*m*-AP, 10 g, 0.092 mol), distilled NMP (90 mL), K_2CO_3 (16.46 g, 0.119 mol), and dry toluene (41 mL) were added to a 250-mL, 3-neck round bottom flask equipped with a mechanical stirrer, Dean-Stark trap, condenser, and N_2 inlet. The mixture was stirred for 4-5 h at 145 °C to azeotrope water. The trap was drained and the excess toluene was removed. SDCDPS (15 g, 0.0305 mol) and distilled NMP (35 mL) were added to the reaction flask. The temperature was increased to 170 °C and the solution was stirred for 24 h. The solution was filtered hot to remove the K_2CO_3 and then precipitated in ethyl acetate. A light brown precipitate formed that was stirred in ethyl acetate overnight. The product was dried under vacuum at 120 °C overnight. >95% yield. 100% disulfonated material was obtained.

3.3.2.2 Synthesis of disulfonated Ultem polyimide with a dimethylethanolammonium counterion

The disulfonated polyimides (s-PISalts) were synthesized via an ester-acid method. Ultem dianhydride (2 g, 3.84 mmol), EtOH (20 mL), and TEA (3 mL) were added to a 100-mL, 3-neck round bottom flask equipped with a condenser and N_2 inlet. The mixture was stirred at reflux until the dianhydride dissolved. Excess EtOH was distilled into a Dean-Stark trap. Once all the EtOH was removed, a viscous liquid remained (the ester-acid). The disulfonated aminofunctional monomer (1) (2.57 g, 3.84 mmol) was added to the reaction flask with distilled NMP (19 mL) and *o*-DCB (5 mL). The reaction temperature was increased to 185 °C and the reaction was stirred for at least 24 h. The

solution was precipitated in a blender into IPA. The triethylammonium sPISalt was filtered and stirred in IPA overnight to remove any residual solvent, then filtered and dried under vacuum at 140 °C overnight. 90% recovered yield.

The disulfonated triethylammonium sPISalt (1.5 g) was added to a 50-mL, round bottom flask equipped with a magnetic stir bar and dissolved in 15 mL of NMP. DMEA (0.0378 mol, 3 mL) was added to the round bottom flask and stirred for at least 15 min. The TEA byproduct of the ion exchange was removed via rotary evaporation at 100 °C. The polymer was precipitated in excess IPA, filtered, and then washed with ethanol. The polymer was dried under vacuum at 160 °C. The dimethylethanolammonium sPISalt structure was confirmed via ^{1}H NMR.

3.3.3 Synthesis of suspending agents - poly(amic acid) salt with a dimethylethanol ammonium counterion

The monomer stoichiometry was adjusted to target a controlled molecular weight poly(amic acid). A procedure for the synthesis of a 20,000 g/mole M_n poly(amic acid) is provided. Ultem dianhydride (11.3804 g, 0.0224 mol) and phthalic anhydride (0.10925 g, 0.0007 mol) were added to a 250-mL, two-neck, round bottom flask equipped with a magnetic stir bar and a N_2 purge inlet. Anhydrous DMAc (70 mL) was added to the flask. The solution was stirred at room temperature and *m*-AP (2.5 g, 0.0231 mol) was added to the flask once a homogeneous solution was obtained. The solution was stirred for at least 12 h at room temperature. A stoichiometric amount of dimethylaminoethanol (5.519 g, 0.0582 mol) was added to the flask and allowed to react for 1 h. The solution of the dimethylethanolammonium PAASalt was stored under N_2.

3.3.4 Fabrication of sub-micron PEI particles by nucleation and growth

PEI powder (0.5 g) and PVA (0.17 g) were dissolved in DMAc (50 mL) at 80 °C in a 100-mL, round bottom flask. In a separate 250-mL, round bottom flask, de-ionized water (100 mL) was heated to 80 °C. The hot water was added to the DMAc solution dropwise while agitating with a mechanical stirrer at 80 °C. The mixture was sonicated at room temperature for 1 h, and stirred at room temperature overnight to afford a milky suspension. The suspension was centrifuged at 10 k rpm for 1 h. The supernatant was decanted, and the remaining solid was collected and re-dispersed in de-ionized water (~150 mL) and boiled for 1 h to remove PVA. Centrifugation was applied again at 10 k rpm for 1 h. After decantation, the precipitate was dried at room temperature under vacuum for 4 h and then at 140 °C overnight to afford sub-micron PEI particles. Yield: ≥ 94%.

A series of suspending agents were investigated to synthesize the sub-micron PEI particles by nucleation and growth. In addition to the PVA, these suspending agents included SDS, Pluronic® F68, PAASalt, and the sPISalt.

3.3.5 Fabrication of PEI particles by homogenization - solvent evaporation

3.3.5.1 Fabrication of PEI particles using the poly(amic acid) dimethylethanolammonium salt (PAASalt) as a suspending agent

PEI pellets (30 g) were dissolved in DCM (300 mL) in a 500-mL, round bottom flask at room temperature. A PAASalt with a molecular weight of ~20k M_n in DMAc (2.49 g of the solution, ~0.3 g of PAASalt) was diluted with de-ionized water (1200 mL) in a 5-L, round bottom flask at room temperature. The PEI organic solution was poured into the PAASalt DMAc/aqueous solution. The mixture was homogenized at 20 k rpm for 10 min in a closed system. The mixture was distilled for 1 h to remove the DCM. The particle suspension was kept for further experiments.

3.3.5.2 Synthesis of PEI particles using a sulfonated polyimide dimethylethanolammonium salt (sPISalt) as a suspending agent

A procedure for fabricating PEI particles using the sulfonated polyimide dimethylethanolammonium salt (s-PISalt) as the suspending agent is provided. PEI pellets (5 g) were dissolved in DCM (50 mL). The sPISalt suspending agent (0.2 g) was dissolved in DMAc (5 mL) and the solution was added to a 3-neck, round bottom flask containing DI water (200 mL). The PEI/DCM solution was added to the round bottom flask and the mixture was homogenized for 5 min. The solvent was removed by distillation, producing a milky, white PEI particle suspension. The particles were used directly without drying.

3.3.6 Carbon fiber coating with PEI particles

3.3.6.1 Coating PEI nanoparticles onto carbon fibers without any functionalization

Polyacrylonitrile (PAN)-based or pitch-based fibers (10 mg) were charged into scintillation vials and soaked in an aqueous PEI-PAASalt dispersion (10 mL of water containing ~10.6 mg of PEI nanoparticles coated with the PAASalt) with sonication for 10 min at room temperature. The liquid was decanted and the fibers were dried under vacuum at room temperature overnight. Experiments with higher amounts of carbon fibers and with the same reagent ratios and reaction conditions were also conducted, and the uptake of PEI particles was determined gravimetrically.

3.3.6.2 Functionalization of carbon fibers with ozone and a cyclic azasilane coupling agent

PAN-based or pitch-based carbon fibers were treated with ozone at a concentration of ~4500 ppm for 3 h at 70 °C. In a cyclic azasilane coupling experiment, either PAN-based or pitch-based carbon fibers (2 g) were dried under vacuum at 130 °C for 4 h, then charged to a flame-dried, nitrogen-filled, 100-mL, round bottom flask. A solution of *N*-(2-aminoethyl)-2,2,4-trimethyl-1-aza-2-

silacyclopentane (the cyclic azasilane, 40 mg) in DCM (20 mL) was charged into the flask containing the pre-weighed carbon fibers via syringe under N_2. The mixture was sonicated for 5 min. The mixture was heated to 80 °C and strong vacuum was applied for 1 h to remove the DCM and any excess cyclic azasilane coupling agent. The functionalized fibers were stored in a desiccator under N_2.

3.3.6.3 Coating PEI particles onto ozone treated carbon fibers

Aqueous PEI-PAASalt particle dispersions were freshly-prepared. Either PAN-based or pitch-based carbon fibers (2 g) with ozone treatment only, or with both ozone and azasilane treatment were charged to a 100-mL, round bottom flask. An aqueous PEI particle dispersion (20 mL of de-ionized water containing 2.12 g of PEI-PAASalt particles) was charged to the flask. The mixture was sonicated for 10 min at room temperature. The liquid was decanted and the PEI-coated fibers were dried at room temperature under vacuum overnight to obtain fibers with PEI particle coatings. The uptake of PEI particles was determined gravimetrically.

3.3.7 Characterization

3.3.7.1 Nuclear Magnetic Resonance (NMR)

^{1}H NMR spectroscopy was performed on an Agilent MR4 spectrometer operating at 400 MHz. The spectra were obtained from 20 % (w/v) 0.7 mL solutions in d_6-DMSO (s-PI and SDCDPS) or $CDCl_3$ (PEIs) using a 30 ° pulse angle, 5 s relaxation delay and 128 scans.

3.3.7.2 Scanning Electron Microscopy (SEM)

SEM was performed using a Phenom Pro operated at an accelerating voltage of 10 kV in high vacuum mode. SEM particle samples were prepared by evaporation of aqueous PEI suspensions onto double-sided carbon tape attached to an SEM pedestal, then dried prior to measurements.

3.3.7.3 Dynamic Light Scattering (DLS)

Intensity average diameters were determined by DLS using a Zetasizer NanoZS (Malvern Instruments, Software v. 7.11) equipped with a 4.0 mW solid-state He-Ne laser (λ= 633 nm) at a scattering angle of 173° and at 25 ± 0.1 °C. DLS uses an algorithm based on Mie theory that converts time-varying scattering intensities to hydrodynamic diameters of particles in suspension. For DLS analysis, each of the PEI nanoparticle types were centrifuged, dried at 130 °C overnight, then dispersed in DI water at a concentration of 1 mg mL^{-1}. Each dispersion was sonicated for 3 min in a 75T VWR Ultra-sonicator (120 W, 45 kHz), then transferred into a polystyrene cuvette for analysis. All measurements were done in triplicate.

3.3.7.4 Size Exclusion Chromatography (SEC)

The molecular weights of the Ultem 1000 and two batches of the PEI particles by the nucleation and growth method that were isolated by the same procedure used for the DLS experiments were measured by SEC. The mobile phase was DMAc distilled from CaH_2 containing dry LiCl (0.1 M). The column set consisted of 3 Agilent PLgel 10-μm Mixed B-LS columns 300 × 7.5 mm (polystyrene/divinylbenzene) connected in series with a guard column having the same stationary phase. The columns and detectors were maintained at 50 °C. An isocratic pump (Agilent 1260 infinity, Agilent Technologies) with an online degasser (Agilent 1260), autosampler and column oven was used for mobile phase delivery and sample injection. A system of multiple detectors connected in series was used for the analyses. A multi-angle laser light scattering detector (DAWN-HELEOS II, Wyatt Technology Corp.), operating at a wavelength of 658 nm and a refractive index detector operating at a wavelength of 658 nm (Optilab T-rEX, Wyatt Technology Corp.) provided online results. The system was corrected for inter-detector delay and band broadening using a 21,000 g/mole polystyrene standard. Data acquisition and analysis were conducted using Astra 6 software from

Wyatt Technology Corp. Validation of the system was performed by monitoring the molar mass of a known molecular weight polystyrene sample by light scattering. The accepted variance of the 21,000 g/mole polystyrene standard was defined as 2 standard deviations (11.5% for M_n and 9% for M_w) derived from 34 runs. Specific refractive index values were calculated based on the assumption of 100% recovery.

3.3.7.5 Thermogravimetric analysis (TGA)

The thermal stability and degradation profiles of the PEI particles coated with PVA, PAASalt, and sPISalt suspending agents were measured using a TA Instruments Thermogravimetric Analyzer Q5000. The TGA was equipped with an autosampler and a nitrogen (ultra high purity) purge inlet.

3.3.7.6 X-ray photoelectron spectroscopy (XPS)

X-ray photoelectron spectroscopy was performed to evaluate the surface compositions of the untreated and treated carbon fibers. Specifically, C, N, O, and Si were measured. The instrument settings were as follows: Spectra were acquired using a monochromatic Al K-alpha X-ray source (1486.6 eV) at 100 W over a 1400 × 100 µm area at a 45° angle. Survey: 280 eV Pass Energy, 1.0 eV/step, 50 ms/step, 3 sweeps; C_{1s}: 26 eV Pass Energy, 0.1 eV/step, 50 ms/step, 6 sweeps; N_{1s}: 26 eV Pass Energy, 0.1 eV/step, 50 ms/step, 36 sweeps; O_{1s}: 26 eV Pass Energy, 0.1 eV/step, 50 ms/step, 6 sweeps; Si_{2p}: 26 eV Pass Energy, 0.1 eV/step, 50 ms/step, 18 sweeps. All binding energies were referenced to adventitious C-C at 284.8 eV. The chemical states of elements were assigned based on the PHI and NIST XPS Databases.

3.4 Results and discussion

Two particle fabrication processes were investigated to prepare sub-micron high-performance PEI particles and dispersions for producing carbon fiber reinforced polymer composites. The first

method, nucleation and growth, utilized DMAc as the solvent and PVA as the suspension stabilizer. The PEI particles nucleated and grew when water was slowly added as a non-solvent, and a stable suspension formed. In the homogenization - solvent evaporation method, two parts were prepared. The PEI was dissolved in a chlorinated solvent such as DCM, and a thermally stable suspension stabilizer such as PAASalt or sPISalt dissolved in DMAc was diluted with water. The two solutions were mixed, then homogenized at high speed to produce a dispersion of fine particles swollen by the organic solvent. The organic solvent was removed by distillation to afford a stable PEI particle suspension in water. The PAASalt-coated PEI particle dispersions were then utilized to coat both surface treated PAN and pitch-based carbon fibers.

3.4.1 Synthesis of suspending agents

PAASalts and sPISalts were synthesized to afford ionic suspending agents that could stabilize PEI particle dispersions in water. These ionic, polymeric suspending agents likely stabilized the particles in water by a combination of steric and electrostatic repulsion forces. Conventional suspending agents such as PVA were not sufficiently thermally stable to withstand the processing and use temperatures of the desired composite materials. Thus when PVA was employed in the particle fabrication process, it was necessary to remove it before using the particles for fabricating the composites. The PAASalt is an ionic intermediate to a polyimide, while the sPISalt is an ionic fully formed polyimide. A potential advantage of the sPISalt is that it should have better chemical stability in aqueous media relative to the PAASalt, and thus may provide improved chemical stability if the materials were to be stored in an aqueous medium for some time.

The disulfonated diamino-functional monomer (1) for the sPISalt was synthesized via a nucleophilic aromatic substitution reaction of the phenolate salt of *m*-aminophenol with sulfonated dichlorodiphenylsulfone (SDCDPS) as shown in Figure 3.1. ^{1}H NMR was used to confirm the

structure of the disulfonated diamine monomer and to ensure that complete substitution of the *m*-aminophenol onto the monomer was obtained (Figure 3.2). The aromatic amine peak, labeled A (5.25 ppm), was used as a reference set at 4.00. The peak labeled B (8.21 ppm) corresponds to the aromatic proton adjacent to the sulfonate group. Quantitative substitution to form the monomer was obtained as shown by the peak labeled B integrating to 2.

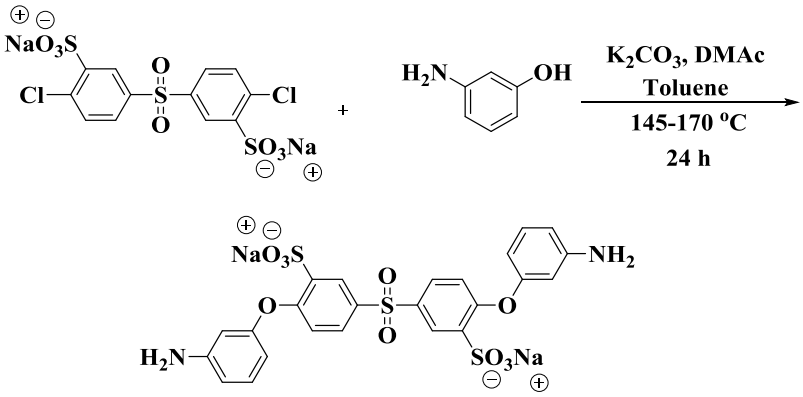

Figure 3.1 Synthesis of the disulfonated diamine monomer (1) for the sPISalt suspending agent.

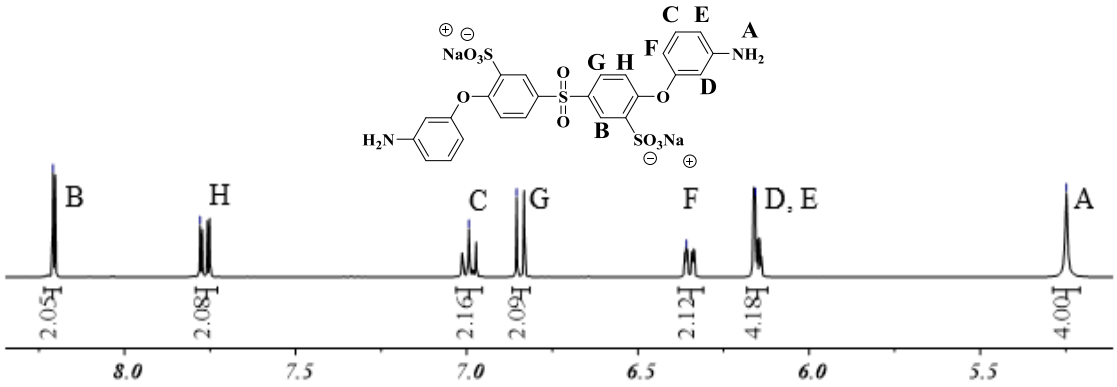

Figure 3.2 ^{1}H NMR of the disulfonated monomer (1).

The sPISalt with a high degree of sulfonation was synthesized in a one-pot, ester-acid solution polymerization method (Figure 3.3). The ester-acid monomer is less sensitive to moisture than the corresponding dianhydrides.[25] ^{1}H NMR was used to confirm the molecular structure of the polymer and confirm the expected degree of disulfonation along the polymer backbone (Figure 3.4). The

isopropylidene protons (1.68 ppm) were used as a reference with the integral set to 6. The degree of disulfonation was calculated using the integral of the peaks corresponding to the proton adjacent to the sulfonate group (8.26 ppm) divided by 2.

The triethylammonium counterion was exchanged with dimethylethanolamine to increase hydrophilicity and increase the boiling point of the corresponding tertiary amine to minimize volatilization during particle fabrication or storage. ^{1}H NMR shows the complete exchange of the triethylammonium counterion to the dimethylethanolammonium counterion (Figure 3.4).

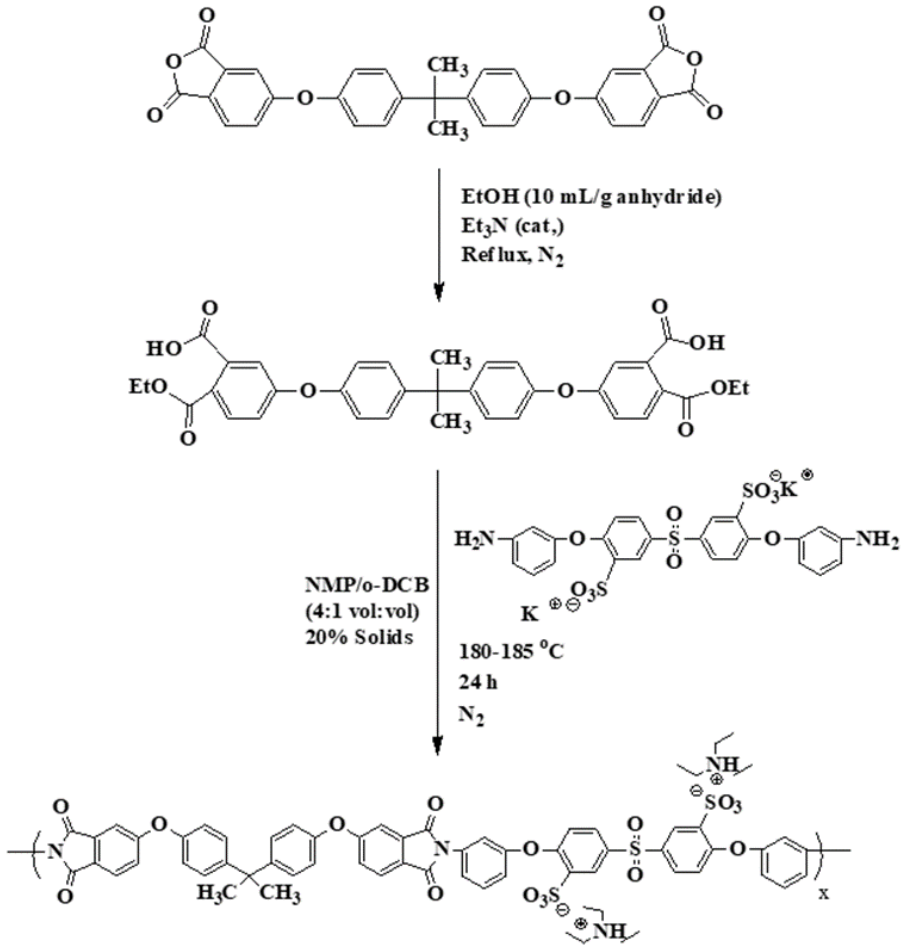

Figure 3.3 Synthesis of sPISalt via an ester-acid method.

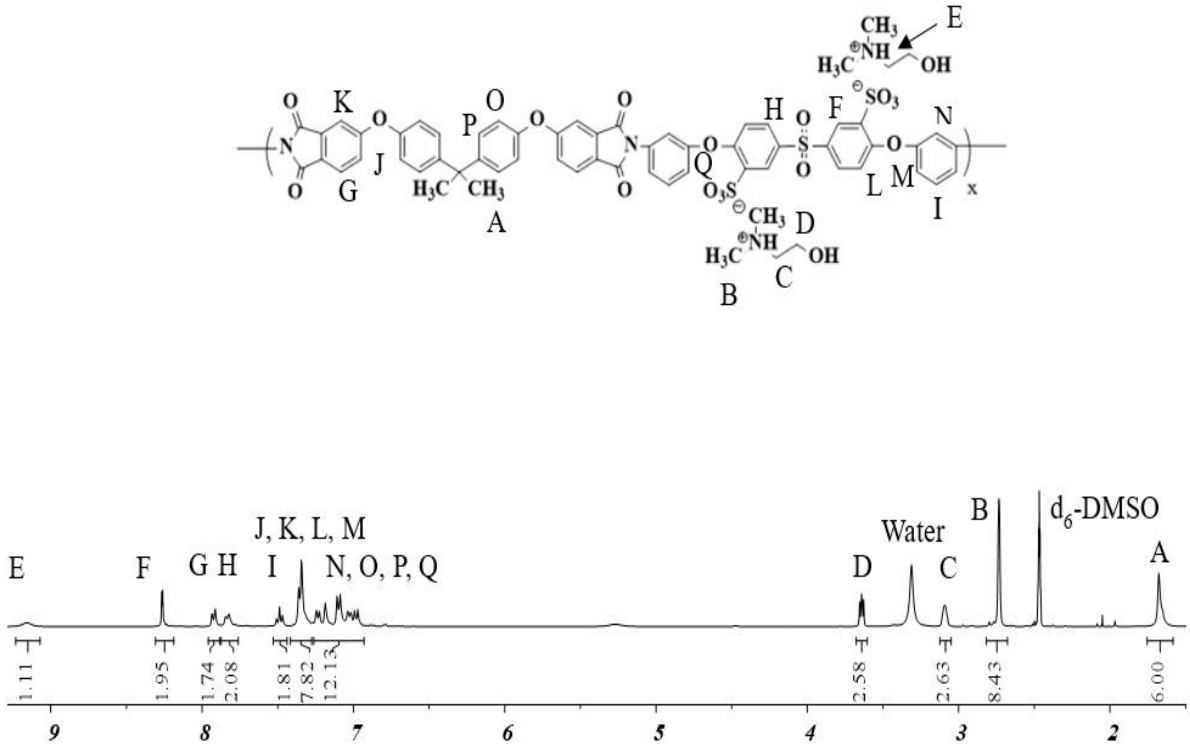

Figure 3.4 ^{1}H NMR of sPISalt with a dimethylethanolammonium counterion.

The PAASalt synthesis was conducted at room temperature with Ultem dianhydride and *m*-phenylenediamine as the co-monomers (Figure 3.5). The molecular weight was targeted by offsetting the stoichiometry of the dianhydride to diamine, with the diamine in excess. To convert the poly(amic acid) to the PAASalt, the carboxylic acid groups were reacted with a slight excess of DMEA (Figure 3.6). The conjugate base was expected to have a longer shelf life and better hydrolytic stability in comparison to the acid form.

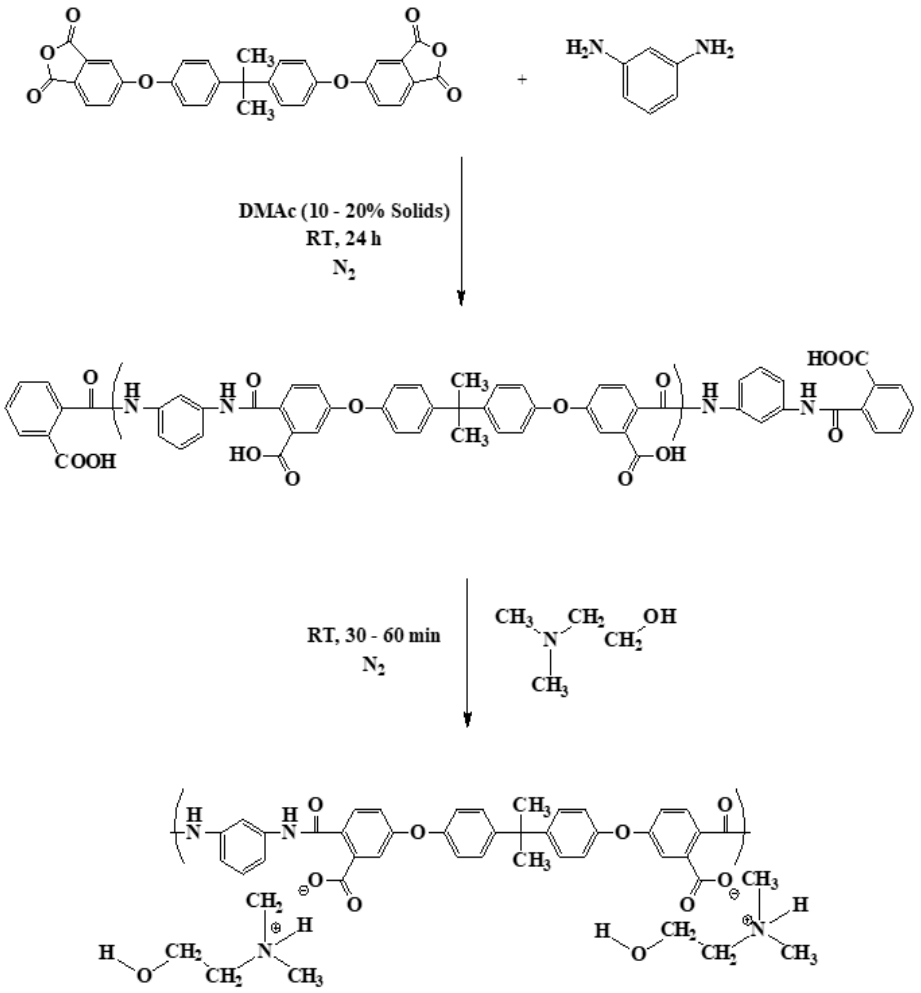

Figure 3.5 Synthesis of the PAASalt with a dimethylethanolammonium counterion.

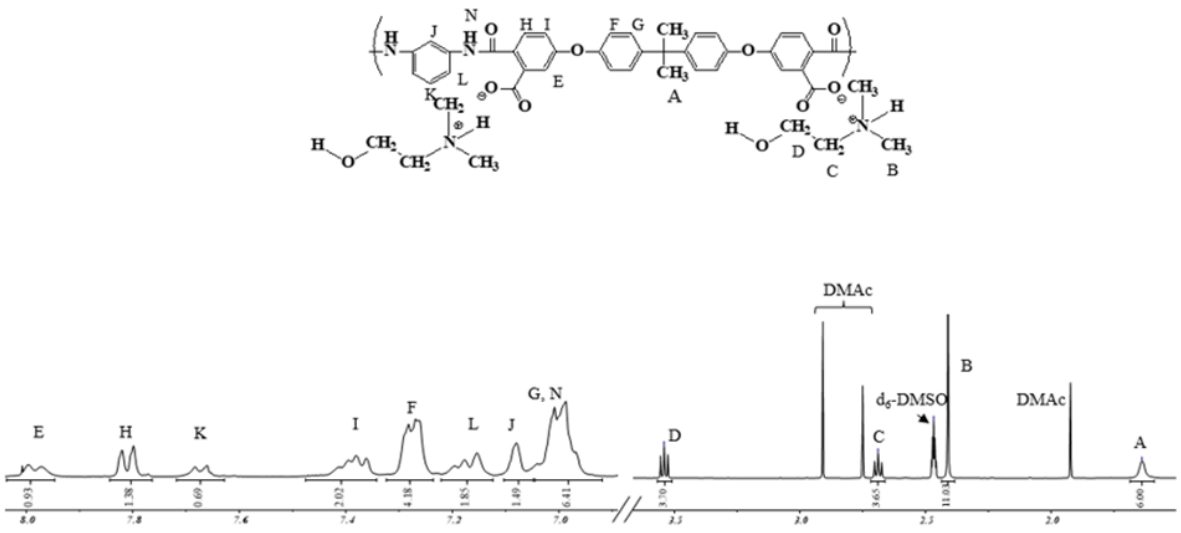

Figure 3.6 ^{1}H NMR of PAASalt with a dimethylethanolammonium counterion.

3.4.2 Fabrication of sub-micron PEI particles

3.4.2.1 Preparation and optimization of PEI particles by nucleation and growth

Sub-micron PEI particles were fabricated with PVA as a steric suspending agent in DMAc (solvent) by adding water (non-solvent). The solvent and non-solvent must be miscible so that the majority of the solvent is extracted in the precipitation process. Once the particles formed, the non-thermally stable PVA suspension stabilizer was removed. This was achieved by centrifugation followed by re-dispersing the particles and boiling in water. At least most of the PVA was removed, as determined by ^{1}H NMR (Figure 3.7). The boiled particles were centrifuged again and dried to afford the PEI particle solids. SEC results (Figure 3.8) of the dried particles showed the same molecular weight compared to the starting PEI, signaling that the nucleation and growth method had not altered the structure of the PEI, and the properties of the PEI were not compromised. SEM was utilized to evaluate the properties of the fabricated and dried particles (Figure 3.9A). It was found that the spherical particles had diameters of 420 ± 10 nm and a fairly narrow size distribution. The intensity

average diameters of the fabricated PEI particles were 792 nm with a polydispersity index of 0.18, as determined by DLS (Figure 3.10, curve A). Both DLS and SEM confirmed the success in the fabrication of fine sub-micron PEI particles. The thermal stability of the dried PEI particles were evaluated using TGA. The TGA degradation curve (Figure 3.11, curve A) showed an initial weight loss of ~2 wt% at around 300 °C. A possible explanation is that some amount of DMAc had become trapped in the PEI particles, and that the DMAc volatilized when the temperature surpassed the glass transition temperature of PEI. It is recommended that this aspect be further explored.

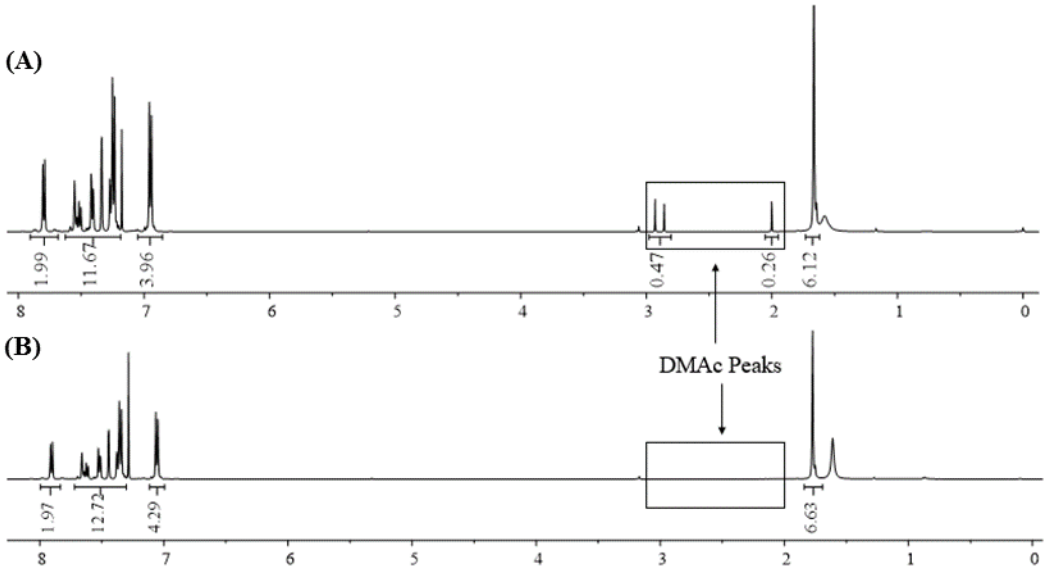

Figure 3.7 ^{1}H NMR of the fabricated PEI particles using nucleation and growth method and dried by different methods. (A: Dried by lyophilization at low temperature; B: Dried under vacuum at 140 °C)

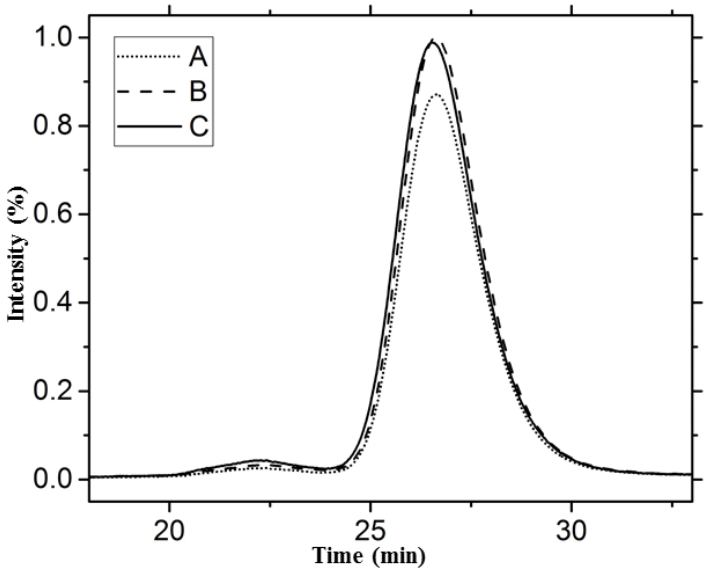

Figure 3.8 SEC light scattering curves from A) the PEI starting material, and B and C) Two batches of PEI after being fabricated into particles by the nucleation and growth method and re-dissolved.

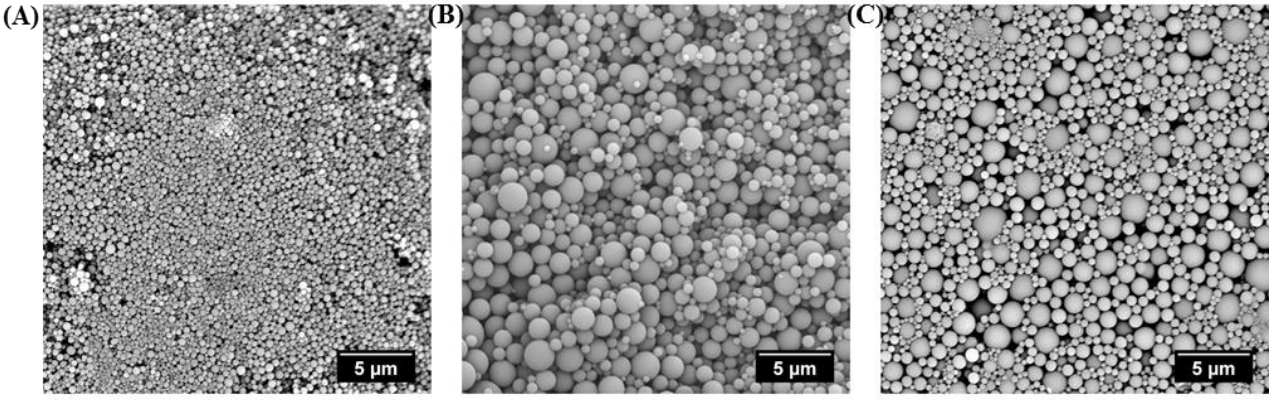

Figure 3.9 SEM images of (A) Nucleation and growth particles; (B) Homogenization – solvent evaporation particles coated with PAASalt; (C) Homogenization – solvent evaporation particles coated with s-PISalt.

Experiments were conducted to optimize the fabrication procedures for the sub-micron PEI particles by nucleation and growth. The variables are listed in Table 3.1. In one set of experiments, the aqueous solution addition rate was varied from 1.5 to 6 to 120 mL/min. The PEI particles had

similar sizes of ~ 1 μm in diameter and narrow size distributions. Thus, in this range, the rate of addition of the non-solvent does not affect the PEI particle sizes, so it does not appear that the properties will be sensitive to this upon scale-up. In another trial, the water to DMAc ratio ranging from 2:1 to 2:5 also did not change the particle size significantly, so the recommended amount of water relative to the DMAc was minimized at 2:5. Another important set of experiments was conducted with PEI concentrations in DMAc varied from 1-10 w/v %. Results showed that the concentration of PEI in DMAc could be as high as 5 w/v % (but not 10%), without compromising the small particle sizes. The concentration of PVA/PEI wt/wt was also investigated to tailor the viscosity of the DMAc solution for the fabrication process. It was found that at a ratio of 1:3, the particle sizes were in the sub-micron range, whereas with a higher amount of PVA (1:1), the particles were larger (a few microns in diameter) and the size distribution was broadened due to the higher viscosity of the mixture.

Table 3.1 Variables in control experiments in the nucleation and growth method.

PEI concentration (w/v)	1, 5, 10
PVA/PEI (wt/wt)	1:1, 1:3
DI-water/DMAc (vol/vol)	2:1, 1:1, 2:5
Addition rate of water (mL/min)	1.5, 6, 120

After particle nucleation with the addition of the non-solvent, it was necessary to stir the dispersion at room temperature overnight prior to isolation, to allow for the growth phase. If the particles are isolated immediately after adding the water, the size distributions became broad.

Various methods to isolate the PEI particles and to remove the PVA and DMAc were also assessed. The recommended procedure requires centrifuging to eliminate any excess PVA and most

of the DMAc remaining in solution, re-dispersion in water and boiling the dispersion to further remove impurities. A final drying step at 140 °C overnight under vacuum could also be used to remove residual high-boiling DMAc. By contrast, freeze-drying at low temperature was insufficient to remove residual DMAc (Figure 3.8).

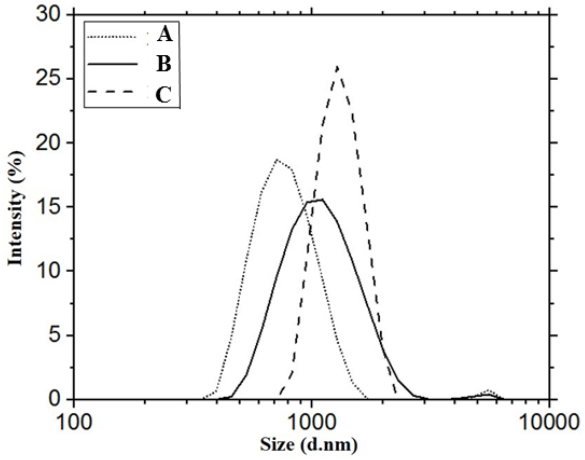

Figure 3.10 Sizes of the fabricated PEI particles after drying as measured by DLS. The dotted line (A) shows the smaller particles prepared by the nucleation and growth method. The solid (s-PISalt) (B) and dashed (PAASalt) (C) lines show particles prepared by the homogenization - solvent evaporation method.

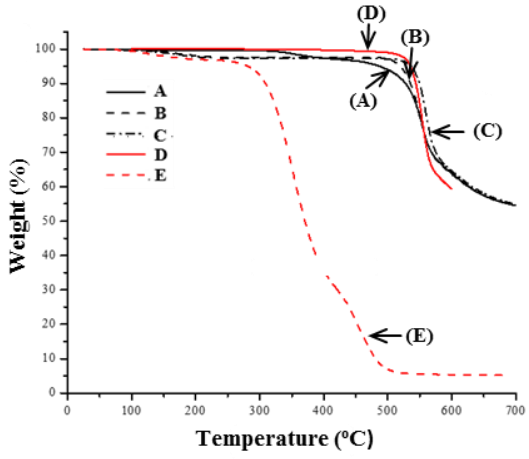

Figure 3.11 TGA degradation curve of the (A) particles prepared by the nucleation and growth method; (B) s-PISalt coated particles and (C) PAASalt coated particles prepared by homogenization - solvent evaporation method; (D) PEI and (E) PVA starting materials.

Although sub-micron PEI particles with narrow size distributions were successfully fabricated with high reproducibility using PVA as a suspension stabilizer by nucleation and growth, alternative suspension stabilizers including the thermally-stable PAASalt and sPISalt failed to generate particle dispersions because the PEI precipitated out as large agglomerates when water was added into the polymer solution. Thus, it was important to remove the PVA from the particles and solution to preserve the desired thermal stability that would be needed for fabricating high-performance composites. This requires isolation by methods such as centrifugation that may be difficult on a large scale.

3.4.2.2 Preparation and optimization of PEI particles by the homogenization - solvent evaporation method

The homogenization - solvent evaporation method involves preparing a solution of PEI in a chlorinated solvent such as chloroform or dichloromethane, dissolving the suspension stabilizer (PAASalt or s-PISalt) in DMAc and diluting it with water, then pouring the organic solution into the aqueous medium. High speed homogenization was applied to the two-phase mixture to disperse the organic phase containing the PEI in the water. Once the dispersion formed, DCM was distilled to leave PEI polymer particles coated with the suspension stabilizer dispersed in the aqueous phase. The particle sizes were larger with this method relative to the nucleation and growth method, and the size distribution was broader. The intensity average diameters of the PAASalt-coated and s-PISalt-coated PEI particles were 1.3 μm and 1.1 μm as measured by DLS (Figure 3.10, curves B and C). SEM micrographs (Figure 3.9B and C) showed that the PAASalt-coated PEI particles had diameters of

0.98±0.30 μm with the sizes ranging from 0.29 to 2.35 μm. The s-PISalt-coated PEI particles had diameters of 0.90±0.30 μm with sizes ranging from 0.20 to 2.15 μm. Their weight loss curves are also shown in Figure 3.11 (curves B and C) using TGA. It showed ~2.5% initial weight loss at around 140 °C. It might be attributable to a combination of the loss of DMEA from the suspending agents together with some loss of trapped DMAc in the particles.

It was speculated that the shear forces during homogenization, and the procedures and time for solvent removal would play an important role in determining particle sizes and size distributions. A series of experiments was conducted to optimize the fabrication process (Table 3.2).

Table 3.2 Variables in control experiments in the homogenization - solvent evaporation method.

Polymer concentration (w/v)	1, 5, 10, 20
DI-water/chloroform (vol/vol)	6.7:1, 4:1, 1:1
PAASalt/PEI (wt%)	1, 3, 10

The first set of experiments focused on the enhancing the PEI concentrations in chloroform to minimize the required volume of solvent while still maintaining a workable viscosity during fabrication. Experiments with 1, 5, 10, and 20% w/v of PEI in chloroform were conducted. It was found that at a concentration of 10%, particles could be fabricated with diameters of ~1 μm. When the concentration was raised to 20%, sediments precipitated during homogenization. The minimum amount of water that was required relative to the organic solvent (6.7:1, 4:1, and 1:1 vol/vol) was investigated. It was found that a water to an organic solvent ratio of 4:1 was able to generate uniform particles, whereas the 1:1 ratio did not. Experiments were also conducted to determine the approximate level of PAASalt suspending agent that was needed relative to PEI (1%, 3%, and 10%).

The particle sizes and distributions were minimally affected, which indicated that 1% of the PAASalt could be used. Different solvents were also explored. Solvents with lower boiling points such as dichloromethane (vs. chloroform) were preferred since they could be removed more easily.

A significant advantage of the homogenization - solvent evaporation method relative to the nucleation and growth method is that, the thermally-stable PAASalt and s-PISalt suspension stabilizers can be employed directly in this process without any PVA. This simplifies the isolation procedure substantially since there is no need to remove PVA. In addition, the low-boiling point DCM solvent used in this method is easier to remove than the polar aprotic solvent required in the nucleation and growth process. These advantages likely outweigh the positive effects of obtaining smaller particles with narrower size distributions using the nucleation and growth method.

3.4.3 PEI particle coating onto carbon fibers

The approach has been to attract the particles through multiple ionic interactions to the carbon fiber surfaces. The fibers were treated with ozone to produce hydroxyl-functional surfaces, then with a cyclic azasilane to yield amino-functional carbon fiber surfaces (Figure 3.12). The strategy for coupling PAASalt-coated PEI particles with amino-functional carbon fiber surfaces was to ion exchange the DMEA counterion on the PAASalt coating with ammonium ions on the carbon fibers (Figure 3.13). Thus, it was envisioned that electrostatic attractions between the ammonium-functional silanes on the fibers and the carboxylates or sulfonates on the particle surfaces would attract the particles to the fibers, even from dilute suspensions.

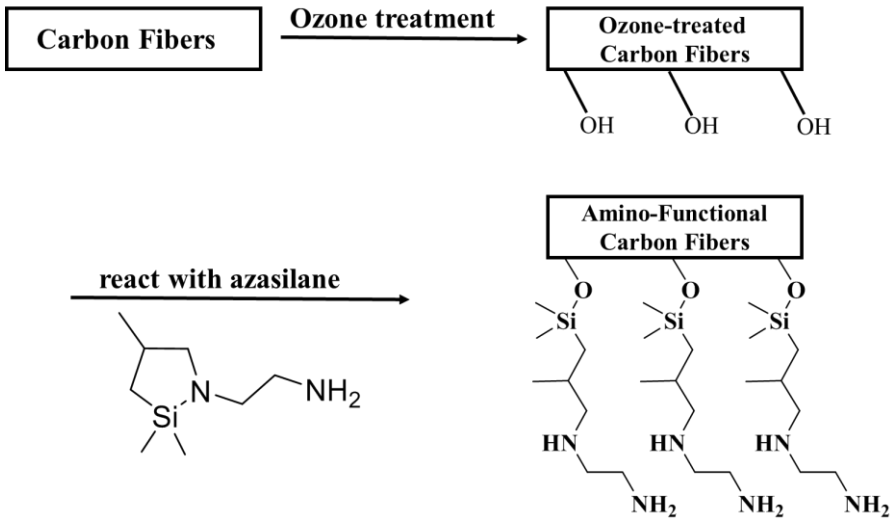

Figure 3.12 The mechanisms of ozone and the cyclic azasilane treatment.

Coating particles onto PAN-based or pitch-based carbon fibers with or without surface treatment was investigated from aqueous dispersions. SEM images of PAN-based and pitch-based carbon fibers with adhered particles are shown in Figure 3.14. The ozone and cyclic azasilane treated carbon fibers attracted significantly more PEI particles (Figure 3.14C and F), compared to fibers without any treatment (Figure 3.14A and D), or with ozone treatment only (Figure 3.14B and E). XPS results showed significantly increased atomic concentrations of Si on the ozone and cyclic azasilane treated carbon fibers. The atomic concentration % of Si was increased from 2.40 to 14.66 for the azasilane treated carbon fibers, which is a convincing indication that the ozone treatment and azasilane functionalization was successful. The coverage of the PAASalt coated particles onto the ammonium-functional fibers was significant (Figure 3.14C and F as well as G and H).

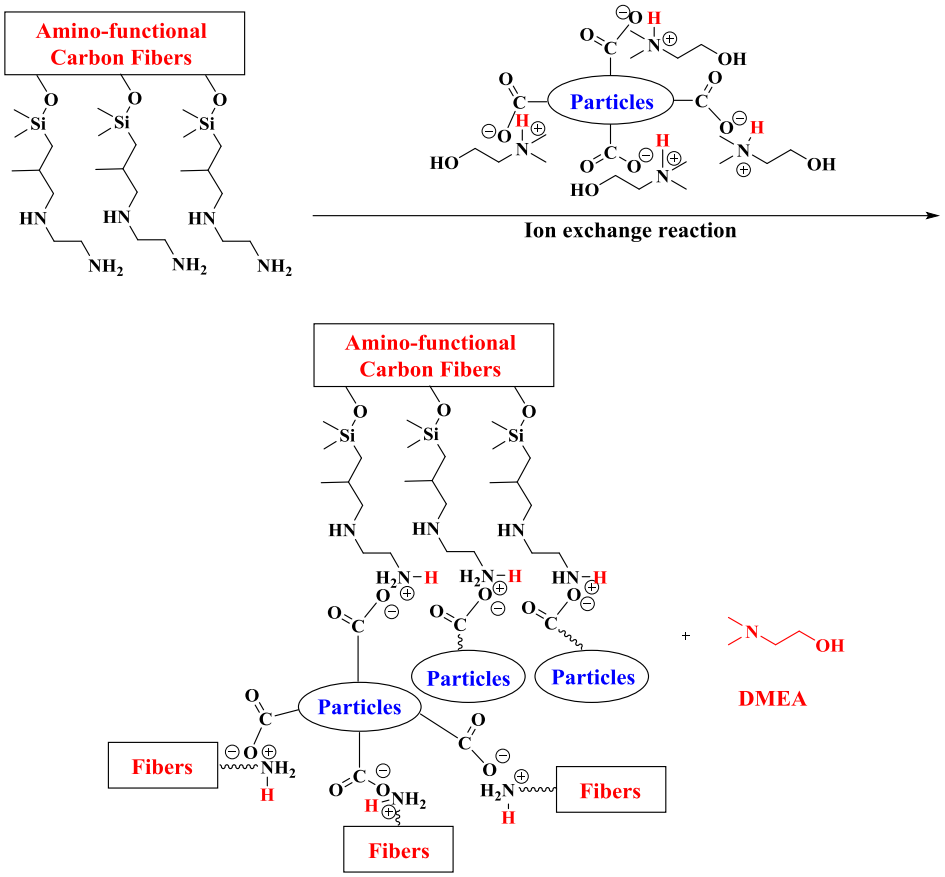

Figure 3.13 Proposed ion exchange reaction between the PAASalt coated PEI particles and the amino-functional carbon fibers.

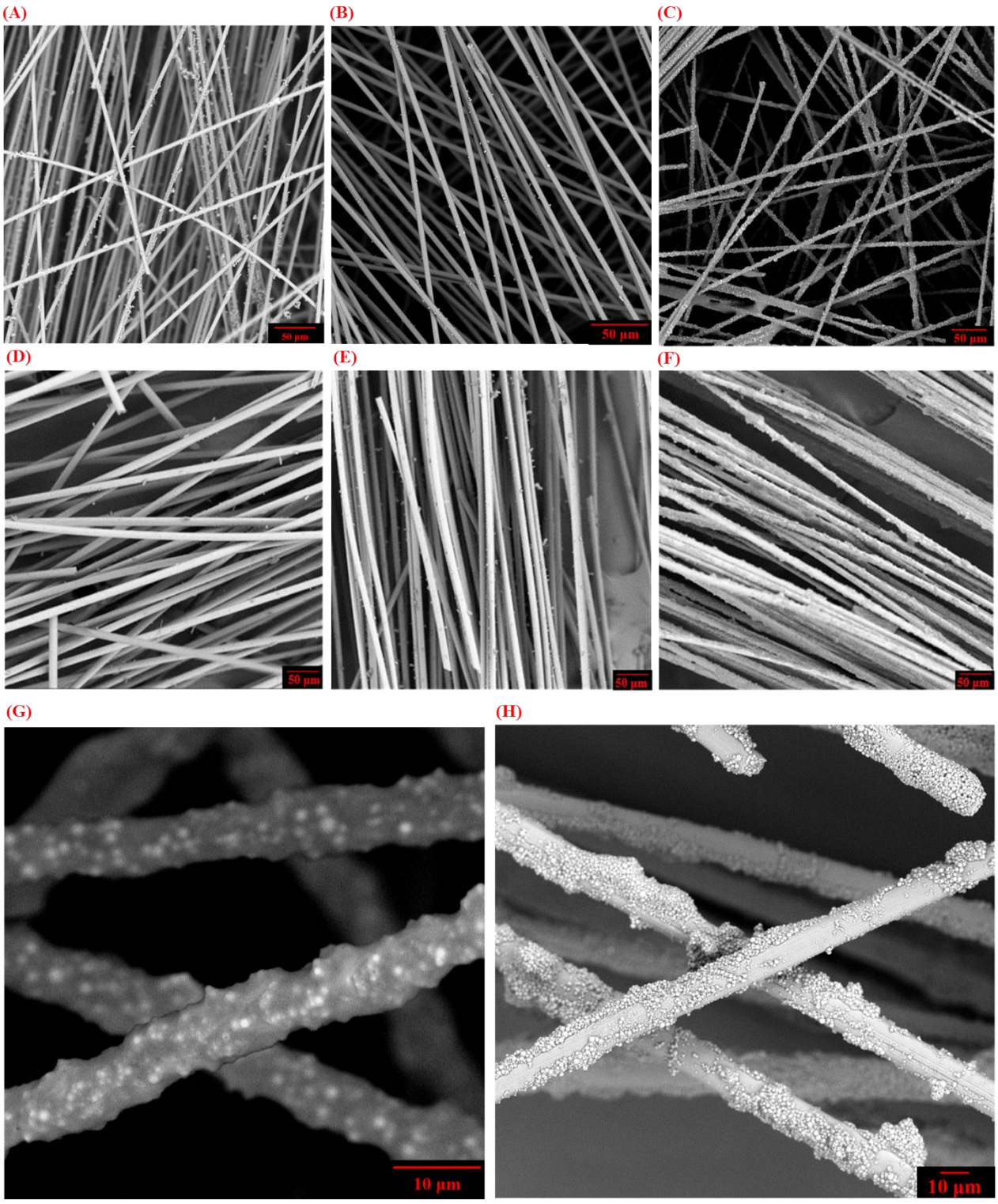

Figure 3.14 PAASalt coated PEI particles coated onto: (A) PAN-based fibers without surface treatment with sparse particle coating; (B) PAN-based fibers with ozone treatment only with sparse

particle coating; (C) PAN-based fibers with both ozone and azasilane treatment with greatly increased particls on their surfaces; (D) Pitch-based fibers without surface treatment and sparse particle coating; (E) Pitch-based fibers with ozone treatment only and sparse particle coating; (F) Pitch-based fibers with both ozone and azasilane treatment and greatly increased particle coating; (G) Higher magnification of sample C; (H) Higher magnification of sample F.

Different particle concentrations (ranging from 126 to 4.125 mg/mL) and charged particle volume % (ranging from 60 to 40 volume %) were investigated. The targeted fiber-matrix composition was 60 volume % of fibers and 40 volume % of PEI. When 50 volume % of PEI particles was charged relative to fibers, it was found that after drying, the amount of particles coated onto the fibers was ~40 volume %. When 40 volume % of particles were charged, ~29 volume % of particles were adhered to the fibers. Thus, very high amounts of particles were attracted to the fiber surfaces by using the strategy of multiple electrostatic attractions. It was also found that more particles were on the surface of the fiber bundle, while there were significantly fewer particles in the gaps between individual fibers. It may be important to separate the fibers or pre-disperse them into individual fibers, to enable functionalization with more uniform coatings.

3.5 Conclusions

In conclusion, we have successfully fabricated water-dispersible, sub-micron, high performance PEI particles using two particle production processes - a nucleation and growth process and the homogenization - solvent evaporation method. The viability of synthesizing and incorporating two thermally stable suspending agents in the homogenization - solvent evaporation method was demonstrated. PAN-based and pitch-based carbon fibers were functionalized with a combination of ozone treatment followed by an azasilane addition to form amino-functional surfaces on the fibers. A

novel method for coating the amino-functional fibers with PEI fine particles having anionic surfaces was developed. It is hypothesized that an ionic exchange reaction between the fibers and particles was responsible for the high surface coverages that were obtained. Further research will focus on consolidation and mechanical properties of carbon fiber reinforced composites using these fine particle-coated fibers.

3.6 Acknowledgements

The authors greatly acknowledge the Defense Advanced Research Projects Agency (DARPA) for funding. The authors also gratefully thank Dr. Xu Feng and the Surface Analysis Laboratory at Virginia Tech for the XPS analysis.

3.7 References

1. Unterweger, C.; Duchoslav, J.; Stifter, D.; Fürst, C., Characterization of carbon fiber surfaces and their impact on the mechanical properties of short carbon fiber reinforced polypropylene composites. *Composites Science and Technology* **2015,** *108*, 41-47.
2. Mallick, P. K., *Fiber-reinforced composites: materials, manufacturing, and design*. CRC press: 2007.
3. Hussain, F.; Hojjati, M.; Okamoto, M.; Gorga, R. E., Polymer-matrix nanocomposites, processing, manufacturing, and application: an overview. *Journal of composite materials* **2006,** *40* (17), 1511-1575.
4. Soutis, C., Carbon fiber reinforced plastics in aircraft construction. *Materials Science and Engineering: A* **2005,** *412* (1), 171-176.
5. Agarwal, B. D.; Broutman, L. J.; Chandrashekhara, K., *Analysis and performance of fiber composites*. John Wiley & Sons: 2017.
6. Friedrich, K.; Almajid, A. A., Manufacturing aspects of advanced polymer composites for automotive applications. *Applied Composite Materials* **2013,** *20* (2), 107-128.
7. Chung, D. D., Tailoring composite materials. *Composite Materials: Science and Applications* **2010**, 157-201.
8. McMahon, P. E., Thermoplastic carbon fibre composites. In *Developments in Reinforced Plastics—4*, Springer: 1984; pp 1-30.
9. Bigg, D.; Hiscock, D.; Preston, J.; Bradbury, E., High performance thermoplastic matrix composites. *Journal of Thermoplastic Composite Materials* **1988,** *1* (2), 146-160.
10. Platt, D. K., *Engineering and high performance plastics market report: a Rapra market report*. iSmithers Rapra Publishing: 2003.
11. High-performance Plastics for Aviation and Aerospace. http://www.sdplastics.com/ensinger/aerodef.pdf (accessed Mar 7, 2018).

12. Ye, L.; Friedrich, K., Processing of thermoplastic composites from powder/sheath-fibre bundles. *Journal of materials processing technology* **1995,** *48* (1-4), 317-324.
13. Allen, K. A., Processing of thermoplastic composites. *Polymer and Composites Processing* **2012**, 1-10.
14. Yu, T.; Davis, R., The effect of processing conditions on the properties of carbon fiber-LaRC TPI composites made by suspension prepregging. *Journal of Thermoplastic Composite Materials* **1993,** *6* (1), 62-90.
15. Texier, A.; Davis, R. M.; Lyon, K. R.; Gungor, A.; McGrath, J. E.; Marand, H.; Riffle, J. S., Fabrication of PEEK/carbon fibre composites by aqueous suspension prepregging. *Polymer* **1993,** *34* (4), 896-906.
16. Wu, G.; Schultz, J., Processing and properties of solution impregnated carbon fiber reinforced polyethersulfone composites. *Polymer composites* **2000,** *21* (2), 223-230.
1. Unterweger, C.; Duchoslav, J.; Stifter, D.; Fürst, C., Characterization of carbon fiber surfaces and their impact on the mechanical properties of short carbon fiber reinforced polypropylene composites. *Composites Science and Technology* **2015,** *108*, 41-47.
2. Mallick, P. K., *Fiber-reinforced composites: materials, manufacturing, and design*. CRC press: 2007.
3. Hussain, F.; Hojjati, M.; Okamoto, M.; Gorga, R. E., Polymer-matrix nanocomposites, processing, manufacturing, and application: an overview. *Journal of composite materials* **2006,** *40* (17), 1511-1575.
4. Soutis, C., Carbon fiber reinforced plastics in aircraft construction. *Materials Science and Engineering: A* **2005,** *412* (1-2), 171-176.
5. Agarwal, B. D.; Broutman, L. J.; Chandrashekhara, K., *Analysis and performance of fiber composites*. John Wiley & Sons: 2017.
6. Friedrich, K.; Almajid, A. A., Manufacturing aspects of advanced polymer composites for automotive applications. *Applied Composite Materials* **2013,** *20* (2), 107-128.
7. Chung, D. D., Tailoring composite materials. *Composite Materials: Science and Applications* **2010**, 157-201.
8. McMahon, P. E., Thermoplastic carbon fibre composites. In *Developments in Reinforced Plastics—4*, Springer: 1984; pp 1-30.
9. Bigg, D.; Hiscock, D.; Preston, J.; Bradbury, E., High performance thermoplastic matrix composites. *Journal of Thermoplastic Composite Materials* **1988,** *1* (2), 146-160.
10. Platt, D. K., *Engineering and high performance plastics market report: a Rapra market report*. iSmithers Rapra Publishing: 2003.
11. High-performance Plastics for Aviation and Aerospace. http://www.sdplastics.com/ensinger/aerodef.pdf (accessed Mar 7, 2018).
12. Ye, L.; Friedrich, K., Processing of thermoplastic composites from powder/sheath-fibre bundles. *Journal of materials processing technology* **1995,** *48* (1-4), 317-324.
13. Allen, K. A., Processing of thermoplastic composites. *Polymer and Composites Processing* **2012**, 1-10.
14. Yu, T.; Davis, R., The effect of processing conditions on the properties of carbon fiber-LaRC TPI composites made by suspension prepregging. *Journal of Thermoplastic Composite Materials* **1993,** *6* (1), 62-90.
15. Texier, A.; Davis, R. M.; Lyon, K. R.; Gungor, A.; McGrath, J. E.; Marand, H.; Riffle, J. S., Fabrication of PEEK/carbon fibre composites by aqueous suspension prepregging. *Polymer* **1993,** *34* (4), 896-906.
16. Wu, G. M.; Schultz, J. M., Processing and properties of solution impregnated carbon fiber reinforced polyethersulfone composites. *Polymer composites* **2000,** *21* (2), 223-230.
17. Ishida, Y.; Ogasawara, T.; Yokota, R., Development of Highly Soluble Addition-type Imide Oligomers for Matrix of Carbon Fiber Composite (I): Imide Oligomers Based on Asymmetric Biphenyltetracarboxylic Dianhydride and 9,9-Bis(4-aminophenyl) fluorene. *High Performance Polymers* **2006,** *18* (5), 727-737.

18. Goodman, K. E.; Loos, A. C., Thermoplastic Prepreg Manufacture. *Journal of Thermoplastic Composite Materials* **1990,** *3* (1), 34-40.
19. Godara, A.; Mezzo, L.; Luizi, F.; Warrier, A.; Lomov, S. V.; van Vuure, A. W.; Gorbatikh, L.; Moldenaers, P.; Verpoest, I., Influence of carbon nanotube reinforcement on the processing and the mechanical behaviour of carbon fiber/epoxy composites. *Carbon* **2009,** *47* (12), 2914-2923.
20. Iyer, S. R.; Drzal, L. T., Manufacture of powder-impregnated thermoplastic composites. *Journal of Thermoplastic Composite Materials* **1990,** *3* (4), 325-355.
21. Giraud, I.; Franceschi-Messant, S.; Perez, E.; Lacabanne, C.; Dantras, E., Preparation of aqueous dispersion of thermoplastic sizing agent for carbon fiber by emulsion/solvent evaporation. *Applied Surface Science* **2013,** *266*, 94-99.
22. Cheng, H. K. F.; Pan, Y.; Sahoo, N. G.; Chong, K.; Li, L.; Chan, S. H.; Zhao, J., Improvement in properties of multiwalled carbon nanotube/polypropylene nanocomposites through homogeneous dispersion with the aid of surfactants. *Journal of Applied Polymer Science* **2012,** *124* (2), 1117-1127.
23. Chai, Z.; Zheng, X.; Sun, X., Preparation of polymer microspheres from solutions. *Journal of Polymer Science Part B: Polymer Physics* **2003,** *41* (2), 159-165.
24. Lin, T.; Stickney, K. W.; Rogers, M.; Riffle, J. S.; McGrath, J. E.; Marand, H.; Yu, T. H.; Davis, R. M., Preparation of submicrometre polyimide particles by precipitation from solution. *Polymer* **1993,** *34* (4), 772-777.
25. Farr, I.; Kratzner, D.; Glass, T.; Dunson, D.; Ji, Q.; McGrath, J., The synthesis and characterization of polyimide homopolymers based on 5 (6) ‐ amino ‐ 1 ‐ (4 ‐ aminophenyl) ‐ 1, 3, 3 ‐ trimethylindane. *Journal of Polymer Science Part A: Polymer Chemistry* **2000,** *38* (15), 2840-2854.

Chapter 4: Design and Synthesis of Pluronic® P85 Block Copolymers for Remote Actuation in Cancer Cell Selective Treatment through Cytoskeletal Disruption

Alyssa M. Master,[1*] Philise N. Williams,[1,2*] Nikorn Pothayee,[3] Nipon Pothayee,[3] Rui Zhang,[3] Hemant M. Vishwasrao,[1,2] Judy S. Riffle ,[3] Marina Sokolsky,[1] Alexander V. Kabanov[1]

* denotes co-first author

[1] Center for Nanotechnology in Drug Delivery, University of North Carolina, Chapel Hill, NC, USA

[2] Department of Pharmaceutical Sciences, University of Nebraska Medical Center, Omaha, NE, USA

[3] Macromolecules and Interfaces Institute, Virginia Polytechnic Institute and State University, Blacksburg, VA, USA

4.1 Abstract

Motion of micron and sub-micron size magnetic particles in alternating magnetic fields can activate mechanosensitive cellular functions or physically destruct cancer cells. However, such effects are usually observed with relatively large magnetic particles (>250 nm) that would be difficult if at all possible to deliver to remote sites in the body to treat disease. Here we show a completely new mechanism of selective toxicity of superparamagnetic nanoparticles (SMNP) of 7 to 8 nm in diameter to cancer cells. These particles are coated by block copolymers, which facilitates their entry into the cells and clustering in the lysosomes, where they are then magneto-mechanically actuated by remotely applied alternating current (AC) magnetic fields of very low frequency (50 Hz). Such fields and treatments are safe for surrounding tissues but produce cytoskeletal disruption and subsequent death of cancer cells while leaving healthy cells intact.

4.2 Introduction

The medicines of the future should be dormant on the way to their target but actuated to execute their therapeutic function once they reach the site of their action within the body. Superparamagnetic iron oxide nanoparticles (SMNP) can be remotely actuated by externally applied magnetic fields to kill cancer cells.[1-4] One of the most studied modes of remote actuation is magnetic hyperthermia, which utilizes the SMNP response to alternating current (AC) magnetic fields of relatively high frequencies, on the order of hundreds of kHz. Once exposed to such fields the SMNPs generate heat through Neél or Brownian relaxation, depending on the SMNP and the surrounding media characteristics.[5-8] This heat leads to temperature increases causing subsequent damage to the surrounding cells. However, magnetic hyperthermia is limited due to challenges in synthesizing non-toxic SMNPs with sufficiently high specific absorption rates (SAR), in reaching sufficient intracellular SMNP concentrations and in restricting heat dissipation from a tumor to adjacent healthy tissues.[5] It is also clear that the thermal conductivity of water is so high that bulk temperature increase is difficult. In response to the issue of the high thermal conductivity of water, the concept of surface heating has been proposed. This concept emphasizes energy dissipation in the absence of measurable bulk heating, and suggests that localized surface heating may be the cause of cell death.

Several studies now document cell damage with exposure to AC magnetic fields even without a perceptible increase in temperature.[9-14] For example, Villanueva et al. reported HeLa tumor cell damage and death after incubation with magnetic manganese oxide nanoparticles that were coated with silica, and exposure to an AC field with a frequency of 10Hz.[9] Rinaldi et al. incubated magnetic iron oxide nanoparticles that were coated with carboxymethyldextran and conjugated with epidermal growth factor (EGF) with MDA-MB-468 cancer cells that have EGFR receptors.[10-11] Upon exposure to an AC field with a strength of 30.5 kA/m and 233 kHz, cell viability was dramatically reduced

without any measured temperature rise from 37 °C.[10] Sanchez and Connord et al. designed and constructed a magnetic field space within a confocal microscope, and viewed cell behavior dynamically upon exposure to an AC field of 53mT at 300 kHz.[12-13] Iron oxide particles with an average diameter of 8.7nm were coated with targeting ligands that facilitated their selective uptake into endocrine cancer cells. Cell responses included lysosome membrane permeabilization with concomitant ROS appearance, followed by cell death, and the responses were largely limited to cells that contained the nanoparticles and also that were exposed to the AC field. Importantly, this suggests that targeted cells could be made to respond to the field without damage to neighboring cells.

Magneto-mechanical actuation of cells or organelles within cells has also been suggested. For example, Zhang et al. designed a rotating AC magnetic field space with a field strength of ~30mT and exposed cells at a very low frequency of ~20Hz.[14] They utilized the field to enhance uptake of iron oxide nanoparticles of 100 nm and above that were conjugated with antibodies for targeting the lysosomal protein marker LAMP-1 Into rat insulinoma tumor cells and human pancreatic cells. They reported intracellular lysosomal membrane permeabilization followed by apoptosis, and proposed that mechanical rotation of the nanoparticles associated with the lysosomal membranes caused membrane disruption. Kim et al. reported utilizing relatively large nanoparticles comprised of a 20/80% Fe/Ni alloy coated with gold in a disc geometry (~60-nm thick and ~1-μm in diameter). The gold surfaces of the discs were functionalized with anti-human-IL13α2R antibodies to target the cell membranes of human glioblastoma cells. They incubated the particles with the cells and exposed them to uniform AC magnetic fields with very low strengths (~8 kA/m) and frequencies (10–20Hz). The glioblastoma cells underwent apoptosis and it was hypothesized that the discs aligned in the field and then somewhat misaligned when the field was changed, thus damaging the cell membranes that they were bound to, and further causing in an ionic signal that resulted in cell apoptosis.[15]

Distinct from these studies, here we show a novel magneto-mechanical mechanism of action of small polymer coated SMNPs actuated inside the cells, also by super low frequency AC magnetic fields as discussed in previous reports of magneto-mechanical actuation.[14-15] Such fields are not expected to cause any damage to biological tissues but they result in magneto-mechanical actuation of the SMNPs and promote cancer cell death. We demonstrate cancer cell selectivity due to the intrinsic difference in cell architecture between cancerous and healthy cells. Previously, we have shown that the activity and conformation of enzymes immobilized on SMNPs were disrupted following exposure to super low frequency AC magnetic fields in a non-heat induced manner.[16] These changes in the enzyme structure were attributed to the motion of SMNPs in the AC magnetic field, which created shear and tensile forces on the surrounding materials. In this work, we demonstrate the concept of magneto-mechanical actuation of small ~7–8 nm diameter magnetite (Fe_3O_4) SMNPs in AC magnetic fields and their effects on the subcellular compartments of cancerous vs non-cancerous cell lines. We show that a non-targeted polymer coated SMNP system is taken up into cell lysosomal compartments and after magnetic field actuation, can cause cytoskeletal disruption in cancer cells while leaving healthy cells intact and viable.

4.3 Materials and Methods

4.3.1 Materials

Lysotracker® Green, TubulinTracker™, Hoechst 33342, Annexin V, Propidium Iodide, fetal bovine serum (FBS) (both dialyzed and heat inactivated), Dulbecco's Modified Eagle's Medium (DMEM), DMEM:F-12, penicillin/streptomycin, human insulin, human epidermal growth factor and Alexa Fluor 647-hydrazine were purchased from Life Technologies (Carlsbad, CA). Hydrogen peroxide was purchased from Thermo Fisher Scientific (Waltham, MA). Lab-Tek II Chambered

Coverglass #1.5 Borosilicate 8 well chambers, used for live cell imaging, were purchased from Fisher Scientific (Waltham, MA). High binding strip plates (2 × 8 MICROLON 96 well) were purchased from Griener Bio-One. MTT reagent (3-(4,5-dimethylthiazol-2-yl)-2, 5-diphenyltetrazolium bromide) was purchased from Research Products International (Prospect, IL). Cytochalasin D (CD), dimethylsulfoxide (DMSO) and nitric acid (HNO3) TRACESELECT purity grade, Atto 647 N-hydroxysuccinimide ester, and Sephadex G-50 were purchased from Sigma Aldrich (St. Louis, MO). Pluronic® P85, poly(ethylene oxide)$_{26}$-*b*-poly(propylene oxide)$_{39}$-*b*-poly(ethylene oxide)$_{26}$ block copolymer was provided by BASF Corp. (Wyandotte, MI). All other chemicals were of reagent grade and used without further purification.

4.3.2 Cell lines

MDA-MB-231 (human triple negative (ER/PR- Her2/neu-) mammary gland adenocarcinoma), BT474 (human breast ductal carcinoma) and MCF10A (human non tumorigenic mammary gland cells) were supplied by ATCC (Manassas, VA). MDA-MB- 231 and BT474 cells were maintained in DMEM (high glucose) containing 10% heat inactivated FBS and 1% penicillin/streptomycin. MCF10A cells were maintained in DME/F12 media containing 10% heat inactivated FBS, 1% penicillin/streptomycin, 10 μL/mL human insulin and 10 ng/mL human epidermal growth factor. All cell cultures were maintained at 37 °C in a 5% CO_2 atmosphere. Human breast cancer cell models were used for this study. MDA-MB-231 human breast cancer cells were initially used to assess the ability of this system to kill a triple negative (ER-/PR-/HER2/neu-) cancer. BT474 human breast ductal carcinoma cells were used to further assess the effects in a cell line with a different cytoskeletal structure. Lastly, MCF10A nontumorigenic human breast cells were used as a control.

4.3.3 Synthesis

4.3.3.1 Synthesis of a Br-P85-Br macro-initiator

Dihydroxyfunctional P85 was reacted with 2-bromoisobutyryl bromide to make a macro-initiator that was used for polymerization of *tert*-butyl acrylate by atom transfer free radical polymerization. P85 (9.7 g, ~2.1 x 10^{-3} mol) was dried under vacuum at 60 °C overnight, then was dissolved in anhydrous THF (100 mL) in a 250-mL round bottom flask. Triethylamine (2.3 mL, 16.5 x 10^{-3} mol) was added. The mixture was cooled in an ice bath and then 2-bromoisobutyryl bromide (2.0 mL, 16.5 x 10^{-3} mol) was added dropwise. The ice bath was removed and the mixture was stirred at room temperature for 45 h. The reaction mixture was filtered twice and THF was removed by rotary evaporation. The mixture was diluted with CH_2Cl_2 (110 mL) and then washed with a saturated aqueous NaCl solution twice. The organic layer was concentrated and precipitated in a 1:1 v:v mixture of chilled hexane and diethylether (800 mL each time) twice. The precipitate was filtered and dried under vacuum at 40 °C overnight.

4.3.3.2 Synthesis of a ptBA-b-P85-b-ptBA copolymer

Br-P85-Br was used as a macro-initiator for polymerization of *tert*-butyl acrylate. Br-P85-Br (M_n ~4,700 g mol^{-1}, 3.0 g, ~6.0 x 10^{-4} mol), *tert*-butyl acrylate (4 mL, 2.8 x 10^{-2} mol), and dry, deoxygenated toluene (8 mL) were added into a 50-mL Schlenk flask. Oxygen was removed with three freeze-pump-thaw procedures. Cuprous bromide (0.26 g, 1.8 x 10^{-3} mol) and *N*,*N*,*N*′,*N*″,*N*″-pentamethyldiethylenetriamine (0.38 mL, 1.8 x 10^{-3} mol) were added quickly under nitrogen. Two additional freeze-pump-thaw procedures were applied. The Schlenk flask was sealed with parafilm and stirred at 80 °C for 19 h. After the polymerization, the reaction mixture was diluted with CH_2Cl_2 (60 mL). The catalyst was removed by filtering the reaction mixture through a neutral alumina column

twice using CH_2Cl_2 as the eluent. The solution was filtered and the solvents were removed by rotary evaporation. The block copolymer was dried under vacuum at room temperature overnight.

4.3.3.3 Deprotection of ptBA-b-P85-b-ptBA to afford PAA-b-P85-b-PAA copolymer

The *tert*-butyl ester groups were selectively removed by a previously reported procedure using trifluoroacetic acid (TFA).[17] P*t*BA-*b*-P85-*b*-P*t*BA (2.4 g, ~2.9 x 10^{-4} mol) was dried in a 100-mL round bottom flask under vacuum at 60 °C overnight. Anhydrous CH_2Cl_2 (30 mL) was added to dissolve the polymer. Trifluoroacetic acid (4.3 mL, 5.6 x 10^{-2} mol) was added dropwise and the reaction mixture was stirred at room temperature for 24 h. The polymer was precipitated into chilled hexane (400 mL). The precipitated polymer was filtered and collected. The solid was then dissolved in THF (10 mL) and dialyzed against DI water (4 L) through a cellulose acetate membrane (MWCO 1,000 g mol^{-1}) for 48 h. The PAA-*b*-P85-*b*-PAA copolymer was recovered by freeze-drying for 2 d. The composition by weight was measured by ^{1}H NMR to have block molecular weights of PAA(1.9k)-PEO(1.1k)-PPO(2.4k)-PEO(1.1k)-PAA(1.9k).

4.3.3.4 Synthesis of Polymer-SMNP (PAA-b-P85-b-PAA-Magnetite Nanoparticle) Complexes

Synthesis of polymer-SMNP complexes utilized a similar procedure to that previously reported to synthesize complexes with magnetite and PEO-*b*-PAA.[18] Oleic acid-coated magnetite nanoparticles (50 mg) were dispersed in anhydrous chloroform (5 mL) in a 20-mL vial. The mixture was sonicated for 10 min. Meanwhile, PAA-*b*-P85-*b*-PAA (100 mg) was charged into a separate vial equipped with a magnetic stir bar. Anhydrous DMF (5 mL) was charged to dissolve the polymer, and the mixture was sonicated for 10 min. The magnetite dispersion was added dropwise into the polymer solution while sonicating, followed by purging with N_2 for 5 min. The reaction mixture was further sonicated for 4 h, and the water in the sonicator was changed every 30 min. The mixture was stirred at room temperature for 48 h. The mixture was precipitated into hexane (20 mL) five times. A

permanent magnet was placed under the vial to attract the complex while the supernatant was decanted to remove any solvent, free oleic acid, and other residues. The remaining solid was washed with diethylether (20 mL) 3X, and the supernatant was decanted. The nanoparticles were partially dried by purging with N_2 for 2 h at room temperature, then were dispersed in de-ionized water (10 mL) and the pH was adjusted to 7.4. The dispersion was sonicated for 20 min. It was subsequently transferred to dialysis tubing with a 12-14k MWCO, and dialyzed against de-ionized water (4 L) for 24 h. Finally the polymer-SMNP complexes were recovered by freeze-drying for 2 d.

4.3.3.5 Labeling of P85 with Atto 647

The mono-amine P85 was prepared as reported previously.[19] Mono-amine P85 (3.1 mg) was reacted with a 2-fold molar excess of Atto 647 *N,N*-hydroxyssuccinimide ester (1 mg) in *N,N*-dimethylformamide (0.5 mL) supplemented with *N,N*-diisopropylethylamine (2 μL). The reaction mixture was incubated at room temperature for 5 d. The P85-Atto 647 conjugate was purified on a size exclusion column (LH-20) with methanol as the eluent. P85-Atto 647 conjugation was confirmed by thin layer chromatography (TLC) prior to use.

4.3.3.6 Labeling of PAA-P85-SMNP with Alexa Fluor®647

PAA-P85 coated SMNP complexes were labeled with the fluorescent dye Alexa- Fluor®647 hydrazine using standard EDC chemistry. Briefly, 4.5 mg of PAA-P85- SMNPs were diluted with 0.35 mL of DI water and sonicated for 30 minutes followed by addition of 10 mg 1-ethyl-3-(-3-dimethylaminopropyl) carbodiimide hydrochloride (EDC). A stock solution of *N*-hydroxysulfosuccinimide (S-NHS) (40 mg/mL in DI water) was prepared and 50 μL of this solution was added to the reaction vial. A stock solution of Alexa Fluor®647 hydrazine (1 mg/mL in DI water) was prepared and 0.1 mL was added to the reaction vial. The vial was protected from light and incubated overnight on a shaker at approximately 100 rpm. Alexa Fluor®647-PAA-P85-SMNP were

purified on a size exclusion column (Sephadex G-50) with PBS as the eluent followed by centrifugal filtration with 100 kDa cutoff Centricons (EMD Millipore, Billerica, MA). The concentration of SMNPs in solution was determined by ICP-MS. Similar to the previously described method, 20 μL of particle solution were mixed with 50 μL of nitric acid and incubated at 70 °C overnight (minimum 12 h). Following the digestion, the volume of the solution was adjusted to 1 mL with DI water and analyzed by ICP-MS.

4.3.4 Characterization

4.3.4.1 Characterization of Polymer-SMNP Complexes

The intensity average diameters, polydispersity and zeta potential of the polymer-SMNP complexes were determined by dynamic light scattering (DLS) using a Zetasizer Nano ZS (Malvern Instruments Ltd., Malvern, UK). All measurements were performed in automatic mode at 25 °C. All measurements were performed at least in triplicate to calculate mean values ± standard deviations.

The polymer content in the polymer-SMNP complexes was determined by thermogravimetric analysis (Q50, TA Instruments, New Castle, DE). Approximately 10- 15 mg of the samples were loaded and exposed to a heat ramp to 110 ^{o}C at a rate of 10 ^{o}C min^{-1}, followed by an isothermal hold for 15 min, and then continued heating to 1000 ^{o}C at 10 ^{o}C min^{-1}.

Iron content in the polymer-SMNP complexes was analyzed by Inductively Coupled Plasma Mass Spectrometry (ICP-MS) (NexION 300D, Perkin Elmer, Waltham, MA). Briefly, 0.5 mL of particle solution (1 mg mL^{-1}) were mixed with 50 μL of nitric acid and incubated at 70 ^{o}C overnight (at least 12 h). Following the digestion, the volume of the solution was adjusted to 1 mL with deionized (DI) water and analyzed by ICP-MS.

4.3.4.2 In vitro Colloidal Stability of Polymer-SMNP Complexes

Polymer-SMNP complexes were dispersed in DI water pH=6.5, PBS pH=7.4 or DMEM media (with 10 % fetal bovine serum and 1 % penicillin–streptomycin) in concentration of 1.5 mg/mL, filtered through a 0.22 μm filter and incubated at 37 ^{o}C. At 1, 24 and 48 h, 0.5-mL aliquots of solution were diluted with 1 mL of the corresponding media to a final particle concentration of 0.5 mg/mL and the effective hydrodynamic diameters (D_{eff}) of the polymer-SMNP complexes were measured by DLS using a Zetasizer Nano ZS (Malvern Instruments Ltd., Malvern, UK). All measurements were performed in automatic mode at 25 °C. All measurements were performed at least in triplicate to calculate mean values ± SD.

4.3.4.3 In vitro Cytotoxicity of Polymer-SMNP Complexes

In vitro cytotoxicity of polymer-SMNP complexes was assessed in MDA-MB-231, BT474 and MCF10A cells by standard MTT assay. Briefly, cells were seeded at 5× 103 cells/well in a 96-well plate and were allowed to adhere for two days. Cells were treated with polymer-SMNP complexes at various doses (0.005–0.5mg/mL polymer-SMNP complexes) for 24 h at 37 °C, washed with acidic saline (pH 3) to remove non-internalized polymer-SMNPs and maintained in complete DMEM for an additional 24 h. All of the samples were tested in triplicate. A standard MTT assay was then performed by addition of 25 μL of 3-(4,5-dimethylthiazol-2-yl)-2,5-diphenyltetrazolium bromide (MTT) dye (5 mg/mL) to each well followed by a 4-h incubation period at 37 °C. The resultant formazan was then solubilized in dimethylsulfoxide (DMSO) and absorption was measured at 570 nm using a spectrofluorometer (SpectraMax M5, Molecular Devices Co., USA). The reading taken from the wells with cells cultured with control medium was used as a 100% viability value. The cell viability was calculated as Asample/Acontrol×100%.

4.3.4.4 Fluorescence Activated Cell Sorting

MDA-MB-231 and BT474 cells were seeded at 100K per well in 12 well plates and allowed to adhere for 3 d. After washing, they were treated with 200 μL of 0.08 μg/mL P85-Atto 647 for 1 h at 37 °C. This concentration is well above the CMC of P85 (6.5×10^{-5} M, 0.35 mg/mL). Cells were washed with PBS 3X, harvested, and resuspended in 10% Bovine Serum Albumin for FACS analysis.

4.3.4.5 Confocal analysis on live cells

MDA-MB-231 and BT474 cells were seeded at 20K per well in Lab-Tek II Chambered Coverglass 8 well plates. Cells were allowed to adhere for 4 d, washed and treated with 200 μL of 0.08 μg/mL P85-Atto 647, Lysotracker® and Transferrin Alexa 488 for 1 h at 37 °C. This concentration is well above the CMC of P85 (6.5×10^{-5}M, 0.35 mg/mL). Cells were washed 3X and kept in complete media for imaging. Live images were acquired using a Zeiss CLSM 510 LSM Confocal Laser Scanning Microscope with the 63X/oil immersion lens.

4.3.4.6 Intracellular Distributions of PAA-P85-SMNP

MDA-MB-231, BT474 and MCF10A cells were seeded at 1×105 cells/well in 8-well Lab-Tek II Chamber slides. Cells were allowed to adhere for 3 days and were treated with a specified dosage of Alexa Fluor®647-PAA-P85-SMNP for 24 h. After thorough washing, the cells were treated with 100nM of Lysotracker™ Green (λex/λem =504/511nm) for 1h and Hoechst 33342 nuclear stain for 15min. Cells were washed 3X with PBS and kept in complete media for imaging. Live cell images were acquired using a Zeiss CLSM 710 Spectral Confocal Laser Scanning Microscope with the 63X/1.4 Oil Plan Apo lens. Lysotracker™ and SMNP colocalization was determined using the Colocalization Threshold tool in ImageJ/Fiji (NIH, Bethesda, MD).

For transmission electron microscopy (TEM), cell monolayers were grown on Thermanox plastic substrates. The cells were treated with 0.1 mg/mL polymer-SMNPs for 24h. Post-treatment, the cells

were washed with PBS and fixed in 2% paraformaldehyde/2.5% glutaraldehyde/0.15M sodium phosphate buffer, pH 7.4, for 1h at room temperature and stored at 4 °C until processed. Following 3 rinses with 0.15M sodium phosphate buffer, pH 7.4, the cells were post-fixed with 1% osmium tetroxide/0.15 M sodium phosphate buffer for 1 h at RT. After washes in DI water, the cells were dehydrated using increasing concentrations of ethanol (30%, 50%, 75%, 100%, 10 min each) and embedded in Polybed 812 epoxy resin (Polysciences, Inc., Warrington, PA). The cells were sectioned en face to the substrate at 70 nm using a diamond knife. Ultrathin sections were collected on 200 mesh copper grids and stained with 4% aqueous uranyl acetate for 15 min, followed by Reynolds' lead citrate for 7 min.[20] Samples were viewed with a LEO EM910 transmission electron microscope (Carl Zeiss Microscopy, LLC, Peabody, MA) with an acceleration voltage of 80 kV. Digital images were taken using a Gatan Orius SC 1000 CCD Camera and DigitalMicrograph 3.11.0 software (Gatan, Inc., Pleasanton, CA).

4.3.4.7 Intracellular Localization of PAA-P85-SMNP

MDA-MB-231 and BT474 cells were seeded at 20K per well in 8-well Lab-Tek II Chamber slides. Cells were allowed to adhere for 4 d and were treated with 0.05 mg/mL Alexa Fluor®647-PAA-P85-SMNP for 24 h. After thorough washing, cells were treated with 100 nM of Lysotracker™ Green ($\lambda_{ex}/\lambda_{em}$=504/511 nm) for 1 h. Cells were washed 3X with acid saline (pH 3) and kept in complete media for imaging. Live cell images were acquired using a Zeiss CLSM 710 Spectral Confocal Laser Scanning Microscope with the 63X/1.4 Oil Plan Apo lens. Fluorescence was quantified using Image J.

4.3.4.8 TEM Images of SMNPs in Cells

MCF7 cells were seeded in 6 well plates containing glass coverslips at a density of $1x10^5$ cells/well. Prior to treatment, cells were starved with incomplete media (no FBS) for 30 min. Cells

were then incubated with SMNPs for 1 h at 37 °C. Cells were then preserved in 4% glutaraldehyde in formaldehyde at room temperature for 24 h, then processed for TEM analysis (Figure 4.1).

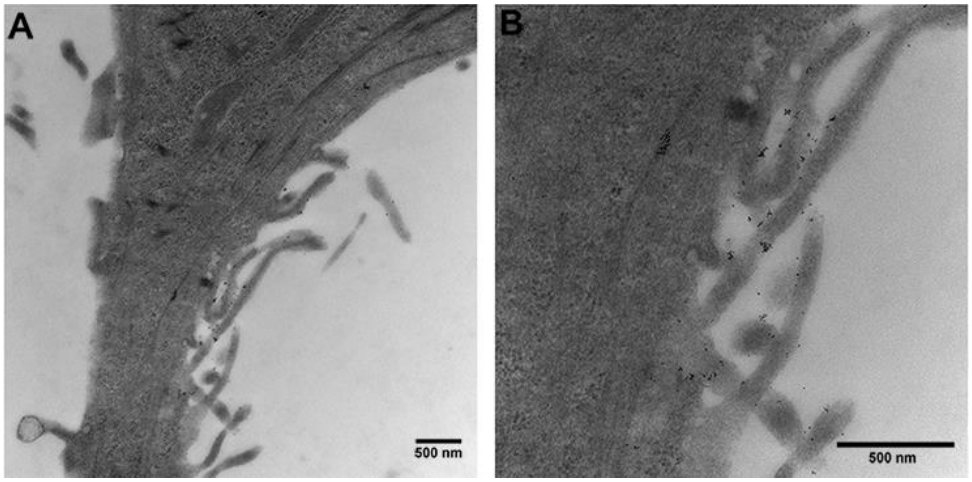

Figure 4.1 Representative TEM images of MCF7 cells treated with PAA-P85-SMNPs. (A) shows the association of the SMNPs with the cytoskeleton of the cells with (B) showing higher magnification.

4.3.4.9 Alternating Current Magnetic Field Generator

The super-low frequency alternating current (AC) magnetic field generator was custom designed and purchased from Nanomaterials Ltd. (Tambov, Russia). The unit contains a sinusoidal current generator with variable power (up to 1.5 kW), frequency (in the range from 30 to 3000 Hz) and variable magnetic field amplitude (from 10 to 100 mT). The unit is equipped with a water-cooled inductor with a ferromagnetic core and a temperature-controlled cuvette. The temperature-controlled holder accommodates one 8-well strip plate at a time. The temperature was maintained at 37 °C for all cellular experiments. For all cell experiments, cells were seeded in the middle wells, which were exposed to a homogeneous field. The experiments were conducted at a frequency of 50 Hz and the magnetic field intensity was 50 or 100 kA m^{-1}. Field frequency and field intensity were measured and monitored by an oscilloscope throughout the application time.

4.3.4.10 Quantitative Uptake of Polymer-SMNP Complexes In Vitro

MDA-MB-231, BT474 and MCF10A cells were seeded at $1x10^6$ cells/well in 6 well plates and allowed to adhere for 3 days. They were then washed and treated with polymer-SMNP complexes at various doses (0.005–0.5 mg mL^{-1} polymer-SMNP complexes) for 1 h or 24 h at 37 °C. Cells were rinsed 3 times with acidic saline (pH 3) and harvested using 0.05% trypsin/EDTA. Cells were pelleted, the supernatant was discarded and the cells were resuspended in 0.5 mL of DI water. The cell suspension was then sonicated with a probe sonicator at 10 kHz for 40 s. The cell suspension was digested using nitric acid as previously described. Following the digestion, the volume of the solution was adjusted to 1 mL with DI water and analyzed by ICP-MS.

4.3.4.11 Effect of Exposure to AC Magnetic Fields on Cell Viability

MDA-MB-231, BT474 and MCF10A cells were seeded at $5x10^3$ cells/well in 2x8 MICROLON 96 well high binding plate strips (Griener Bio Inc.) and were allowed to adhere for 3 d. Cells were treated with PAA-P85-SMNP complexes at various concentrations (0.05 - 0.5 mg mL^{-1} polymer-SMNP complexes) for 24 h at 37 °C, washed with acidic saline (pH 3) and exposed to AC magnetic fields of 50 kA m^{-1} or 100 kA m^{-1} and 50 Hz as specified in the legends. In the continuous mode, the cells were exposed to the field for 30 min. In the pulsed exposure mode, the cells were exposed to the field with a 10 min on, 5 min off pattern for 30 min in total. During the experiments the temperature was maintained at 37 °C. All the samples were tested in triplicate. A standard MTT assay was then performed.

4.3.4.12 Intracellular Distributions of PAA-P85-SMNP Complexes After Exposure to an AC Field

MDA-MB-231, BT474 and MCF10A cells were seeded at $1x10^5$ cells/well in 8-well Lab-Tek II Chamber slides. Cells were allowed to adhere for several days and were treated with a specified dosage of Alexa Fluor®647-PAA-P85-SMNPs. After 24 h, the cells were washed and then exposed

to an AC magnetic field (50 Hz, 50 kA m^{-1}) using the pulsed exposure regime for a total of 30 min. Twenty four hours post exposure, the cells were treated with 100 nM of Lysotracker™ Green ($\lambda_{ex}/\lambda_{em}$=504/511 nm) for 1 h and Hoechst 33342 nuclear stain for 15 min. Cells were washed 3X with PBS and kept in complete media for imaging. Live cell images were acquired using a Zeiss CLSM 710 Spectral Confocal Laser Scanning Microscope with the 63X/1.4 Oil Plan Apo lens.

4.3.4.13 Assessment of Lysosomal Membrane Permeabilization

MDA-MB-231, BT474 and MCF10A cells were seeded at $1x10^5$ cells/well in 8- well Lab-Tek II Chamber slides. Cells were allowed to adhere for several days and were treated with PAA-P85-SMNPs at a concentration of 0.1 mg mL^{-1}. After 24 h, the cells were washed and then exposed to an AC magnetic field (50 Hz, 50 kA m^{-1}) using the pulsed exposure regime for a total of 30 min. Three hours post exposure, cells were treated for 15 min with 10 μg mL^{-1} acridine orange stain. The cells were washed 3X with PBS and kept in complete media for imaging. Positive control cells were treated with 150 μM hydrogen peroxide for 3 h followed by thorough washing and staining with acridine orange. Live cell images were acquired using a Zeiss CLSM 710 Spectral Confocal Laser Scanning Microscope with the 63X/1.4 Oil Plan Apo lens.

4.3.4.14 Effect of Cytoskeleton Modulation on the Response to an AC Magnetic Field

For cell viability studies, MDA-MB-231, BT474 and MCF10A cells were seeded at $5x10^3$ cells per well in 2x8 96-well high binding strip plates (Griener Bio Inc.) and were allowed to adhere for 2 d. The cells were treated with PAA-P85-SMNPs at various doses for 24 h at 37 °C followed by washing with acidic saline. After washing to remove non-internalized polymer-SMNP complexes, test cells were exposed to a 100 nM sub- lethal dosage of cytochalasin D (CD) for 1 h. After washing, the cells were exposed to the AC magnetic field and viability was tested 24 h post exposure using a MTT assay as previously described. Appropriate controls of cells exposed to just one of the

compounds (either PAA-P85-SMNP alone or CD alone) as well as cells without field exposure were used.

For confocal studies, MDA-MB-231, BT474 and MCF10A cells were plated on Lab-Tek II Chamber slides at a concentration of 1 × 105 cells/well and allowed to grow overnight. The cells were then treated with 0.1 mg/mL Alexa Fluor® 647-PAA-P85-SMNP for 24 h followed by thorough washing with acid saline and replacement with complete media. The cells were incubated with 100-nM CD for 1 h to enact cytoskeletal damage in a nonlethal capacity. After washing, the cells were exposed to the pulsed AC magnetic field (50 Hz, 50 kA/m) (10 min on, 5 min off, total exposure 30 min on). Appropriate controls included cells not exposed to the magnetic field and untreated cells. Cells were then incubated at 37 °C for 24 h, fixed using 4% paraformaldehyde and permeabilized using 0.5% Triton-X 100. Fixed cells were stained with ActinGreen 488 (Life Technologies, Carlsbad, CA), a phalloidin-based actin stain and Hoechst 33342. Images were acquired using a Zeiss CLSM 710 Spectral Confocal Laser Scanning Microscope with the 63X/1.4 Oil Plan Apo lens.

4.3.4.15 Mechanism of Cell Death by Flow Cytometry

Cells were seeded in 8-well chamber slides and allowed to grow for several days. Cells were then treated with 0.1 mg mL^{-1} SMNPs for 24 h. Following incubation, cells were washed 3X with saline and then their media was replaced. Cells were then exposed to the magnetic field. For magnetic field exposure, a 50 Hz field (50 kA m^{-1} field strength) was utilized. The pulsed regime of 10 min on, 5 min off was used. Twenty-four h post-field exposure, the Annexin V/Dead Cell Apoptosis Kit with PI from Life Technologies (Carlsbad, CA) was used as per the manufacturer's instructions. The results seen in Figure 4.2 corroborate data found through MTT assays. In this figure, Q1 indicates purely necrotic cells, Q2 is a mixture of late stage apoptotic cells and necrotic cells, Q3 is early stage apoptotic cells and Q4 is live cells. This further confirms that the MCF10A cells remain unaffected

by the combination of SMNP and pulsed field exposure. Similarly, the MDA-MB-231 and BT474 cells yielded significant cell death after SMNP and field exposure. The figure shows that the majority of cells are in late stage apoptosis or necrosis but it is important to note that this is a snapshot of the cell death after 24 hours. Therefore, it is possible that cells that underwent apoptosis soon after field exposure may become sensitive to the PI dye by the 24-hour timepoint.

4.3.4.16 Statistical Analysis

Statistical analyses were performed using GraphPad Prism (GraphPad Software, Inc, La Jolla, CA). ANOVA or two-tailed Student's t-tests was used to analyze data. Where applicable, reported p-values have been adjusted for multiple comparisons using the Ryan-Einot-Gabriel-Welsch post-hoc method. Significance was reported for $p<0.05$.

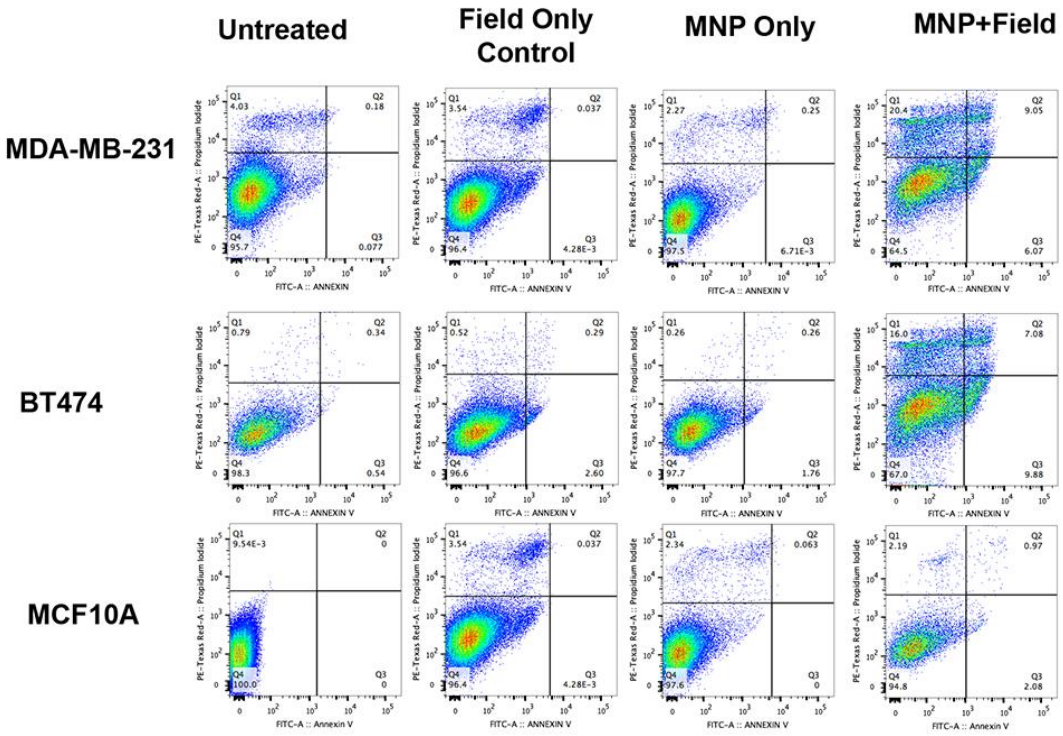

Figure 4.2 Results of flow cytometry assay 24 hours after pulsed field exposure. The controls of field and SMNPs only show little death. In contrast, the MDA-MB-231 and BT474 show high cell amounts of late stage apoptosis and necrosis after exposure to SMNPs and the pulsed field. The MCF10As remain unaffected by SMNP and pulsed field exposure.

4.3.4.17 Estimate of a Number of SMNP per Cell.

Assuming magnetite SMNP take up 500 Fe ng/mg cell protein ≈ 700 Fe_3O_4 ng/mg cell protein and magnetite density ~ 5.2 g/cm^3 the total volume of magnetite taken up by cells is $7 \cdot 10^{-7}$ / 5.2 ≈ $1.34 \cdot 10^{-4}$ cm^3/g cell protein. The volume of one magnetite particle having a radius R_m = 4 nm is approximately 4/3 x π $(4 \times 10^{-7})^3 \approx 2.7 \cdot 10^{-19}$ cm^3. For mammalian cells, a value for protein density of ~ 0.2 g/mL was reported.[21] This leads to estimates of ~ $0.5 \cdot 10^{15}$ particles/g cell protein or ~$1 \cdot 10^{14}$ particles/mL cell volume. Assuming mammalian cell volume ranging from ~1000 to 10,000 μm^3.[22] the final estimate is from ~$1 \cdot 10^5$ to ~$1 \cdot 10^6$ magnetite particles per cell.

4.4 Results

4.4.1 Quantitative Intracellular Uptake of Polymer-SMNP Complexes

A series of block copolymers with a polyanion block and poly(ethylene glycol) (PEG) was synthesized to evaluate the effect of polymer coating composition on the polymer-SMNP complexes' uptake in cancer cells. The polyanion block was either polyacrylic acid (PAA) or polymethacrylic acid (PMA), which differ in their hydrophobicity. The more hydrophobic PMA was expected to interact better with the hydrophobic cell membrane and improve particle uptake. Another strategy to improve the internalization of polymer coated SMNPs was incorporation of Pluronic P85 (P85) into the polymer coating. P85 effectively accumulated in the cells across all the cell lines tested as was analyzed by flow cytometry (Figure 4.3) and confocal microscopy (Figure 4.4). Representative

confocal microscopy images of BT474 (Figure 4.4 A-D) and MDA-MB-231 (Figure 4.4 E-H) indicate that in both cell lines P85 preferentially accumulates in lysosomes. Due to this favorable uptake pattern, P85 was incorporated in the polymer coatings of several of our tested SMNP-complexes by complexation of SMNPs with a PAA-*b*-P85-*b*-PAA pentablock copolymer. The physicochemical characteristics of the formed polymer-SMNP complexes are summarized in Table 4.1. The sizes (D_{eff}) of the polymer-SMNP complexes were in the range of 30-70 nm with ζ-potential values of -35 to -50 mV and with a polydispersity index (PDI) of 0.18, as measured by dynamic light scattering (DLS). The polymer content in all the complexes was around 60 wt% as measured by thermogravimetric analysis (TGA), and this was in excellent agreement with the iron concentration measured by inductively coupled plasma-mass spectrometry (ICP-MS). All the polymer-SMNP complexes were small clusters with several SMNP cores incorporated together as observed by TEM (Figure 4.5).

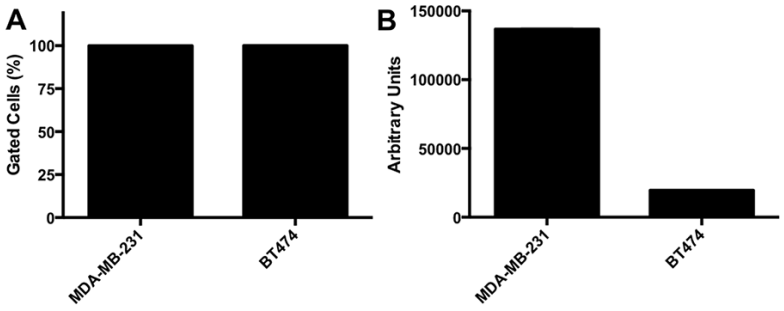

Figure 4.3 Flow Cytometry of P85-Atto 647. Cells were exposed to 0.08 ug/mL P85-Atto 647 for 1 hour, washed, trypsinized, and resuspended in PBS with 10% BSA for FACS analysis. 10,000 events were analyzed. (A) % Gated cells shows uptake into 100% of cells exposed to P85. (B) Mean fluorescence shows significant internalization of P85 into both cell lines.

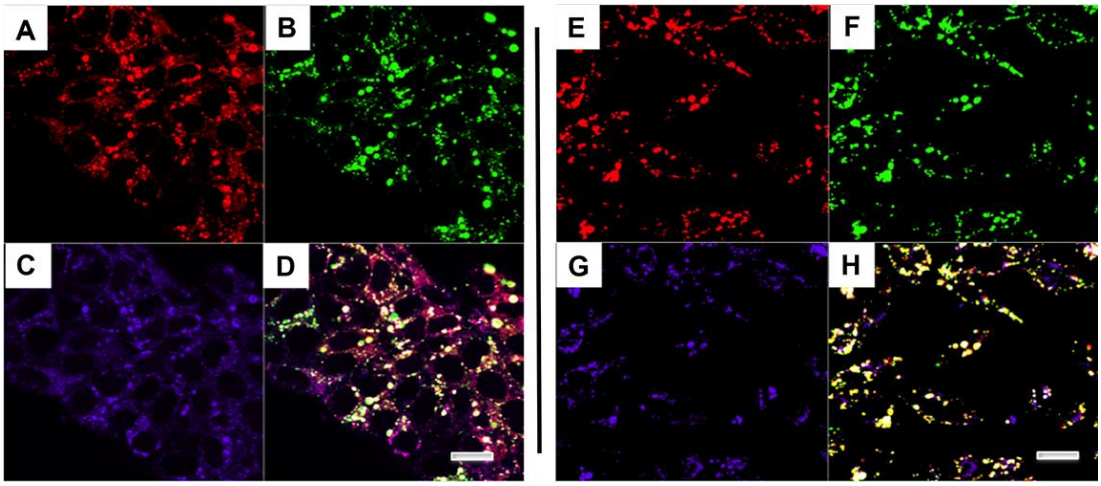

Figure 4.4 Confocal Microscopy of Internalized P85 in BT474 cells (left panel) and MDA-MD-231 cells (right panel). Cells were incubated with (A,E) Lysotracker Red, (B,F) 40 μg/mL Transferrin-Alexa Fluor® 488 (green), and (C,G) P85-Atto 647 1% (v/v) (purple) for 1 hour. Cells were washed and visualized by a Zeiss 510 LSM via the 63X oil immersion lens under live cell conditions. Triple colocalization is shown in the composite photo (D,H) as white punctate structures.

Table 4.1 Summary of polymer-SMNP complexes used in this study.

Polymer composition	Polymer block lengths (kDa)[a]	Abbreviation	D_{eff} (nm)[b]	PDI[c]	ζ-potential, mV[d]	Polymer content in complex (%, w/w)[e]
Polyacrylic acid-PEG	7.7K-2K	PAA-PEG-SMNP	67.0 ± 3.9	0.19 ± 0.01	-39.01 ± 1.17	59.5
Polymethacrylic acid-PEG	7.2K-2K	PMA –PEG-SMNP	55.7 ± 0.7	0.18 ± 0.01	-47.03 ± 0.95	63.1
1:1 w/w blend of Polyacrylic acid-PEG and Polyacrylic acid- P85	7.7K-2K/ 4.6K-3K	PAA-PEG/ PAA-P85-SMNP	38.2 ± 0.1	0.29 ± 0.01	-44.23 ± 2.61	64.1
Polyacrylic acid- P85-Polyacrylic acid	1.9K-4.6K-1.9K	PAA-P85-SMNP	30.2 ± 0.1	0.41±0.001	-34.31 ± 5.2	65.3

[a] Polymer block length is defined as the length of the polyacid block-length of the PEG or P85 block.

[b,c,d] D_{eff}, PDI and ζ-potential were measured by DLS with Nano-ZS in de-ionized water at concentration of 0.5 mg/mL at 25°C. D_{eff} is reported as an intensity averaged diameter.

[c] Polydispersity index.

[e] Polymer content in the complex was measured by thermogravimetric analysis (TGA). Briefly, 10-15 mg samples were heated at 10 °C/min to 110 °C, held isothermally for 15 min and then heated at 10 °C/min to 700 °C.

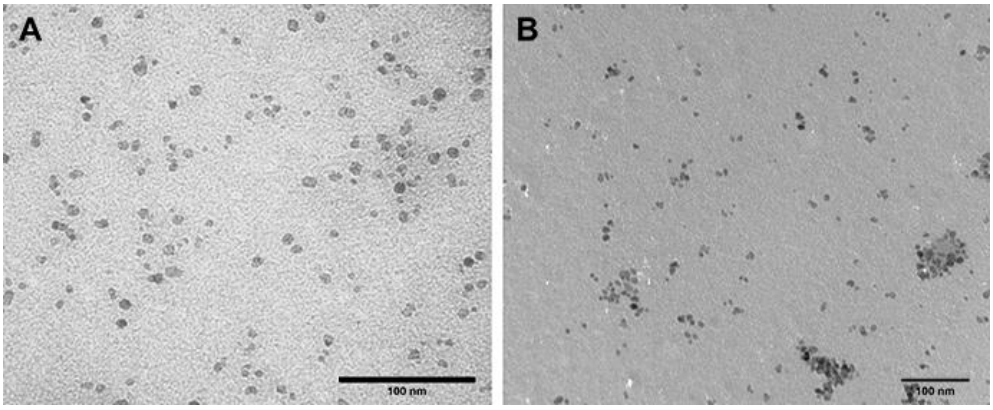

Figure 4.5 Representative TEM images of (A) PAA-P85 coated SMNP and (B) PAA-PEG coated SMNP.

All the polymer-SMNP complexes were stable in aqueous dispersion for over 48 hours under different ionic environments (deionized (DI) water, phosphate buffered saline (PBS), and complete media) (Figure 4.6). The saturation magnetization values of all the clusters were in the 60-70 emu/g Fe_3O_4 range. Preliminary cytotoxicity studies showed that all tested polymer-SMNP complexes were minimally toxic in MDA-MB-231, BT474 and MCF10A cells at all tested concentrations (Figure 4.7).

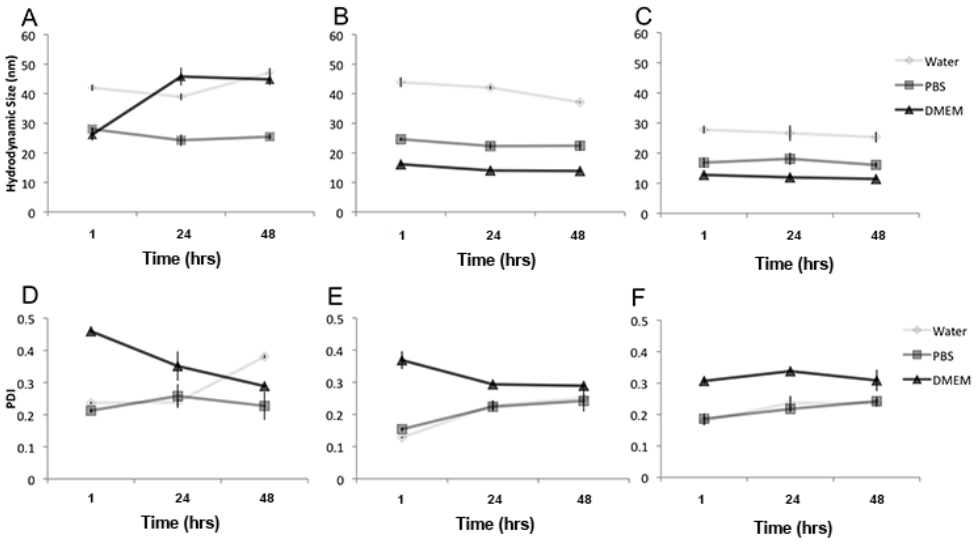

Figure 4.6 *In vitro* Colloidal Stability of Polymer-SMNP Complexes. Particles were dispersed in solvent, sonicated, filtered at 0.22 um, allowed to stand for 45 minutes, and then measured by DLS. This graph represents three independent experiments. Row 1: Hydrodynamic diameters of (A) PAA-P85-SMNP, (B) PAA-PEG-SMNP, and (C) PMA-PEG-SMNP; Row 2: Polydispersity of (D) PAA-P85-SMNP, E) PAA-PEG-SMNP, and F) PMA-PEG-SMNP.

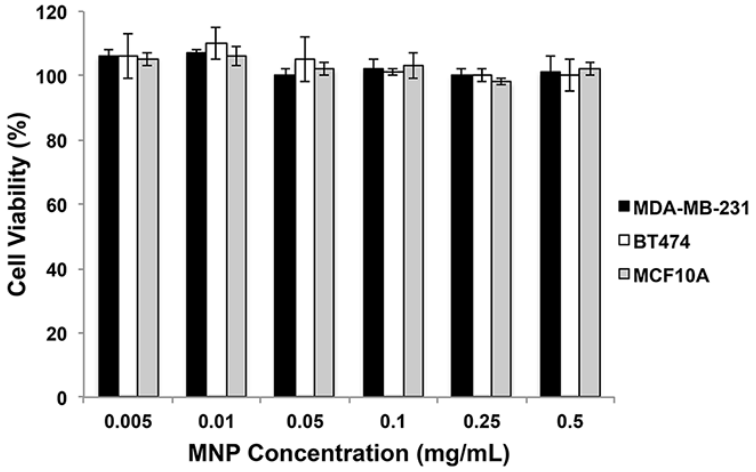

Figure 4.7 Cytotoxicity of polymer-SMNPs in the absence of AC magnetic field exposure in MDA-MB-231, BT474 and MCF10A cells. The cells were incubated with increasing concentrations of

polymer-SMNP complexes for 24 h and washed with acid saline to remove any membrane-bound SMNP complexes. Cell viability was assessed by MTT assay 24 hours post incubation.

Internalization of the polymer-SMNP complexes was evaluated following 1 h and 24 h of incubation and was determined by the amount of Fe/mg protein in the cells (Figure 4.8a). All polymer-SMNP complexes showed time and concentration dependent uptake in all experimental cell lines. PMA-PEG-SMNP showed slightly enhanced uptake compared to PAA-PEG-SMNP, especially in BT474 cells but these differences were not statistically significant. Incorporation of P85, with its relatively hydrophobic central block, into the polymer chain effectively promoted internalization of the PAA-P85-SMNPs. Interestingly, this effect of PAA-P85 was lost when PAA-P85 was mixed with PAA-PEG in the PAA-PEG/PAA-P85 blend coated SMNP. Comparable accumulation of PAA-P85-SMNP was observed in BT474 and MCF10A cells after 24 h while uptake in MDA-MB-231 was lower (Figure 4.8b). Due to significantly higher uptake the following studies focused exclusively on the PAA-P85-SMNP complexes.

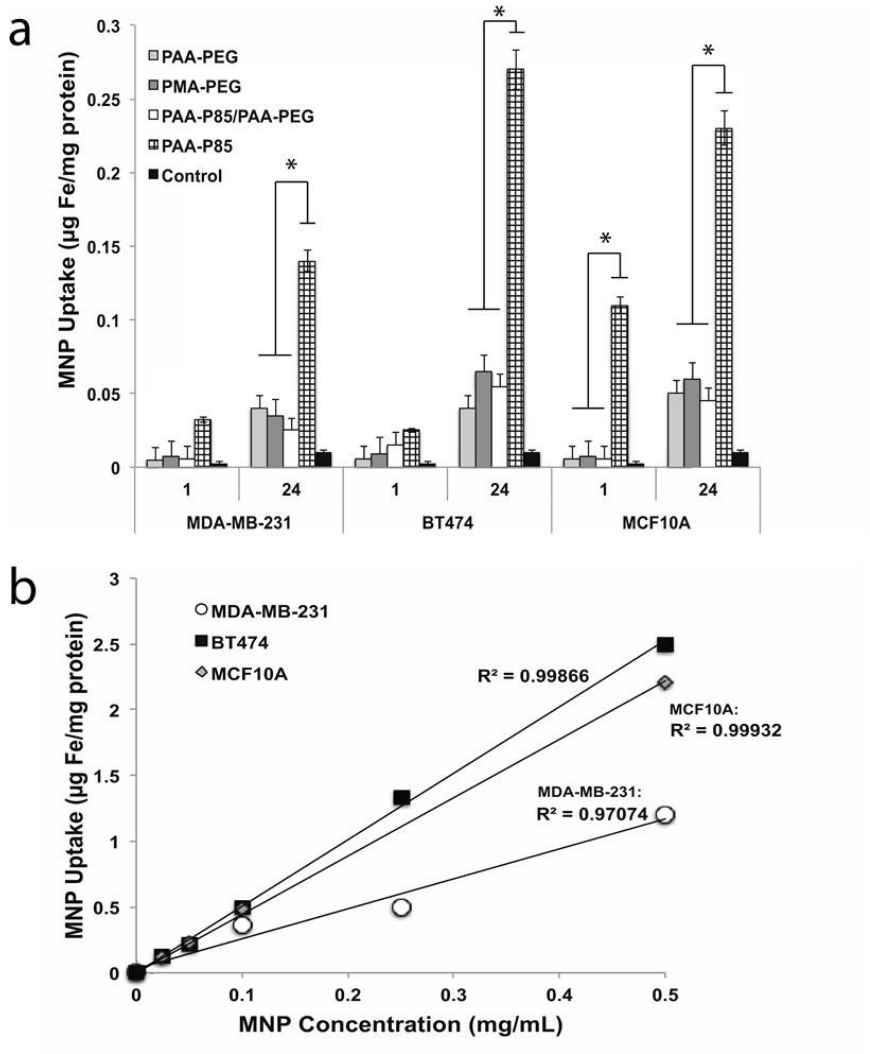

Figure 4.8 Intracellular uptake of polymer-SMNP complexes in MDA-MB-231, BT474 and MCF10A cells. a) Uptake of the polymer-SMNP complexes after incubation with complexes for 1h or 24h (b) dose dependent uptake of PAA-P85-SMNP in all three cell lines (*$p<0.05$).

4.4.2 Intracellular Distribution of PAA-P85-SMNP

Intracellular distributions of the PAA-P85-SMNP complexes were studied by confocal microscopy in MDA-MB-231, BT474 and MCF10A cells. For this experiment, the nuclei were labeled with DAPI (blue), lysosomes were labeled with Lysotracker Green and the PAA-P85-SMNPs were labeled with Alexa Fluor®647 (red). The overlap of the Lysotracker and SMNP labels indicates

colocalization. Our preliminary studies suggested that the intracellular localization of the AA-P85-SMNPs varied at different dosing concentrations. Therefore, this study dosed with both a low (0.05 mg/mL or 0.1 mg/mL) and high (0.5 mg/mL) concentration. Figure 4.9(a-c) shows representative confocal images of intracellular distributions of Alexa Fluor®647-PAA-P85-SMNP complexes following incubation for 24 h. As can be seen at the low concentration of 0.05 mg/ml PAA-P85-SMNP complexes are accumulated in lysosomes, while at the high concentration of 0.5 mg/ml the PAA-P85-SMNPs also spread throughout the cytoplasm. These observations are further confirmed by the colocalization quantitative data shown in Figure 4.9d. This data shows that in all three cell lines colocalization of the Polymer- SMNP complexes with lysosomes remains quite high (80%) at low exposure concentrations of 0.05 and 0.1 mg/mL, but drops off significantly to about 30% at the high exposure concentration of 0.5 mg/mL. Figure 4.9e shows TEM data of PAA-P85- SMNPs in cells to further confirm high amounts of lysosomal accumulation.

4.4.3 *In Vitro* Exposure to Super Low Frequency AC Field

Following incubation with various concentrations of PAA-P85-SMNPs for 24 h, the cells were exposed to a super low frequency AC magnetic field (50 Hz) with field strengths of 50 or 100 kA/m utilizing two exposure regimes termed ‘continuous’ (30 min) or ‘pulsed’ (10 min on, 5 min off, total 30 min on. A remarkable difference in the response of cancerous (MDA-MB-231 and BT474) versus non-cancerous (MCF10A) cells was observed. There was a significant reduction in cell viability at as low as 0.05 mg/mL of PAA-P85-SMNPs in both MDA-MB-231 (Figure 4.10a) and BT474 cells (Figure 4.10b) regardless of the field exposure regime utilized. However, as seen in Figure 4.10c, despite similar internalization rates and SMNP concentration inside the MCF10A cells there was no noticeable decrease in cell viability after AC magnetic field exposure (all tested regimes). For the cancerous MDA-MB-231 and BT474 cells, the effect on cell viability did not occur in a dose

dependent manner and was not enhanced with increased field strength. Interestingly, in the MDA-MB-231 cell line, field exposure using the continuous field regime caused little toxicity up to 0.25 mg/mL PAA-P85-SMNP complexes while in the BT474 cells, this same exposure regime caused a 50% decrease in cell viability following incubation with only 0.05 mg/mL PAA-P85-SMNP complexes. However, in both cell lines, the pulsed field regime was significantly more effective compared to the continuous field regime (50% for pulsed versus 100% cell viability for continuous field in MDA-MB-231 and 25% for pulsed versus 50% cell viability for continuous field in BT474). Exposure of the cells in the absence of PAA-P85-SMNPs to either a continuous or pulsed field regime remained minimally toxic for both cell lines. Cell viability after exposure to 0.5 mg/mL SMNPs was assessed but did not yield any higher efficacy in any of the cell lines. Due to these results, further experiments were done using a 50 kA/m field strength and the pulsed field regime.

These results show that the BT474 cells are more sensitive to the treatment than the MDA-MB-231 cells, and the healthy MCF10A cells do not seem to be affected at all. To further determine a mechanistic understanding of this observation, we first needed to determine if lysosomal membrane permeabilization (LMP) or cellular heating was responsible for the observed cell death. It has been determined, based upon our previous experimental results as well as theoretical calculations, that the observed effects cannot be explained by bulk or surface heat.[16] Previously we have clearly shown that exposure of PAA-P85-SMNP dispersions to super low frequency AC magnetic fields does not result in a temperature increase of the surrounding medium, and that change in the physical structure of a conjugated enzyme were significantly different from a temperature-induced structural deformation.[16] Thus, we can conclude that the cell death observations are not due to heating effects.

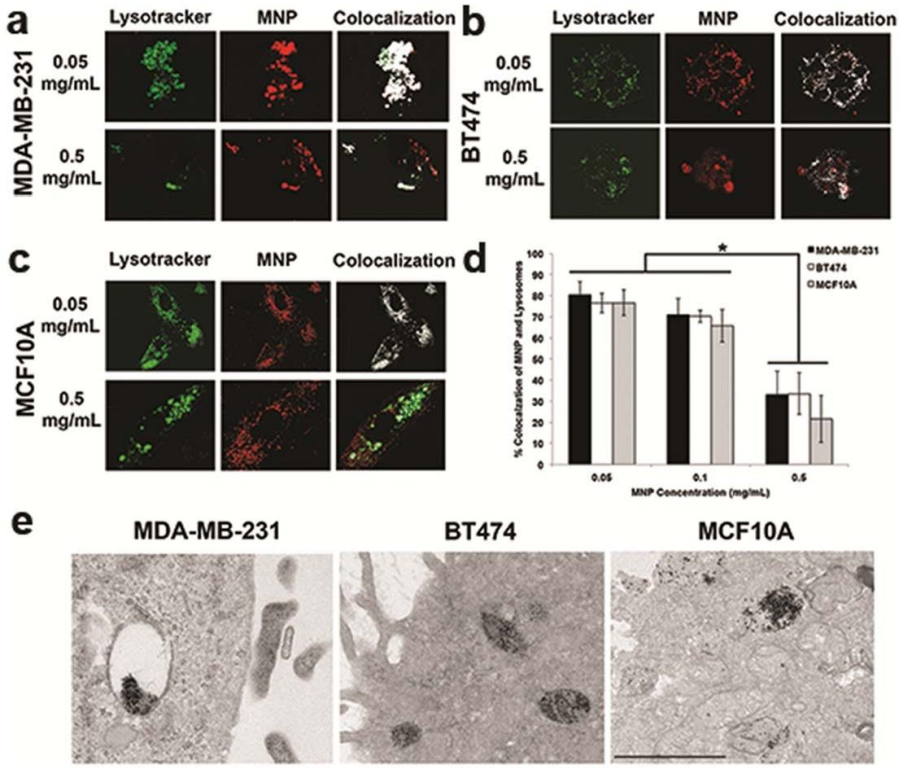

Figure 4.9 Intracellular Distribution of PAA-P85-SMNP: Intracellular distributions of PAA-P85-SMNPs in a) MDA-MB-231 b), BT474 and c) MCF10A cells after 24 hours of incubation with 0.05 or 0.5 mg/ml PAA-P85-SMNPs. d) The quantification of the colocalization of Alexa Fluor®647-PAA-P85-SMNPs with lysosomes as determined by ImageJ/Fiji. ($p<0.01$). Lysosomal encapsulation of SMNPs seen in e) TEM images.

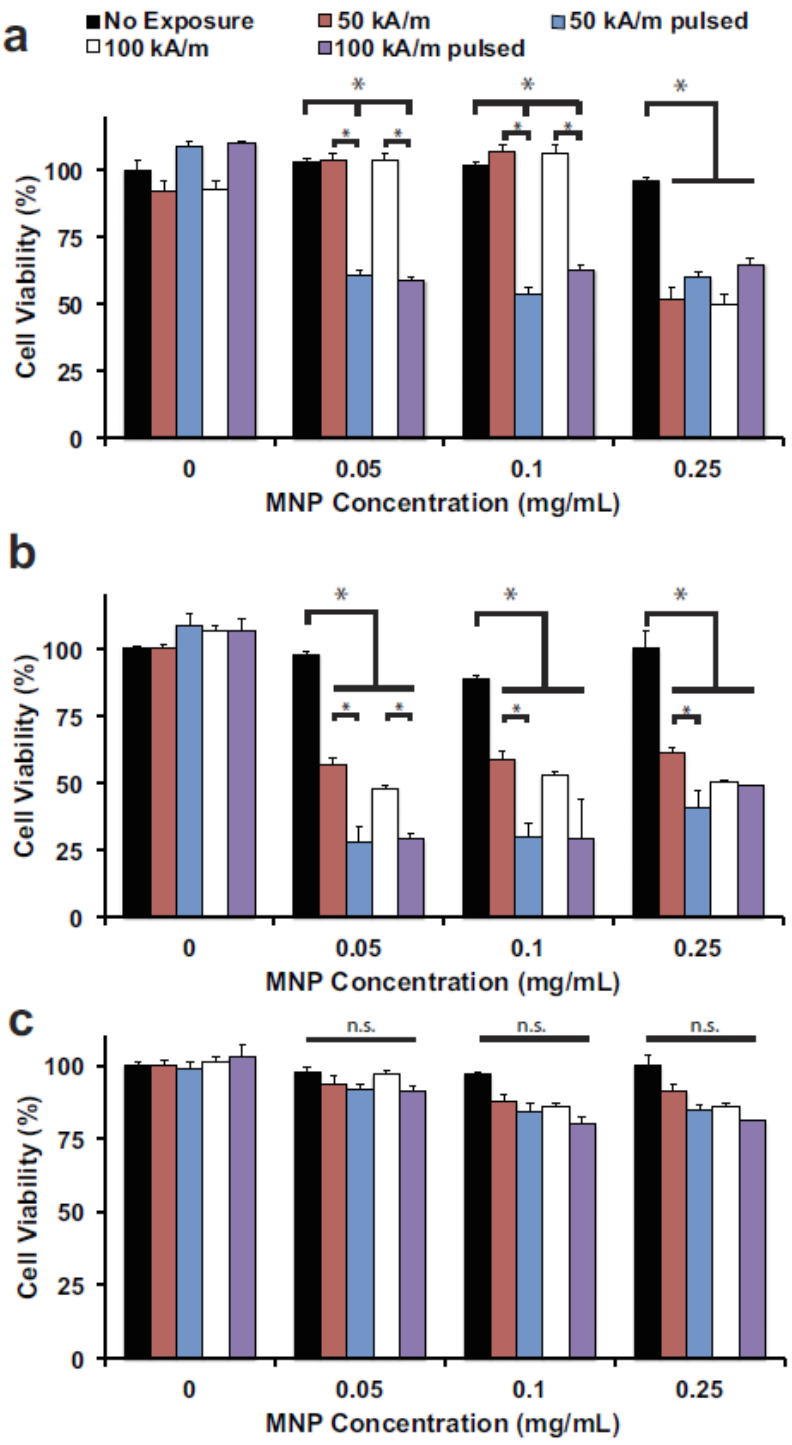

Figure 4.10 *In Vitro* Exposure to Super Low Frequency AC Field: Effect of exposure to 50 Hz AC magnetic fields on cell viability. Cells were incubated with various concentrations of PAA-P85 SMNPs for 24h, washed with acid saline and exposed to the field. Viability of MDA-MB-231 (A),

BT474 (B) and MCF10A (C) cells was assessed following exposure to a 50kA/m, 50 Hz or 100 kA/m, 50 Hz AC magnetic field. For each of the field strengths, two different exposure regimes were used: continuous (30 min) or pulsed (10 min on/5 min off) magnetic field. Data shown are mean ± SEM (n=15), $p<0.05$, n.s.=not significant.

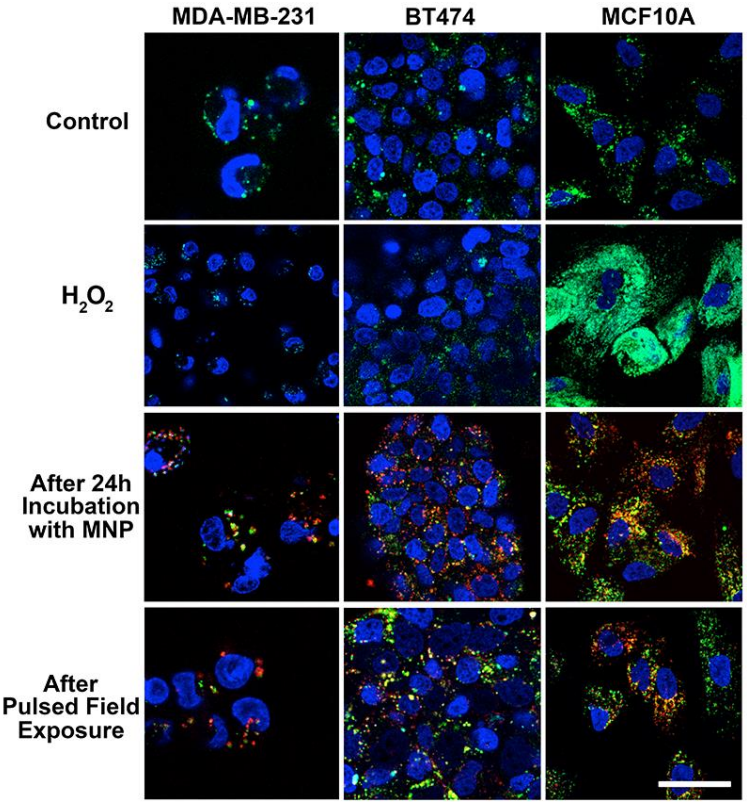

Figure 4.11 Intracellular distribution of the PAA-P85-SMNP in MDA-MB-231, BT474 and MCF10A cells before and after field exposure. Cells were incubated with Alexa Fluor 647-PAA-P85-SMNP for 24 h at 37 °C, washed with acid saline, incubated with Lysotracker Green (Alexa 488) for 1 h and exposed to a 50kA/m, 50 Hz pulsed (10 min on/5 min off) AC magnetic field. Co-localization (yellow green) of the MNPs with the Lysotracker indicated lysosomal uptake. This figure also shows lack of lysosomal membrane permeabilization (LMP) after field exposure. The positive control (cells exposed to hydrogen peroxide) indicates Lysotracker staining after LMP. Scale bar = 20 μm.

An acridine orange assay, a more robust method to detect LMP, was also conducted. Acridine orange is a lysosomotropic stain that can be used to measure the lysosome membrane functionality. The stain is excited by UV light and emits red/orange fluorescence when in lysosomes and green fluorescence when present in the nucleus or cytosol. Cells with intact lysosomes display punctate red/orange fluorescence but this red/orange fluorescence reduces significantly after LMP.[23-25] Hydrogen peroxide was used as a positive control because it is known to induce LMP.[26] Figure 4.12 shows that SMNP incubation along with pulsed field exposure does not cause loss of lysosomal fluorescence as observed in the positive hydrogen peroxide control. The lysosomes retain the punctate red/orange fluorescence before and after field exposure in all three cell lines, which indicates a lack of LMP.

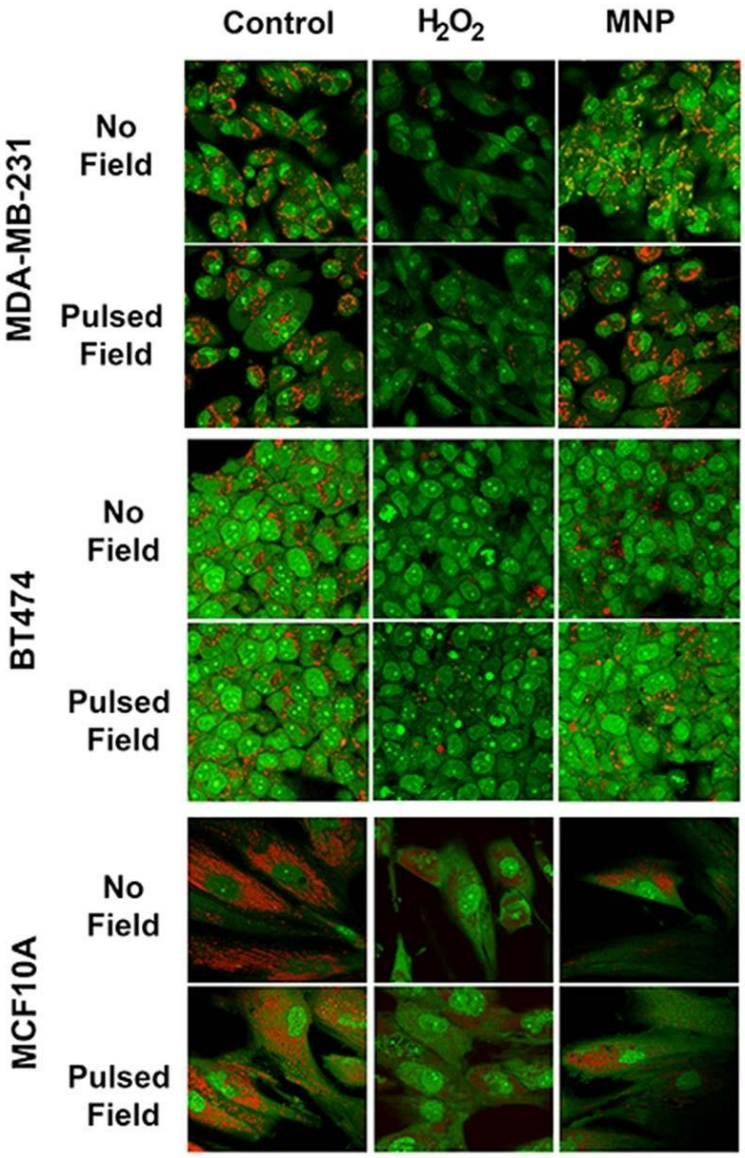

Figure 4.12 LMP detection using acridine orange in SMNP-treated MDA-MB-231, BT474 and MCF10A cells before and after pulsed field exposure. Cells were incubated with PAA-P85-SMNP for 24 h at 37 °C, washed and exposed to the 50Hz pulsed AC magnetic field. (50 kA/m). After three hours, cells were incubated with 10 μg/mL acridine orange for 15 min. Positive control cells were treated with 150 μM hydrogen peroxide for three hours. The cells exposed to hydrogen peroxide exhibit loss of punctate red fluorescence while negative controls and cells treated with SMNPs do not.

Once heating and LMP were eliminated as potential explanations for our observations, we looked to the differing cytoskeletal architectures of the cell lines for a mechanism. Cytoskeletal damage as a cause of cell death has been well reported in the literature. Actin filaments are one of the main components involved in maintaining cell structure as well as assisting with transport of organelles and vesicles throughout the cell. Previous research has shown that interference with cytoskeletal components can cause cessation of the cell cycle and lead to apoptosis.[27-28] Lysosomes are anchored to microtubule highways and highly associated with actin filaments. The hypothesis for this system is that the PAA-P85-SMNPs accumulate in lysosomes and upon remote actuation by the AC magnetic field can rotate inside of the lysosome, thus inducing torques and shear stresses on the underlying cytoskeleton, all without causing lysosomal leakage. A schematic of this event progression can be seen in Figure 4.13. The cytoskeleton in cancerous cells is more sensitive to mechano-transduction leading to subsequent damage and cell death. Thus, it is suggested that while the generated forces are insufficient to cause damage to the underlying cytoskeleton of the stiffer, benign cells, less mechanical force is required to cause cytoskeletal deformation to the cytoskeleton of non-cancerous cells.[29-31]

The theory of actin damage as the cause of cell death was studied by first determining the effect of the AC magnetic field on actin structure using confocal microscopy (Figure 4.14). MDA-MB-231 and BT474 control cells show an actin filament structure very typical of cancer cells while the nontumorigenic MCF10A cells show actin structures very typical of healthy epithelial cells. Following exposure to 0.1 mg/mL of Alexa Fluor 647® labeled PAA-P85-SMNPs and a pulsed 50 Hz, 50 kA/m AC magnetic field, the confocal images revealed significant disruption of the actin cytoskeleton in the cancerous MDA-MB-231 and BT474 cells but not in the nontumorigenic MCF10A cells (Figure 4.14 left panel). This is in excellent agreement with the previously discussed cytotoxicity data (Figure 4.10). To further test the correlation between the mechanical properties of

the cells and treatment effects, the cells were incubated with Cytochalasin D (CD). CD disrupts actin polymerization and in sub-lethal doses decreases the mechanical stiffness of cells (as measured by Atomic Force Microscopy). Therefore, exposure of non-cancerous cells to CD reduces their stiffness to the levels comparable to cancer cells.[30] Notably after exposure to CD and SMNPs the pulsed AC magnetic field regime enacts significant cytoskeletal damage in MCF10A cells as can be seen in the insert of Figure 4.14c. The damage is comparable to the damage observed in the cancerous cells following exposure to the SMNPs and pulsed AC magnetic field (Figures 4.14a-b). No significant differences in the cytoskeleton structure were observed in cancerous cells incubated with CD alone following exposure to a pulsed AC magnetic field.

Cell viability data confirmed these observations. Addition of CD to SMNP exposed MCF10A cells sensitizes them to both the continuous and pulsed AC magnetic field regimes (Figure 4.14 right panel). The MCF10A cell viability decreased to 25% following exposure to the 50Hz, 50kA/m AC field. It was also interesting to see that CD appeared to sensitize the cancer cells to forces created by the SMNP in the continuous field regime.

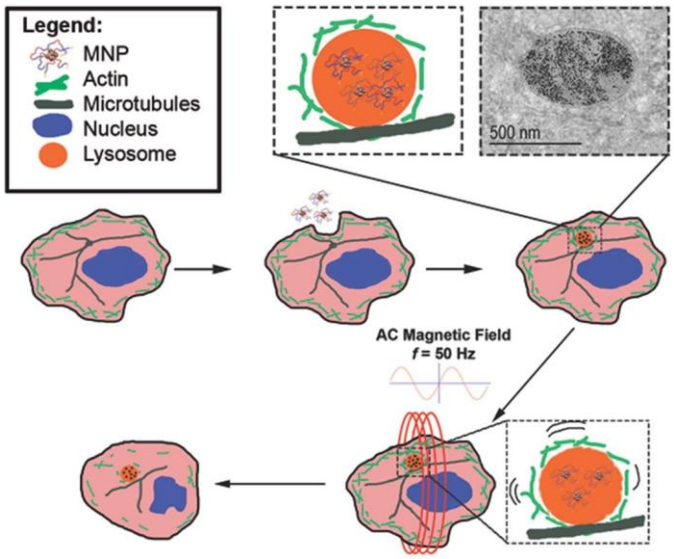

Figure 4.13 Schematic representation of SMNP uptake into lysosomes followed by mechanical movement of the lysosomes to generate forces leading to cytoskeletal disruption.

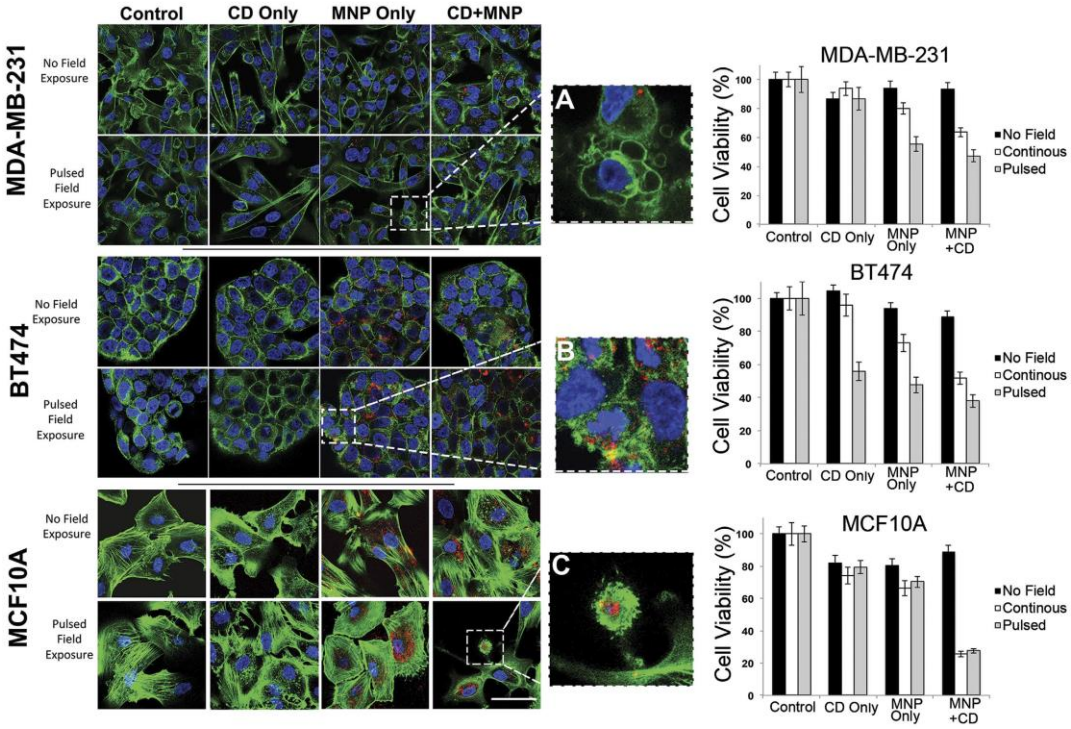

Figure 4.14 The left panel shows representative confocal images of actin (green) of the MDA-MB-231, BT474 and nontumorigenic MCF10A cell before and after exposure to a pulsed AC magnetic field with or without treatment with CD and/or PAA-P85-SMNP (red). Insets show a large image of the actin cytoskeleton of a dead (A) MDA-MB-231, (B) BT474 and (C) MCF10A. The right panel shows corresponding cell viability for the same conditions in the three cell lines.

The proposed mechanism of mechanical disruption of the cytoskeleton is in very good agreement with the differences in cytotoxicity observed for MDA-MB-231 cells versus BT474 cells. BT474 cells grow in multilayer colonies and their complex cytoskeletal structure is very important to their growth. Interestingly, we have observed colocalization of PAA-P85-SMNPs with the basal cells rather than in the top layer (Figures 4.15-4.16). It may be that when the cytoskeletons of the basal cells in the

colony are compromised, this causes a subsequent loss to the apical cells in the colony as well which results in the lower cell viability we observed in Figure 4.10.

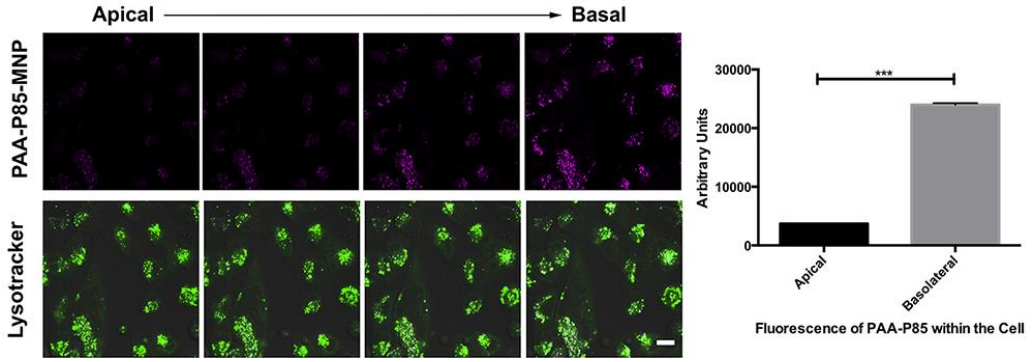

Figure 4.15 Confocal microscopy of MDA-MB-231 treated for 24 hours with 0.05 mg/mL AlexaFluor 647-PAA-P85-SMNP. This z-stack shows that the intracellular distribution of SMNPs increases towards the basal part of the cell. Quantification of this fluorescence is seen in the graph.

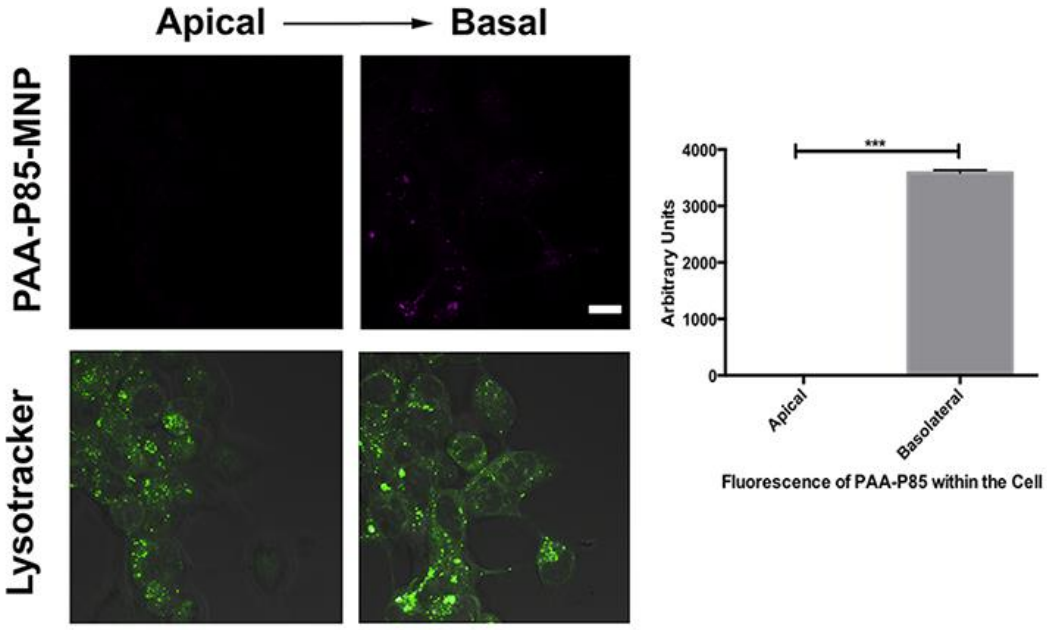

Figure 4.16 Confocal microscopy of BT474 cells treated for 24 h with 0.05 mg/mL AlexaFluor 647-PAA-P85-SMNP. This z-stack shows that the intracellular distribution of SMNPs increases towards the basal part of the cell. Quantification of this fluorescence is seen in the graph.

4.5 Discussion

We observed a new mechanism of toxicity of SMNPs in non-heating super low frequency AC magnetic fields to cancerous cells that involves cytoskeletal disruption, and it can be selectively enacted upon cancerous cells while leaving healthy cells intact. The selective cytotoxic effect was dependent on the cell mechanical properties rather than on intracellular uptake disparities between cancerous and healthy cells reported elsewhere.[14-15, 32] Notably, cancerous and non-cancerous cell lines differ in mechanical properties of the cytoskeleton. Cancerous cells are mechanically softer than their benign counterparts due to their need to remodel during transformation and metastasis.[29] For example, the Young's modulus of malignant MDA-MB-231 cells is less than half that of the non-malignant MCF10A cells.[33] It has previously been shown that SMNPs conjugated to signaling proteins can control the assembly of cytoskeletal components such as microtubules in an applied magnetic field.[34-35] It was also shown that SMNPs under AC magnetic fields can form linear aggregates.[8, 36] In addition, in high frequency magnetic fields, SMNPs can oscillate mechanically and generate ultrasound waves.[37] While the movement of individual particles cannot induce forces high enough to generate biological responses, forces generated by an assembly of SMNPs, such as those observed here in lysosomes, are sufficient to induce cellular responses.[37] However, our experiments were carried out in the absence of the magnetic field gradient, using at least 1/10 of the field amplitude and nearly 104 lower field frequencies than those predicted to generate the ultrasound waves. Therefore, we believe that we may observe a different effect.[37]

We have previously reported that exposure to an AC field can cause mechanical movement of SMNPs, which generates stress forces and deformation of the surrounding polymer coating and attached biological molecules.[38] In one study, the aggregates of PAA-PEG coated SMNPs with enzymes conjugated to the PAA chains were reported to denature the enzyme in the AC field without

heating.[39] The estimates of the forces for the AC fields used herein (50 Hz, 50 to 100 kA/m) suggest that the movement of individual magnetite particles of ~7-8 nm in diameter is unlikely to induce forces high enough to generate biological responses. However, these fields can produce forces ranging from several dozen to ~300 pN, if single particles form aggregates with a greater net magnetic moment. Such forces may exceed the strength of the filaments in the cells and result in their damage.[40] The literature states that actin-actin bonds will break at 600 pN under straight pulling and at 320 pN under twisting forces.[41] Notably, these estimates of strength were obtained with a monotonously increasing load applied to the filaments as a whole. The aggregates of the SMNPs accumulated in lysosomes can actually affect filaments locally and multiple times (~ $3 \cdot 10^4$ loading cycles during 10 min at 50 Hz AC field). It is well known that due to fatigue dynamic strength of the materials is 3–4 times lower than their static strength.

Interestingly we did not observe permeabilization of lysosomes in contrast to Zhang *et al.* who described the use of a rotating magnetic field to rotate particles, mostly within lysosomes (and attached to the lysosome membranes).[9] Therefore, we believe that there are major differences in both mechanism and result from the work of Zhang *et al.* The present work does not invoke rotating fields and importantly the particle size ~7-8 nm is at least an order of magnitude less than that of Zhang *et al.* (they used particles of 100 nm and more). Such small particles aggregate within the lysosomes upon internalization in the cells. Each lysosome may contain from several hundred to several thousands of particles, which is not surprising since we estimate that each cell takes up from ~105 to ~106 particles (see Supplementary information). The pentablock copolymer coating of the particles may be very important since upon the accumulation of the particles in the lysosomes their hydrophobic poly(propylene oxide) chains of P85 may interact with each other (alike formation of Pluronic micelles). This should lead to a formation of a dense physical nanogel SMNP-polymer

network. Moreover, poly(propylene oxide) chains may also form multiple "anchors" to the lysosome membrane. As a result the giant SMNPs aggregates and the surrounding lysosomes would move as a whole with much of the load affecting their points of attachment to the actin filaments and only relatively little stress produced upon the lysosomal membranes (Figure 4.17).

Notably, effects of the continuous AC magnetic field depend more specifically on the SMNP concentration inside the cells and lysosomes while exposure to the pulsed AC magnetic field generates more cell damage at each tested concentration. The exposure to CD sensitizes the cancerous cells to a continuous AC magnetic field, suggesting that less force is generated by continuous exposure. This difference between exposure to continuous and pulsed AC magnetic fields might be due to the fact that following the application of force, stress-relaxation processes can occur in the cells. Connord *et al.* reported that during the AC field application (300 kHz, 53 mT) lysosomes containing magnetite nanoparticles of nearly same size as in the present work can align within cells in needle-like structures along the direction of the field.[13] Once the field is switched off the lysosomes disassemble. Assembling and disassembling occurs during minutes, i.e. same time scale as the on/off field exposures in the present work. So it is likely that similar assembling/disassembling can also proceed in the conditions of our experiment. At lower frequencies, such 50 Hz AC field the alignment of magnetite-loaded lysosome is even more likely. In this case the rupture of the cytoskeleton may take place in the areas of greatest stress due to a combination of strain and torque. (The torque produced by AC field appears to be essential, since no toxicity was observed upon repeated exposure of cancer cells to DC field.) Once the lysosomes disassemble the strain is released, but when the field is applied again the assembly of the lysosomes may cause stress in the new areas of the cytoskeleton.

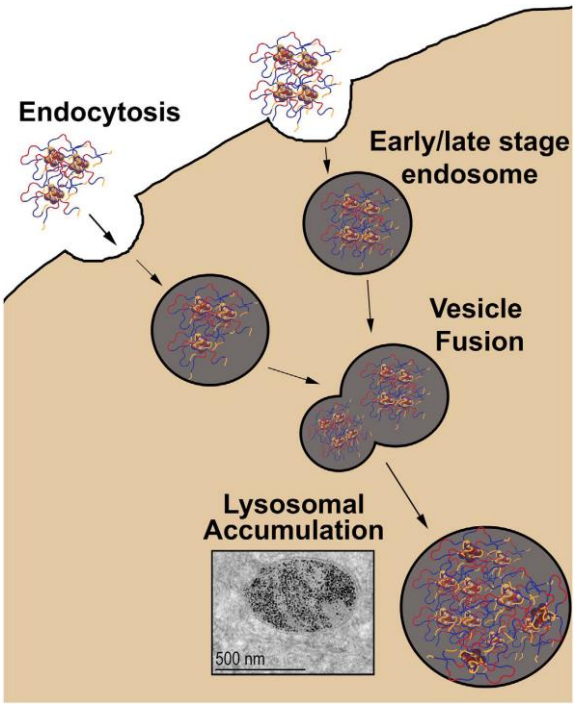

Figure 4.17 Scheme illustrating assembly of PAA-P85-SMNP during endocytosis and trafficking in the cells. The SMNP (brown spheres) are coated with the pentablock copolymer attached to the particles through the PAA chains (yellow). Upon accumulation in the lysosomes the coated SMNP form large aggregates, in which individual magnetite particles are interconnected via swollen hydrophilic poly(ethylene oxide) chains (blue) and hydrophobic poly(propylene oxide) chains (red) that interact with each other and the lysosomal membrane.

4.6 Conclusions

Our results demonstrate that polymer coats can enhance the intracellular uptake of SMNPs and allow subsequent magneto-mechanical actuation of these nanoparticles through the use of super low frequency AC magnetic fields. The work demonstrates that cytoskeletal disruption and subsequent cell death can be selectively enacted upon cancerous cells while leaving healthy cells intact. This type of system which allows for enhanced intracellular uptake, remotely controlled actuation and most importantly cancer cell selectivity has a high impact potential for cancer therapy and could serve as a

platform technology in other biomedical applications.

4.7 Acknowledgements

The Carolina Partnership, a strategic partnership between the UNC Eshelman School of Pharmacy, The University Cancer Research Fund through the Lineberger 32 Comprehensive Cancer Center and the grant from the UNC Eshelman Institute for Innovation, in part supported this work.

4.8 References

1. Urries, I.; Muñoz, C.; Gomez, L.; Marquina, C.; Sebastian, V.; Arruebo, M.; Santamaria, J., Magneto-plasmonic nanoparticles as theranostic platforms for magnetic resonance imaging, drug delivery and NIR hyperthermia applications. *Nanoscale* **2014,** *6* (15), 9230-9240.
2. Ansari, C.; Tikhomirov, G. A.; Hong, S. H.; Falconer, R. A.; Loadman, P. M.; Gill, J. H.; Castaneda, R.; Hazard, F. K.; Tong, L.; Lenkov, O. D., Development of Novel Tumor ‐ Targeted Theranostic Nanoparticles Activated by Membrane ‐ Type Matrix Metalloproteinases for Combined Cancer Magnetic Resonance Imaging and Therapy. *Small* **2014,** *10* (3), 566-575.
3. He, H.; David, A.; Chertok, B.; Cole, A.; Lee, K.; Zhang, J.; Wang, J.; Huang, Y.; Yang, V. C., Magnetic nanoparticles for tumor imaging and therapy: a so-called theranostic system. *Pharmaceutical Research* **2013,** *30* (10), 2445-2458.
4. Yoo, D.; Lee, J.-H.; Shin, T.-H.; Cheon, J., Theranostic magnetic nanoparticles. *Accounts of chemical research* **2011,** *44* (10), 863-874.
5. Di Corato, R.; Espinosa, A.; Lartigue, L.; Tharaud, M.; Chat, S.; Pellegrino, T.; Ménager, C.; Gazeau, F.; Wilhelm, C., Magnetic hyperthermia efficiency in the cellular environment for different nanoparticle designs. *Biomaterials* **2014,** *35* (24), 6400-6411.
6. Andrä, W.; d'Ambly, C.; Hergt, R.; Hilger, I.; Kaiser, W., Temperature distribution as function of time around a small spherical heat source of local magnetic hyperthermia. *Journal of Magnetism and Magnetic Materials* **1999,** *194* (1-3), 197-203.
7. Sonvico, F.; Mornet, S.; Vasseur, S.; Dubernet, C.; Jaillard, D.; Degrouard, J.; Hoebeke, J.; Duguet, E.; Colombo, P.; Couvreur, P., Folate-conjugated iron oxide nanoparticles for solid tumor targeting as potential specific magnetic hyperthermia mediators: synthesis, physicochemical characterization, and in vitro experiments. *Bioconjugate Chemistry* **2005,** *16* (5), 1181-1188.
8. Salunkhe, A. B.; Khot, V. M.; Pawar, S., Magnetic hyperthermia with magnetic nanoparticles: a status review. *Current topics in medicinal chemistry* **2014,** *14* (5), 572-594.
9. Villanueva, A.; De La Presa, P.; Alonso, J.; Rueda, T.; Martinez, A.; Crespo, P.; Morales, M.; Gonzalez-Fernandez, M.; Valdes, J.; Rivero, G., Hyperthermia HeLa cell treatment with silica-coated manganese oxide nanoparticles. *The Journal of Physical Chemistry C* **2010,** *114* (5), 1976-1981.
10. Creixell, M.; Bohorquez, A. C.; Torres-Lugo, M.; Rinaldi, C., EGFR-targeted magnetic nanoparticle heaters kill cancer cells without a perceptible temperature rise. *ACS Nano* **2011,** *5* (9), 7124-7129.
11. Domenech, M.; Marrero-Berrios, I.; Torres-Lugo, M.; Rinaldi, C., Lysosomal membrane permeabilization by targeted magnetic nanoparticles in alternating magnetic fields. *ACS Nano* **2013,** *7* (6), 5091-5101.

12. Sanchez, C.; El Hajj Diab, D.; Connord, V.; Clerc, P.; Meunier, E.; Pipy, B.; Payré, B.; Tan, R. P.; Gougeon, M.; Carrey, J., Targeting a G-protein-coupled receptor overexpressed in endocrine tumors by magnetic nanoparticles to induce cell death. *ACS Nano* **2014,** *8* (2), 1350-1363.
13. Connord, V.; Clerc, P.; Hallali, N.; El Hajj Diab, D.; Fourmy, D.; Gigoux, V.; Carrey, J., Real‐Time Analysis of Magnetic Hyperthermia Experiments on Living Cells under a Confocal Microscope. *Small* **2015,** *11* (20), 2437-2445.
14. Zhang, E.; Kircher, M. F.; Koch, M.; Eliasson, L.; Goldberg, S. N.; Renström, E., Dynamic magnetic fields remote-control apoptosis via nanoparticle rotation. *ACS Nano* **2014,** *8* (4), 3192-3201.
15. Kim, D.-H.; Rozhkova, E. A.; Ulasov, I. V.; Bader, S. D.; Rajh, T.; Lesniak, M. S.; Novosad, V., Biofunctionalized magnetic-vortex microdiscs for targeted cancer-cell destruction. *Nature materials* **2010,** *9* (2), 165.
16. Klyachko, N. L.; Sokolsky‐Papkov, M.; Pothayee, N.; Efremova, M. V.; Gulin, D. A.; Pothayee, N.; Kuznetsov, A. A.; Majouga, A. G.; Riffle, J. S.; Golovin, Y. I., Changing the Enzyme Reaction Rate in Magnetic Nanosuspensions by a Non‐Heating Magnetic Field. *Angewandte Chemie International Edition* **2012,** *51* (48), 12016-12019.
17. Pothayee, N.; Pothayee, N.; Hu, N.; Zhang, R.; Kelly, D. F.; Koretsky, A. P.; Riffle, J. S., Manganese graft ionomer complexes (MaGICs) for dual imaging and chemotherapy. *Journal of Materials Chemistry B* **2014,** *2* (8), 1087-1099.
18. Pothayee, N.; Pothayee, N.; Jain, N.; Hu, N.; Balasubramaniam, S.; Johnson, L. M.; Davis, R. M.; Sriranganathan, N.; Riffle, J. S., Magnetic Block Ionomer Complexes for Potential Dual Imaging and Therapeutic Agents. *Chemistry of Materials* **2012,** *24* (11), 2056-2063.
19. Yi, X.; Batrakova, E.; Banks, W. A.; Vinogradov, S.; Kabanov, A. V., Protein conjugation with amphiphilic block copolymers for enhanced cellular delivery. *Bioconjugate Chemistry* **2008,** *19* (5), 1071-1077.
20. Reynolds, E. S., The use of lead citrate at high pH as an electron-opaque stain in electron microscopy. *The Journal of cell biology* **1963,** *17* (1), 208.
21. Milo, R., What is the total number of protein molecules per cell volume? A call to rethink some published values. *Bioessays* **2013,** *35* (12), 1050-1055.
22. Hevia, D.; Rodriguez-Garcia, A.; Alonso-Gervós, M.; Quirós-González, I.; Cimadevilla, H. M.; Gómez-Cordovés, C.; Sainz, R. M.; Mayo, J. C., Cell volume and geometric parameters determination in living cells using confocal microscopy and 3D reconstruction. *Protocol Exchange* **2011**.
23. Trincheri, N. F.; Nicotra, G.; Follo, C.; Castino, R.; Isidoro, C., Resveratrol induces cell death in colorectal cancer cells by a novel pathway involving lysosomal cathepsin D. *Carcinogenesis* **2006,** *28* (5), 922-931.
24. Michallet, M.-C.; Saltel, F.; Flacher, M.; Revillard, J.-P.; Genestier, L., Cathepsin-dependent apoptosis triggered by supraoptimal activation of T lymphocytes: a possible mechanism of high dose tolerance. *The Journal of Immunology* **2004,** *172* (9), 5405-5414.
25. Boya, P.; Andreau, K.; Poncet, D.; Zamzami, N.; Perfettini, J.-L.; Metivier, D.; Ojcius, D. M.; Jäättelä, M.; Kroemer, G., Lysosomal membrane permeabilization induces cell death in a mitochondrion-dependent fashion. *Journal of Experimental Medicine* **2003,** *197* (10), 1323-1334.
26. Antunes, F.; Cadenas, E.; Brunk, U. T., Apoptosis induced by exposure to a low steady-state concentration of H2O2 is a consequence of lysosomal rupture. *Biochemical Journal* **2001,** *356* (Pt 2), 549.
27. Atencia, R.; Asumendi, A.; Garcia-Sanz, M., Role of cytoskeleton in apoptosis. **2000**.
28. Ndozangue-Touriguine, O.; Hamelin, J.; Bréard, J., Cytoskeleton and apoptosis. *Biochemical pharmacology* **2008,** *76* (1), 11-18.

29. Swaminathan, V.; Mythreye, K.; O'Brien, E. T.; Berchuck, A.; Blobe, G. C.; Superfine, R., Mechanical stiffness grades metastatic potential in patient tumor cells and in cancer cell lines. *Cancer research* **2011,** *71* (15), 5075-5080.
30. Wakatsuki, T.; Schwab, B.; Thompson, N. C.; Elson, E. L., Effects of cytochalasin D and latrunculin B on mechanical properties of cells. *Journal of cell science* **2001,** *114* (5), 1025-1036.
31. Lee, M.-H.; Wu, P.-H.; Staunton, J. R.; Ros, R.; Longmore, G. D.; Wirtz, D., Mismatch in mechanical and adhesive properties induces pulsating cancer cell migration in epithelial monolayer. *Biophysical journal* **2012,** *102* (12), 2731-2741.
32. Wen, J.; Jiang, S.; Chen, Z.; Zhao, W.; Yi, Y.; Yang, R.; Chen, B., Apoptosis selectively induced in BEL-7402 cells by folic acid-modified magnetic nanoparticles combined with 100 Hz magnetic field. *International journal of nanomedicine* **2014,** *9*, 2043.
33. Nikkhah, M.; Strobl, J. S.; Schmelz, E. M.; Agah, M., Evaluation of the influence of growth medium composition on cell elasticity. *Journal of biomechanics* **2011,** *44* (4), 762-766.
34. Hoffmann, C.; Mazari, E.; Lallet, S.; Le Borgne, R.; Marchi, V.; Gosse, C.; Gueroui, Z., Spatiotemporal control of microtubule nucleation and assembly using magnetic nanoparticles. *Nature nanotechnology* **2013,** *8* (3), 199.
35. Hoffmann, C. l.; Mazari, E.; Gosse, C.; Bonnemay, L.; Hostachy, S.; Gautier, J. r. m.; Gueroui, Z., Magnetic control of protein spatial patterning to direct microtubule self-assembly. *ACS Nano* **2013,** *7* (11), 9647-9654.
36. Saville, S. L.; Qi, B.; Baker, J.; Stone, R.; Camley, R. E.; Livesey, K. L.; Ye, L.; Crawford, T. M.; Mefford, O. T., The formation of linear aggregates in magnetic hyperthermia: Implications on specific absorption rate and magnetic anisotropy. *Journal of Colloid and Interface Science* **2014,** *424*, 141-151.
37. Carrey, J.; Connord, V.; Respaud, M., Ultrasound generation and high-frequency motion of magnetic nanoparticles in an alternating magnetic field: toward intracellular ultrasound therapy? *Applied Physics Letters* **2013,** *102* (23), 232404.
38. Golovin, Y. I.; Gribanovsky, S. L.; Golovin, D. Y.; Klyachko, N. L.; Majouga, A. G.; Master, A. M.; Sokolsky, M.; Kabanov, A. V., Towards nanomedicines of the future: Remote magneto-mechanical actuation of nanomedicines by alternating magnetic fields. *Journal of Controlled Release* **2015,** *219*, 43-60.
39. Klyachko, N. L.; Sokolsky-Papkov, M.; Pothayee, N.; Efremova, M. V.; Gulin, D. A.; Pothayee, N.; Kuznetsov, A. A.; Majouga, A. G.; Riffle, J. S.; Golovin, Y. I.; Kabanov, A. V., Changing the Enzyme Reaction Rate in Magnetic Nanosuspensions by a Non-Heating Magnetic Field. *Angewandte Chemie International Edition* **2012,** *51* (48), 12016-12019.
40. Suresh, S., Biomechanics and biophysics of cancer cells. *Acta Materialia* **2007,** *55* (12), 3989-4014.
41. Noy, A.; Vezenov, D. V.; Lieber, C. M., Chemical force microscopy nanoscale probing of fundamental chemical interactions. In *Handbook of Molecular Force Spectroscopy*, Springer: 2008; pp 97-122.

Chapter 5: Ammonium Bisphosphonate Polymeric Magnetic Nanocomplexes for Platinum Anticancer Drug Delivery and Imaging, with Potential Hyperthermia and Temperature-Dependent Drug Release

Rui Zhang,[†] Benjamin Fellows,[‡] Nikorn Pothayee,[§] Nan Hu,[†] Nipon Pothayee,[†] Ami Jo,[†] Ana C. Bohórquez,[⁄⁄] Carlos Rinaldi,[⁄⁄] O. Thompson Mefford,[‡] Richey M. Davis[†] and Judy S. Riffle[*†]

[†]Department of Chemistry, Department of Chemical Engineering, and Macromolecules Innovation Institute, Virginia Tech, Blacksburg, VA 24061

[‡]Department of Materials Science and Engineering and the Center for Optical Materials Science and Engineering (COMSET), Clemson University, Clemson, SC 29634

[§]Laboratory of Functional and Molecular Imaging, National Institute of Neurological Disorders and Stroke, National Institutes of Health, Bethesda, MD 20892

[⁄⁄]J. Crayton Pruitt Family Department of Biomedical Engineering and Department of Chemical Engineering, University of Florida, Gainesville, FL 32611

Corresponding Author *E-mail: jriffle@vt.edu

5.1 Abstract

Novel Magnetite - ammonium bisphosphonate Graft Ionic Copolymer nanocomplexes (*MGICs*) have been developed for potential drug delivery, magnetic resonance imaging, and hyperthermia applications. The complexes displayed relatively uniform sizes with narrow size distributions upon self-assembly in aqueous media and their sizes were stable under simulated physiological conditions for at least 7 days. The anticancer drugs, cisplatin and carboplatin, were loaded into the complexes,

and sustained release of both drugs was observed. The transverse NMR relaxivities (r_2's) of the complexes were 244 s^{-1} $(mM\ Fe)^{-1}$ which is fast compared to either the commercial T_2-weighted MRI agent Feridex IV® as well as our previously reported magnetite-block ionomer complexes. Phantom MRI images of the complexes demonstrated excellent negative contrast effects of such complexes. Thus, the bisphosphonate-bearing *MGICs* could be promising candidates for dual drug delivery and magnetic resonance imaging. Moreover, the bisphosphonate *MGICs* generate heat under an AC magnetic field of 30 kA m^{-1} at 206 kHz. The temperature of the *MGICs* dispersion in deionized water increased from 37 to 41 °C after exposure to the magnetic field for 10 minutes, corresponding to a specific absorption rate of 77.0 W g^{-1}. This suggests their potential as hyperthermia treatment agents as well as the possibility of heat-induced drug release, making the nanocomplexes more versatile in potential drug delivery applications.

5.2 Introduction

Nanoscale drug delivery and imaging systems have received tremendous interest in the past few decades.[1-12] They enjoy some intrinsic advantages over conventional drug delivery approaches. Due to the small sizes of the nanoparticles, they can transport through capillaries and enter cells, therefore leading to higher drug accumulation at the desired site.[2] Drug release depends on the interaction between the drug and the carrier, and this can be carefully designed and fabricated. Such systems can also lead to long drug circulation times.[13]

With the aim of improving drug bioavailability and minimizing cytotoxicity, a multitude of drug delivery systems have been developed to address the issues of drug efficacy and circulation time in the bloodstream during delivery.[14-15] Micellar polymeric drug carriers have been of particular interest due to the advantages of self-assembly in water and their potential for large-scale industrial production. These carriers can form core-shell micelles *via* self-assembly with therapeutic and

diagnostic agents in water, and they can be either amphiphilic nonionic or ionic block copolymers.[16-20] They feature a water soluble segment, and a hydrophobic segment or an ionic segment. The hydrophobic or ionic segment can be designed to bind metal or metal oxide nanoparticles, and to form complexes with hydrophobic drugs. Those components form the cores of micellar complexes in water. Interactions in the core among the different components are largely non-covalent, and can include electrostatic interactions, hydrophobic interactions, hydrogen bonding, and metal-ligand complexation.[2] Specifically for the block or graft ionic copolymers that contain a hydrophilic segment and an ionic segment, the interactions can combine both electrostatic and metal-ligand interactions. This leads to the formation of core-shell micellar structures with a nonionic hydrophilic shell and an ionic core that is comprised of the anionic polymer segment as well as the bound transition metals or metal oxides. The residual unbound ionic segment provides binding sites for drug loading via ionic complexation.[21] The hydrophilic segment, which is typically poly(ethylene oxide), plays the role of improving dispersibility and biocompatibility of the complexes.[22]

Iron oxide nanoparticles, particularly magnetite nanoparticles (MNPs), have been reported to be a versatile and powerful probe in biomedical applications such as nanoparticle-based imaging and cancer therapy approaches.[23-25] They have been utilized as effective contrast enhancement agents for transverse (T_2-weighted) magnetic resonance imaging (MRI) due to their low toxicity and high magnetization in magnetite-polymer complexes.[21] MNPs of certain sizes can generate heat upon exposure to an alternating magnetic field (AMF), making them potentially useful for local magnetic hyperthermia therapy, or for triggered drug release if drugs are encapsulated in the magnetite-based nanocarriers.[6, 26] MNPs are usually coated with natural or synthetic biocompatible macromolecules such as dextran or poly(ethylene oxide)-containing copolymers to prevent aggregation for biomedical applications.[27-28] This increases their colloidal stability in physiological media and minimizes

toxicity.[29-31] The magnetite-ionic copolymer complexes can be used as contrast agents for MRI. Colloidally stable magnetite-copolymer complexes can also serve as carriers for selectively storing and releasing small molecules which make them potentially attractive drug carriers for cancer therapy. Cancer is a major public health problem in the United States and worldwide.[32] It is reported to be the second leading cause of death in the United States and is approaching the rate for the current number one cause, cardiovascular/heart diseases.[33-34] More than 85% of cancers eventually lead to the formation of solid tumors.[35] Many therapies have been developed, aimed at blocking the biological activities of tumor cells and killing them. A family of platinum therapeutic agents is in clinical use to treat various cancer types.[36] A first-generation platinum drug, cisplatin, a second-generation drug, carboplatin, and a third-generation analog, oxaliplatin, are potent anti-tumor drugs which have achieved success in treating some types of malignant tumors such as testicular, lung, ovarian, and colon tumors.[37-41] However, due to their lack of selectivity and to drug resistance complications, as well as their low solubility and high cytotoxicity, especially in the case of cisplatin, their applications have been limited.[36, 42] Nanocarrier-based delivery of platinum complexes is a therapeutic alternative that has evolved over the last decade as an approach to cancer therapy.[42-43] Compared to low molecular weight drugs which rapidly pass through the cell membranes of both normal and cancerous tissues, drugs which are loaded into nanocarriers of certain sizes can passively accumulate into solid tumors via the enhanced permeability and retention effect, promoting drug uptake into tumor sites with reduced off-target toxicity effects.[44] In addition, nanoparticle drug delivery systems have shown improvement of the pharmacokinetic and pharmacodynamic profiles of the chemotherapeutic payloads and have promoted controlled and sustained release of platinum drugs.[45-47] Use of these nanocarriers may enable high intracellular concentration in cancer cells and achieve potential stimuli-responsive drug release, while suppressing the development of multidrug resistance.[43, 48-50]

Hyperthermia has also generated research interest for biomedical applications such as cancer treatment and drug/gene delivery.[51-56] Magnetic nanoparticles can act as a heating source via magnetically mediated hyperthermia that involves heating of specific tissues or organs to between 41 and 46 ºC.[52] When the temperature is raised to 41-43 ºC, tumor cells can be irreversibly damaged while normal tissues may not be, because tumor cells are more sensitive to heat than normal cells.[57-58] Since magnetic fields can penetrate human tissues, treatment by hyperthermia may serve as a non-invasive method to kill cancer cells.[59] Moreover, it has been found that hyperthermia greatly enhances treatments by radiotherapy or chemotherapy for several cell lines including those found in brain tumors.[60-62] Hyperthermia studies on rats and dogs have shown positive results as well.[57] Magnetite nanoparticles can have a high specific absorption rate (SAR) of energy, which is ideal for hyperthermia applications.[63] Utilization of iron oxide nanoparticles for magnetically induced hyperthermia has been reported to kill cancer cells and these are in clinical trials for brain and prostate cancer patients.[60, 64-66]

Phosphonic acid-containing polymers have recently triggered interest in biomedical fields, and there have been multiple reports of their potential for drug delivery.[67-69] Denizot *et al*. studied different types of polymer coatings for iron oxide nanoparticles, which included sulfonates, phosphonates, and carboxylates.[70] The phosphonate-bearing polymer-magnetite complexes displayed much better hydrodynamic stability at pH 7.0 compared to the stability of analogous carboxylate-containing complexes. The hydrodynamic sizes of the particles remained unchanged for over two weeks. Mohapatra and coworkers modified the surfaces of magnetite nanoparticles with 2-carboxyethyl phosphonic acid and carboxylic acid.[71] Subsequently, the carboxylic acids were conjugated with folic acid. The sizes of the nanoparticles with and without conjugated folic acid remained unchanged over a pH range of 4.5-8, indicating strong binding between the magnetite and the phosphonate groups.

Previously our group[47, 72] prepared ammonium bis(phosphonate)-functional poly(*N*-isopropylacrylamide)-magnetite and poly(ammonium bisphosphonic acid methacrylate)-*g*-PEO-manganese (II) nanoparticles. Both complexes were colloidally stable in phosphate buffered saline (PBS) at pH 7.4 for an extended period. Thus, phosphonate-containing polymers can be promising candidates for making colloidally stable nanocarriers for drug delivery.

In this paper, we report novel magnetite-graft ionomer complexes (*MGICs*) that were made by adsorbing poly(ammonium bisphosphonic acid methacrylate)-*g*-poly(ethylene oxide) onto magnetite. Analogous poly(acrylic acid)-bearing graft ionic copolymers were also used to make comparisons. A portion of either the bisphosphonic acid or the acrylic acid of the copolymer was complexed with the magnetite surfaces to form a core, while the poly(ethylene oxide) (PEO) component extended into water to form the shell to provide colloidal stability in aqueous solutions. Cisplatin and carboplatin were loaded into the complexes, and drug release was measured in simulated endosomal (pH = 4.6) and physiological conditions (pH = 7.4). Physicochemical properties, charge characteristics, and hydrodynamic stabilities were measured and compared to other previously reported systems to evaluate the potential of such nanoparticles for drug delivery. The specific absorption rate of hexyl bisphosphonate *MGICs* in an aqueous dispersion was measured to evaluate the potential of the complexes for heat-induced drug release and/or hyperthermia treatment. Transverse relaxivities and phantom MRI images were obtained to evaluate their potential for T_2-weighted magnetic resonance imaging.

5.3 Experimental

5.3.1 Materials

Diethyl vinyl phosphonate (Epsilon-Chimie, >98%), anhydrous dimethylsulfoxide (DMSO) and dichloromethane (EMD Chemicals, anhydrous, 99.8%) were used as received. Phosphate buffered saline (PBS) was obtained from Mediatech. Acetate buffer solution (ABS) was purchased from Fluka Analytical. Methanol (anhydrous, 99.9%), hexane (99.9%), dichloromethane (99.9%), chloroform (99.9%), diethyl ether (anhydrous, 99.8%), nitric acid aqueous solution (69.3%) and dialysis tubing (Spectra/Por, 3,500 and 12,000 MWCO), all from Fisher Scientific, were used as received. *N*,*N*-Dimethylformamide (DMF, 99.9%), 3-amino-1-propanol (>99%), 6-amino-1-hexanol (>99%), sodium sulfate (anhydrous, 99%), triethylamine (>99.5%), sodium hydroxide (97%), poly(ethylene oxide) monomethyl ether (M_n=5,085), 2,2'-azobisisobutyronitrile (AIBN, 98%), sodium chloride (>99.5%), oleic acid (90%, technical grade), iron(III) chloride hexahydrate (97%), trioctylamine, sodium oleate, and aqueous tetramethylammonium hydroxide solution (25% wt/v) were purchased from Sigma-Aldrich and used as received. Acryloyl chloride (97%), methacryloyl chloride (97%) and bromotrimethylsilane (TMSBr, 97.0%) were fractionally distilled before use. Deionized water was obtained through a MilliQ A10 water purification system (EMD Millipore, MA). Slide-A-Lyzer dialysis cassettes (MWCO 3500) were obtained from Thermo Scientific. Centrifugal filter units (MWCO 10k) were obtained from EMD Millipore. A permanent magnet made of NdFeB with a diameter of 11/16" and a thickness of 1/4" was purchased from K&J Magnetics. It was axially magnetized with a surface field of 3880 Gauss.

5.3.2 Synthesis and fabrication

5.3.2.1 Synthesis of an acrylate-functional poly(ethylene oxide) macromonomer

Poly(ethylene oxide) methyl ether (20 g, Mn = 5,000 g mol^{-1}, 4.0 mmol) was dried under vacuum at 50 °C overnight in a flame-dried 250-mL round bottom flask. Triethylamine (4.0 g, 40 mmol) and 100 mL of anhydrous dichloromethane were charged to the flask via syringe. Acryloyl chloride (3.6 g, 40 mmol) was added dropwise to the flask via syringe. The reaction mixture was stirred at room temperature overnight. The mixture was diluted with chloroform and washed with an aqueous solution of sodium hydroxide (0.1 N, 3 x 50 mL). The organic phase was washed with water (2 x 50 mL), dried over anhydrous sodium sulfate and concentrated by evaporation. The concentrated mixture was precipitated in hexane, filtered and dried under vacuum at room temperature to afford a pale yellow PEO-acrylate powder.

5.3.2.2 Synthesis of methacrylate-functional bisphosphonate monomers

The synthetic scheme for the hexylamino bisphosphonate methacrylate monomer is shown in Figure 5.1. The propylamino bisphosphonate methacrylate monomer can be prepared by the same procedure, by using 3-amino-1-propanol instead of 6-amino-1-hexanol. The acrylate-functional PEO oligomer was synthesized by reacting a commercial ~5000 M_n poly(ethylene oxide) monomethyl ether with freshly-distilled acryloyl chloride.

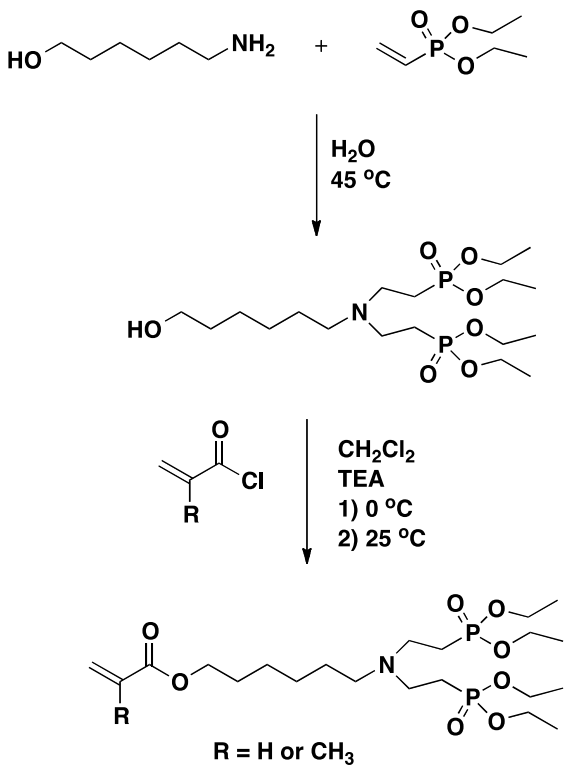

Figure 5.1 Synthesis of hexylamino bisphosphonate methacrylate monomer.

5.3.2.3 Synthesis of an acrylic acid-containing graft copolymer

Conventional free radical polymerization was utilized to synthesize the acrylate-containing graft copolymers. *tert*-Butyl acrylate monomer (2.05 g, 16 mmol) and an acrylate-PEO (1.15 g, 0.23 mmol) were charged to a flame-dried, 25-mL Schlenk flask equipped with a stir bar. Anhydrous toluene (14 mL) was added to the Schlenk flask and the reaction mixture was deoxygenated for 30 min. AIBN (150 mg, 0.9 mmol) was dissolved in degassed toluene (5 mL) in a separate 20-mL vial. The freshly prepared AIBN solution (1 mL) was added to the Schlenk flask via syringe. After three freeze-pump-thaw cycles, the reaction mixture was heated at 70 °C for 24 h. The copolymer was precipitated in a cold mixture of 1:1 v:v anhydrous diethyl ether:hexane (2 x 400 mL) and the resulting copolymer was vacuum dried at room temperature overnight. The *tert*-butyl ester groups were removed by dissolving P(*t*BA)-g-PEO (0.8 g, 0.6 x 10^{-2} eq of *tert*-butyl ester groups) in 30 mL of dichloromethane.

Trifluoroacetic acid (3.5 mL, 4.6 x 10^{-2} mol) was added and the reaction mixture was stirred at room temperature for 24 h. The copolymer was precipitated into hexane and dried under vacuum at room temperature. The copolymer was dissolved in a 9:1 v:v THF:water mixture and dialyzed against 4 L of DI water through a cellulose acetate membrane (MWCO 3,500 g mol^{-1}) for 24 h. The final product was recovered by freeze-drying.

5.3.2.4 Synthesis of Poly(ammonium bisphosphonic acid-g-ethylene oxide) Copolymers.

Synthesis methods for making a poly(hexyl ammonium bisphosphonic acid methacrylate-*g*-ethylene oxide) and a poly(propyl ammonium bisphosphonic acid methacrylate-*g*-ethylene oxide) polymers have been previously reported.[73] Conventional free radical polymerization was utilized to synthesize the bisphosphonate-containing graft copolymers, as is shown in Figure 5.2. The phosphonate esters were then selectively hydrolyzed without affecting the carboxylic esters by a mild approach using bromotrimethylsilane in dichloromethane.

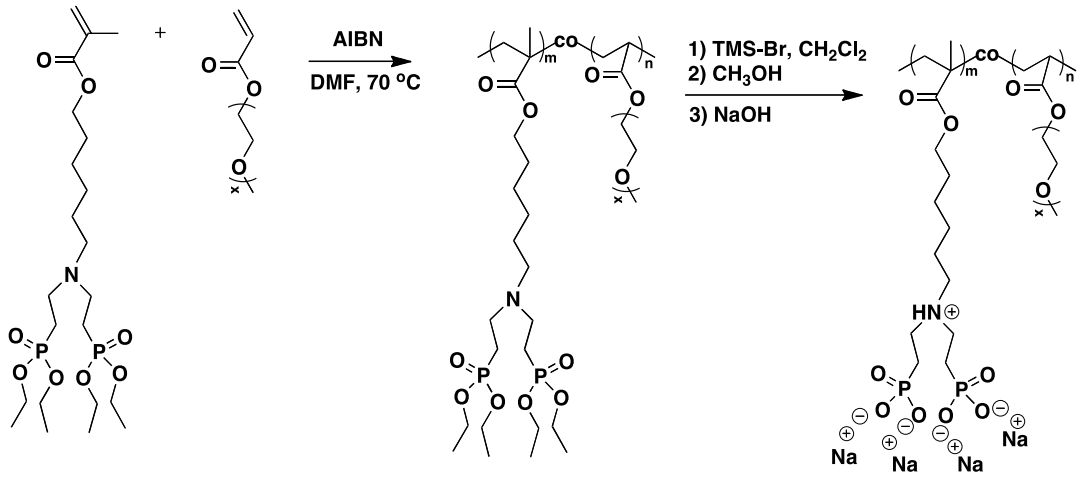

Figure 5.2 Synthesis of poly(hexyl ammonium bisphosphonic acid methacrylate)-*g*-PEO copolymers.

5.3.2.5 Synthesis of Magnetite Nanoparticles (25 nm).

Magnetite nanoparticles were synthesized by a known procedure that utilized thermal decomposition of an iron oleate precursor in trioctylamine as a high-boiling solvent.[74-75] The synthesis consisted of two steps: (1) Synthesis of the iron oleate precursor, and (2), its conversion to magnetite nanoparticles. Iron(III) chloride hexahydrate (6.50 g, 0.95 mmol) was dissolved in deionized water (24 mL) in a 250-mL beaker and sonicated for 10 min. Sodium oleate (21.9 g, 71.9 mmol), then deionized water (12 mL), ethanol (48 mL) and hexane (84 mL) were added. The mixture was placed in a 500-mL, three-neck, round-bottom flask equipped with a heating mantle and mechanical agitation (200 rpm) and purged with N_2 for 5 min. The mixture was heated to 70 ºC with a constant heating rate of 6.7 ºC/min and was kept at 70 ºC for another 4 h. The iron-oleate complex, which partitioned into the upper organic layer, was washed three times with deionized water (20 mL each) in a separatory funnel. The organic layer was collected, and the solvent was removed by rotary evaporation. The viscous product was dried under vacuum at 70 ºC for 24 h to yield the iron-oleate precursor.

The magnetite nanoparticles were prepared by mixing the iron oleate precursor (20.5 g) with oleic acid (3.3 g, 11.7 mmol) and trioctylamine (114 mL) and sonicating for 15 min. The mixture was charged to a 500-mL, three-neck, round-bottom flask equipped with a heating mantle and mechanical agitation (200 rpm) and purged with N_2 for 30 min. The reaction mixture was heated to 350 ºC at a constant rate of 3.3 ºC/min, then kept at 350 ºC for 30 min. The reaction mixture was cooled to room temperature and diluted with cold ethanol. The mixture was placed in centrifuge tubes and centrifuged at 7500 rpm for 15 min. The liquid was decanted and the oleic acid and amine-coated magnetite nanoparticles were recovered from the centrifuge tubes. The magnetite nanoparticles were purged with N_2 overnight at room temperature to yield a black solid.

5.3.2.6 Synthesis of Magnetite-Graft Ionomer Complexes (MGICs).

The synthetic method for preparing the magnetite-graft ionomer complexes (*MGICs*) was adapted from a previously reported method developed by our group.[21] The oleic acid-coated magnetite nanoparticles (50 mg) were dispersed in anhydrous chloroform (5 mL) in a 20-mL vial and the mixture was sonicated for 10 min. Poly(ammonium bisphosphonic acid methacrylate-*g*-PEO) (100 mg) or poly(acrylic acid-*g*-PEO) (100 mg) was charged into a separate vial equipped with a magnetic stir bar. Anhydrous DMF (5 mL) was added to dissolve the polymer, and the mixture was sonicated for 10 min. The magnetite dispersion was added dropwise into the polymer solution while sonicating, followed by purging with N_2 for 5 min. The reaction mixture was further sonicated for 4 h, and the water in the sonicator was changed every 30 min. The mixture was stirred at room temperature for 48 h. The mixture was then precipitated into hexane (20 mL) five times. A permanent magnet was placed under the vial to attract the complexes while the supernatant was decanted to remove any solvent, free oleic acid or other residues. The remaining solid was washed with diethyl ether (20 mL) 3 times, and the supernatant was decanted. The nanoparticles were purged with N_2 for 2 h to remove most of the solvent, then they were dispersed in deionized water (10 mL) and the pH was adjusted to 7.4 using a 1 N aqueous NaOH solution. The dispersion was sonicated for 20 min. It was transferred to dialysis tubing with a 12k MWCO and dialyzed against deionized water (4 L) for 24 h. Finally, the *MGICs* were recovered by freeze-drying for 2 days. The polymer-magnetite complexation process is shown in Figure 5.3.

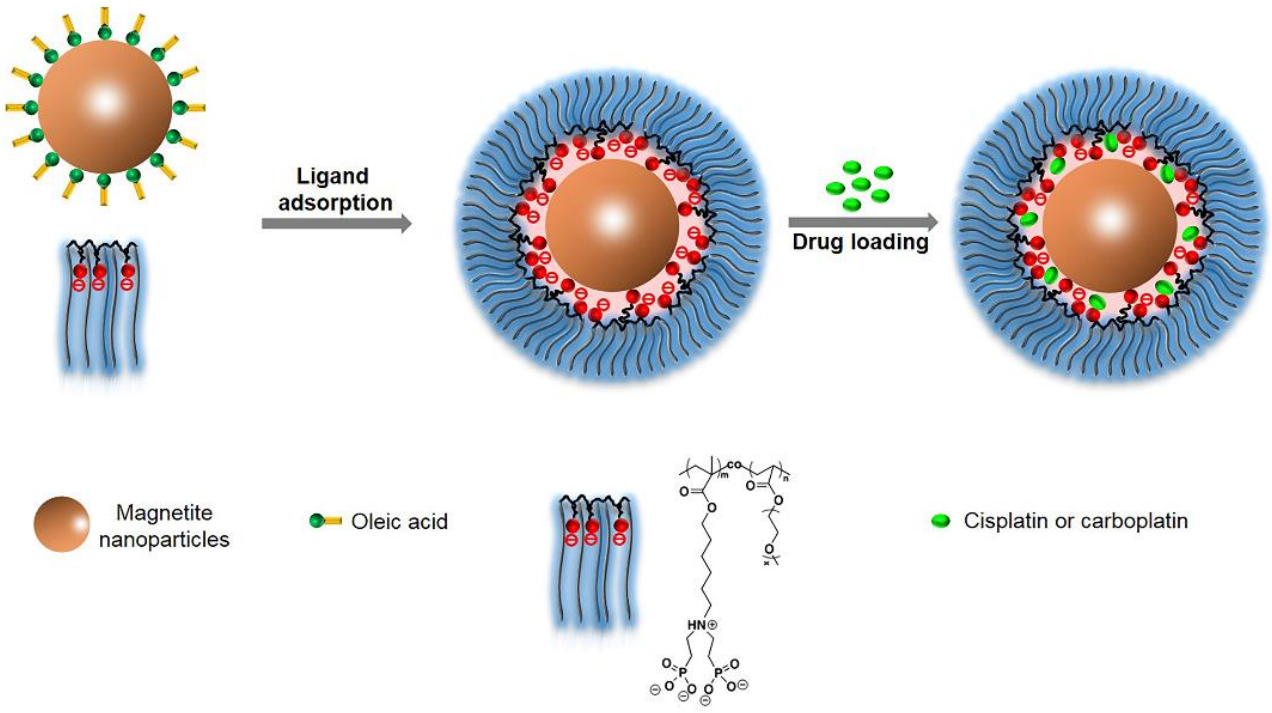

Figure 5.3 Fabrication of the *MGICs* and cisplatin and carboplatin loading.

5.3.2.7 Synthesis of Cisplatin-Loaded MGICs.

The magnetite complex with the poly(hexyl ammonium bisphosphonic acid methacrylate-*g*-PEO) was used to load drugs. *MGICs* (50 mg) were dispersed in deionized water (4.5 mL) in a 20-mL vial equipped with a magnetic stir bar. The dispersion was sonicated for 5 min. Cisplatin (20.1 mg) was charged into a separate vial, and DMSO (0.5 mL) was added to dissolve the cisplatin. This was followed by sonication for 5 min. The cisplatin solution was added dropwise into the *MGICs* dispersion while sonicating. The mixture was sonicated for 5 min, then stirred at room temperature for 12 h. The mixture was transferred to a membrane centrifuge unit with a 10k MWCO and was centrifuged at 5k rpm for 1 h. The particles were collected from the membrane, dispersed in deionized water (10 mL), and transferred to a 20-mL vial. The dispersion was freeze-dried for 2 days. The

targeted wt% of platinum was 20%, and this was the same for both cisplatin and carboplatin. The drug loading process is shown in Figure 5.3.

5.3.2.8 Synthesis of Carboplatin-Loaded MGICs.

MGICs (50 mg) were dispersed in phosphate buffer (0.01 N, 5 mL) in a 20-mL vial equipped with a magnetic stir bar and sonicated for 5 min. Carboplatin (30.7 mg) was charged into a separate vial, and phosphate buffer (0.01 N, 5 mL) was added to dissolve the carboplatin. The solution was sonicated for 5 min. The carboplatin solution was added dropwise into the *MGICs* dispersion while sonicating, and the mixture was sonicated for 5 additional min. The mixture was stirred at room temperature for 24 h. The work-up procedures were the same as described for cisplatin.

5.3.3 Characterization

5.3.3.1 ^{1}H and ^{31}P Nuclear Magnetic Resonance (NMR)

^{1}H NMR spectral analyses were performed on a Bruker Avance II-500 NMR operating at 500 MHz. ^{31}P NMR spectral analyses were obtained on a Varian Inova 400 NMR operating at 161.91 MHz. Parameters utilized for the ^{31}P NMR were a 45° pulse and 1 s relaxation delay with 128 scans. All spectra of the monomers and phosphonate polymers were obtained in $CDCl_3$. Spectra of the phosphonic acid polymers were obtained in D_2O by adjusting the pH to 7.4 with NaOD.

5.3.3.2 Dynamic Light Scattering (DLS)

Intensity average diameters were determined by Dynamic Light Scattering (DLS) measurements using the Zetasizer NanoZS (Malvern Instruments, Software v. 7.11) equipped with a 4.0 mW solid-state He-Ne laser (λ= 633 nm) at a scattering angle of 173° and at 25 ± 0.1 ºC. DLS uses an algorithm based on Mie theory that converts time-varying scattering intensities to hydrodynamic diameters of particles in suspension. For DLS analysis, the drug-free or drug-loaded complexes were dispersed in

deionized water at a concentration of 1 mg mL^{-1}. Each dispersion was sonicated for 3 min in a 75T VWR Ultra-sonicator (120 W, 45 kHz) before transferring it into a polystyrene cuvette for analysis. All measurements were done in triplicate and the averages are reported.

5.3.3.3 Inductively Coupled Plasma Atomic Emission Spectroscopy (ICP-AES)

The amounts of platinum that were loaded into the complexes were quantified by ICP-AES. The amount of iron in both the drug-free and drug-loaded complexes was also quantified by ICP-AES. The drug-free or drug-loaded complexes (2.5 mg) were dispersed in deionized water (10 mL) in a 20-mL vial and sonicated for 3 min. The dispersion (1 mL) was then charged to a new vial and concentrated nitric acid (4 mL) was added to digest the magnetite into their water-soluble nitrate salts with vigorous stirring for 72 h. The obtained solution (1 mL) was diluted with DI water (9 mL) and was submitted for ICP-AES measurements. All experiments were performed in triplicate and the averages are reported.

5.3.3.4 Transmission electron microscopy (TEM)

TEM was performed on a Philips EM-420 field emission gun TEM operating at an acceleration voltage of 120 kV. The sample with the hexyl bisphosphonate *MGICs* was prepared by casting a drop of its dilute aqueous dispersion (0.2 mg mL^{-1}) onto an amorphous carbon-coated copper grid. TEM images were acquired at a magnification of 96,000x, which corresponded to a resolution of 3.88 pixels nm^{-2}.

5.3.3.5 Phantom Magnetic Resonance Imaging (MRI)

Phantom magnetic resonance imaging was performed to demonstrate T_2 shortening effects of the *MGICs*. The particles were dispersed in PBS at iron concentrations ranging from 0 to 200 μM Fe. The dispersions were transferred to 1.5-mL Eppendorf tubes and mounted in a 1.5 wt% agarose gel in a

glass container. MRI was performed on a 4.7 T small animal MRI scanner with a 40-cm horizontal bore (Bruker). T_2-weighted MR images were acquired with a spin-echo sequence with repetition time (TR) = 2500 ms, echo time (TE) = 100 ms, flip angle = 180°, matrix size = 128 x 128, and slice thickness = 1 mm.

5.3.3.6 Relaxivity Measurements

Proton transverse relaxation times (T_2) and longitudinal relaxation times (T_1) were measured on a Model MQ-60 NMR Analyzer (Bruker Minispec) at a magnetic field strength of 1.4 T corresponding to a proton Larmor frequency of 60 MHz. T_2's were obtained from fitting a monoexponential decay curve to signal data generated by a Carr-Purcell-Meiboom-Gill (CPMG) spin−echo pulse sequence with an echo spacing of 0.5 ms and a repetition time of 5 s. T_1's were obtained from fitting a monoexponential recovery curve to signal data generated with an inversion recovery pulse sequence using ten logarithmically spaced inversion times between 50 and 10,000 ms. Either drug-free or drug-loaded *MGICs* were dispersed in deionized water to generate a series of dispersions with concentrations of 0.1, 0.08, 0.04, 0.02, 0.01 mg mL^{-1} and each was sonicated for 3 min in a 75T VWR Ultrasonicator (120 W, 45 kHz). Each dispersion (500 µL) was transferred into a 7.5-mm NMR tube and measurements were made at 37.5 ºC after equilibration for 15 min. The transverse relaxivities (r_2s) and longitudinal relaxivities (r_1s) were calculated from the least-square fits of the relaxation rates (R_2, R_1), which were the inverses of the relaxation times (T_2, T_1) as a function of iron concentration (mM Fe). To measure the concentration of Fe in each tube, each dispersion (1 mL) was charged to a 20-mL vial and concentrated nitric acid (4 mL) was added. The vials were sealed with Parafilm and shaken vigorously for 72 h. Each solution (1 mL) was diluted with deionized water (9 mL) and was submitted for ICP-AES to measure the concentrations of iron. This was done in triplicate and the averages are reported.

5.3.3.7 In vitro Release of Cisplatin or Carboplatin from MGICs

To determine the release of cisplatin (carboplatin) from the drug-loaded *MGICs*, a drug release study was performed at 37 ºC for 24 h. ABS (pH 4.6) was used to simulate the endosomal environment and PBS (pH 7.4) was used to mimic physiological conditions. ABS or PBS (150 mL) was charged into a 250-mL beaker equipped with a magnetic stir bar. The solution was heated to 37 ºC for 1 h. A dialysis cassette with a 4k MWCO was hydrated with de-ionized water, then ABS (or PBS). Cisplatin (carboplatin)-loaded *MGICs* (20 mg), or free cisplatin (carboplatin) (10 mg), were dispersed in ABS or PBS (5 mL each). The dispersion was sonicated for 1 min. Each dispersion (3 mL) was transferred into a dialysis cassette. An aliquot of the remaining dispersion (1 mL) was charged into another vial, followed by dilution with ABS or PBS (9 mL), and was submitted for ICP-AES measurement to determine the wt% of Pt. Each cassette was placed into a beaker equipped with a stir bar and either ABS or PBS (150 mL). The beakers were sealed with Parafilm to avoid evaporation of the liquid. The beakers were stirred at 37 ºC for 24 h. At 0, 1, 3, 6, 9, 12, 18 and 24 h, the beakers were shaken vigorously by hand, and the reception media were flushed with a syringe a few times. Solutions from the reception media (10 mL) were charged into separate vials. At each time point, fresh ABS or PBS (10 mL) was replenished to maintain constant volume in the reception media. All the samples of reception media, as well as the starting dispersions in the vials, were submitted for ICP-AES measurements to determine the wt% of Pt.

5.3.3.8 Calorimetry measurement

The SAR of the hexyl bisphosphonate *MGICs* was measured and calculated with an EasyHeat Induction Heating System produced by Ameritherm. The calorimetric measurement setup is described in Figure 5.4. Data was collected using an EasyHeat Induction Heating System produced by Ameritherm. The five-turn induction coil contained a polycarbonate recirculating water bath designed

to regulate sample temperature. The temperature changes in each sample were measured using a fiber optic temperature sensor from NeoptixTM. The sample was allowed to reach thermal equilibrium prior to turning on the magnetic field. Temperature was recorded every five seconds. Measurements were conducted at a frequency of 205 kHz and a magnetic field strength of 30 kA m^{-1} that was verified using an AC field probe (AMF Life Science). The hexyl *MGICs* dispersion (3.5 mg mL^{-1}, 0.5 mL) was used to measure the heating rate. The SAR of the *MGICs* was calculated from its heat capacity (C), the initial slope of the temperature versus time curve ($\Delta T/\Delta t$, K s^{-1}), and the total mass of the *MGICs* dispersion, divided by the mass of iron as determined from ICP-AES.[76]

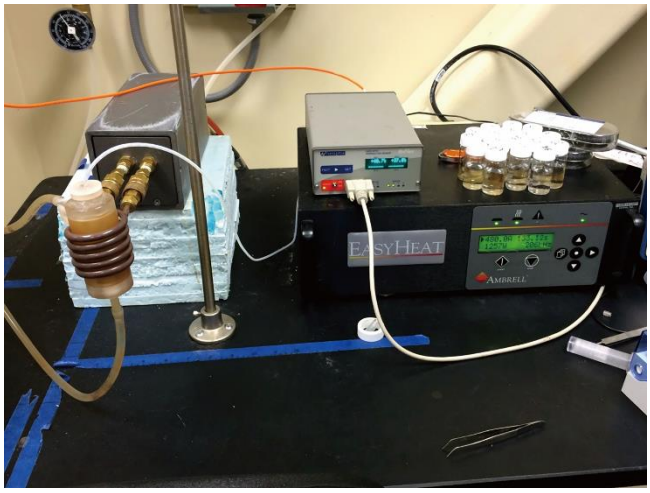

Figure 5.4 Experimental setup for calorimetric measurements.

5.4 Results and Discussion

5.4.1 Overview

A primary research interest in our group is on developing metal oxide/ionic-copolymer nanocomplexes for potential applications such as magnetic resonance imaging and drug delivery. We have previously reported magnetite-block ionomer complexes with an average magnetite diameter of 8 nm that were coated with a PEO-poly(acrylic acid) diblock copolymer.[21, 23] Their capabilities to

encapsulate and release the cationic antibiotic, gentamicin, were investigated as agents to treat Brucella melitensis, which is a zoonotic bacterial disease.[77] Carboxylate anions on the copolymer associated electrostatically with the cationic drug to provide sustained release kinetics. Those complexes showed excellent colloidal stability in PBS and good size distributions as measured by dynamic light scattering. They also had high transverse NMR relaxivities compared to commercial iron oxide-based contrast agents such as Feridex IV®.[78]

In this contribution, we designed magnetite nanoparticles coated with ammonium bisphosphonate graft copolymers to bind strongly to platinum-based cancer drugs via ionic interactions. This is in part because the release kinetics of platinum-based drugs from such magnetite-phosphonate-containing ionic copolymer complexes and their MRI potentials have not been studied to date. There is evidence that phosphonate ions bind well to platinum drugs, likely by coordination of the phosphonate anions to the electropositive metal atoms.[47] In addition, magnetite nanoparticles are known to be excellent MRI contrast agents, and they normally function as negative (T_2) contrast agents, thus appearing predominantly dark on MRI images.[75, 79-80] Moreover, magnetite nanoparticles could respond to an alternating magnetic field.[6, 26] By combining both phosphonate-bearing ionic graft copolymers and magnetite nanoparticles and making corresponding magnetite-copolymer complexes, a multifunctional drug delivery system that generates heat and enables potential triggered drug release by exposing them to an alternating magnetic field was created.[81-82]

5.4.2 Synthesis of the bisphophosphonic acid and acrylic acid-containing ionic graft copolymers

^{1}H and ^{31}P NMR spectra of the poly(propyl ammonium bisphosphonate methacrylate)-g-PEO before and after phosphonate ester hydrolysis are shown in Figures 5.5 and 5.6. The poly(hexyl ammonium bisphosphonate methacrylate)-g-PEO had similar spectra. Due to solubility issues, the graft copolymers before and after selective hydrolysis were analyzed in different deuterated solvents.

The ^{1}H NMR spectra featured the disappearance of protons corresponding to the methyl and methylene groups of the phosphonate esters (peaks h and i in the top spectrum in Figure 5.5). The methyl protons (peak i) had a chemical shift at ~1.3 ppm, and this peak completely disappeared after hydrolysis. The methylene protons on the phosphonate esters (peak h) had a chemical shift of 4 ppm, very close to the methylene proton resonance on the carboxylic ester of the bisphosphonate graft segment (peak c). Before hydrolysis, peaks c and h combined indicated that 10 Hs per phosphonate monomer unit were present. After selective hydrolysis, only 2 Hs remained due to the carboxylic ester methylene. This was confirmed by the integrals in the spectra. The protons on the poly(ethylene oxide) segment (peaks l and m) remained unchanged, indicating that the carboxylic esters on the PEO segment were not affected by the hydrolysis procedure. The spectra indicated that the phosphonate esters had been selectively deprotected, with little to no effects on the carboxylic esters. ^{31}P NMR spectra (Figure 5.6) further demonstrated the success of the removal of the phosphonate esters. The single phosphorus resonance shifted from 31 to 16 ppm, which was in good agreement with our previous study with polymer end groups.[73]

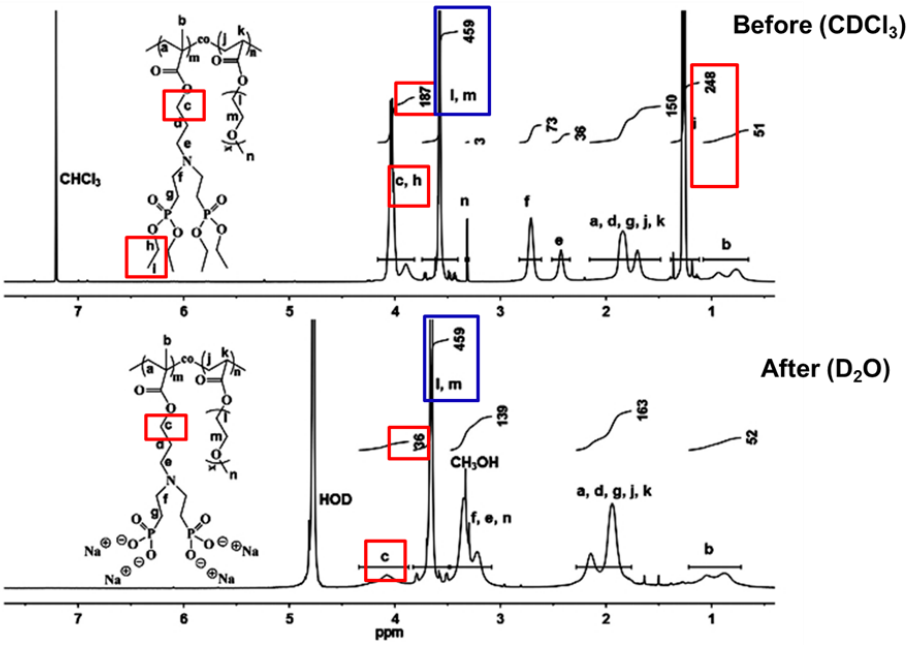

Figure 5.5 ^{1}H NMR spectra show successful deprotection of the phosphonate esters of the poly(propyl ammonium bisphosphonate methacrylate)-*g*-PEO copolymers with minimal effect on carboxylic esters.

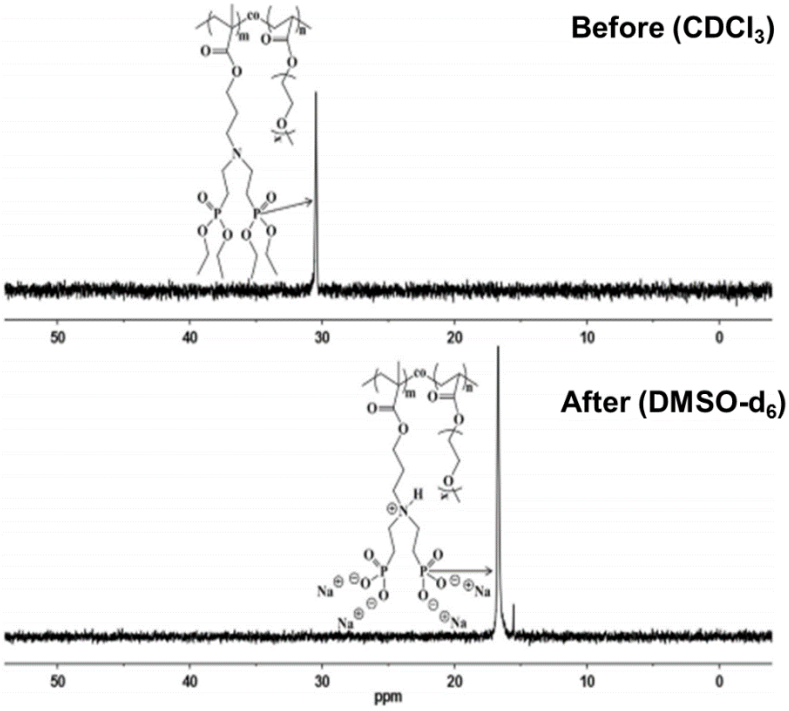

Figure 5.6 ^{31}P NMR spectra of the poly(propyl ammonium bisphosphonate methacrylate)-*g*-PEO.

The ^{1}H NMR spectrum of the PEO-*g*-PAA is shown in Figure 5.7. The integrals indicated that there were ~75 acrylate repeat units per PEO graft. Based on this, the graft copolymer contained about 50 wt% of PEO and 50 wt% of poly(sodium acrylate).

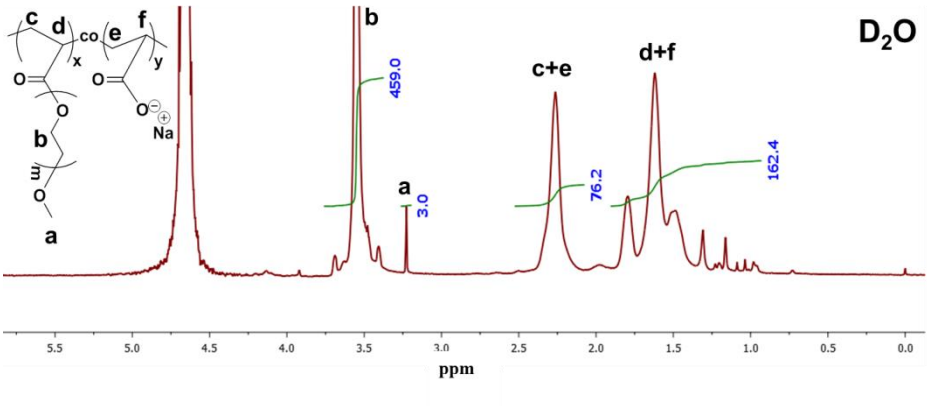

Figure 5.7 ^{1}H NMR spectrum of the PEO-*g*-PAA.

5.4.3 Synthesis of Magnetite Nanoparticles Coated with Ammonium Bisphosphonate-PEO Graft Copolymers *(MGICs)*.

The ammonium bisphosphonate-PEO graft copolymers reported herein were prepared by free radical copolymerization of PEO-monoacrylate macromonomers with an ammonium bisphosphonate methacrylate monomer.[73] An analogous polyacrylate-PEO graft copolymer was also prepared so that the properties of the complexes could be compared in terms of using carboxylates versus phosphonates. Magnetite nanoparticles were synthesized by thermal decomposition of an organometallic precursor as described by Park *et al*. with some modifications.[83] During the preparation of the magnetite-graft copolymer complexes, the phosphonate anions displaced part of the oleic acid coating on the surface of the nanoparticles to produce a core-shell particle.[84-85] The process required homogeneous dispersion of the ionomers and the oleic acid-coated magnetite in organic solvents so that the ionic copolymers could adsorb onto the magnetite core without significant repulsion of the anionic charges in the copolymer. The copolymers were readily soluble in *N*,*N*-dimethylformamide (DMF), while the oleic acid-coated magnetite nanoparticles were dispersible in chloroform. A mixed solvent system of 1:1 v:v DMF:chloroform was used for the adsorption step.

The mixture was sonicated for 4 hours, then stirred at room temperature for 48 hours. The nanoparticles were then precipitated and washed extensively with hexane and diethyl ether to remove free oleic acid, low molecular weight impurities and any residual trioctylamine solvent derived from the magnetite formation process. The particles were first dried under a nitrogen purge at room temperature, then recovered by freeze-drying to avoid nanoparticle aggregation that might occur by drying at an elevated temperature.

5.4.4 Physicochemical Properties of the *MGICs.*

It was of great interest to examine whether the bisphosphonate-containing and the acrylate-bearing graft copolymers would bind to magnetite with conspicuous differences in terms of physicochemical properties, charge characteristics, and hydrodynamic stabilities. A previous study by our group utilizing similar graft copolymers to complex with manganese (II) indicated that the bisphosphonate graft copolymers bound more strongly to manganese than the carboxylate copolymer.[47] Table 1 lists the intensity average diameters, polydispersity indices and zeta potentials of the graft copolymer-magnetite complexes and drug-loaded *MGICs*. All of the complexes had low polydispersity indices (PDIs) as measured by DLS, which indicated that the sizes of these nanocomplexes were relatively uniform in hydrodynamic diameters without noticeable aggregation/agglomeration. This eliminated any concern that the *MGICs* (*i.e.*, with graft copolymers) would not form complexes with desirable sizes and PDIs that were as uniform as with block copolymers made in controlled free radical polymerizations. The complexes were designed to incorporate an excess of anions in the magnetite-ionomer complexes, so that either residual carboxylate or phosphonate groups could provide binding sites for charged or metal-containing drugs such as doxorubicin and cisplatin. The zeta potentials of all the *MGICs* were strongly negative as measured by DLS, indicating that substantial amounts of anions still existed (Table 5.1). The

relatively uniform sizes, discrete size distributions and zeta potentials of the *MGICs* lead to the conclusion that ionic graft copolymers can be used to form complexes with magnetite for potential drug delivery applications. Further experiments may be needed to compare the colloidal stability between the carboxylate-containing and phosphonate-bearing complexes.

TEM images of the hexyl bisphosphonate *MGICs* are shown in Figure 5.8. It is noted that only the primary magnetite nanoparticles can be observed. Based on the TEM image, the magnetite core of the complexes has a relatively uniform size with a narrow size distribution. It has a spherical shape and a mean average diameter of 20.4 ± 1.4 nm. It has been reported that biocompatible magnetic nanoparticles with core sizes above 20 nm can provide large specific heating power.[86-87] It has also been reported that ideally the sizes of polymeric micellar drug delivery systems should be within 10-200 nm so they could avoid fast filtration and elimination by the kidneys or spleen.[22, 88-90] The sizes of our magnetite cores (~20 nm) and as-prepared nanocomplexes (~100 nm) are within the size ranges and with narrow size distributions, thus bearing the potential for the proposed drug delivery and hyperthermia applications.

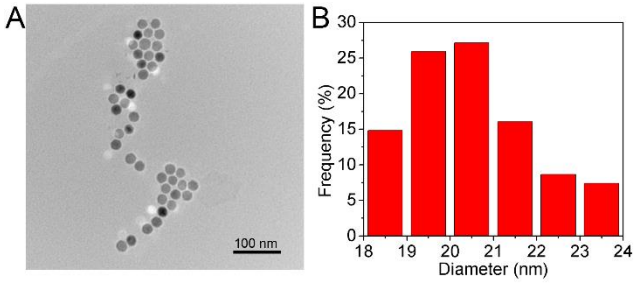

Figure 5.8 TEM micrograph (A) and the particle size distributions (B) of the poly(hexyl ammonium bisphosphonic acid methacrylate)-*g*-poly(ethylene oxide)-magnetite complexes.

Table 5.1 The intensity average diameters, polydispersity indices and zeta potentials of *MGICs* and magnetite-block ionomer complexes.

Sample	Polymer Coating Composition	Intensity Average Diameter (nm)	PDI	Zeta Potential (mV)
MGICs carboxylate	PAA-*g*-PEO (50:50 wt:wt)	131±3	0.13	-56±1
MGICs propyl bisphosphonate	Poly(propyl ammonium bisphosphonic acid)-*g*-PEO (60:40 wt:wt)	100±2	0.16	-47±1
MGICs hexyl bisphosphonate	Poly(hexyl ammonium bisphosphonic acid)-*g*-PEO (60:40 wt:wt)	105±2	0.14	-49±1
Cisplatin-*MGICs* hexyl bisphosphonate	Poly(hexyl ammonium bisphosphonic acid)-*g*-PEO (60:40 wt:wt)	141±1	0.15	-43±1
Carboplatin-*MGICs* hexyl bisphosphonate	Poly(hexyl ammonium bisphosphonic acid)-*g*-PEO (60:40 wt:wt)	130±1	0.15	-44±1

5.4.5 Colloidal Stability of the *MGICs.*

Colloidal stability under physiological conditions is one of the most important factors in considering potential biological applications of nanomaterials.[86] To evaluate the potential of the *MGICs* for drug delivery, it is of vital importance that the *MGICs* be hydrodynamically stable in deionized water under physiological conditions. The hydrodynamic sizes of both acrylate-containing and bisphosphonate-bearing *MGICs* were monitored by DLS in PBS at pH 7.4 and 37 ºC over 24 hours to mimic physiological conditions. The hydrodynamic sizes of the dispersed nanocomplexes were measured again after 7 days. Their intensity average diameters measured by DLS over 24 hours are shown in Figure 5.9. Based on these tests, the *MGICs* had stable sizes in simulated physiological conditions for at least 24 hours, and the sizes remained unchanged even after 7 days. Our prior experience has shown that if the polymer begins to desorb from the nanoparticle surface, it leads to aggregation over time and eventually to sedimentation of the metal or metal oxides.[69, 87] The relatively stable sizes of these *MGICs* suggest that adhesion between the polymers and the magnetite surfaces was sufficient for the polymers to remain stably bound.

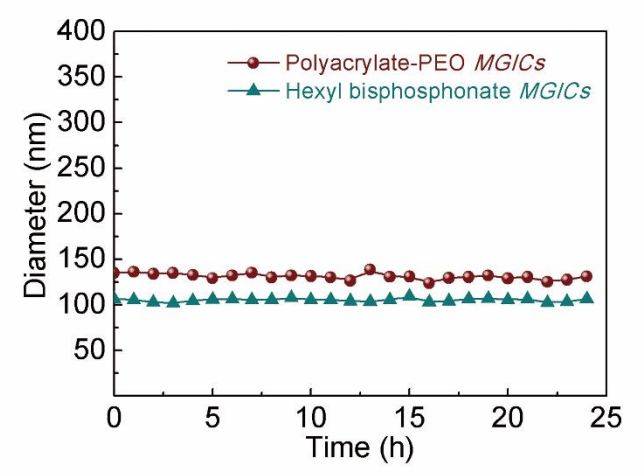

Figure 5.9 Hydrodynamic stability tests in simulated physiological conditions.

5.4.6 Cisplatin and Carboplatin-Loaded *MGICs.*

To evaluate the potential of the *MGICs* as drug carriers, cisplatin and carboplatin were loaded into the hexyl bisphosphonate *MGICs*. The targeted amounts of both platinum drugs were 20 wt%. *Cis*-dichlorodiammineplatinum(II) (cisplatin, CPT) and *cis*-diammine(cyclobutane-1,1-dicarboxylate-O,O')platinum(II) (carboplatin, CAPT) are well-known platinum anticancer drugs. Cisplatin is one of the first generation platinum drugs that remains one of the top choices for treatments of numerous malignant tumors including breast and prostate cancer.[91] However, it has poor water solubility and low selectivity towards tumor cells. It causes severe side effects such as acute nephrotoxicity and chronic neurotoxicity.[92] Carboplatin, a cisplatin analogue, belongs to the second generation cancer drugs and has better water solubility and less toxicity. Carboplatin is now widely used to treat ovarian cancer.[36] Encapsulating these platinum drugs into the *MGIC* nanocarriers may solve the problem of low water solubility for cisplatin.

It is known that the chloride ligands on cisplatin can be substituted by reactive groups such as carboxylates and phosphonates.[21, 47] The cisplatin and carboplatin drug loading into the magnetite-

graft ionomer complexes utilized a similar experimental procedure that was employed for synthesizing manganese (II)-graft ionomer complexes.[47] The cisplatin loading utilized a mixed solvent of 9:1 deionized water: dimethylsulfoxide (DMSO) by dissolving the drug in DMSO and dispersing the magnetite-graft ionomer complex in water (due to the poor water solubility of the drug). An unsuccessful attempt to load the cisplatin in only water as the reaction medium was made. Carboplatin has good water solubility and thus the loading process was performed in complete aqueous media. It is noteworthy that the dicarboxylate ligand in carboplatin binds to the platinum more strongly than individual chlorides on cisplatin. A recent study indicated that the ligands in carboplatin are not replaced under the conditions that were used for loading the drug into the complexes in the present work.[93] It is likely that the phosphonate anions chelate the platinum without replacing the dicarboxylate ligands. Residual free drug was removed by centrifuging the dispersions through a membrane cassette. The cisplatin (carboplatin)-loaded *MGICs* were re-dispersed in deionized water and were recovered by freeze-drying. This drying procedure was necessary to avoid premature drug release and any agglomeration of the nanoparticles that might have been introduced by heating.

Based on inductively coupled plasma atomic emission spectroscopy (ICP-AES) results, 8.7 wt% of platinum was loaded in the cisplatin-loaded *MGICs*, while 6.9 wt% was incorporated into the carboplatin-loaded *MGICs*. The targeted amount of platinum was 20 wt% in both cases. Although the drug loading efficiencies were significantly lower than the charged amount of platinum, the results do suggest that the *MGICs* have the capacity to encapsulate platinum drugs. A possible explanation for the relatively low drug loadings is that the magnetite was in the form of small aggregates, and that such aggregates prevented loading of more platinum drugs into the complexes. It could also be attributed to insufficient reaction times for the loading processes, so additional work would be

required to understand how the reaction times affect the drug loading capacities. It was also found that the drug loading procedures did not cause significant loss of magnetite (within 0.5 wt%), as determined by ICP-AES. The physicochemical properties of the cisplatin and carboplatin-loaded hexyl bisphosphonate *MGICs* were measured as shown in Table 5.1. The sizes increased slightly after drug loading, and the PDIs remained unchanged. This indicated that the drug had not affected the colloidal stability of the *MGICs*. Their zeta potentials decreased slightly, and this can be explained by the fact that part of the remaining anions on the polymers was sequestered into the cores of the micellar *MGICs*. These results are in good agreement with our previous studies on drug-loaded complexes, which indicate successful drug loading.[21] The results also strongly suggest that there is sufficient binding strength between the magnetite and the graft copolymers.

5.4.7 Transverse Relaxivities of *MGICs.*

Magnetite nanoparticles have been demonstrated to be versatile MRI contrast agents.[24-25, 94-95] To evaluate the potential for MRI applications with the *MGICs*, the proton transverse relaxivities (r_2's) were measured at the physiological temperature (37 °C) and a magnetic field strength of 1.4 Tesla (corresponding to a proton Larmor frequency of 60 MHz). This corresponds to a common clinical field strength. There are two types of NMR relaxations which generate magnetic resonance images: longitudinal relaxation (T_1-recovery) and transverse relaxation (T_2-decay). When magnetic nanoparticles such as magnetite are delivered in tissues, contrast enhancement is generated by shortening of both types of relaxations of surrounding protons. While MRI contrast agents affect both T_1 and T_2, magnetite nanoparticles are typically categorized as T_2 contrast agents by applying T_2-weighted pulse sequences.[96] T_2 contrast agents decrease signal intensity, thus creating negative (dark) contrast enhancements in T_2-weighted images.[97] For magnetite nanoparticles, r_2 is a normalized transverse contrast enhancement indicator. It can be calculated based on the slope of the measured

transverse relaxation rate (R_2) over iron concentration (mM Fe). Higher values of r_2 correlate with greater contrast.[98]

The transverse relaxivities of the hexyl bisphosphonate *MGICs* were compared to our previously reported magnetic block ionomer complexes (*MBICs)* and *MBIClusters* as well as to a commercial T_2-weighted MRI contrast agent Feridex IV®. The hexyl bisphosphonate *MGICs* had a transverse relaxivity (r_2) of 244 s^{-1} (mM Fe)$^{-1}$ and a longitudinal relaxivity (r_1) of 3.3 s^{-1} (mM Fe)$^{-1}$. The high transverse relaxivity value is 2-4 times higher than the *MBICs* and almost six-fold higher than the commercial iron T_2 contrast agent Ferridex IV® (r_2 = 41 s^{-1} (mM Fe)$^{-1}$ at 37 ºC and 1.5 T).[21, 78] The *MGICs* may be in the form of small clusters based on DLS results. Previous findings in our group suggested that small aggregates lead to significant increases in relaxivities.[99] Such a high relaxivity suggests that the *MGICs* may be sensitive contrast agents for MRI applications.

To further demonstrate that the *MGICs* have potential as negative contrast agents, phantom MRI images using the hexyl bisphosphonate *MGICs* were obtained (Figure 5.10). Significant contrast was observed at an iron concentration of 100 μM and complete signal losses were observed at an Fe concentration of 200 μM. The relaxivities of the *MGICs* are in the range with the results from our and other previous reports of magnetic iron oxide nanoparticles that have similar sizes.[21, 100-101]

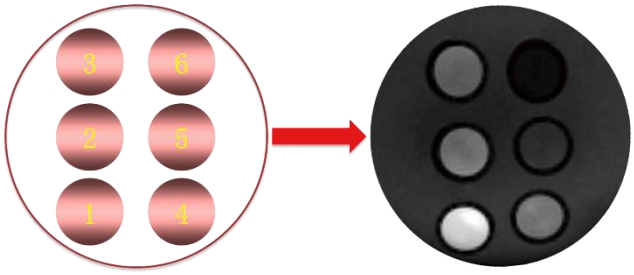

Figure 5.10 Phantom MRI images of the hexyl bisphosphonate *MGICs* at 4.7 Tesla. Concentrations of iron in each tube were (1) 0, (2) 12.5, (3) 25, (4) 50, (5) 100 and (6) 200 μM Fe.

Comparisons of transverse relaxivities between the drug-free and drug-loaded hexyl bisphosphonate *MGICs* were made (Figure 5.11). It was found that the cisplatin-loaded *MGICs* had a transverse relaxivity of 409 s^{-1} (mM Fe)$^{-1}$, while the carboplatin-loaded complex was 335 s^{-1} (mM Fe)$^{-1}$. The transverse relaxivity of the *MGICs* without a platinum drug was 244 s^{-1} (mM Fe)$^{-1}$. The longitudinal relaxivities increased slightly from 3.3 to 4.3 s^{-1} (mM Fe)$^{-1}$ after drug loading. Since higher transverse relaxivities correlate with better contrast and magnetite generates dark (black) images, the drug-loaded hexyl bisphosphonate *MGICs* generate darker T_2-weighted images than drug-free ones. It remains unclear whether the drug-free and drug-loaded complexes can generate T_2-weighted images with significant differences in vivo. If they can generate MRI images with striking differences and such differences can be quantified, it may indicate the ability to track drug release by MRI, and this would represent a significant advance to understand and take advantage of the drug release kinetics of such complexes.

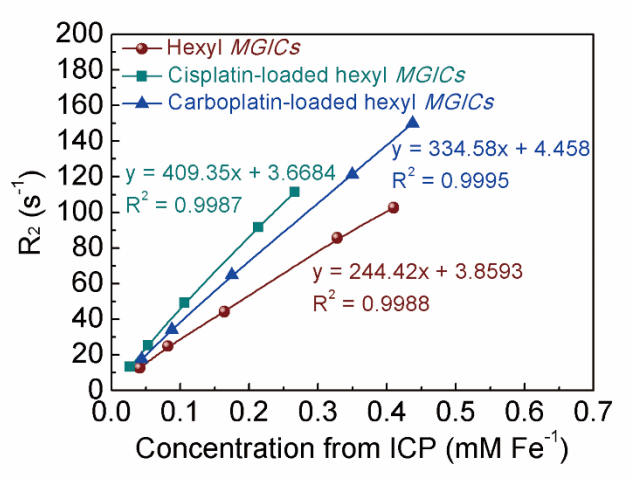

Figure 5.11 Transverse relaxivities of drug-free and drug-loaded hexyl bisphosphonate *MGICs*.

5.4.8 *In Vitro* Release Profiles of Cisplatin and Carboplatin from *MGICs* at pH 4.6 and 7.4

The drug release profiles from cisplatin and carboplatin-loaded hexyl bisphosphonate *MGICs* were measured at 37 ºC by dialyzing the complexes and measuring platinum concentrations in the reception media by ICP-AES. The buffers used for the experiments were acetate buffer solution (ABS, pH 4.6) to simulate the endosomal environment, and PBS (pH 7.4) to mimic the physiological pH. The experiments were performed over 24 hours. The amount of accumulated drug release as a function of time is shown in Figure 5.12. Free cisplatin and carboplatin fully transported into the reception medium over 12 hours. Cisplatin and carboplatin-loaded hexyl bisphosphonate *MGICs* released the drugs more slowly and in a sustained manner. After 24 hours, approximately 40 wt% of the platinum was released. It has been reported that the pK_{a1}s of such ammonium-bearing phosphonic acids were below 4 while the pK_{a2}s were between 6-7.4.[102] This indicated that the amount of phosphonate anions at pH 4.6 was only half that at pH 7.4. Still, the rates of drug release at pH 4.6 and 7.4 were not significantly different. This demonstrated strong binding between the phosphonate and the magnetite and platinum drugs. With fewer phosphonate anions present at lower pH, the drugs did not release significantly faster. Overall, sustained release of cisplatin and carboplatin was achieved by loading them into the *MGIC* nanocarriers. The *MGIC* complexes represent promising candidates as drug carriers for delivery applications.

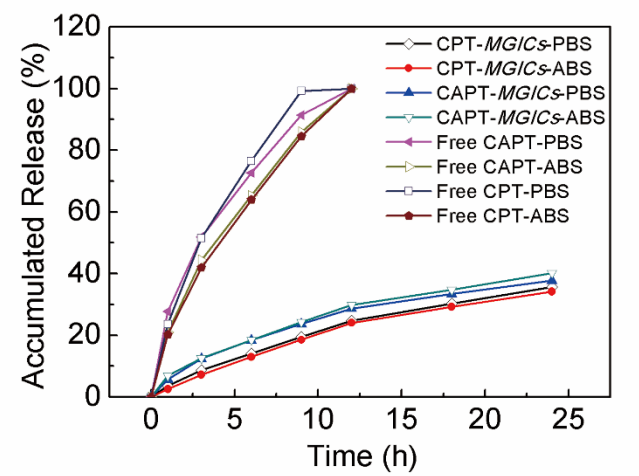

Figure 5.12 Drug release profiles with and without *MGIC* nanocarriers in ABS and PBS at 37 °C.

5.4.9 SAR Measurements

A hexyl bisphosphonate *MGIC* aqueous dispersion (3.5 mg mL^{-1}, 0.5 mL) was found to release heat upon exposure to an AC magnetic field at 480 A and 206 kHz. The temperature of the nanoparticle dispersion increased from 37 to 41 °C after applying the AC magnetic field for 10 minutes (Figure 5.13). The SAR values of the hexyl bisphosphonate *MGICs* was calculated to be 77.0 W g^{-1} at a field strength of 30 kA m^{-1} and a frequency of 206 kHz.[103-105] This may potentially allow hyperthermia treatment and/or heat-induced drug release. More importantly, our recent study and report on utilizing an ultra-low frequency (50 Hz) AC magnetic field at the field strength of 50 or 100 kA m^{-1} for remote actuation of magnetite nanoparticles coated with poly(acrylic acid)-functionalized Pluronic® P85 block copolymers revealed that cancerous cells were selectively killed while normal cells remained intact.[106] Further investigation showed that cytoskeletal disruption instead of hyperthermia or other known mechanisms caused the selective cell death upon exposure to the low frequency field. It is hypothesized that under the higher frequency AC fields investigated in this work, both hyperthermia effects and nanoparticle motion-induced cytoskeletal disruption might

occur, leading to increased cytotoxicity to the cells. This may further increase the versatility of these *MGICs* for drug delivery.

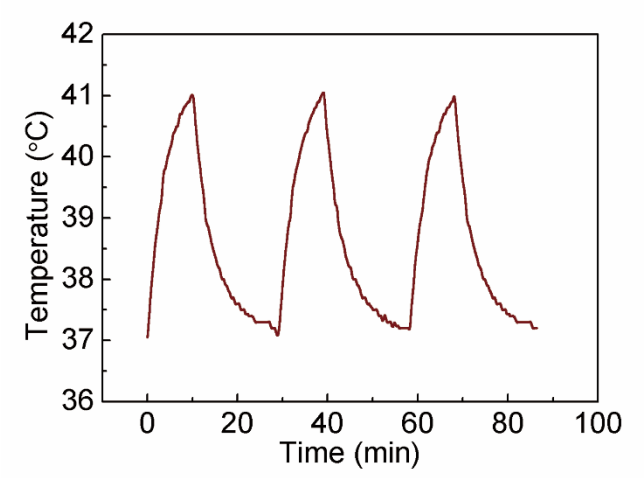

Figure 5.13 Calorimetric measurement of the hexyl bisphosphonate *MGICs.*

5.5 Conclusions

In summary, novel bisphosphonate graft ionic copolymer-magnetite complexes have been synthesized and characterized. They displayed relatively uniform sizes with narrow size distributions after self-assembly in aqueous media. They also showed good colloidal stability in simulated physiological conditions for at least to 7 days. The anticancer drugs, cisplatin and carboplatin, were successfully loaded into the *MGICs.* Sustained drug release of both cisplatin and carboplatin were achieved in both simulated endosomal and physiological conditions. The drug-free and drug-loaded *MGICs* exhibited excellent contrast enhancements in comparison with the commercial T_2-weighted MRI agent Feridex IV®. Therefore, the bisphosphonate graft ionic copolymer-magnetite complexes may be promising candidates for dual MRI imaging and drug delivery, with the possibility of triggered drug release and hyperthermia treatment, making it more versatile in potential drug delivery applications.

5.6 Acknowledgements

The authors are grateful for the support of the National Science Foundation under contracts DMR 0805179, DMR 1106182 and DMR 1263248.

5.7 References

1. Kim, D. K.; Dobson, J., Nanomedicine for targeted drug delivery. *Journal of Materials Chemistry* **2009,** *19* (35), 6294-6307.
2. Kabanov, A. V.; Batrakova, E. V.; Alakhov, V. Y., Pluronic® block copolymers as novel polymer therapeutics for drug and gene delivery. *Journal of Controlled Release* **2002,** *82* (2–3), 189-212.
3. Sherlock, S. P.; Tabakman, S. M.; Xie, L.; Dai, H., Photothermally Enhanced Drug Delivery by Ultrasmall Multifunctional FeCo/Graphitic Shell Nanocrystals. *ACS Nano* **2011,** *5* (2), 1505-1512.
4. Tu, Y.; Peng, F.; André, A. A. M.; Men, Y.; Srinivas, M.; Wilson, D. A., Biodegradable Hybrid Stomatocyte Nanomotors for Drug Delivery. *ACS Nano* **2017,** *11* (2), 1957-1963.
5. Yuan, X.; Marcano, D. C.; Shin, C. S.; Hua, X.; Isenhart, L. C.; Pflugfelder, S. C.; Acharya, G., Ocular Drug Delivery Nanowafer with Enhanced Therapeutic Efficacy. *ACS Nano* **2015,** *9* (2), 1749-1758.
6. Mura, S.; Nicolas, J.; Couvreur, P., Stimuli-responsive nanocarriers for drug delivery. *Nature materials* **2013,** *12* (11), 991.
7. Nicolas, J.; Mura, S.; Brambilla, D.; Mackiewicz, N.; Couvreur, P., Design, functionalization strategies and biomedical applications of targeted biodegradable/biocompatible polymer-based nanocarriers for drug delivery. *Chemical Society Reviews* **2013,** *42* (3), 1147-1235.
8. Nishiyama, N.; Matsumura, Y.; Kataoka, K., Development of polymeric micelles for targeting intractable cancers. *Cancer Science* **2016,** *107* (7), 867-874.
9. Kinoh, H.; Miura, Y.; Chida, T.; Liu, X.; Mizuno, K.; Fukushima, S.; Morodomi, Y.; Nishiyama, N.; Cabral, H.; Kataoka, K., Nanomedicines Eradicating Cancer Stem-like Cells in Vivo by pH-Triggered Intracellular Cooperative Action of Loaded Drugs. *ACS Nano* **2016,** *10* (6), 5643-5655.
10. Li, F.; Li, C.; Liu, J.; Liu, X.; Zhao, L.; Bai, T.; Yuan, Q.; Kong, X.; Han, Y.; Shi, Z.; Feng, S., Aqueous phase synthesis of upconversion nanocrystals through layer-by-layer epitaxial growth for in vivo X-ray computed tomography. *Nanoscale* **2013,** *5* (15), 6950-6959.
11. Li, C.; Li, F.; Li, T.; Bai, T.; Wang, L.; Shi, Z.; Feng, S., A facile synthesis and photoluminescence properties of water-dispersible Re3+ doped CeF3 nanocrystals and solid nanocomposites with polymers. *Dalton Transactions* **2012,** *41* (16), 4890-4895.
12. Li, F.; Li, C.; Liu, X.; Bai, T.; Dong, W.; Zhang, X.; Shi, Z.; Feng, S., Microwave-assisted synthesis and up-down conversion luminescent properties of multicolor hydrophilic LaF3:Ln3+ nanocrystals. *Dalton Transactions* **2013,** *42* (6), 2015-2022.
13. Guzman, L. A.; Labhasetwar, V.; Song, C.; Jang, Y.; Lincoff, A. M.; Levy, R.; Topol, E. J., Local Intraluminal Infusion of Biodegradable Polymeric Nanoparticles: A Novel Approach for Prolonged Drug Delivery After Balloon Angioplasty. *Circulation* **1996,** *94* (6), 1441-1448.
14. Torchilin, V., Micellar Nanocarriers: Pharmaceutical Perspectives. *Pharmaceutical Research* **2007,** *24* (1), 1-16.
15. Torchilin, V. P., Structure and design of polymeric surfactant-based drug delivery systems. *Journal of Controlled Release* **2001,** *73* (2–3), 137-172.

16. Gaucher, G.; Dufresne, M.-H.; Sant, V. P.; Kang, N.; Maysinger, D.; Leroux, J.-C., Block copolymer micelles: preparation, characterization and application in drug delivery. *Journal of Controlled Release* **2005,** *109* (1–3), 169-188.
17. Oh, K. T.; Bronich, T. K.; Bromberg, L.; Hatton, T. A.; Kabanov, A. V., Block ionomer complexes as prospective nanocontainers for drug delivery. *Journal of Controlled Release* **2006,** *115* (1), 9-17.
18. Kamimura, M.; Kim, J. O.; Kabanov, A. V.; Bronich, T. K.; Nagasaki, Y., Block ionomer complexes of PEG-block-poly(4-vinylbenzylphosphonate) and cationic surfactants as highly stable, pH responsive drug delivery system. *Journal of Controlled Release* **2012,** *160* (3), 486-494.
19. Xiong, X.-B.; Falamarzian, A.; Garg, S. M.; Lavasanifar, A., Engineering of amphiphilic block copolymers for polymeric micellar drug and gene delivery. *Journal of Controlled Release* **2011,** *155* (2), 248-261.
20. Kataoka, K.; Harada, A.; Nagasaki, Y., Block copolymer micelles for drug delivery: design, characterization and biological significance. *Advanced Drug Delivery Reviews* **2001,** *47* (1), 113-131.
21. Pothayee, N.; Pothayee, N.; Jain, N.; Hu, N.; Balasubramaniam, S.; Johnson, L. M.; Davis, R. M.; Sriranganathan, N.; Riffle, J. S., Magnetic Block Ionomer Complexes for Potential Dual Imaging and Therapeutic Agents. *Chemistry of Materials* **2012,** *24* (11), 2056-2063.
22. Lavasanifar, A.; Samuel, J.; Kwon, G. S., Poly(ethylene oxide)-block-poly(l-amino acid) micelles for drug delivery. *Advanced Drug Delivery Reviews* **2002,** *54* (2), 169-190.
23. Pothayee, N.; Balasubramaniam, S.; Pothayee, N.; Jain, N.; Hu, N.; Lin, Y.; Davis, R. M.; Sriranganathan, N.; Koretsky, A. P.; Riffle, J. S., Magnetic nanoclusters with hydrophilic spacing for dual drug delivery and sensitive magnetic resonance imaging. *Journal of Materials Chemistry B* **2013,** *1* (8), 1142-1149.
24. Vishwasrao, H. M.; Master, A. M.; Seo, Y. G.; Liu, X. M.; Pothayee, N.; Zhou, Z.; Yuan, D.; Boska, M. D.; Bronich, T. K.; Davis, R. M.; Riffle, J. S.; Sokolsky-Papkov, M.; Kabanov, A. V., Luteinizing Hormone Releasing Hormone-Targeted Cisplatin-Loaded Magnetite Nanoclusters for Simultaneous MR Imaging and Chemotherapy of Ovarian Cancer. *Chemistry of Materials* **2016,** *28* (9), 3024-3040.
25. Pothayee, N.; Cummings, D.; Schoenfeld, T.; Dodd, S.; Cameron, H.; Belluscio, L.; Koretsky, A., Magnetic resonance imaging of odorant activity-dependent migration of neural precursor cells and olfactory bulb growth. *NeuroImage* **2017**.
26. Regmi, R.; Bhattarai, S. R.; Sudakar, C.; Wani, A. S.; Cunningham, R.; Vaishnava, P. P.; Naik, R.; Oupicky, D.; Lawes, G., Hyperthermia controlled rapid drug release from thermosensitive magnetic microgels. *Journal of Materials Chemistry* **2010,** *20* (29), 6158-6163.
27. Herrera, A. P.; Barrera, C.; Rinaldi, C., Synthesis and functionalization of magnetite nanoparticles with aminopropylsilane and carboxymethyldextran. *Journal of Materials Chemistry* **2008,** *18* (31), 3650-3654.
28. Barrera, C.; Herrera, A. P.; Rinaldi, C., Colloidal dispersions of monodisperse magnetite nanoparticles modified with poly (ethylene glycol). *Journal of Colloid and Interface Science* **2009,** *329* (1), 107-113.
29. Lutz, J.-F.; Stiller, S.; Hoth, A.; Kaufner, L.; Pison, U.; Cartier, R., One-Pot Synthesis of PEGylated Ultrasmall Iron-Oxide Nanoparticles and Their in Vivo Evaluation as Magnetic Resonance Imaging Contrast Agents. *Biomacromolecules* **2006,** *7* (11), 3132-3138.
30. Ghosh, S.; GhoshMitra, S.; Cai, T.; Diercks, D.; Mills, N.; Hynds, D., Alternating Magnetic Field Controlled, Multifunctional Nano-Reservoirs: Intracellular Uptake and Improved Biocompatibility. *Nanoscale Research Letters* **2010,** *5* (1), 195-204.

31. Creixell, M.; Herrera, A. P.; Latorre-Esteves, M.; Ayala, V.; Torres-Lugo, M.; Rinaldi, C., The effect of grafting method on the colloidal stability and in vitro cytotoxicity of carboxymethyl dextran coated magnetic nanoparticles. *Journal of Materials Chemistry* **2010,** *20* (39), 8539-8547.
32. Siegel, R.; Ma, J.; Zou, Z.; Jemal, A., Cancer statistics, 2014. *CA: A Cancer Journal for Clinicians* **2014,** *64* (1), 9-29.
33. Wyatt, S. W.; Maynard, W. R.; Risser, D. R.; Hakenewerth, A. M.; Williams, M. A.; Garcia, R., All-Cancers Mortality Rates Approaching Diseases of the Heart Mortality Rates as Leading Cause of Death in Texas. *Southern Medical Journal* **2014,** *107* (1), 19-23 10.1097/SMJ.0000000000000046.
34. Chilkoti, A.; Dreher, M. R.; Meyer, D. E.; Raucher, D., Targeted drug delivery by thermally responsive polymers. *Advanced Drug Delivery Reviews* **2002,** *54* (5), 613-630.
35. Jain, R. K., Delivery of Molecular Medicine to Solid Tumors. *Science* **1996,** *271* (5252), 1079-1080.
36. Kostova, I., Platinum complexes as anticancer agents. *Recent patents on anti-cancer drug discovery* **2006,** *1* (1), 1-22.
37. Pignata, S.; Scambia, G.; Katsaros, D.; Gallo, C.; Pujade-Lauraine, E.; De Placido, S.; Bologna, A.; Weber, B.; Raspagliesi, F.; Panici, P. B.; Cormio, G.; Sorio, R.; Cavazzini, M. G.; Ferrandina, G.; Breda, E.; Murgia, V.; Sacco, C.; Cinieri, S.; Salutari, V.; Ricci, C.; Pisano, C.; Greggi, S.; Lauria, R.; Lorusso, D.; Marchetti, C.; Selvaggi, L.; Signoriello, S.; Piccirillo, M. C.; Di Maio, M.; Perrone, F., Carboplatin plus paclitaxel once a week versus every 3 weeks in patients with advanced ovarian cancer (MITO-7): a randomised, multicentre, open-label, phase 3 trial. *The Lancet Oncology* **2014,** *15* (4), 396-405.
38. Pujade-Lauraine, E.; Wagner, U.; Aavall-Lundqvist, E.; Gebski, V.; Heywood, M.; Vasey, P. A.; Volgger, B.; Vergote, I.; Pignata, S.; Ferrero, A.; Sehouli, J.; Lortholary, A.; Kristensen, G.; Jackisch, C.; Joly, F.; Brown, C.; Fur, N. L.; Bois, A. d., Pegylated Liposomal Doxorubicin and Carboplatin Compared With Paclitaxel and Carboplatin for Patients With Platinum-Sensitive Ovarian Cancer in Late Relapse. *Journal of Clinical Oncology* **2010,** *28* (20), 3323-3329.
39. André, T.; Boni, C.; Navarro, M.; Tabernero, J.; Hickish, T.; Topham, C.; Bonetti, A.; Clingan, P.; Bridgewater, J.; Rivera, F.; Gramont, A. d., Improved Overall Survival With Oxaliplatin, Fluorouracil, and Leucovorin As Adjuvant Treatment in Stage II or III Colon Cancer in the MOSAIC Trial. *Journal of Clinical Oncology* **2009,** *27* (19), 3109-3116.
40. Scagliotti, G. V.; Parikh, P.; Pawel, J. v.; Biesma, B.; Vansteenkiste, J.; Manegold, C.; Serwatowski, P.; Gatzemeier, U.; Digumarti, R.; Zukin, M.; Lee, J. S.; Mellemgaard, A.; Park, K.; Patil, S.; Rolski, J.; Goksel, T.; Marinis, F. d.; Simms, L.; Sugarman, K. P.; Gandara, D., Phase III Study Comparing Cisplatin Plus Gemcitabine With Cisplatin Plus Pemetrexed in Chemotherapy-Naive Patients With Advanced-Stage Non–Small-Cell Lung Cancer. *Journal of Clinical Oncology* **2008,** *26* (21), 3543-3551.
41. Kelland, L., The resurgence of platinum-based cancer chemotherapy. *Nature reviews. Cancer* **2007,** *7* (8), 573.
42. Nishiyama, N.; Okazaki, S.; Cabral, H.; Miyamoto, M.; Kato, Y.; Sugiyama, Y.; Nishio, K.; Matsumura, Y.; Kataoka, K., Novel Cisplatin-Incorporated Polymeric Micelles Can Eradicate Solid Tumors in Mice. *Cancer research* **2003,** *63* (24), 8977-8983.
43. Oberoi, H. S.; Nukolova, N. V.; Kabanov, A. V.; Bronich, T. K., Nanocarriers for delivery of platinum anticancer drugs. *Advanced Drug Delivery Reviews* **2013,** *65* (13), 1667-1685.
44. Maeda, H.; Nakamura, H.; Fang, J., The EPR effect for macromolecular drug delivery to solid tumors: Improvement of tumor uptake, lowering of systemic toxicity, and distinct tumor imaging in vivo. *Advanced Drug Delivery Reviews* **2013,** *65* (1), 71-79.

45. Haxton, K. J.; Burt, H. M., Polymeric drug delivery of platinum‐based anticancer agents. *Journal of pharmaceutical sciences* **2009,** *98* (7), 2299-2316.
46. Cheng, K.; Peng, S.; Xu, C.; Sun, S., Porous Hollow Fe3O4 Nanoparticles for Targeted Delivery and Controlled Release of Cisplatin. *Journal of the American Chemical Society* **2009,** *131* (30), 10637-10644.
47. Pothayee, N.; Pothayee, N.; Hu, N.; Zhang, R.; Kelly, D. F.; Koretsky, A. P.; Riffle, J. S., Manganese graft ionomer complexes (MaGICs) for dual imaging and chemotherapy. *Journal of Materials Chemistry B* **2014,** *2* (8), 1087-1099.
48. Duncan, R., Polymer conjugates as anticancer nanomedicines. *Nat Rev Cancer* **2006,** *6* (9), 688-701.
49. Yin, Q.; Shen, J.; Zhang, Z.; Yu, H.; Li, Y., Reversal of multidrug resistance by stimuli-responsive drug delivery systems for therapy of tumor. *Advanced Drug Delivery Reviews* **2013,** *65* (13), 1699-1715.
50. Livney, Y. D.; Assaraf, Y. G., Rationally designed nanovehicles to overcome cancer chemoresistance. *Advanced Drug Delivery Reviews* **2013,** *65* (13), 1716-1730.
51. Kozissnik, B.; Bohorquez, A. C.; Dobson, J.; Rinaldi, C., Magnetic fluid hyperthermia: Advances, challenges, and opportunity. *International Journal of Hyperthermia* **2013,** *29* (8), 706-714.
52. Jordan, A.; Scholz, R.; Wust, P.; Fähling, H.; Roland, F., Magnetic fluid hyperthermia (MFH): Cancer treatment with AC magnetic field induced excitation of biocompatible superparamagnetic nanoparticles. *Journal of Magnetism and Magnetic Materials* **1999,** *201* (1–3), 413-419.
53. Jung, B.-K.; Lee, Y. K.; Hong, J.; Ghandehari, H.; Yun, C.-O., Mild Hyperthermia Induced by Gold Nanorod-Mediated Plasmonic Photothermal Therapy Enhances Transduction and Replication of Oncolytic Adenoviral Gene Delivery. *ACS Nano* **2016,** *10* (11), 10533-10543.
54. Bae, K. H.; Park, M.; Do, M. J.; Lee, N.; Ryu, J. H.; Kim, G. W.; Kim, C.; Park, T. G.; Hyeon, T., Chitosan Oligosaccharide-Stabilized Ferrimagnetic Iron Oxide Nanocubes for Magnetically Modulated Cancer Hyperthermia. *ACS Nano* **2012,** *6* (6), 5266-5273.
55. Al-Ahmady, Z. S.; Al-Jamal, W. T.; Bossche, J. V.; Bui, T. T.; Drake, A. F.; Mason, A. J.; Kostarelos, K., Lipid–Peptide Vesicle Nanoscale Hybrids for Triggered Drug Release by Mild Hyperthermia in Vitro and in Vivo. *ACS Nano* **2012,** *6* (10), 9335-9346.
56. Shah, B. P.; Pasquale, N.; De, G.; Tan, T.; Ma, J.; Lee, K.-B., Core–Shell Nanoparticle-Based Peptide Therapeutics and Combined Hyperthermia for Enhanced Cancer Cell Apoptosis. *ACS Nano* **2014,** *8* (9), 9379-9387.
57. Gupta, A. K.; Gupta, M., Synthesis and surface engineering of iron oxide nanoparticles for biomedical applications. *Biomaterials* **2005,** *26* (18), 3995-4021.
58. Neuberger, T.; Schöpf, B.; Hofmann, H.; Hofmann, M.; von Rechenberg, B., Superparamagnetic nanoparticles for biomedical applications: Possibilities and limitations of a new drug delivery system. *Journal of Magnetism and Magnetic Materials* **2005,** *293* (1), 483-496.
59. Deatsch, A. E.; Evans, B. A., Heating efficiency in magnetic nanoparticle hyperthermia. *Journal of Magnetism and Magnetic Materials* **2014,** *354*, 163-172.
60. Maier-Hauff, K.; Rothe, R.; Scholz, R.; Gneveckow, U.; Wust, P.; Thiesen, B.; Feussner, A.; von Deimling, A.; Waldoefner, N.; Felix, R., Intracranial Thermotherapy using Magnetic Nanoparticles Combined with External Beam Radiotherapy: Results of a Feasibility Study on Patients with Glioblastoma Multiforme. *Journal of Neuro-Oncology* **2007,** *81*.
61. Kenichi Kakinuma; Ryuichi Tanaka; Hideaki Takahashi; Masato Watanabe; Tadashi Nakagawa; Mizuo Kuroki, Targeting chemotherapy for malignant brain tumor using thermosensitive liposome and localized hyperthermia. *Journal of Neurosurgery* **1996,** *84* (2), 180-184.

62. Issels, R. D., Hyperthermia adds to chemotherapy. *European Journal of Cancer* **2008,** *44* (17), 2546-2554.
63. Zhang, L.-Y.; Gu, H.-C.; Wang, X.-M., Magnetite ferrofluid with high specific absorption rate for application in hyperthermia. *Journal of Magnetism and Magnetic Materials* **2007,** *311* (1), 228-233.
64. Ito, A.; Tanaka, K.; Honda, H.; Abe, S.; Yamaguchi, H.; Kobayashi, T., Complete regression of mouse mammary carcinoma with a size greater than 15 mm by frequent repeated hyperthermia using magnetite nanoparticles. *Journal of Bioscience and Bioengineering* **2003,** *96* (4), 364-369.
65. Fortin, J.-P.; Wilhelm, C.; Servais, J.; Ménager, C.; Bacri, J.-C.; Gazeau, F., Size-Sorted Anionic Iron Oxide Nanomagnets as Colloidal Mediators for Magnetic Hyperthermia. *Journal of the American Chemical Society* **2007,** *129* (9), 2628-2635.
66. Jordan, A.; Scholz, R.; Wust, P.; Fähling, H.; Krause, J.; Wlodarczyk, W.; Sander, B.; Vogl, T.; Felix, R., Effects of Magnetic Fluid Hyperthermia (MFH) on C3H mammary carcinoma in vivo. *International Journal of Hyperthermia* **1997,** *13* (6), 587-605.
67. Gitsov, I.; Johnson, F. E., Synthesis and hydrolytic stability of poly(oxyethylene-H-phosphonate)s. *Journal of Polymer Science Part A: Polymer Chemistry* **2008,** *46* (12), 4130-4139.
68. Xu, X.; Yu, H.; Gao, S.; Mao, H.-Q.; Leong, K. W.; Wang, S., Polyphosphoester microspheres for sustained release of biologically active nerve growth factor. *Biomaterials* **2002,** *23* (17), 3765-3772.
69. Sandiford, L.; Phinikaridou, A.; Protti, A.; Meszaros, L. K.; Cui, X.; Yan, Y.; Frodsham, G.; Williamson, P. A.; Gaddum, N.; Botnar, R. M.; Blower, P. J.; Green, M. A.; de Rosales, R. T. M., Bisphosphonate-Anchored PEGylation and Radiolabeling of Superparamagnetic Iron Oxide: Long-Circulating Nanoparticles for in Vivo Multimodal (T1 MRI-SPECT) Imaging. *ACS Nano* **2013,** *7* (1), 500-512.
70. Portet, D.; Denizot, B.; Rump, E.; Lejeune, J.-J.; Jallet, P., Nonpolymeric Coatings of Iron Oxide Colloids for Biological Use as Magnetic Resonance Imaging Contrast Agents. *Journal of Colloid and Interface Science* **2001,** *238* (1), 37-42.
71. Mohapatra, S.; Mallick, S. K.; Maiti, T. K.; Ghosh, S. K.; Pramanik, P., Synthesis of highly stable folic acid conjugated magnetite nanoparticles for targeting cancer cells. *Nanotechnology* **2007,** *18* (38), 385102.
72. Pothayee, N.; Balasubramaniam, S.; Davis, R. M.; Riffle, J. S.; Carroll, M. R. J.; Woodward, R. C.; St. Pierre, T. G., Synthesis of 'ready-to-adsorb' polymeric nanoshells for magnetic iron oxide nanoparticles via atom transfer radical polymerization. *Polymer* **2011,** *52* (6), 1356-1366.
73. Hu, N.; Johnson, L. M.; Pothayee, N.; Pothayee, N.; Lin, Y.; Davis, R. M.; Riffle, J. S., Synthesis of ammonium bisphosphonate monomers and polymers. *Polymer* **2013,** *54* (13), 3188-3197.
74. Cui, X.; Green, M.; Blower, P.; Zhou, D.; Yan, Y.; Zhang, W.; Djanashvili, K.; Mathe, D.; Veres, D.; Szigeti, K., Al (OH) 3 facilitated synthesis of water-soluble, magnetic, radiolabelled and fluorescent hydroxyapatite nanoparticles. *Chemical Communications* **2015,** *51* (45), 9332-9335.
75. Huang, J.; Bu, L.; Xie, J.; Chen, K.; Cheng, Z.; Li, X.; Chen, X., Effects of nanoparticle size on cellular uptake and liver MRI with polyvinylpyrrolidone-coated iron oxide nanoparticles. *ACS Nano* **2010,** *4* (12), 7151-7160.
76. Vreeland, E. C.; Watt, J.; Schober, G. B.; Hance, B. G.; Austin, M. J.; Price, A. D.; Fellows, B. D.; Monson, T. C.; Hudak, N. S.; Maldonado-Camargo, L., Enhanced nanoparticle size control by extending LaMer's mechanism. *Chemistry of Materials* **2015,** *27* (17), 6059-6066.
77. Jain-Gupta, N.; Pothayee, N.; Pothayee, N.; Tyler, R., Jr.; Caudell, D.; Balasubramaniam, S.; Hu, N.; Davis, R.; Riffle, J.; Sriranganathan, N., Efficacies of gentamicin-loaded magnetite block ionomer

complexes against chronic Brucella melitensis infection. *Journal of Nanoparticle Research* **2013,** *15* (11), 1-13.
78. Rohrer, M.; Bauer, H.; Mintorovitch, J.; Requardt, M.; Weinmann, H. J., Comparison of magnetic properties of MRI contrast media solutions at different magnetic field strengths. *Invest Radiol* **2005,** *40* (11), 715-24.
79. Balasubramaniam, S.; Kayandan, S.; Lin, Y.-N.; Kelly, D. F.; House, M. J.; Woodward, R. C.; St. Pierre, T. G.; Riffle, J. S.; Davis, R. M., Toward Design of Magnetic Nanoparticle Clusters Stabilized by Biocompatible Diblock Copolymers for T2-Weighted MRI Contrast. *Langmuir* **2014,** *30* (6), 1580-1587.
80. Shi, X.; Wang, S. H.; Swanson, S. D.; Ge, S.; Cao, Z.; Van Antwerp, M. E.; Landmark, K. J.; Baker, J. R., Dendrimer-Functionalized Shell-crosslinked Iron Oxide Nanoparticles for In-Vivo Magnetic Resonance Imaging of Tumors. *Advanced Materials* **2008,** *20* (9), 1671-1678.
81. Brazel, C., Magnetothermally-responsive Nanomaterials: Combining Magnetic Nanostructures and Thermally-Sensitive Polymers for Triggered Drug Release. *Pharmaceutical Research* **2009,** *26* (3), 644-656.
82. Peiris, P. M.; Abramowski, A.; Mcginnity, J.; Doolittle, E.; Toy, R.; Gopalakrishnan, R.; Shah, S.; Bauer, L.; Ghaghada, K. B.; Hoimes, C.; Brady-Kalnay, S. M.; Basilion, J. P.; Griswold, M. A.; Karathanasis, E., Treatment of Invasive Brain Tumors Using a Chain-like Nanoparticle. *Cancer Research* **2015,** *75* (7), 1356-1365.
83. Park, J.; An, K.; Hwang, Y.; Park, J.-G.; Noh, H.-J.; Kim, J.-Y.; Park, J.-H.; Hwang, N.-M.; Hyeon, T., Ultra-large-scale syntheses of monodisperse nanocrystals. *Nat Mater* **2004,** *3* (12), 891-895.
84. Davis, K.; Cole, B.; Ghelardini, M.; Powell, B. A.; Mefford, O. T., Quantitative Measurement of Ligand Exchange with Small-Molecule Ligands on Iron Oxide Nanoparticles via Radioanalytical Techniques. *Langmuir* **2016,** *32* (51), 13716-13727.
85. Davis, K.; Qi, B.; Witmer, M.; Kitchens, C. L.; Powell, B. A.; Mefford, O. T., Quantitative measurement of ligand exchange on iron oxides via radiolabeled oleic acid. *Langmuir* **2014,** *30* (36), 10918-10925.
86. Hergt, R.; Hiergeist, R.; Zeisberger, M.; Schüler, D.; Heyen, U.; Hilger, I.; Kaiser, W. A., Magnetic properties of bacterial magnetosomes as potential diagnostic and therapeutic tools. *Journal of Magnetism and Magnetic Materials* **2005,** *293* (1), 80-86.
87. Hergt, R.; Hiergeist, R.; Zeisberger, M.; Glöckl, G.; Weitschies, W.; Ramirez, L.; Hilger, I.; Kaiser; WA, Enhancement of AC-losses of magnetic nanoparticles for heating applications. *Journal of Magnetism and Magnetic Materials* **2004,** *280* (2), 358-368.
88. Oh, K. T.; Bronich, T. K.; Kabanov, A. V., Micellar formulations for drug delivery based on mixtures of hydrophobic and hydrophilic Pluronic® block copolymers. *Journal of Controlled Release* **2004,** *94* (2), 411-422.
89. Lin, W.-J.; Juang, L.-W.; Lin, C.-C., Stability and release performance of a series of pegylated copolymeric micelles. *Pharmaceutical Research* **2003,** *20* (4), 668-673.
90. Allen, C.; Maysinger, D.; Eisenberg, A., Nano-engineering block copolymer aggregates for drug delivery. *Colloids and Surfaces B: Biointerfaces* **1999,** *16* (1–4), 3-27.
91. Boulikas, T.; Vougiouka, M., Recent clinical trials using cisplatin, carboplatin and their combination chemotherapy drugs (Review). *Oncology Reports* **2004,** *11* (3), 559-595.
92. Pinzani, V. B., F.; Hang, I. J., Galtier, M.; Blayac, J. P.; Balmes, P. , Cisplatin-induced renal toxicity and toxicity -modulating strategies: review. *Cancer Chemother. Pharmacol.* **1994,** *35*, 1-9.
93. Hu, N. Block and Graft Copolymers Containing Carboxylate or Phosphonate Anions. Dissertation, Virginia Polytechnic Institute and State University, 2014.

94. Narayanan, S.; Sathy, B. N.; Mony, U.; Koyakutty, M.; Nair, S. V.; Menon, D., Biocompatible Magnetite/Gold Nanohybrid Contrast Agents via Green Chemistry for MRI and CT Bioimaging. *ACS Applied Materials & Interfaces* **2012,** *4* (1), 251-260.
95. Xiao, L.; Li, J.; Brougham, D. F.; Fox, E. K.; Feliu, N.; Bushmelev, A.; Schmidt, A.; Mertens, N.; Kiessling, F.; Valldor, M.; Fadeel, B.; Mathur, S., Water-Soluble Superparamagnetic Magnetite Nanoparticles with Biocompatible Coating for Enhanced Magnetic Resonance Imaging. *ACS Nano* **2011,** *5* (8), 6315-6324.
96. Sun, C.; Lee, J. S. H.; Zhang, M., Magnetic nanoparticles in MR imaging and drug delivery. *Advanced Drug Delivery Reviews* **2008,** *60* (11), 1252-1265.
97. Stephen, Z. R.; Kievit, F. M.; Zhang, M., Magnetite nanoparticles for medical MR imaging. *Materials Today* **2011,** *14* (7–8), 330-338.
98. Jun, Y.-w.; Lee, J.-H.; Cheon, J., Chemical Design of Nanoparticle Probes for High-Performance Magnetic Resonance Imaging. *Angewandte Chemie International Edition* **2008,** *47* (28), 5122-5135.
99. Balasubramaniam, S.; Pothayee, N.; Lin, Y.; House, M.; Woodward, R. C.; St. Pierre, T. G.; Davis, R. M.; Riffle, J. S., Poly(N-isopropylacrylamide)-Coated Superparamagnetic Iron Oxide Nanoparticles: Relaxometric and Fluorescence Behavior Correlate to Temperature-Dependent Aggregation. *Chemistry of Materials* **2011,** *23* (14), 3348-3356.
100. Wu, C.; Xu, Y.; Yang, L.; Wu, J.; Zhu, W.; Li, D.; Cheng, Z.; Xia, C.; Guo, Y.; Gong, Q.; Song, B.; Ai, H., Negatively Charged Magnetite Nanoparticle Clusters as Efficient MRI Probes for Dendritic Cell Labeling and In Vivo Tracking. *Advanced Functional Materials* **2015,** *25* (23), 3581-3591.
101. Cui, X.; Green, M. A.; Blower, P. J.; Zhou, D.; Yan, Y.; Zhang, W.; Djanashvili, K.; Mathe, D.; Veres, D. S.; Szigeti, K., Al(OH)3 facilitated synthesis of water-soluble, magnetic, radiolabelled and fluorescent hydroxyapatite nanoparticles. *Chemical Communications* **2015,** *51* (45), 9332-9335.
102. Jose Sanchez-Moreno, M.; Gomez-Coca, R. B.; Fernandez-Botello, A.; Ochocki, J.; Kotynski, A.; Griesser, R.; Sigel, H., Synthesis and acid-base properties of (1H-benzimidazol-2-yl-methyl)phosphonate (Bimp2-). Evidence for intramolecular hydrogen-bond formation in aqueous solution between (N-1)H and the phosphonate group. *Organic & Biomolecular Chemistry* **2003,** *1* (10), 1819-1826.
103. Ma, M.; Wu, Y.; Zhou, J.; Sun, Y.; Zhang, Y.; Gu, N., Size dependence of specific power absorption of Fe 3 O 4 particles in AC magnetic field. *Journal of Magnetism and Magnetic Materials* **2004,** *268* (1), 33-39.
104. Darwish, M. S.; El-Sabbagh, A.; Stibor, I., Hyperthermia properties of magnetic polyethylenimine core/shell nanoparticles: influence of carrier and magnetic field strength. *Journal of Polymer Research* **2015,** *22* (12), 239.
105. Vreeland, E. C.; Watt, J.; Schober, G. B.; Hance, B. G.; Austin, M. J.; Price, A. D.; Fellows, B. D.; Monson, T. C.; Hudak, N. S.; Maldonado-Camargo, L.; Bohorquez, A. C.; Rinaldi, C.; Huber, D. L., Enhanced Nanoparticle Size Control by Extending LaMer's Mechanism. *Chemistry of Materials* **2015,** *27* (17), 6059-6066.
106. Master, A. M.; Williams, P. N.; Pothayee, N.; Pothayee, N.; Zhang, R.; Vishwasrao, H. M.; Golovin, Y. I.; Riffle, J. S.; Sokolsky, M.; Kabanov, A. V., Remote Actuation of Magnetic Nanoparticles For Cancer Cell Selective Treatment Through Cytoskeletal Disruption. *Scientific Reports* **2016,** *6*.

Chapter 6: Additional synthesis and fabrication

6.1 Synthesis of poly(lactide) homopolymers and copolymers

6.1.1 Materials

6-Mercapto-1-hexanol (97%), tin(II) 2-ethylhexanoate (92.5-100.0%), and (3S)-*cis*-3,6-dimethyl-1,4-dioxane-2,5-dione (98%) were purchased from Sigma-Aldrich and used as received. Anhydrous diethyl ether (99.8%) was purchased from Fisher Chemicals Co. and used as received. Anhydrous toluene (99.8%) was purchased from EMD Chemicals, dried over 3 Å molecular sieves and distilled before use. Anhydrous ethanol (200 proof) was purchased from Decon Laboratories Inc. and used as received. 2,2'-Azobis(2-methyl propionitrile) (AIBN, 98%, Sigma-Aldrich) was recrystallized from anhydrous methanol (Fisher Scientific, HPLC grade, 99.9%) twice. Acrylic acid (AA, anhydrous, 99%) was distilled under vacuum. 3,6-Dimethyl-1,4-dioxane-2,5-dione (99%, Sigma-Aldrich) was recrystallized from anhydrous acetone (Fisher Scientific, HPLC grade, 99.8%) and dried at room temperature under vacuum for 24 h.

6.1.2 Synthesis of poly(ethylene oxide)-*b*-poly(DL-lactide)

The synthesis of poly(ethylene oxide)-*b*-poly(DL-lactide) followed a previously reported procedure.[1] A 250-mL, round bottom flask was flame-dried with a nitrogen purge and cooled 3X. Anhydrous toluene was dried over 3 Å molecular sieves. Poly(ethylene oxide) methyl ether (PEG 5k) was dried at 60 °C overnight under vacuum. 3,6-Dimethyl-1,4-dioxane-2,5-dione (DL-Lactide monomer, 8.88 g), dry poly(ethylene oxide) methyl ether (4.44 g), and dry toluene (34 mL) were charged to a dry, round bottom flask. Tin(II) 2-ethylhexanoate (stannous octoate, 0.2 mL) was charged into a 25-mL scintillation vial, and dry toluene (9.8 mL) was added and mixed well, then a fraction

of the solution (1 mL) was charged to the reaction mixture via syringe. The mixture was stirred and reacted at 105 °C for 48 h. Afterward, the reaction mixture was allowed to cool down and precipitated in cold diethyl ether. The precipitate was filtered by suction and dried at 40 °C for 40 h under vacuum. A white solid of poly(ethylene oxide)-*b*-poly(DL-lactide) (PEO-*b*-PDLLA) was obtained. Yield: 85%.

6.1.3 Synthesis of poly(acrylic acid)-*b*-poly(DL-lactide)

6.1.3.1 Synthesis of hydroxyl-terminated poly(acrylic acid)

Hydroxyl-terminated poly(acrylic acid) (PAA-OH) was synthesized by conventional free-radical polymerization using 2,2'-azobis(2-methyl propionitrile) (AIBN) as an initiator and 6-mercapto-1-hexanol as a chain transfer agent.[2] A 100-mL, round bottom flask was flame-dried 3X under a nitrogen purge, and anhydrous ethanol (50 mL) was charged. Recrystallized AIBN (50 mg), 6-mercapto-1-hexanol (125 μL) in dry ethanol (1 mL), and distilled AA (2.1 mL) was added and dissolved. The mixture was purged with nitrogen heavily for 10 min. The mixture was then heated to 70 °C and reacted for 6 h. The solvent was partially removed by rotary evaporation and precipitated in chilled ether (250 mL each) 5X. The precipitate was filtered and dried under vacuum at 60 °C overnight to afford the PAA-OH macroinitiator for the next step.

6.1.3.2 Synthesis of a poly(acrylic acid)-b-poly(DL-lactide) copolymer

Poly(acrylic acid)-*b*-poly(DL-lactide) (PAA-*b*-PDLLA) copolymer was synthesized by ring opening polymerization using PAA-OH as the macroinitiator and DL-lactide as the monomer. PAA-OH was dried at 60 °C under vacuum overnight. A 100-mL, round bottom flask was flame-dried 3X under a nitrogen purge, and the PAA-OH (0.5 g) and DL-lactide (2.81 g) were charged. Dry toluene (10 mL) was added and the temperature was raised to 80 °C to dissolve the reagents. After a clear solution was formed, tin(II) 2-ethylhexanoate (8.5 μL) in dry toluene (1 mL) was charged. The temperature of the mixture was then raised to 105 °C to reflux for 48 h under nitrogen. The mixture

was cooled slightly and precipitated in diethyl ether (250 mL each) 2X and filtered. The solid was dried at 80 °C under vacuum for 24 h to afford the PAA-*b*-PDLLA copolymer.

6.1.4 Synthesis of a PLLA homopolymer

A PLLA homopolymer with a targeted M_n of 11,000 g mol^{-1} was prepared with benzyl alcohol as the initiator.[3] (3S)-*cis*-3,6-Dimethyl-1,4-dioxane-2,5-dione (L-lactide monomer, 2.05 g, 0.01 mol) and toluene (6.5 mL) were charged into a 100-mL, round-bottom flask equipped with a stir bar and condenser. Benzyl alcohol (0.36 mL of a 0.51 M solution in toluene, 0.18 mmol) was added to the stirring reaction via syringe. Stannous octoate catalyst solution (0.31 mL, 0.012 g/mL) in toluene was added to the flask. The polymerization was conducted at 120 °C for 48 h. The polymer was isolated by precipitation into cold diethyl ether and collected by vacuum filtration. The product was vacuum dried at 40 °C for 40 h and 1.65 g of PLLA homopolymer was obtained. Yield: 80%.

6.2 Fabrication of poly(dimethylsiloxane)-magnetite magnetic fluids

6.2.1 Materials

Hexamethylcyclotrisiloxane (D_3, 98%) was purchased from Gelest Inc. and sublimed under vacuum before use. Trivinylchlorosilane (95%) was purchased from Gelest Inc. and used as received. Thioglycolic acid (mercaptoacetic acid, ≥99%), benzyl alcohol (99-100.5% by GC), iron(III) chloride hexahydrate (ACS reagent, crystallized, 98.0-102%), iron(II) chloride tetrahydrate (ReagentPlus®, 98%), iron(III) acetylacetonate (99.9+%), calcium hydride (powder, reagent grade, 90-95%), sodium (lump, in kerosene, 99%), *n*-butyl lithium solution (2.5 M in hexanes), and benzophenone (ReagentPlus®, 99%) were purchased from Sigma-Aldrich and used as received. Hydrochloric acid (3.0 M) was purchased from LabChem Inc. and used as received. Magnesium sulfate (certified anhydrous) was purchased from Fisher Chemical Co. and used as received. Toluene (anhydrous,

99.8%) was purchased from Sigma-Aldrich, washed with concentrated sulfuric acid (ACS reagent, 95-98%, Spectrum Chemical Corp.) 2X for 30 min each time at room temperature, dried over magnesium sulfate for 1 h, dried over calcium hydride for 12 h, and distilled before use. Tetrahydrofuran (THF, anhydrous, ≥99.9%, inhibitor-free) was purchased from Fisher Chemical Co., dried over calcium hydride, distilled, and dried over sodium and benzophenone under N_2, stirred until the solution became deep purple, and re-distilled before use. Cyclohexane (anhydrous, 99.5%, Fisher Chemical Co.) was stirred with concentrated sulfuric acid for 48 h at room temperature to remove any unsaturated impurities and washed with de-ionized water until neutral. The organic layer was then separated and dried over magnesium sulfate and calcium hydride, and distilled under reduced pressure and stored in a desiccator until the addition of sodium with a nitrogen purge. The cyclohexane was re-distilled over sodium before use. 2,2′-Azobis(2-methylpropionitrile) (AIBN, 98%) was purchased from Sigma-Aldrich and recrystallized from anhydrous methanol (Fisher Scientific, HPLC grade, 99.9%) twice. Ammonium hydroxide solution was purchased from Alfa Aesar and used as received. Oleic acid (≥99% by GC), dichloromethane (DCM, 99.9%), methanol (certified ACS grade, Assay: ≥99.8%), and chloroform (99.99%) were purchased from Fisher Chemical Co. and used as received. NdFeB doughnut-shaped magnets that were magnetized through the thickness were purchased from Engineered Concepts.

6.2.2 Synthesis of a trivinyl-functional poly(dimethylsiloxane) by anionic ring opening polymerization

The synthesis of a poly(dimethylsiloxane) (PDMS) has been previously established by our group.[4-5] Freshly-sublimed hexamethylcyclotrisiloxane (34.6 g) was prepared in a 250-mL, two-neck round bottom flask. Ultra-dry cyclohexane (60 mL) was charged via a cannula and the mixture was stirred at room temperature to dissolve the monomer. The *n*-butyl lithium initiator (4.5 mL, 2.5 M)

was added to the reaction flask via a cannula, and stirred at r.t. for 30 min. Dry THF (15 mL) was then added to promote the ring opening polymerization. The mixture was stirred at r.t. overnight. After 95% conversion as determined by ^{1}H NMR, trivinylchlorosilane (1.5 equivalents relative to the initiator, 2.6 mL) was added dropwise to terminate and end-cap the PDMS. The mixture was stirred overnight. The reaction mixture was subsequently diluted with chloroform (150 mL), and washed with de-ionized water (100 mL) 3X. The organic layer was separated, and the solvent was partially removed via rotary evaporation, then coagulated in chilled methanol (800 mL) 2X. The precipitate was filtered by suction, charged to a 250-mL, round bottom flask, and dried at 80 °C overnight. After the removal of methanol and trace amounts of water, the polymer became a transparent yet viscous liquid.

6.2.3 Synthesis of a tricarboxylic acid-functional PDMS via thiol-ene reaction

A 100-mL, round-bottom flask was flame-dried and purged with nitrogen 3X to remove moisture. Trivinyl-functional PDMS (3281 mol^{-1}, 27.93 g, 25.54 mmol vinyl) was added into the flask and dissolved in distilled toluene (25 mL). Nitrogen was purged through the solution for 2 h to deoxygenate the mixture. AIBN (63 mg, 0.3831 mmol) and mercaptoacetic acid (2.7 mL, 38.3 mmol) were added and the flask was purged with nitrogen. After thorough mixing by stirring, the mixture was heated to 80 °C and stirred for 1.5 h. Reaction completion was monitored by observing the disappearance of the vinyl proton peaks at ~6 ppm in the ^{1}H NMR spectra. The solvent was subsequently removed under vacuum at 80 °C overnight, and the polymer was dissolved in methanol (30 mL) and stirred for 30 min. Deionized water was added to the solution until the polymer coagulated as a solid, and then it was collected via filtration. The methanol/deionized water coagulation process was repeated 5X, and the targeted tricarboxylic acid-functional PDMS was dried under vacuum at 80 °C overnight.

6.2.4 Synthesis of magnetite nanoparticles via co-precipitation of iron chlorides with ammonium hydroxide

Synthesis of magnetite nanoparticles by chemical co-precipitation of iron salts was achieved via the following established procedure.[6] Iron(III) chloride hexahydrate (3.50 g, 0.013 mol) and iron(II) chloride tetrahydrate (1.28 g, 0.0064 mol) were weighed into separate round-bottom flasks, and each was dissolved in deoxygenated water (20 mL, previously boiled for 10 min and purged with nitrogen for 60 min) The two iron salt solutions were then added to a 500 mL, three-neck round-bottom flask fitted with an Ultra-Turrax T25 Digital Homogenizer, a calibrated pH meter, and a nitrogen purge. The mixture was stirred at 13,000 rpm with the homogenizer and the ammonium hydroxide solution (~40 mL) was charged via syringe until the rapidly stirring solution turned black and reached a pH of 9-10, as determined by pH meter. Magnetite nanoparticles were formed and used directly without purification and storage.

6.2.5 Synthesis of magnetite nanoparticles using thermo-decomposition with benzyl alcohol as the solvent

The synthesis of magnetite using a thermo-decomposition method with benzyl alcohol as the solvent has been previously reported by our group.[7] $Fe(acac)_3$ (2.14 g, 8.4 mmol) and benzyl alcohol (45 mL, 0.43 mol) were charged to a 250-mL, three-neck, round-bottom flask equipped with a water condenser and placed in a Belmont metal bath with an overhead stirrer with thermostatic (±l °C) control. The solution was dehydrated at 110 °C for 1 h under a N_2 stream. The temperature was increased in 25 °C increments and held at each step temperature for 1 h until it reached the reflux temperature of benzyl alcohol at 205 °C, then the temperature was maintained for 40 h. The reaction was cooled to room temperature and the particles were collected by centrifugation (4000 rpm, 30 min). The magnetite nanoparticles were washed 3X with acetone (100 mL each), and they were

subsequently dispersed in chloroform (20 mL) containing oleic acid (0.3 g) and sonicated for 30 min. The solvent was removed by purging with nitrogen at room temperature, and the oleic acid-stabilized magnetite nanoparticles were washed 3X with acetone (20 mL each) to remove any excess oleic acid. The particles were dried by purging with nitrogen for 2 h and stored in a refrigerator.

6.2.6 Preparation of PDMS-coated magnetite magnetic fluid with a targeted composition of 70:30 wt:wt

The preparation of PDMS-coated magnetite magnetic fluid has been previously reported by our group.[5] The experimental conditions describe a method to obtain a PDMS stabilizer:magnetite complex comprised of ~30 wt% magnetite and ~70 wt% PDMS as the dispersion stabilizer. Typically, A PDMS dispersion stabilizer (3.54 g) was dissolved in DCM (60 mL), and this solution was added to a freshly-prepared basic magnetite dispersion described in 6.2.4 and stirred for 30 min. Aqueous HCl (3.0 M) was then slowly added until a slightly acidic pH was obtained (~13 mL was required to reach pH 5-6). The heterogeneous dispersion was stirred for 1 h, and then the DCM was removed via rotary evaporation. The PDMS-coated magnetite magnetic fluid was collected with a permanent magnet and the water was decanted, and then it was washed 3X with water (20 mL each) and methanol (20 mL each) before drying at 50 °C under reduced pressure overnight. A black viscous fluid was obtained, which is the PDMS-coated magnetite magnetic fluid.

6.3 Preparation of silver nanoparticle-embedded polymer membranes by solvent casting

6.3.1 Materials

Polyethylene glycol (M_n 2k g mol^{-1}) and silver nitrate (ACS reagent, ≥99.0%) were purchased from Sigma-Aldrich and used as received. Ethanol (200 proof) was purchased from Decon Labs. Chloroform (99.9%) was purchased from Fisher Scientific and used as received. A bisphenol A-based

poly(arylene ether ketone) was synthesized from 4,4'-difluorobenzophenone and bisphenol A (both were kindly donated by Solvay) by Dr. Wenrui Zhang.[8] Poly(*para*-phenylene oxide) (1.6k) was synthesized from 2,6-dimethylphenol also by Dr. Wenrui Zhang.[8]

6.3.2 Fabrication of pegylated silver nanoparticles

Polyethylene oxide (PEO, 4 g, Mn of 2k g mol^{-1}) was dried at 50 °C under vacuum overnight. The PEO was melted at 80 °C, and $AgNO_3$ (100 mg) was charged and the mixture was purged with nitrogen for 5 min. The mixture was stirred at 80 °C for 1 h. The hot solution was precipitated in cold ethanol (~40 mL) and the supernatant was decanted. The particles were washed with ethanol (40 mL each) twice and decanted. The remaining mixture was centrifuged at 8k rpm for 30 min. The supernatant was decanted again, and the remaining solid was subsequently purged with nitrogen for 1 h, and then dried under vacuum at room temperature overnight.

6.3.3 Fabrication of silver nanoparticle-containing polymer membranes by solution casting

To solution cast the silver nanoparticle-containing polymer membranes, chloroform was used as the solvent. Pegylated silver nanoparticles (150 mg) were dispersed in chloroform (2 mL) in a scintillation vial and stirred to mix well. Poly(*para*-phenylene oxide) (200 mg) and the bisphenol A based poly(arylene ether ketone) (400 mg) were also dissolved in a separate vial and mixed thoroughly. The polymer solutions were filtered through a 0.45 μm PTFE syringe filter and mixed well with the silver nanoparticle dispersion by stirring for 10 min. The mixed solution was then cast on a glass plate (6 in" by 6 in"). A controlled nitrogen stream (2 standard cubic feet per hour, scfh) was purged over the surface of the glass plate for 30 min. The glass plate was then placed in a vacuum oven and dried at 55 °C without vacuum for 30 min, followed by drying under vacuum at 55 °C for 2 d. A silver

nanoparticle-containing polymer membrane was obtained and peeled off from the glass plate with a blade, without soaking in water.

6.4 Preparation of phosphonate-bearing ionic graft copolymer – manganese (II) complexes for dual drug delivery and imaging

6.4.1 Materials

Dimethyl sulfoxide (HPLC grade) was purchased from Fisher Scientific and used as received. cis-diamineplatinum(II) dichloride (cisplatin, 99%), carboplatin, manganese (II) chloride tetrahydrate, sodium hydroxide solution (NaOH, 1.0 N), and hydrochloric acid (HCl, 1.0 N) were purchased from Sigma-Aldrich. Poly(ethylene oxide)-*g*-poly(acrylic acid) (PEO-*g*-PAA), poly(ammonium bisphosphonate methacrylate)-*g*-poly(ethylene oxide) (PABP-*g*-PEO) polymers with three and six carbon spacers, and a poly(acrylamide phosphonate)-*g*-PEO was previously reported and used.[9-10] Slide-A-Lyser dialysis cassettes (MWCO 3,500) were obtained from Thermo scientific. Centrifugal filter units (MWCO 10,000) were obtained from EMD Millipore. Manganese dipyroxyl diphosphate (Mn-DPDP, Teslascan®) was obtained from GE Healthcare. Deionized water was obtained through a MilliQ A10 synthesis water purification system (EMD Millipore, MA).

6.4.2 Synthesis of manganese (II) - graft ionic copolymer complexes (*MaGICs*)

To fabricate *MaGICs*, graft copolymers (100 mg) were dissolved in de-ionized water (10 mL) and filtered through a 1.0-μm syringe-driven filter unit (PTFE, Millipore) and subsequently added to a 20-mL vial equipped with magnetic stir bar. The graft copolymer solution was adjusted to pH 7.4 with 1.0 N NaOH. Manganese (II) chloride tetrahydrate solution (20.0 mg mL^{-1} in DI water) was added slowly into the polymer solution under stirring. The initial molar ratio of manganese to phosphorus (Mn:P) was kept at 1:2 which formed a clear solution. The mixture was stirred at room

temperature for 5 h and then transferred into a dialysis cassette (MWCO = 3,500 g mol^{-1}) and dialyzed against 2 L of DI water for 2 d, with two changes of water daily. The final complexes were recovered by freeze-drying for 2 d.

6.4.3 Cisplatin loading into the *MaGICs*

The *MaGICs* for drug loading utilized the poly(hexyl ammonium bisphosphonate methacrylate)-*g*-poly(ethylene oxide)-Mn complex. Cisplatin loading was performed at different feed weight ratios of platinum to *MaGICs* of 5, 10 and 20 wt %. For a targeted 20 wt % platinum, cisplatin (38.50 mg) was dispersed in DMSO (0.5 mL) and added dropwise to the *MaGICs* solution (100 mg in 4.5 mL phosphate buffer) with stirring. The solution was sonicated for 5 min followed by stirring at room temperature for 12 h. Unincorporated drugs and DMSO were removed by dialysis against DI water (4 L, 24 h). The external medium was renewed one time in the course of dialysis. Then the solution was freeze-dried to obtain cisplatin-loaded *MaGICs*. The percent of loaded cisplatin in the *MaGICs* was quantified by ICP-AES.

6.4.4 Carboplatin loading into the *MaGICs*

The *MaGICs* for drug loading utilized the poly(hexyl ammonium bisphosphonate methacrylate)-*g*-poly(ethylene oxide)-Mn complex. Carboplatin-loaded *MaGICs* were prepared with platinum contents at 5, 10, and 20 wt % relative to *MaGICs*. To prepare complexes with a targeted content of 20 wt %, carboplatin (24 mg) was dispersed in phosphate buffer (3 mL, pH 7.4) and added dropwise to the *MaGICs* solution (50 mg in 5 mL phosphate buffer, pH 7.4). The mixture was sonicated for 5 min followed by stirring at room temperature for 24 h. The complex solution was transferred to a centrifugal filter unit equipped with a cellulose acetate membrane (MWCO of 10,000 g mol^{-1}). Free drugs and salts were removed by centrifuging the dispersion at 4000 rpm for 1 h. This allowed the

liquid to pass through the membrane into the bottom of the centrifugation unit, and the particles were collected on the membrane. They were removed from the membrane by re-dispersing them in DI water (5 mL), and then the dispersion was freeze-dried to obtain carboplatin loaded *MaGICs*. The amount of loaded platinum was measured by ICP-AES.

6.5 Results and Discussion

6.5.1 Synthesis of poly(lactide) homopolymers and copolymers

Poly(lactide)-based polymers are an important class of biocompatible and biodegradable polymers and are widely used in biomedical applications.[11-12] Poly(lactide) can be synthesized by living ring opening polymerization to afford the polymers with target molecular weights and narrow molecular weight distributions.[13] Poly(lactide) is relatively hydrophobic, and it can be easily functionalized to form copolymers with tailored hydrophobicity/hydrophilicity. In this study, we synthesized several poly(lactide) homopolymers and copolymers to build drug delivery systems (DDS) with imaging capability by loading a fluorescent probe, TIPS pentacene, into the core of the systems. The structures of the poly(lactide) polymers and TIPS pentacene are shown in Figure 6.1. Specifically, a PEO-*b*-PDLLA amphiphilic block copolymer was used as the primary structure for the DDS, and the micellar DDS was fabricated using flash nanoprecipitation.[14-15] In order to study the relationship between the micellar core sizes of the DDS and the capabilities of probe loading, a PLLA homopolymer was used as a filler to increase the core sizes without interrupting the surface functionalities, up to 40 wt% of the overall complexes. PAA-*b*-PDLLA was also used as a filler in order to introduce anions onto the surface of the nanocomplexes, so that it could be used for targeted delivery. In this study, carboxylate anions on the PAA block were used to bind a protein, streptavidin, by using carbodiimide crosslinking chemistry (EDC/NHS) which has been widely used in such

applications.[16-17] The carboxylate anions on the surface of the nanocomplexes were coupled to the amine groups from streptavidin with the aid of 1-ethyl-3-(3-dimethylaminopropyl)carbodiimide as a crosslinking reagent. The streptavidin was bound to biotin enable further functionalization, such as conjugation with bacteria. The highest fluorescence occurred when 0.5 wt% of the TIPS pentacene relative to the poly(lactide) core was loaded, as measured by UV-Vis and fluorescence spectroscopy. Such systems may have potential for dual drug delivery and fluorescent imaging, with the capability for fine-tuning the loading capacity and surface functionality.

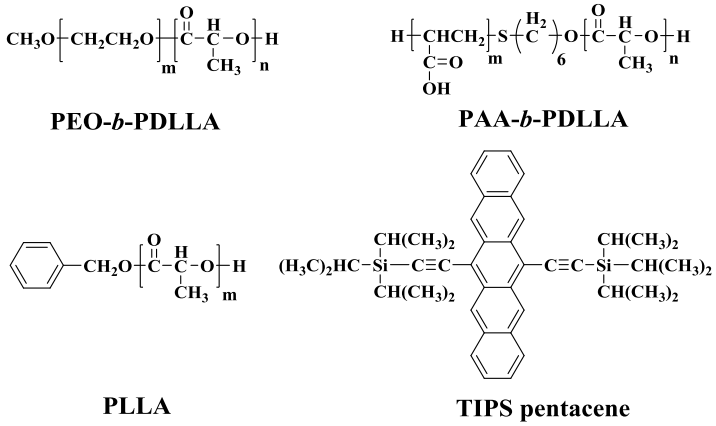

Figure 6.1 The structures of the poly(lactide) polymers and TIPS pentacene.

6.5.2 Fabrication of poly(dimethylsiloxane)-magnetite magnetic fluids

Magnetite nanoparticles have garnered tremendous research interest and have been used in a multitude of applications, such as hyperthermia, drug delivery, and magnetic resonance imaging.[7, 18-20] Magnetite-bearing concrete has been widely used for radiation shielding in nuclear plants.[21] Magnetite nanoparticles containing poly(vinyl alcohol) films were recently prepared by co-precipitation for use in gamma ray shielding and protection.[22] In this project, the aim was to develop a magnetite-bearing polymeric fluid which could be used for gamma ray shielding. We decided to fabricate a poly(dimethylsiloxane) (PDMS)-magnetite magnetic fluid for the proposed applications.

PDMS is a well-known, biocompatible polymer which can be synthesized by living ring opening polymerization, so that the polymers have targeted molecular weights and narrow molecular distributions. It has been widely used in biomedical applications.[11-12] In addition, it is easy to functionalize the PDMS to enable coupling to magnetite nanoparticles. More importantly, low molecular weight PDMS is a liquid polymer, which meets our requirement excellently. Therefore, we utilized n-butyl lithium as the initiator, hexamethylcyclotrisiloxane (D_3) as the monomer, cyclohexane as the solvent, and THF as the promoter to perform the living anionic ring opening polymerization, to obtain the PDMS. After the reaction, trivinylchlorosilane was charged to the reaction mixture, so that trivinyl-functional PDMS was obtained. In the next step, a thiol-ene reaction was performed by reacting the trivinyl-functional PDMS with mercaptoacetic acid, using AIBN to form the free radicals. This afforded the tricarboxylic acid-functional PDMS, which was a transparent liquid polymer. The synthesis of the tricarboxylic acid-functional PDMS is shown in Figure 6.2. Magnetite was synthesized by either a co-precipitation method or a thermo-decomposition method. The polysiloxane-based magnetic fluid was then fabricated, and the process is shown in Figure 6.3. The ^{1}H NMR (Figure 6.4) confirmed the structure of our trivinyl-functional PDMS and allowed for calculating the molecular weight of the polymer. The carboxylic acid groups on the PDMS could bind to the surface of the magnetite, forming a stable fluid-like material with magnetic properties. The polymer compositions were characterized by ^{1}H NMR, while the magnetic fluid was evaluated by TEM and ICP-AES (after digesting the magnetite with nitric acid). The ICP-AES results indicated that the wt% of Fe_3O_4 in the complex was 27.7% with the charged ratio having been 29.7%. The results indicated that most magnetite nanoparticles were bound to the PDMS. Our preliminary data indicated that the magnetic fluid was able to shield gamma rays, and further work is underway.

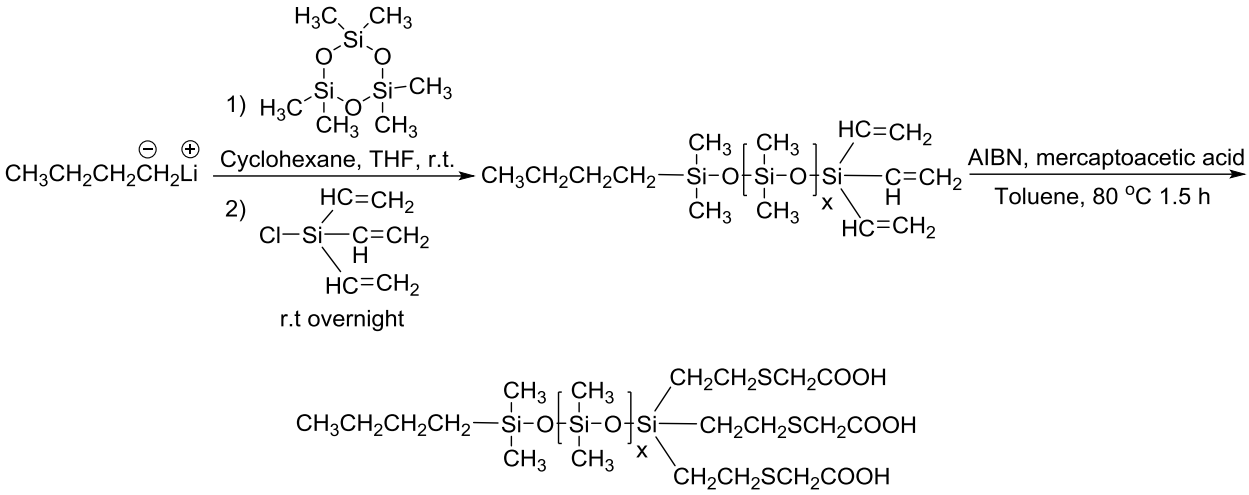

Figure 6.2 The synthesis of the tricarboxylic acid-functional PDMS.

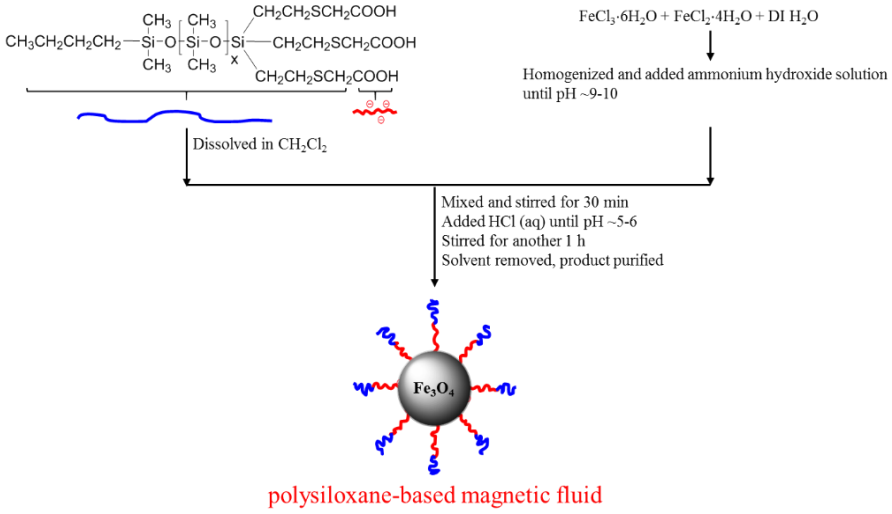

Figure 6.3 The fabrication of polysiloxane-based magnetic fluid.

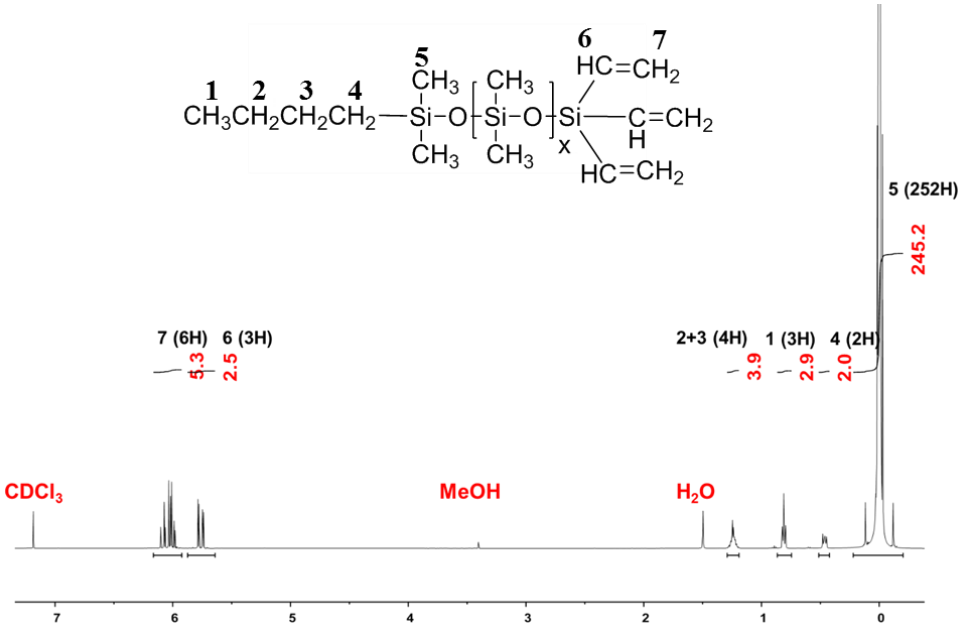

Figure 6.4 ^{1}H NMR spectrum of the synthesized trivinyl-functional PDMS.

6.5.3 Preparation of silver nanoparticle-embedded polymer membranes by solvent casting

Silver nanoparticles have received a lot of research interest in many different fields.[23-27] More recently, silver nanoparticles embedded in polymer membranes were fabricated and evaluated for potential gas separations.[23, 28] It has been reported that silver nanoparticle or silver salt doped polymeric membranes may enable gas separations of olefin/paraffin mixtures due to a mechanism known as facilitated olefin transport.[29-30]

In this study, to fabricate silver nanoparticles, we used silver nitrate as the starting material, and PEO as the solvent, reducing agent and capping agent. The use of PEO has been reported in fabrications of silver nanoparticles as it has several advantages.[31] It is commercial and safe to use. PEO is a well-known host for polymer electrolytes and can coat silver *in situ*.[31] Excess PEO can be removed from the nanoparticles easily. The reaction was performed at 80 °C so that the PEO was in the liquid state. After formation of the silver nanoparticles, precipitation was accomplished in ethanol,

and pegylated silver nanoparticles were obtained by centrifugation. ICP-AES was used to measure the wt% of silver in the complex, and it was found that the complexes contained 0.35 wt% of silver. Since the charged wt% of silver was 1.55%, it seemed that the precipitation and centrifugation steps need to be optimized in order to reduce the loss of silver nanoparticles. Dynamic light scattering was used to measure the sizes and size distributions of the silver nanoparticles. It was found that the particles had an intensity average diameter of 84.5 nm, with a PDI of 0.2. Such results indicated that the fabricated silver nanoparticles had relatively uniform sizes and good size distributions.

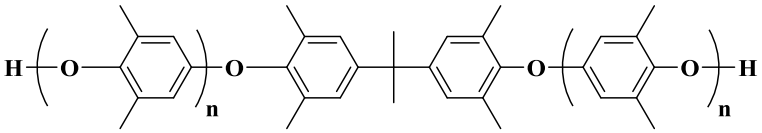

1.6k Poly(*p*-phenylene oxide) PPO

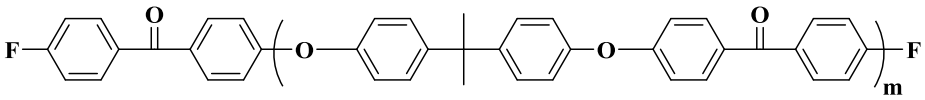

28k Bisphenol A Based Poly(arylene ether ketone) BPA-based PAEK

Figure 6.5 The structures of the PPO and BPA-based PAEK used in this study.

After successfully obtaining the pegylated silver nanoparticles, polymer blend membranes were cast. A poly(phenylene oxide) (PPO) polymer (1.6k) and a bisphenol A-based poly(arylene ether ketone) (28k) were synthesized and used, together with the pegylated silver nanoparticles.[32] The polymer structures are shown in Figure 6.5. The target was to prepare 2 wt% of the polymers in chloroform, with the PPO composition of 33 wt% in the polymer blends. The blended polymer solution was filtered to remove dust before mixing well with the silver nanoparticle dispersion. After mixing, a clear solution was obtained that was poured onto the glass plate meticulously. A nitrogen stream was applied to avoid potential oxidation of the silver nanoparticles. The drying temperature and time were designed so that the solvent could be removed completely at a moderate speed. Finally,

the membrane was obtained, as is shown in Figure 6.6. However, the membrane was not transparent. It was established that such polymer blends were miscible as measured by DSC. Because the membrane contained silver nanoparticles, TGA and DSC were not performed due to the concern that it may damage the equipment. ^{1}H NMR was performed by taking samples from either the center or the side of the membrane. From the NMR results, it seemed that the membrane compositions were identical from different parts. Miscibility tests were performed to identify the cause of the opaqueness. It has been reported by our group that the PPO and BPA-based PAEK polymers used in this study can form transparent membranes. Thus, mixing PEO with the other two polymers with different ratios were tested. It was found that PEO and PPO are miscible, at 33 wt% of PEO. The problem came from the immiscibility between PEO and the PAEK. Therefore, additional research is needed to address this issue. Utilization of another miscible polymer may be needed to make the proposed silver-containing, clear polymer membranes. Another potential issue is the wt% of the silver in the final membrane. It is unclear how much silver particles would be needed, and their locations in the prepared membranes (i.e., at the membrane surface *vs* uniformed dispersed in the whole membranes) could be very important in enabling the "carrier facilitated olefin transport."

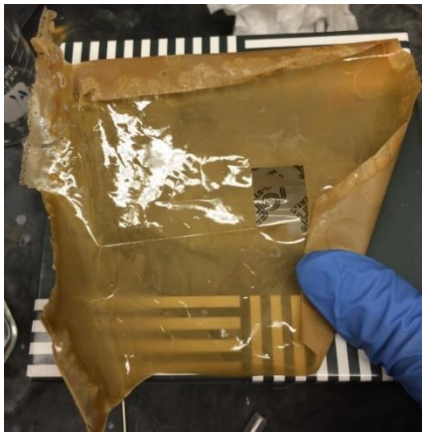

Figure 6.6 The as-prepared silver particle-embedded polymer membrane.

6.5.4 Preparation of phosphonate-bearing ionic graft copolymer – manganese (II) complexes for dual drug delivery and imaging

In our group, we are interested in making biocompatible polymeric nanocomplexes for biomedical applications, with the focus on drug delivery and imaging. In this project, we synthesized various ionic graft copolymers with different acid anchoring groups, all with biocompatible, water-soluble PEO segments. Copolymers with an anionic polyelectrolyte block and a nonionic water-soluble PEO block were known to bind electrostatically with cation-bearing species such as calcium to form block ionomer complexes via self-assembly in aqueous media.[33-42] In this study, we investigated self-assembly between Mn^{2+} ions and various graft copolymers and made a comparison regarding their sizes, size distributions, colloidal stabilities, etc. The polymers used to fabricate *MaGICs* is shown in Figure 6.7. Fabrication of *MaGICs* was performed by simply mixing Mn^{2+} salts with various graft copolymer solutions. Ionic complexes formed spontaneously through electrostatic interactions and possibly also chelation between Mn^{2+} cations and the polymers. ICP-AES revealed that the amount of manganese in these complexes and the molar ratios of phosphorus or carbon to Mn in the final complexes were calculated to be ~3 (Table 6.1). The physicochemical properties are also listed in Table 6.1. The colloidal stabilities of the *MaGICs* under simulated physiological conditions were measured. Their hydrodynamic sizes in PBS containing 0.14 M NaCl were recorded as a function of time over 24 hours. It was found that all phosphonate-containing *MaGICs* had stable sizes under such conditions, while the sizes of the carboxylate-bearing *MaGICs* increased with time, signaling its instability. Therefore, the carboxylate graft ionomer-manganese complexes may not be used for drug delivery applications. Release profiles of Mn^{2+} from *MaGICs* were also explored at pH 7.4 in PBS at 37 °C. The carboxyl *MGICs* released almost half of the bound Mn^{2+}, while the propyl and hexyl bisphosphonate analog released 7% and 0%, respectively. The phosphonate amide *MaGICs*

also displayed minimal amount (0.5-0.7%) of Mn^{2+} release. Therefore, the hexyl bisphosphonate and phosphonate amide polymer-based *MaGICs* may be good candidates for drug delivery due to their excellent stability. To determine the feasibility of the *MaGICs* to be potent positive MRI contrast agents, the proton longitudinal relaxivities (r_1's) and transverse relaxivities (r_2's) were measured in water at the clinically-relevant field strength of 1.4 T and physiological temperature (37 °C). Table 6.2 shows relaxivities of *MaGICs* compared to $MnCl_2$ and a commercial positive contrast agent, Mn-DPDP. Although carboxyl *MaGICs* displayed a longitudinal relaxivity which was 20-fold higher than commercial positive contrast agent Mn-DPDP, its terrible colloidal stability rendered it inappropriate for these biomedical applications. The propyl and hexyl bisphosphonate counterparts were colloidally stable, and their longitudinal relaxivities were 12 and 8 fold excess compared to the commercial agent, thus bearing the potentially for use as dual drug delivery carriers and positive contrast agents. The phosphonate amide *MaGICs* displayed excellent stability while possessing a longitudinal relaxivity which is almost 20 fold excess and could be an excellent contrast agent and drug delivery vehicle.

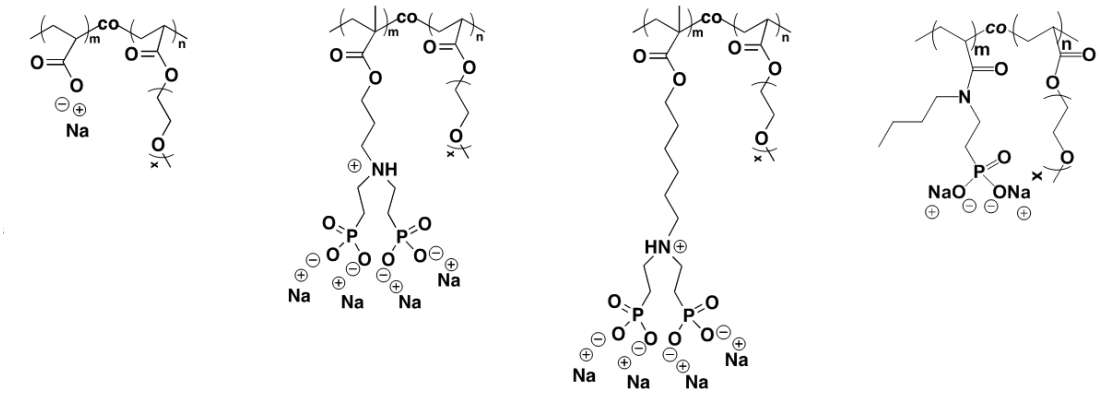

Figure 6.7 The polymers used to fabricate the *MaGICs.*

Table 6.1 Compositions and Physicochemical properties of the *MaGICs.*

Sample	Mn (wt%)	Mole of P(C) to Mn	Intensity average diameter (nm)	PDI	Zeta Potential (mV)
Carboxyl *MaGICs*	7.5	3.3	114	0.23	-36
Propyl *MaGICs*	4.7	3.3	64	0.20	-38
Hexyl *MaGICs*	3.7	3.3	56	0.20	-37
Amide *MaGICs*	2.8	3.0	65	0.20	-

Table 6.2 Relaxivity studies of the *MaGICs.*

Sample	Longitudinal relaxivity (r_1)	r_2/r_1
$MnCl_2$	5.6	11.9
Mn-DPDP	2.3	1.7
Carboxyl *MaGICs*	40.9	1.6
Propyl *MaGICs*	25.7	1.6
Hexyl *MaGICs*	16.9	1.7
Amide *MaGICs*	42.4	2.0

Table 6.3 Charged and achieved Pt wt% in the *hexyl bisphosphonate MaGICs.*

Sample	Charged Pt wt%	Achieved Pt wt%
MaGICs-cisplatin-5.0	5.0	5.0
MaGICs-cisplatin-9.7	10.0	9.7
MaGICs-cisplatin-16.0	20.0	16.0
MaGICs-carboplatin-4.7	5.0	4.7
MaGICs-carboplatin-7.7	10.0	7.7
MaGICs- carboplatin-13.0	20.0	13.0

To further evaluate the potential of the poly(hexyl ammonium bisphosphonate methacrylate)-g-poly(ethylene oxide)-based *MaGICs* for drug delivery, anti-tumor platinum drugs, cisplatin and carboplatin, were loaded into the complexes, with the charged wt% of platinum being 5, 10, and 20%. The obtained wt% of platinum was measured by ICP-AES and listed in Table 6.3. Drug release experiments similar to the ones described in Chapter 5 were performed under simulated endosomal (pH 4.5) and physiological (pH 7.4) conditions at 37 °C. Free drugs, or drug-loaded hexyl *MaGICs*

were used. Accumulated drug release was measured and calculated, as is shown in Figure 6.8 for cisplatin and Figure 6.9 for carboplatin. In all cases, free drugs were released very quickly, while the drugs loaded into the *MaGICs* released much slower. For cisplatin, the drug release rate in either pH 4.5 or pH 7.4 was similar. Less than 20% of the cisplatin was released after 24 hours for the *MaGICs* with the highest platinum load. The less platinum loaded *MaGICs* released cisplatin even less or not at all. The trend is similar for carboplatin, but much more carboplatin was released in all cases. It is estimated that the binding strength between cisplatin and *MaGICs* were stronger compared to carboplatin-*MaGICs* counterparts. The leaving groups on cisplatin are chlorine and may be easily replaced by the remaining anions on the *MaGICs*. On the other hand, the ligand on carboplatin may not be easily substituted, therefore the binding strength may be lower. Overall, sustained release of platinum anti-cancer drugs was achieved, further demonstrating the potential of such phosphonate-bearing ionic graft copolymer-manganese (II) complexes in dual drug delivery and magnetic resonance imaging applications.

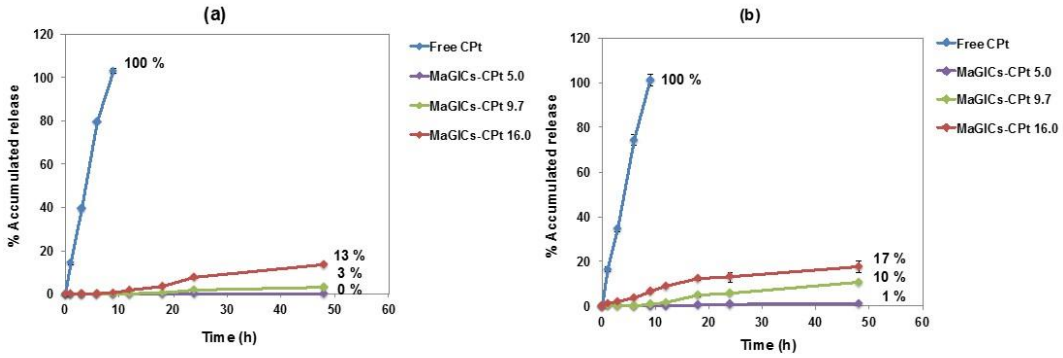

Figure 6.8 Drug release profiles of free cisplatin and cisplatin-loaded *MaGICs* from a) pH 4.5; b) pH 7.4.

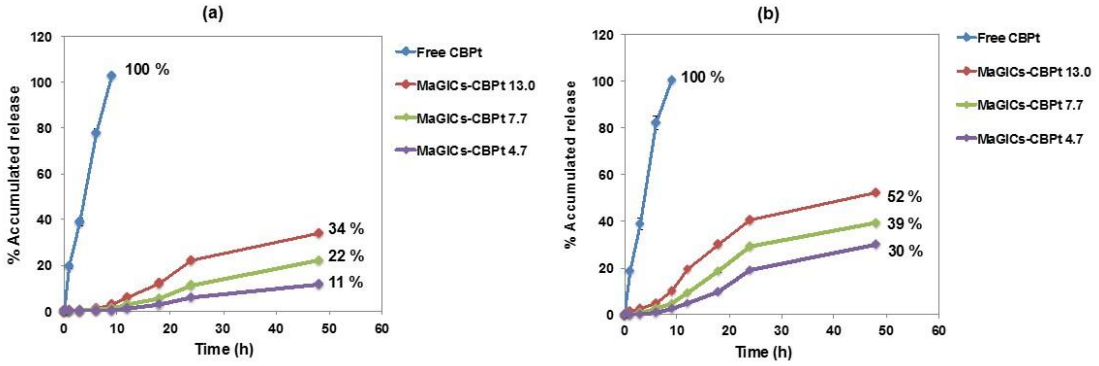

Figure 6.9 Drug release profiles of free carboplatin and carboplatin-loaded *MaGICs* from a) pH 4.5; b) pH 7.4.

6.6 References

1. Balasubramaniam, S.; Kayandan, S.; Lin, Y.-N.; Kelly, D. F.; House, M. J.; Woodward, R. C.; St. Pierre, T. G.; Riffle, J. S.; Davis, R. M., Toward Design of Magnetic Nanoparticle Clusters Stabilized by Biocompatible Diblock Copolymers for T2-Weighted MRI Contrast. *Langmuir* **2014,** *30* (6), 1580-1587.
2. Xue, Y.-N.; Huang, Z.-Z.; Zhang, J.-T.; Liu, M.; Zhang, M.; Huang, S.-W.; Zhuo, R.-X., Synthesis and self-assembly of amphiphilic poly(acrylic acid-b-dl-lactide) to form micelles for pH-responsive drug delivery. *Polymer* **2009,** *50* (15), 3706-3713.
3. Kayandan, S. Synthesis and Characterization of Poly (lactide) Functional Oligomers and Block Copolymers. Virginia Tech, 2013.
4. Mefford, O. T.; Carroll, M. R. J.; Vadala, M. L.; Goff, J. D.; Mejia-Ariza, R.; Saunders, M.; Woodward, R. C.; St. Pierre, T. G.; Davis, R. M.; Riffle, J. S., Size Analysis of PDMS−Magnetite Nanoparticle Complexes: Experiment and Theory. *Chemistry of Materials* **2008,** *20* (6), 2184-2191.
5. Mefford, O. T.; Vadala, M. L.; Goff, J. D.; Carroll, M. R. J.; Mejia-Ariza, R.; Caba, B. L.; St. Pierre, T. G.; Woodward, R. C.; Davis, R. M.; Riffle, J. S., Stability of Polydimethylsiloxane-Magnetite Nanoparticle Dispersions Against Flocculation: Interparticle Interactions of Polydisperse Materials. *Langmuir* **2008,** *24* (9), 5060-5069.
6. Wilson, K.; Goff, J.; Riffle, J.; Harris, L.; St Pierre, T., Polydimethylsiloxane‐magnetite nanoparticle complexes and dispersions in polysiloxane carrier fluids. *Polymers for advanced technologies* **2005,** *16* (2‐3), 200-211.
7. Pothayee, N.; Pothayee, N.; Jain, N.; Hu, N.; Balasubramaniam, S.; Johnson, L. M.; Davis, R. M.; Sriranganathan, N.; Riffle, J. S., Magnetic Block Ionomer Complexes for Potential Dual Imaging and Therapeutic Agents. *Chemistry of Materials* **2012,** *24* (11), 2056-2063.
8. Shaver, A.; Moon, J. D.; Savacool, D.; Zhang, W.; Narang, G.; Miller, G.; Vondrasek, B.; Lesko, J. J.; Freeman, B. D.; Riffle, J. S.; McGrath, J. E., Poly(2,6-dimethyl-1,4-phenylene oxide) blends with a poly(arylene ether ketone) for gas separation membranes. *Polymer* **2017,** *114*, 135-143.
9. Pothayee, N.; Pothayee, N.; Hu, N.; Zhang, R.; Kelly, D. F.; Koretsky, A. P.; Riffle, J. S., Manganese graft ionomer complexes (MaGICs) for dual imaging and chemotherapy. *Journal of Materials Chemistry B* **2014,** *2* (8), 1087-1099.

10. Hu, N.; Peralta, A.; Roy Choudhury, S.; Zhang, R.; Davis, R. M.; Riffle, J. S., Acrylamide monomers and polymers that contain phosphonate ions. *Polymer* **2015,** *65*, 124-133.
11. Oh, J. K., Polylactide (PLA)-based amphiphilic block copolymers: synthesis, self-assembly, and biomedical applications. *Soft Matter* **2011,** *7* (11), 5096-5108.
12. Albertsson, A.-C.; Varma, I. K., Recent Developments in Ring Opening Polymerization of Lactones for Biomedical Applications. *Biomacromolecules* **2003,** *4* (6), 1466-1486.
13. Penczek, S.; Cypryk, M.; Duda, A.; Kubisa, P.; Słomkowski, S., Living ring-opening polymerizations of heterocyclic monomers. *Progress in Polymer Science* **2007,** *32* (2), 247-282.
14. McDaniel, D. K.; Jo, A.; Ringel-Scaia, V. M.; Coutermarsh-Ott, S.; Rothschild, D. E.; Powell, M. D.; Zhang, R.; Long, T. E.; Oestreich, K. J.; Riffle, J. S.; Davis, R. M.; Allen, I. C., TIPS pentacene loaded PEO-PDLLA core-shell nanoparticles have similar cellular uptake dynamics in M1 and M2 macrophages and in corresponding in vivo microenvironments. *Nanomedicine : nanotechnology, biology, and medicine* **2017,** *13* (3), 1255-1266.
15. Liu, Y.; Cheng, C.; Prud'homme, R. K.; Fox, R. O., Mixing in a multi-inlet vortex mixer (MIVM) for flash nano-precipitation. *Chemical Engineering Science* **2008,** *63* (11), 2829-2842.
16. Liu, E. Y.; Jung, S.; Yi, H., Improved Protein Conjugation with Uniform, Macroporous Poly(acrylamide-co-acrylic acid) Hydrogel Microspheres via EDC/NHS Chemistry. *Langmuir* **2016,** *32* (42), 11043-11054.
17. Anselmo, A. C.; Modery-Pawlowski, C. L.; Menegatti, S.; Kumar, S.; Vogus, D. R.; Tian, L. L.; Chen, M.; Squires, T. M.; Gupta, A. S.; Mitragotri, S., Platelet-like Nanoparticles (PLNs): Engineering Shape, Flexibility and Surface Chemistry of Nanocarriers to Target Vascular Injuries. *ACS Nano* **2014,** *8*, 11243-11253.
18. Guo, S.; Li, D.; Zhang, L.; Li, J.; Wang, E., Monodisperse mesoporous superparamagnetic single-crystal magnetite nanoparticles for drug delivery. *Biomaterials* **2009,** *30* (10), 1881-1889.
19. Kim, J.; Kim, H. S.; Lee, N.; Kim, T.; Kim, H.; Yu, T.; Song, I. C.; Moon, W. K.; Hyeon, T., Multifunctional uniform nanoparticles composed of a magnetite nanocrystal core and a mesoporous silica shell for magnetic resonance and fluorescence imaging and for drug delivery. *Angewandte Chemie International Edition* **2008,** *47* (44), 8438-8441.
20. Ito, A.; Tanaka, K.; Honda, H.; Abe, S.; Yamaguchi, H.; Kobayashi, T., Complete regression of mouse mammary carcinoma with a size greater than 15 mm by frequent repeated hyperthermia using magnetite nanoparticles. *Journal of Bioscience and Bioengineering* **2003,** *96* (4), 364-369.
21. Maslehuddin, M.; Naqvi, A. A.; Ibrahim, M.; Kalakada, Z., Radiation shielding properties of concrete with electric arc furnace slag aggregates and steel shots. *Annals of Nuclear Energy* **2013,** *53*, 192-196.
22. Badawy, S. M.; El‐Latif, A. A. A., Synthesis and characterizations of magnetite nanocomposite films for radiation shielding. *Polymer composites* **2017,** *38* (5), 974-980.
23. Kang, Y. S.; Kang, S. W.; Kim, H.; Kim, J. H.; Won, J.; Kim, C. K.; Char, K., Interaction with Olefins of the Partially Polarized Surface of Silver Nanoparticles Activated by p‐Benzoquinone and Its Implications for Facilitated Olefin Transport. *Advanced Materials* **2007,** *19* (3), 475-479.
24. Ahmed, S.; Ahmad, M.; Swami, B. L.; Ikram, S., A review on plants extract mediated synthesis of silver nanoparticles for antimicrobial applications: a green expertise. *Journal of advanced research* **2016,** *7* (1), 17-28.
25. Aslan, K.; Zhang, J.; Lakowicz, J. R.; Geddes, C. D., Saccharide sensing using gold and silver nanoparticles-A review. *Journal of Fluorescence* **2004,** *14* (4), 391-400.
26. Rai, M.; Yadav, A.; Gade, A., Silver nanoparticles as a new generation of antimicrobials. *Biotechnology advances* **2009,** *27* (1), 76-83.

27. Austin, L. A.; Mackey, M. A.; Dreaden, E. C.; El-Sayed, M. A., The optical, photothermal, and facile surface chemical properties of gold and silver nanoparticles in biodiagnostics, therapy, and drug delivery. *Archives of toxicology* **2014,** *88* (7), 1391-1417.
28. Chae, I. S.; Kang, S. W.; Park, J. Y.; Lee, Y. G.; Lee, J. H.; Won, J.; Kang, Y. S., Surface Energy‐Level Tuning of Silver Nanoparticles for Facilitated Olefin Transport. *Angewandte Chemie International Edition* **2011,** *50* (13), 2982-2985.
29. Hong, S.; Jin, J. H.; Won, J.; Kang, Y., Polymer–salt complexes containing silver ions and their application to facilitated olefin transport membranes. *Advanced Materials* **2000,** *12* (13), 968-971.
30. Kang, S. W.; Char, K.; Kang, Y. S., Novel application of partially positively charged silver nanoparticles for facilitated transport in olefin/paraffin separation membranes. *Chemistry of Materials* **2008,** *20* (4), 1308-1311.
31. Luo, C.; Zhang, Y.; Zeng, X.; Zeng, Y.; Wang, Y., The role of poly (ethylene glycol) in the formation of silver nanoparticles. *Journal of Colloid and Interface Science* **2005,** *288* (2), 444-448.
32. Shaver, A. T. Advanced Polymeric Membranes and Multi-Layered Films for Gas Separation and Capacitors. Virginia Tech, 2016.
33. Kabanov, A. V.; Bronich, T. K.; Kabanov, V. A.; Yu, K.; Eisenberg, A., Soluble Stoichiometric Complexes from Poly(N-ethyl-4-vinylpyridinium) Cations and Poly(ethylene oxide)-block-polymethacrylate Anions. *Macromolecules* **1996,** *29* (21), 6797-6802.
34. Bronich, T. K.; Popov, A. M.; Eisenberg, A.; Kabanov, V. A.; Kabanov, A. V., Effects of Block Length and Structure of Surfactant on Self-Assembly and Solution Behavior of Block Ionomer Complexes. *Langmuir* **1999,** *16* (2), 481-489.
35. Bronich, T. K.; Nehls, A.; Eisenberg, A.; Kabanov, V. A.; Kabanov, A. V., Novel drug delivery systems based on the complexes of block ionomers and surfactants of opposite charge. *Colloids and Surfaces B: Biointerfaces* **1999,** *16* (1–4), 243-251.
36. Bronich, T. K.; Kabanov, A. V.; Kabanov, V. A.; Yu, K.; Eisenberg, A., Soluble Complexes from Poly(ethylene oxide)-block-polymethacrylate Anions and N-Alkylpyridinium Cations. *Macromolecules* **1997,** *30* (12), 3519-3525.
37. Kataoka, K.; Harada, A.; Yasugi, K.; Matsumoto, T.; Katayose, S., Spontaneous formation of polyion complex micelles with narrow distribution from antisense oligonucleotide and cationic copolymer in physiological saline. *Macromolecules* **1996,** *29*, 8556-8557.
38. Harada, A.; Kataoka, K., Formation of Polyion Complex Micelles in an Aqueous Milieu from a Pair of Oppositely-Charged Block Copolymers with Poly(Ethylene Glycol) Segments. *Macromolecules* **1995,** *28*, 5294-5299.
39. Voets, I. K.; de Keizer, A.; Cohen Stuart, M. A., Complex coacervate core micelles. *Advances in Colloid and Interface Science* **2009,** *147,Äì148* (0), 300-318.
40. Oh, K. T.; Bronich, T. K.; Bromberg, L.; Hatton, T. A.; Kabanov, A. V., Block ionomer complexes as prospective nanocontainers for drug delivery. *Journal of Controlled Release* **2006,** *115* (1), 9-17.
41. Bromberg, L.; Temchenko, M.; Hatton, T. A., Dually Responsive Microgels from Polyether-Modified Poly(acrylic acid):‚Äâ Swelling and Drug Loading. *Langmuir* **2002,** *18* (12), 4944-4952.
42. Bromberg, L., Polymeric micelles in oral chemotherapy. *Journal of Controlled Release* **2008,** *128*, 99-112.

Chapter 7: Recommended future work

7.1 Preparation of functional silane-treated carbon fibers for enhanced adhesion to particle matrices

The azasilane coupling agent treatment with carbon fibers seems to have significantly increased the adhesion between carbon fibers and PEI particles. But there were a few drawbacks. First, the azasilane did not enable crosslinking between individual linkers, so the adhesion may not have been sufficiently strong, particularly when the fibers and particles were exposed under shear to aqueous dispersions. Second, the interaction between the functional carbon fibers and the poly(amic acid) salt-coated PEI particles was primarily electrostatic. That also may not be strong enough. Third, the azasilane coupling agent is relatively expensive, and large-scale applications would significantly increase the overall cost. Therefore, using alternative coupling agents which also have more potential binding sites is desirable. For example, 3-aminopropyltrimethoxysilane can be used to couple with hydroxyfunctional carbon fibers, and it provides the same surface functional groups while having 3 leaving groups, leading to potential crosslinking and increased binding strength. Other silane coupling agents, such as (3-glycidoxypropyl)trimethoxysilane and *O*-(propargyl)-*N*-(triethoxysilylpropyl) carbamate could also be introduced with the advantage of enabling further functionalization due to the presence of terminal alkyne or glycidyl groups. Amine or azide groups could be introduced onto the PEI particles, so that the particles and fibers could be covalently bonded, and it is expected that this may lead to increased stability of the polymer-carbon fiber composites. Similar solvents and reaction conditions could be used. For example, dichloromethane and toluene may be used as solvents for the coupling reactions. Alternatively, acid or base-catalyzed hydrolysis of the silane coupling agents could be employed. Acetic acid or sodium hydroxide could be used together with a water-

soluble organic solvent such as ethanol and deionized water. XPS and SEM could be used to characterize the surface compositions of the functionalized carbon fibers as well as the fiber-polymer composites.

7.2 Design and synthesis of Pluronic P85 analog copolymers for potential drug delivery

P85-based nanocarriers are promising as they have achieved success both *in vitro* and *in vivo* and they are undoubtedly excellent candidates for potential drug delivery. However, the drawback of P85 is that it is non-biodegradable. It would be ideal to have a biodegradable block copolymer with similar or even superior properties in terms of biological activities compared to P85. In order to mimic the properties such as hydrophobicity, a carefully designed and bio-degradable block copolymer of PEO-*b*-poly(δ-hexalactone), is proposed. The design was inspired by the structure of P85. Similar to caprolactone, δ-hexalactone (6-methyltetrahydro-2H-pyran-2-one or 6-methyloxan-2-one) can be polymerized via ROP and is biodegradable. The hydrophobic propylene oxide unit in P85 has an atomic composition of C_3H_6O compared to δ-hexalactone, which is $C_6H_{10}O_2$. δ-Hexalactone has approximately twice the molecular weight of the propylene oxide repeat unit. Both polymers have branched methyl groups, which likely leads to increased hydrophobicity. More importantly, the solubility parameter (δ) was taken into consideration, as it is ideal for the novel hydrophobic polymer to be similar in hydrophobicity with poly(propylene oxide). Closer values indicate more similarity in hydrophobicity, thus the new polymer is more likely to have similar solution properties, micellar stability, drug loading and releasing capability, and interactions with biological entities.

It is known that polymer solubility is primarily determined by its chemical structure, and the physical state of the polymer is also an important factor.[1] In order to determine the theoretical solubility of a given polymer, the concept of a solubility parameter (δ) was proposed. It is widely used for evaluating polymer-solvent and polymer-polymer interactions and can be deduced by calculating

the square root of the cohesive energy density.[2] The cohesive energy is comprised of three different parts: contributions of dispersion forces, polar forces, and hydrogen bonding, and is expressed in Equation 7.1. Therefore, the solubility parameter δ, which is based on the cohesive energy per unit volume, is expressed in Equation 7.2. The van Krevelen and Hoftyzer method, which used atomic group contributions, has been employed to calculate the solubility parameters for polymers.[1] The solubility parameter components are calculated from group contributions, as are shown in Equations 7.3-7.5. Group contribution to the dispersion component (F_{di}), group contribution to the polar component (F_{pi}), hydrogen bonding energy (E_{hi}), and molar volume (V) for structural groups are known. Table 7.1 shows solubility parameters of poly(propylene oxide) as compared to some biodegradable polymers.

$$E_{coh} = E_d + E_p + E_h \tag{7.1}$$

$$\delta = \sqrt{\delta_d^2 + \delta_p^2 + \delta_h^2} \tag{7.2}$$

$$\delta_d = \frac{\sum F_{di}}{V} \tag{7.3}$$

$$\delta_p = \frac{\sqrt{\sum F_{pi}^2}}{V} \tag{7.4}$$

$$\delta_h = \sqrt{\frac{\sum E_{hi}}{V}} \tag{7.5}$$

Table 7.1 Solubility parameters of poly(propylene oxide) and several biodegradable polymers.

Polymer	Solubility Parameter
Poly(propylene oxide)	18.9
Poly(δ-hexalactone)	19.7
Poly(lactide)	23.3
Poly(δ-valerolactone)	20.9
Poly(caprolactone)	20.2

Solubility parameter unit: $J^{1/2} / cm^{3/2}$.

The synthetic strategy begins with monohydroxy-functional PEO (1k) and grows a poly(δ-hexalactone) block using ROP from the poly(ethylene oxide). Since P85 is a triblock copolymer, the PEO-*b*-poly(δ-hexalactone) with an OH end group on the lactone is designed to form "dimers" through the reaction with a linker to form the triblock copolymers. The compositions were also carefully structured to mimic P85. The diblock copolymer is designed to have approximately 22 repeating units of ethylene oxide and 9 repeating units of δ-hexalactone. The reaction will be performed in bulk using either $Sn(Oct)_2$ as a catalyst, or an anionic polymerization. The triblock copolymer may be formed by reacting the diblock copolymer with a diacyl chloride, which was inspired by the excellent work of Uhrich et al.[3] for the synthesis of salicylic acid-derived poly(anhydride-esters) (Polyaspirin). The synthesis of the proposed triblock copolymer is shown in Figure 7.1. Based on the research conducted by Carbone et al.,[4] the degradation profiles of the poly(anhydride-esters) can be tailored by changing the type of linker, such as being aliphatic versus aromatic, and the linker length. It is likely that such an advantage could be applicable to this new proposed copolymer. Once the polymer is synthesized, we may use it to make polymer-drug nanocomplexes with or without transition metal oxides or salts. The physicochemical properties and

hydrodynamic stabilities of the nanocomplexes would then be evaluated. Cytotoxicity of this polymeric nanocarrier could be investigated with standard MTT assays in vitro. Drugs or antibiotics, such as cisplatin, doxorubicin, and gentamicin might be loaded into the novel nanocarrier, and their release profiles may be studied. In conclusion, if the degradation profiles of this novel polymer could be tailor-made by varying the linker type and length, and the polymer could interact with biological moieties in a similar way to P85, the novel PEO-*b*-poly(δ-hexalactone)-*b*-PEO based micellar nanocomplexes might be a quite promising candidate for drug delivery vehicles.

After an initial synthesis and evaluation of the PEO-*b*-poly(δ-hexalactone)-*b*-PEO for interactions with biological entities, we could further introduce functional groups, such as hydroxyl groups, or other polymer chains, such as poly(acrylic acid), onto the terminals of the poly(ethylene oxide). This could be achieved by using dual-functional initiators at the beginning of the polymer synthesis. For example, 3-hydroxypropyldimethylvinylsilane was used to synthesize vinyldimethylsilylpropoxy-terminated poly(ethylene oxide).[5] The PEO was endowed with the hydroxyl group on the terminal end while possessing a vinylsilyl bond on the other end. The existing hydroxyl end group could be used to initiate the copolymerization reaction with poly(δ-hexalactone). The newly-introduced vinylsilyl terminus could be further functionalized by reaction with various reagents. For example, carboxylic acid groups can be introduced to the PEO terminal vinylsilyl group by thiol-ene chemistry using mercaptoacetic acid.[5] Similarly, cysteamine or 3-mercapto-1-propanol could be used to endow the polymer terminals with amine or hydroxyl groups. These would allow us to compare and contrast PEO-*b*-poly(δ-hexalactone)-*b*-PEO with various surface functional groups, or with different extra polymer blocks, to tailor drug delivery profiles.

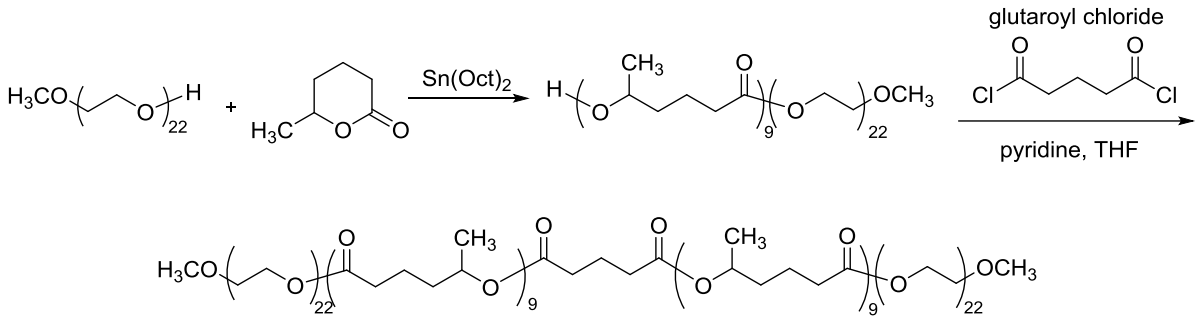

Figure 7.1 Synthesis of PEO-*b*-poly(δ-hexalactone)-*b*-PEG triblock copolymer.

7.3 Design and synthesis of polymeric micellar drug delivery systems using substituted amino acid monomers for potential drug delivery

Versatile, biodegradable polymeric micellar drug delivery systems (DDSs) are proposed utilizing functional amino acids as monomers. A multitude of polymeric micellar DDS using synthetic polymers have been developed and evaluated, many of which were found to be promising candidates for drug delivery.[6-8] Peptoids, which are *N*-substituted glycines with the potential to be used in DDSs, have been synthesized and many building blocks with different side groups have been introduced. [9-13] By converting these peptoids into *N*-carboxyanhydride-functional cyclic monomers, ring opening polymerization (ROP) could be used to synthesize homopolymers or copolymers of the peptoids. However, other substituted functional amino acids have not been studied and the necessary corresponding monomers are not available. In addition, biodegradable polymeric micellar DDSs using the substituted amino acids have not been evaluated for potential delivery applications. Therefore, a great opportunity exists to build substituted amino acid libraries and develop DDSs with them. Even an extra methyl group or functional group in the monomers could significantly change the physicochemical properties of a micellar DDS. More importantly, DDSs using substituted amino acids would be biodegradable and potentially biocompatible. Not meeting such needs may impose cytotoxicity.

A long-term goal would be to build key substituted amino acid monomers to develop versatile, biodegradable DDSs by incorporating them into polymers. It is envisioned that these amino acids could be synthesized by conventional organic synthetic methods with protection and deprotection reactions. It is also conceivable that micellar DDSs could be built with these monomers that would have excellent hydrolytic and hydrodynamic stability, low toxicity and good biocompatibility. It has been reported that polymeric micelles comprised partially of *N*-substituted poly(aspartamide) bearing 1,2-diaminoethane side chains display excellent micellar stability and negligible cytotoxicity, thus having potential as DDSs.[14] Studies have also suggested that *N*-substituted glycine and related building blocks can be synthesized.[15-16] It is proposed that once the targeted monomers and block copolymers with different functionalities are synthesized, biodegradable DDSs with predesigned capability and functionality could be fabricated.

Polymers have received tremendous research interest for drug delivery applications. Many polymeric DDSs have been fabricated that have displayed promising results. One example is a Pluronic® copolymer-based DDS developed by Kabanov et al.,[6] which is under phase III clinical evaluation.[17] In spite of such prominent progress, there is still a need for biodegradable and biocompatible analogs for such applications due to safety concerns. A critical gap in the knowledge base pertains to the synthesis of substituted, functional amino acids to form block copolymers to build DDSs. The proposed idea herein is to generalize the synthesis of substituted amino acid monomers and block polymers, as well as the building of DDS. This would be significant because it would enable screening and selection of appropriate substituted amino acids for building DDS with excellent biodegradability and biocompatibility. For example, by tuning the side chain of the proposed monomers, amphiphilic or ionic block copolymer-based DDSs could be fabricated with desirable

functionality that would add active targeting sites or thermo-responsive moieties for specific drug delivery applications.

7.3.1 Design and synthesis of substituted *N*-carboxyanhydride-functional amino acid monomers

N-substituted glycines have been synthesized and peptoid monomer libraries have been built. It would be interesting however, to have substituted amino acids other than glycines. Thus, it is proposed that select substituted, *N*-carboxyanhydride-functional cyclic amino acid monomers be synthesized. The synthesis could be achieved by using well-known organic synthesis/protection/deprotection methods.

We could synthesize select *N*-substituted amino acids without other functional groups, with the original amino acids being, for example, alanine, leucine or phenylalanine. Side groups to be introduced could be alkyl or allyl groups with different chain lengths. The synthetic method would be based on previously reported procedures,[18] as exemplified in Figure 7.2. A primary amine and an α-keto acid would be reacted in chloroform at room temperature, then acidified to afford intermediate 1. The intermediate would be suspended in toluene at low temperature and reacted with an excess of aqueous sodium hydroxide, then functionalized with benzyl chloroformate. After isolation, the cyclic monomers would be obtained by refluxing intermediate 2 with acetyl chloride and acetic anhydride.

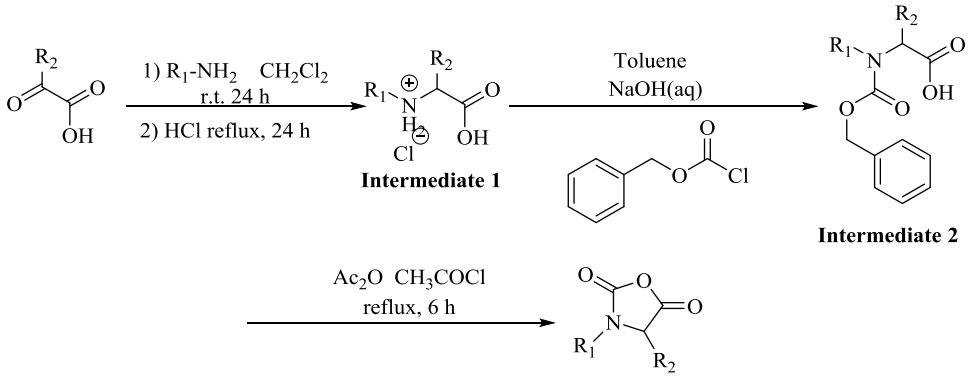

Figure 7.2 The proposed synthetic route for *N*-substituted cyclic amino acid monomers without other functional groups.

We could also synthesize select monomers with functional groups by post-reactions of the monomers or polymers. A straightforward synthetic approach for introducing a vinyl group on a side chain has been reported,[19] as shown in Figure 7.3. 2-Propen-1-amine and substituted α-bromo esters (depends on the desired amino acid) could be utilized as starting materials. After formation of the cyclic amino acid monomers with an allyl substituent, other functional groups could be introduced onto the monomer side chains by using thiol-ene reactions with 2,2'-azobis(2-methylpropionitrile) (AIBN) (Figure 7.4).[20] Carboxylic acids, amines, and other functional groups could be introduced by this method.

It is expected that a key group of substituted, cyclic monomers to be investigated as components in block copolymers for DDS would be provided by these methods. This would enable selection and polymerization to create DDS for potential specific applications, and would also enable a study of structure-property relationships between the constituents and the DDS.

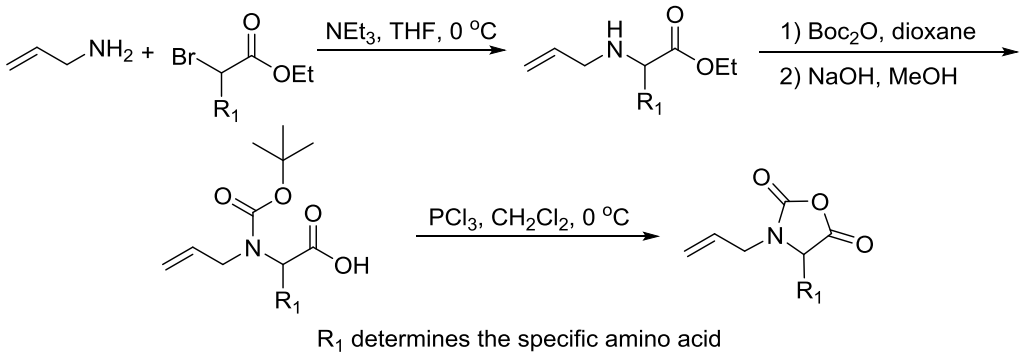

Figure 7.3 Proposed synthetic route for *N*-carboxyanhydride, cyclic amino acid monomers with an allyl substituent.

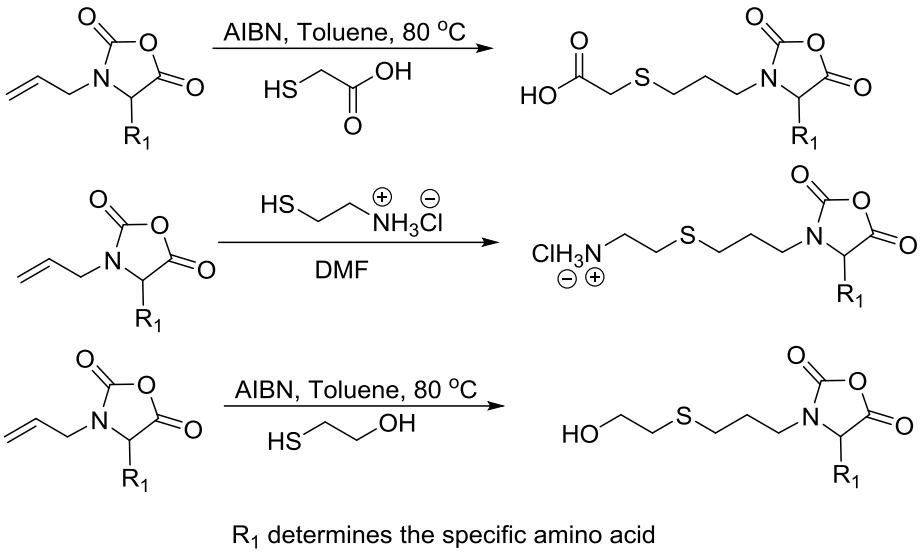

Figure 7.4 Introduction of functional groups onto the *N*-carboxyanhydride cyclic amino acid monomers

7.3.2 Design of DDSs using the substituted amino acid monomers

Biodegradable poly(amino acid)-based DDS would be excellent candidates for drug delivery. The targeted copolymers could be synthesized by sequential ROP, and micellar DDSs would then be fabricated via self-assembly in aqueous media. Two types of DDSs could be built. The first type would be amphiphilic block copolymers with a non-ionic hydrophilic block and a hydrophobic block. This may be achievable by tuning the length of the substituted hydrocarbon chains. The second type would incorporate ionic block copolymers with either an anionic, cationic, or zwitterionic block, as well as a hydrophilic non-ionic block.

Sequential ROP would be employed to synthesize the amphiphilic block copolymers. Benzylamine could be used as the initiator for these *N*-carboxyanhydride polymerizations as exemplified in Figure 7.5. One plan would be to investigate growing the relatively hydrophobic block

then crossing over to the second hydrophilic block. The targeted MW of the copolymers should likely be ~8k to 10k grams per mole.

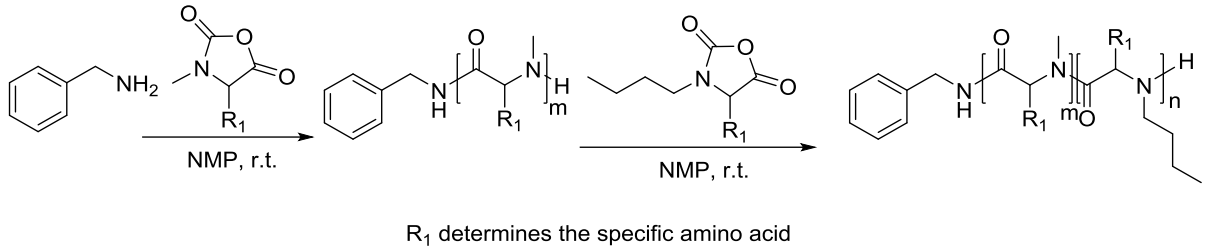

Figure 7.5 Synthesis of an amphiphilic block copolymer for building DDS.

Sequential ROP could also be employed to synthesize the ionic block copolymers as shown in Figure 7.6. The same initiator and similar reaction conditions would be investigated. The ionic groups could be introduced after the polymerization.

In order to form stable micellar ionic block copolymer DDSs, oppositely charged species (other ionic (co)polymers, surfactants, drugs etc.), or transition metal oxides or salts (magnetite, manganese chlorides, etc.) would be needed to complex with the polymers via electrostatic interactions and/or chelation. The complexation could be conducted in non-aqueous media to avoid ionic repulsion.

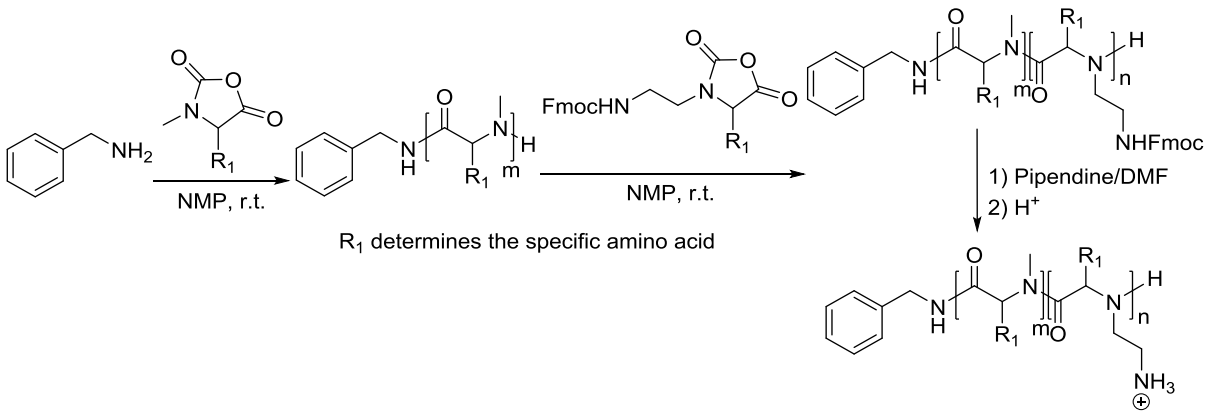

Figure 7.6 Synthesis of an ionic block copolymer for building DDS

After the DDSs are fabricated, their potentials for drug delivery applications could be evaluated. Such a study would include evaluations of hydrodynamic stability of aqueous suspensions and toxicity, then sample drugs could be investigated drug release experiments. Transmission electron microscopy (TEM), DLS, and spectroscopic characterization techniques could be used to characterize the drug-free and drug-loaded delivery systems. The experimental results would shed light on structure-property relationships between the individual monomers, block copolymers, and the corresponding DDSs.

The DDSs would be prepared by dissolving the amphiphilic block copolymers in aqueous media above their critical micelle concentration (CMC) (Figure 7.7). Hydrodynamic stability and *in vitro* toxicity tests would be used to evaluate the suitability of the DDSs since they must be colloidally stable in physiological conditions for an extended period and be non-toxic to cells. If positive results were obtained, then sample drugs would such as cisplatin would be used to load into the micelles. The loading would be investigated using a facile and well-known method: flash nanoprecipitation.[21] Drug release experiments would be performed in simulated physiological conditions.

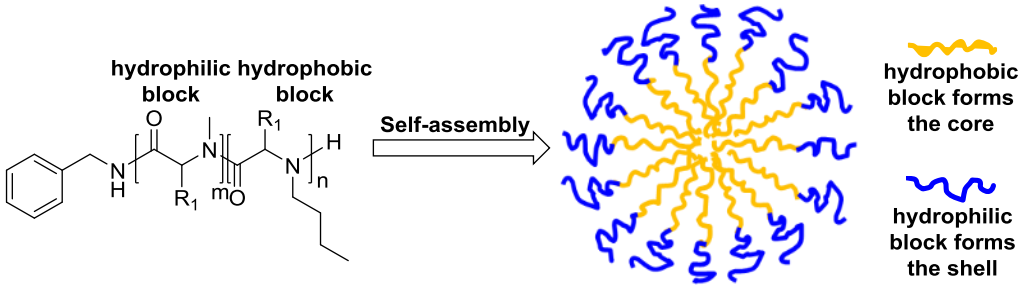

Figure 7.7 Self-assembly of an amphiphilic block copolymer into core-shell micelles.

The ionic DDSs would be fabricated by mixing the ionic block copolymer with another oppositely charged ionic copolymer. An example of one pair of such ionic block copolymers is shown in Figure 7.8. An equal amount of the two ionic copolymers (based on the equivalents of ions) could be mixed in a non-aqueous organic solution to form the micelles. Complexation with transition metal-based drugs could also be attempted. Drug release experiments and a structure-property relationship study with an emphasis on the amount and characteristics of the charge would be pursued.

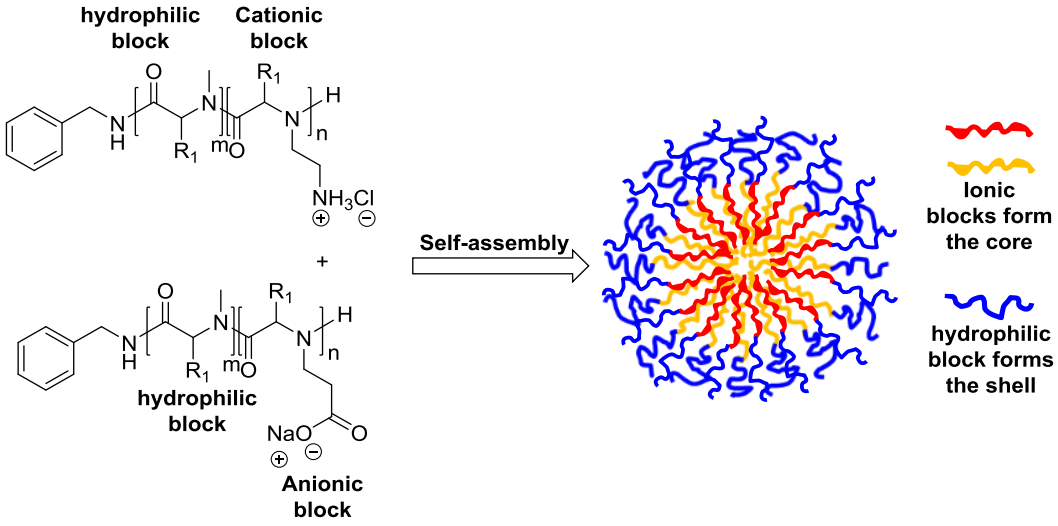

Figure 7.8 Self-assembly of two oppositely charged ionic block copolymers into core-shell micelles.

7.4 References

1. Van Krevelen, D. W.; Te Nijenhuis, K., *Properties of polymers: their correlation with chemical structure; their numerical estimation and prediction from additive group contributions*. Elsevier: 2009.
2. Eldrissi, A.; El Barkany, S.; Amhamdi, H.; Maaroufi, A.; Hammouti, B., New approach to predict the solubility of polymers. Application: Cellulose Acetate at various DS, prepared from Alfa „Stipa-tenassicima "of Eastern Morocco. *J. Mater. Environ. Sci* **2012,** *3*, 270.
3. Erdmann, L.; Uhrich, K. E., Synthesis and degradation characteristics of salicylic acid-derived poly(anhydride-esters). *Biomaterials* **2000,** *21* (19), 1941-1946.
4. Carbone, A. L.; Uhrich, K. E., Design and Synthesis of Fast-Degrading Poly(anhydride-esters). *Macromolecular Rapid Communications* **2009,** *30* (12), 1021-1026.
5. Kayandan, S. Synthesis and Characterization of Poly (lactide) Functional Oligomers and Block Copolymers. Virginia Tech, 2013.
6. Kabanov, A. V.; Batrakova, E. V.; Alakhov, V. Y., Pluronic® block copolymers as novel polymer therapeutics for drug and gene delivery. *Journal of Controlled Release* **2002,** *82* (2–3), 189-212.

7. Kataoka, K.; Harada, A.; Nagasaki, Y., Block copolymer micelles for drug delivery: design, characterization and biological significance. *Advanced Drug Delivery Reviews* **2001,** *47* (1), 113-131.
8. Park, J.-S.; Akiyama, Y.; Yamasaki, Y.; Kataoka, K., Preparation and Characterization of Polyion Complex Micelles with a Novel Thermosensitive Poly(2-isopropyl-2-oxazoline) Shell via the Complexation of Oppositely Charged Block Ionomers†. *Langmuir* **2006,** *23* (1), 138-146.
9. Holub, J. M.; Jang, H.; Kirshenbaum, K., Clickity-click: highly functionalized peptoid oligomers generated by sequential conjugation reactions on solid-phase support. *Organic & biomolecular chemistry* **2006,** *4* (8), 1497-1502.
10. Robertson, E. J.; Proulx, C.; Su, J. K.; Garcia, R. L.; Yoo, S.; Nehls, E. M.; Connolly, M. D.; Taravati, L.; Zuckermann, R. N., Molecular Engineering of the Peptoid Nanosheet Hydrophobic Core. *Langmuir* **2016,** *32* (45), 11946-11957.
11. Gorske, B. C.; Jewell, S. A.; Guerard, E. J.; Blackwell, H. E., Expedient synthesis and design strategies for new peptoid construction. *Organic letters* **2005,** *7* (8), 1521-1524.
12. Wu, C. W.; Sanborn, T. J.; Zuckermann, R. N.; Barron, A. E., Peptoid oligomers with α-chiral, aromatic side chains: effects of chain length on secondary structure. *Journal of the American Chemical Society* **2001,** *123* (13), 2958-2963.
13. Yoo, B.; Kirshenbaum, K., Peptoid architectures: elaboration, actuation, and application. *Current Opinion in Chemical Biology* **2008,** *12* (6), 714-721.
14. Miyata, K.; Oba, M.; Nakanishi, M.; Fukushima, S.; Yamasaki, Y.; Koyama, H.; Nishiyama, N.; Kataoka, K., Polyplexes from poly (aspartamide) bearing 1, 2-diaminoethane side chains induce pH-selective, endosomal membrane destabilization with amplified transfection and negligible cytotoxicity. *Journal of the American Chemical Society* **2008,** *130* (48), 16287-16294.
15. Zuckermann, R. N.; Kerr, J. M.; Kent, S. B.; Moos, W. H., Efficient method for the preparation of peptoids [oligo (N-substituted glycines)] by submonomer solid-phase synthesis. *Journal of the American Chemical Society* **1992,** *114* (26), 10646-10647.
16. Figliozzi, G. M.; Goldsmith, R.; Ng, S. C.; Banville, S. C.; Zuckermann, R. N., [25] synthesis of N-substituted glycine peptoid libraries. In *Methods in enzymology*, Elsevier: 1996; Vol. 267, pp 437-447.
17. Zhang, Y.; Chan, H. F.; Leong, K. W., Advanced materials and processing for drug delivery: The past and the future. *Advanced Drug Delivery Reviews* **2013,** *65* (1), 104-120.
18. Fetsch, C.; Grossmann, A.; Holz, L.; Nawroth, J. F.; Luxenhofer, R., Polypeptoids from N-Substituted Glycine N-Carboxyanhydrides: Hydrophilic, Hydrophobic, and Amphiphilic Polymers with Poisson Distribution. *Macromolecules* **2011,** *44* (17), 6746-6758.
19. Robinson, J. W.; Schlaad, H., A versatile polypeptoid platform based on N-allyl glycine. *Chemical Communications* **2012,** *48* (63), 7835-7837.
20. Boutevin, G.; Ameduri, B.; Boutevin, B.; Joubert, J.-P., Synthesis and use of hydroxyl telechelic polybutadienes grafted by 2-mercaptoethanol for polyurethane resins. *Journal of Applied Polymer Science* **2000,** *75* (13), 1655-1666.
21. Pustulka, K. M.; Wohl, A. R.; Lee, H. S.; Michel, A. R.; Han, J.; Hoye, T. R.; McCormick, A. V.; Panyam, J.; Macosko, C. W., Flash Nanoprecipitation: Particle Structure and Stability. *Molecular Pharmaceutics* **2013,** *10* (11), 4367-4377.